5-2-2011 12:00 AM

Uncertainty Estimation of Extreme Precipitations Under Climate Change: A Non-Parametric Approach

Tarana A. Solaiman, *The University of Western Ontario*

Supervisor: Slobodan P. Simonovic, *The University of Western Ontario*
A thesis submitted in partial fulfillment of the requirements for the Doctor of Philosophy degree
in Civil and Environmental Engineering
© Tarana A. Solaiman 2011

Recommended Citation

UNCERTAINTY ESTIMATION OF EXTREME PRECIPITATIONS UNDER CLIMATE CHANGE: A NON-PARAMETRIC APPROACH

(Spine Title: Uncertainty of Future Extreme Precipitation Events)

(Thesis Format: Monograph)

By

Tarana Aftab **Solaiman**

Graduate Program in Engineering Sciences
Department of Civil and Environmental Engineering

A thesis submitted in partial fulfillment
of the requirements for the degree of
Doctor of Philosophy

The School of Graduate and Postdoctoral Studies
The University of Western Ontario
London, Ontario, Canada

THE UNIVERSITY OF WESTERN ONTARIO
School of Graduate and Postdoctoral Studies

CERTIFICATE OF EXAMINATION

Supervisor

_____
Dr. Slobodan P. Simonovic

_____

Examining Board

_____
Dr. Craig Miller

_____
Dr. Clare Robinson

_____
Dr. Gordon McBean

_____
Dr. Donald Burn

The thesis by

Tarana Aftab Solaiman

entitled:

UNCERTAINTY ESTIMATION OF EXTREME PRECIPITATIONS UNDER CLIMATE CHANGE: A NON-PARAMETRIC APPROACH

is accepted in partial fulfillment of the
requirements for the degree of
Doctor of Philosophy

_____
Date

_____
Chair of the Thesis Examination Board

II

ABSTRACT

Assessment of climate change impacts on hydrology at watershed scale incorporates (a) downscaling of global scale climatic variables into local scale hydrologic variables and (b) assessment of future hydrologic extremes. Atmosphere-Ocean Global Climate Models (AOGCM) are designed to simulate time series of future climate responses accounting for human induced greenhouse gas emissions. The present study addresses the following limitations of climate change impact research: (i) limited availability of observed historical information; (ii) limited research on the detection of changes in hydrologic extremes; and (iii) coarse spatio-temporal resolution of AOGCMs for use at regional or local scale. Downscaled output from a single AOGCM with a single emission scenario represents only a single trajectory of all possible future climate realizations and cannot be representative of the full extent of climate change. Present research, therefore addresses the following questions: (i) how should the AOGCM outputs be selected to assess the severity of extreme climate events?; (ii) should climate research adopt equal weights from AOGCM outputs to generate future climate?; and (iii) what is the probability of the future extreme events to be more severe? Assessment of regional reanalysis hydro-climatic data has shown promising potential as an addition to the observed data in data scarce regions. A new approach using statistical downscaling based nonparametric data-driven kernel estimator is developed for quantifying uncertainties from multiple AOGCMs and emission scenarios. The results are compared with a Bayesian reliability

ensemble average method. The generated future climate scenarios represent the nature and progression of uncertainties from several global climate models and their emission scenarios. Treating the extreme precipitation indices as independent realization at every time step, the kernel estimator provides variable weights to the multi-model quantification of uncertainties. The probabilities of the extreme indices have added useful insight into future climate conditions. Finally, the current method of developing future rainfall intensity-duration-frequency curves is extended by introducing a probabilistic weighted curve to include AOGCM and emission scenario uncertainties using the plug-in kernel. Present research has thus expanded the existing knowledge of dealing with the uncertainties of extreme events.

Keywords: Climate change, Continuous hydrologic modeling, Reanalysis project, Extreme precipitation indices, Uncertainty estimation, K nearest neighbor weather generator, Principal component analysis, Annual maximum series, Kernel density estimation, Bayesian reliability ensemble average, Plug in kernel, Least square cross validation, Intensity-duration-frequency curve.

DEDICATION

To my idols, my parents

ACKNOWLEDGEMENTS

Mahbubul Hasan, Dr. Shahidul Islam for helping me time to time which made my life easier.

Finally my grateful acknowledgement goes to my family members, my always inspiring mother (Professor Momena Akhtar Khodeja) and father (Dr. Muhammad Solaiman), my sisters (Dr. Tamanna Solaiman and Dr. Mahjabeen Solaiman), my sister-in-law (Dr. Javed Iqbal) and my loving husband, Ali Jayed for their support and for giving me strength during hard times. Without all your loves, encouragements, and understanding it would never be possible for me to continue my studies. Above all, thanks to the Almighty for guiding us to the right path.

TABLE OF CONTENTS

LIST OF FIGURES

LIST OF TABLES

LIST OF APPENDICES

CHAPTER ONE

INTRODUCTION

1.1 Climate Change

Climate is a complex and interactive system comprising of the atmosphere, land, snow and ice, oceans, other water bodies and living objects. Two factors such as, Earth's internal dynamics and changes by the external factors (forcing) mainly influence climate's variation over time. External forcing can be natural phenomena such as volcanic eruptions, solar variations or it can also be changes in the atmospheric compositions due to human activities. From the period of industrial revolution since 200 years ago human activities have increased the concentration of greenhouse gases (GHG) in the atmosphere. This enhanced GHG effect is the result of anthropogenic emissions of greenhouse gases which has been trapping heat in the atmosphere and has increased the absorption of infrared radiation. Of many greenhouse gases, such as carbon dioxide (CO_2) and water vapor, methane (CH_4), nitrous oxide (N_2O) and some halocarbons such as perfluorocarbons (PFCs), hydroflourocarbons (HFCs) and sulphur hexafluoride (SF_6), etc, carbon dioxide has caused the most severe threat by releasing 60% of manmade emissions since late 18th century. Global warming is nothing but the progressive gradual increase of the Earth's surface temperature resulting from these greenhouse gases and responsible for the changes in climatic patterns.

The consequences of global warming are reflected in global as well as regional climate in terms of changes in the key climate variables such as temperature, precipitation, humidity, snow cover, extent of land and sea ice, sea level and atmospheric and oceanic circulation patterns. Continuous increase of global temperature is expected to raise the sea level by melting glaciers and thermal expansion. Significant changes in precipitation include shifting global precipitation patterns, intensity and frequency of extreme events such as, floods and droughts. The Intergovernmental Panel on Climate Change (IPCC) has reported $0.74^0 \pm 0.18^0C$ increase of global mean temperature in the 20th century. It is observed that eleven of the twelve years between 1995-2006 ranked among the twelve warmest years in the instrumental record of global surface temperature (since 1850) (IPCC, 2007). There is evidence of the changes in the precipitation pattern in the mid and high latitudes of the Northern Hemisphere (Figure 1.1).

1.2 Climate Change Impact on Hydrology

Water is the most vulnerable resource to climate change (Minville et al., 2008; Srikanthan and McMohan, 2001; Xu and Singh, 2004) resulting in an increased evaporation due to higher temperatures, changes in the amount, variability, and frequency of regional precipitation. Studies related to the impact of climate change on water resources have shown significant changes in the mean annual discharge with any modification in the intensity and frequency of precipitation (Whitfield and Cannon, 2000; Muzik, 2001), larger changes in reservoir storage because of a modest shift in the natural

inflow or even a changed effect in the energy production and flood control measure due to any effect in the hydrologic cycle (Xu and Singh, 2004).
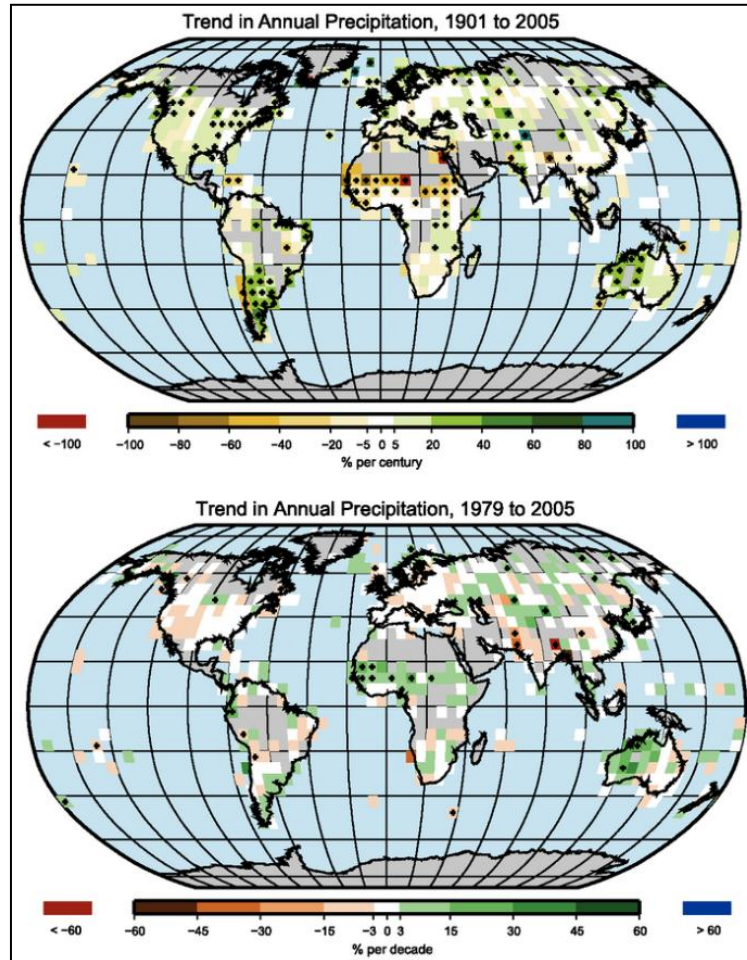
Figure 1.1: Trend of Annual Land Precipitation Amounts for 1901 to 2005 (Top, % per Century) and 1979 to 2005 (Bottom, % per Decade (IPCC, 2007))

Hydrologic research and modeling is largely dependent on climatological inputs due to the inextricable link of water with climate. Climate modeling studies involving anthropogenic increase in the concentration of greenhouse gases have suggested an increase in the frequency and intensity of climatic extremes in a warmer world (Pall, 2011; Cubasch et al., 2001). The evidence of an altered climate has already become

noticeable. Recent studies related to the Canadian climate have indicated a 12% increase of precipitation in southern Canada during the twentieth century (Min et al., 2011; Zhang et al., 2000; Vincent and Mekis, 2006). Such changes can play a major role in water resources planning and management. The most significant impact of climate change on water resources is expected to be on local (basin) scale. The increase in precipitation and extreme events in the form of floods or droughts will demand revision of current safety standards and protection measures designed for extreme conditions as well as development and implementation of new water resources planning, design and management strategies.

1.3 Climate Change Research Tools

1.3.1 Atmosphere Ocean Global Climate Model

Assessment of climate change impacts on hydrology incorporates projection of climate variables into a global scale, downscaling of global scale climatic variables into local scale hydrologic variables and computations of risk of future hydrologic extremes for purposes of water resources planning and management. Global scale climate variables are commonly projected by coupled Atmosphere-Ocean Global Climate Models (AOGCMs), which provide a numerical representation of climate systems based on the physical, chemical and biological properties of their components and feedback interactions between them (IPCC, 2007). These models are currently the most reliable tools available for obtaining the physics and chemistry of the atmosphere and oceans and for deriving projections of meteorological variables (temperature, precipitation, wind speed, solar

radiation, humidity, pressure, etc). They are based on various assumptions about the effects of the concentration of greenhouse gases in the atmosphere coupled with projections of CO_2 emission rates (Smith et al., 2009). More information about the AOGCMs are presented in Appendix A.

Extraction of climatological inputs from any global climate model can be performed by two simple approaches, namely (i) using the grid box information at original model resolution, and (ii) using interpolation to a finer resolution. Using AOGCM values from the nearest grid box to the study area provides the simplest mean of extracting climate information. However, this method suffers from many drawbacks. Firstly, lack of confidence in regional estimates of climate change has led to the suggestions that the minimum effective spatial resolution should be defined by at least four grid boxes. Secondly, sites within close proximity but falling in different grid boxes while having a very similar baseline climate may be assigned a quite different scenario climate. Furthermore, a site on land may be located in a grid box defined as ocean. For these reasons, change fields from nearby grid boxes are interpolated to the site or the region of interest. This method overcomes the problems of discontinuities in change between adjacent sites in different grid boxes.

The accuracy of AOGCMs decreases at finer spatial and temporal scales; a typical resolution of AOGCMs ranges from 250 km to 600 km, but the need for impact studies conversely increases at finer scales (Figure 1.2). The representation of regional precipitation is distorted due to this coarse resolution and thus it cannot capture the subgrid-scale processes required for the formation of site-specific precipitation conditions. While some models are parameterized, details of the land-water distribution

5

or topography in others are not represented at all (Widmann et al., 2003). Studies have found that the models failed to predict the high variability in daily precipitation and could not accurately simulate present-day monthly precipitation amounts (Trigo and Palutikof, 2001; Brissette et al., 2006).

A number of techniques have been developed to enhance the information from AOGCMs in order to bridge the gap between the climate model outputs from global to local scale. Downscaling, in the water resources context, is a method used to predict hydrologic variables at a smaller scale based on large scale climatological variables simulated by the AOGCMs. Poor performances of AOGCMs at local scales have led to the development of two basic downscaling approaches: dynamic and statistical downscaling.

Dynamic downscaling approach incorporates limited area models (LAMs) where a fine computational grid over a limited domain is nested within the coarse grid of any AOGCM (Jones et al, 1995). The complicated design, inflexibility due to need of area specific experiments and higher computational time has restricted its use in the climate change impact assessment studies (Crane and Hewitson, 1998; Ghosh and Mujumder, 2007). The statistical downscaling, on the other hand, derives regional and local information by determining a statistical model to relate with large scale climate variables to regional or local scale hydrologic variables. Further details of the downscaling methods are presented in Chapter 2.
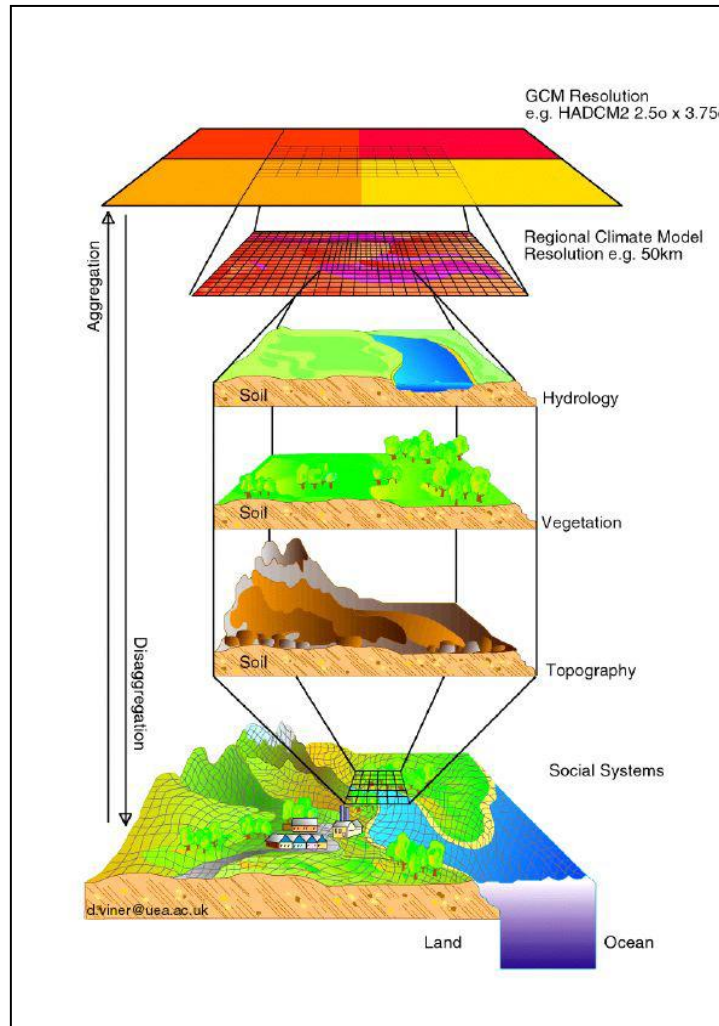
Figure 1.2: Spatial Downscaling

(Source: CCCSN Website; Retrieved from http://cccsn.ca/downscaling, on 3/01/2011)

1.3.2 Reanalysis Project

The reanalysis are essentially diagnostic atmospheric models, which are used 'in concert with observations via data assimilation' (Pielke, 2002). The reanalysis data are advantageous because they are based on the AOGCMs with a fixed dynamical core, physical parameterizations and data assimilation system (Castro et al., 2007). A reanalysis is generally a model-run constrained by observations. The space and time

resolution of the data generated through these reanalysis projects are independent of the number of observations, since the areas void of observations are filled with dynamically and physically consistent model-generated information. Although they provide datasets for any period of time, it is evident that their usefulness crucially depends on the quality and distribution of the observations in time and space. At the same time, it is important to note that to date this is the most accurate way of interpolating data in time and space as well as a superior way to obtain dynamical consistency between different atmospheric variables. It is also more representative because it provides an opportunity to examine local effects, such as those caused by urbanization and agricultural effects (Kalnay and Cai, 2003).

For any specific region if only few observations are available, the constraints to set for the model is considered weak and the model produces datasets based on its own variability. When enough observations are available, the model is more forced to follow the observed variability rather than its own built-in variability. Assuming that different datasets have their own variability, there may be instances where at least one of the reanalyses products does not represent the correct scenario. Comparing results from at least two reanalyses may offer a more correct evaluation of their performances. If the results agree, the observational constraint can be considered large enough to force the models to follow the real variability of the atmosphere. Conversely, a difference in the results indicates weak constraints set for that spatio-temporal domain and at least one of the products does not represent the correct variability (Sterl, 2004).

With a satisfactory presentation of any region's variability, these gridded daily datasets can often be used to initialize climatic, ecological or hydrological models (Jolly et al.,

2005; Kittel et al., 2004; Ensor and Robeson, 2008). More information on the Global and Regional Reanalysis project can be found in Kalnay et al. (1996) and Mesinger et al. (2006).

1.4 Definition and Types of Uncertainties

A proper understanding of the uncertainties resulting from human induced climate change will help decision makers to interpret different projected hydrologic impacts with confidence. Three broad areas of uncertainties have been identified by Colglazier (1991):

- Predicting future climate

- Predicting future impacts

- Assessing costs and benefits of policy responses

The first two areas, related to the present research, are described here.

Predictions of the timing and magnitude of any future global warming are associated with (i) uncertainties in estimating future anthropogenic emissions of greenhouse gases; (ii) understanding the resulting changes in the carbon cycle, especially the uptake of carbon by the oceans; (iii) understanding the dynamic climatic response with all the relevant feedback mechanisms, such as those from clouds and ocean currents; (iv) projecting regional variations; and (v) estimating the frequency of severe events such as, hurricanes and droughts (Colglazier, 1991). Although the basic theory of the enhanced greenhouse gas effect is now well established, and the rise in carbon dioxide concentrations since the industrial revolution has also been well documented, there is still much debate regarding the timing and quantity of warming. For decades AOGCMs have

been used to predict these values; however there is continued uncertainty even with the improvements of the resolution of AOGCMs.

The interpretation of uncertainties from climate models can be described from five sources. 'Forcing uncertainty' consists of using the future elements/aspects that are not a part of the climate system, but have the potential to affect it. One possible form of forcing uncertainty arises from using climate model simulations based on different scenarios of future concentrations of atmospheric GHGs, which depend entirely on the actions taken to control the GHG emissions (Cubasch et al., 2001).

'Initial condition uncertainty' involves uncertainty arising from an initial state or ensemble of states (Stainforth et al., 2007) applied to the climate models. It can be 'macroscopic' and found in state variables with relatively large slowly mixing scales, such that the predicted distribution is affected by the imprecise knowledge of the current state of the system. 'Microscopic' uncertainty, on the other hand, has no significant effect on the targeted climate distribution; the effects are only identified during weather forecast.

'Model imperfection' describes the uncertainty that results from a limited understanding and ability to simulate the Earth's climate. It is sub-divided into two types: 'uncertainty' and 'inadequacy'. 'Model uncertainty' describes uncertainties in the most relevant parameter values to be used in the model (Murphy et al., 2004). It characterizes the impact of known uncertainties and can be large at regional scales. Climate models, in this respect, are considered rather complicated. Extending this from parameter values to parameterizations enables an improved representation of various processes within the

model and makes model uncertainty an extended form of the 'parameter uncertainty'(Kennedy and O'Hagan, 2001). 'Model inadequacy' results from the limited ability of the climate models to represent natural systems. These models provide no information on important processes related to climate change on decadal to centennial time scales, such as the carbon cycle, atmospheric and oceanic chemistry and stratospheric circulation. They further suffer from limited spatial resolution, inadequate representation of hurricanes, the diurnal cycle of tropical precipitation, characteristics of El Nino Southern Oscillation (ENSO) and the inter tropical convergence zone (Trenberth et al., 2003).

Present research focuses on uncertainties due to inter-model variability (AOGCM uncertainty) and inter-scenario variability (Scenario uncertainty) arising from different climate experiments.

1.5 Intensity-Duration-Frequency Analysis

Reliable rainfall intensity estimates are necessary for hydrologic analyses, planning and design problems. The rainfall intensity-duration-frequency (IDF) curve is one of the most common tools for urban drainage designer. Information from IDF curves are used to describe the frequency of extreme rainfall events of various intensity and durations. According to the guideline for 'Development, Interpretation and Use of Rainfall Intensity-Duration-Frequency (IDF) Information: A Guideline for Canadian Water Resources Practitioners" developed by Canadian Standards Association (CSA, 2010), there is a major increase in demand for rainfall IDF information:

- *Due to increased understanding and documentation of the special heterogeneity of extreme rainfall patterns, the demand for "locally relevant" IDF information has increased*

- *Expansions of urban areas have converted watersheds less permeable to rainfall and runoff. As a result of this, many older water systems are facing deficit and failing to deliver the services according to their designed capacity. For a complete understanding of the full magnitude of this deficit, information on the maximum inputs (extreme rainfall events) must be known*

- *Climate change is expected to result in an increase in the intensity and frequency of extreme precipitation events in most regions in future. As a result, IDF values will optimally need to be updated more frequently than in the past and climate change scenarios might eventually be drawn upon in order to inform IDF calculations.*

The establishment of rainfall IDF curves typically involves three steps. First, a probability density function (PDF) or cumulative distribution function (CDF) is fitted to each group comprised of the data value for any specific duration. The maximum rainfall intensity for each time interval is related to the corresponding return period from the cumulative distribution function. For a given return period T, the cumulative frequency F can be expressed as:

$$F = 1 - \frac{1}{T} \tag{1.1}$$

or,

$$T = \frac{1}{1 - F} \tag{1.2}$$

If the cumulative frequency is known, the maximum rainfall intensity can be determined using an appropriate theoretical distribution function (such as Generalized Extreme Value (GEV), Gumbel, Pearson Type III, etc). In the presence of climate change, the theoretical distribution based on historical observations is expected to be different for the future conditions. The issue gets further complicated due to the presence of various uncertainties from global climate models and emission scenarios.

1.6 Research Contribution

Climate change impact studies related to hydrology suffer from the following limitations:

- Limited availability of observed historical information from weather stations

- Decade long history of the climate change impact assessment focuses on studying the changes of means, although extremes usually have the greatest and the most direct impact on our everyday lives, communities and the environment. Study on the detection of changes in extremes is limited and needs further investigation.

- There is a high level of confidence that AOGCMs are able to capture large scale circulation patterns and correctly model smoothly varying fields, such as surface pressure, especially at continental or larger scales. However, it is extremely unlikely that these models can properly reproduce highly variable fields, such as precipitation (IPCC, 2007; Hughes and Guttorp, 1994), on a regional scale, let alone for small to medium watersheds. Although confidence has increased in the ability of AOGCMs to simulate

extreme events, such as hot and cold spells, the frequency and the amount of precipitation during intense events are still underestimated.

- In the presence of human induced warming trends added to Earth's natural variability, it is unlikely that the future distribution of climate extremes will be the same as in the past.

- Downscaled outputs from a single AOGCM with a single climate change emissions scenario characterizes only a single trajectory of all possible realizations derived from different AOGCMs and scenarios and cannot be representative of future climate change.

- Consideration of equal weights for multi-model ensemble of climate experiments

- No quantified probability is provided with the derived results.

Present research addresses the following important questions related to the studies of climate extremes: (i) how should the AOGCM outputs from different global climate models and scenarios be selected to assess the severity of extreme climate events? (ii) should climate change studies adopt equal weights from the global climate model information while modeling uncertainty?; (iii) what are the chances for the future extreme precipitation events to be more severe?. This has a huge impact in climate science, especially due to the differences in the structure, initialization and parameterization of the future climatic responses from the global climate models.

Specific objectives of the study include:

- To assess the performances of the global and regional reanalysis data (stated in section 1.3.2) as an addition/ alternate for (a) climate change and (b) hydrologic modelling studies

- To develop a classification scheme for determining the severity of extreme precipitation events from the downscaled AOGCM outputs;

- To quantify uncertainties associated with different AOGCMs and scenarios;

- To model AOGCM and scenario uncertainties using nonparametric methods;

- To develop intensity-duration-frequency design curves under different climates; and

- To develop a probabilistic approach for future intensity-duration-frequency analysis.

With a view to achieve the above goals, several methods are applied. Firstly, the performance of global and regional reanalysis outputs is interpolated to basin scale and compared with the historical observed information for their potential use in climate change impact studies. Next, a continuous hydrologic model is used to test the reanalysis outputs for hydrologic modeling.

Secondly, AOGCM and scenario uncertainties in modeling climate change impacts are analyzed by two different methods. First, the Bayesian Reliability Ensemble Average (BA-REA) is applied to estimate uncertainties from AOGCM outputs directly. In the next step, a nonparametric approach is developed. It includes statistical downscaling method (i.e. the weather generator) for generating long series of precipitation containing future

climate information. To reduce the dimensionality and multi-collinearity of the predictors, the principal component analysis (PCA) is integrated into the weather generator. The non-parametric kernel density estimators are finally used to quantify uncertainties of the downscaled outputs. Non-parametric approach has proved to be competitive to the parametric methods that involve a specific distribution fit for the data sample. Non-parametric approaches such as, Monte Carlo simulations (Adamowski, 1985, 1996), kernel estimators (Guo et al., 1996; Moon and Lall, 1994) are found to provide more accurate results when compared to log-Pearson (III) distribution and several tail estimators for estimating flood-frequency and low-flow quantiles. The bias and root-mean-square error are found to be less in the above studies, thereby suggesting the non-parametric methods as a viable alternative to its parametric counterparts.

Three extreme precipitation indices are used to derive extreme precipitation information from the downscaled outputs. A percentile based classification scheme is next developed to assess the severity of the extreme precipitation events. By treating the annual values of each extreme precipitation indices as random in every time step, methodology based on data-driven kernel density estimator is used to derive the non-parametric probability density function information for different categories of indices.

Finally, downscaled outputs are used to design rainfall intensity-duration-frequency design curves for different climates. The daily outputs are disaggregated into hourly intervals using a disaggregation scheme and then applied in derivation of rainfall intensity frequency information. The generated IDF information from different climate model outputs are next used to derive weighted IDF curves in a probabilistic manner.

Recommendations for revising existing water resources management standards and guidelines are included.

1.7 Structure of the Thesis

This thesis is composed of six chapters, including introduction in Chapter 1. Chapter 2 covers literature reviewed for the purpose of this research. A brief review of different downscaling methods, uncertainty estimation methods, their advantages and limitations, and approaches for developing IDF curves for assessment of climate change impact on hydrology have been presented.

Chapter 3 describes the methodology along with different model parameters, used to develop the theoretical framework for assessment of climate change impacts. Schematics of the framework for each stage of the work are also presented.

Chapter 4 emphasizes the details related to the applications of the methodology in the Upper Thames River basin. Technical details focusing on different databases, selection of appropriate inputs, parameter values, and model set-up process are explained.

Chapter 5 summarizes the results obtained from the application of the methodologies for the Upper Thames River basin. First, the comparative performances of the reanalysis datasets are presented. Performance of multi-model uncertainty estimation method based on the Bayesian Reliability Ensemble Average technique is analyzed. Performance of the PCA integrated weather generator is next evaluated for deriving future climate signals. A total of 15 different scenarios are derived. They are used to estimate uncertainties using

non-parametric kernel estimators. The results are compared with results obtained from the BA-REA method. Selection of appropriate kernel method is further tested for examining extreme precipitation events. The results are presented in terms of probability density estimates. Finally, input for the development of a probability based rainfall intensity-duration-frequency (IDF) curves using 27 different climate signals are presented.

Finally, the concluding remarks based on the major findings and recommendations for future works are presented in Chapter 6.

CHAPTER 2

LITERATURE REVIEW

This chapter presents the literature related to climate change impact assessment studies in hydrology. Use of reanalysis data for water resources studies are presented in next section. Different downscaling techniques in terms of their application, comparative advantages and limitations are discussed next. Implications of different uncertainty estimation techniques for assessment of hydrologic variables under climate change are presented in the subsequent sections. Methodologies adopted for developing IDF curves under future climate are presented at the end.

2.1 Reanalysis Hydro-Climatic Data

Reanalysis data from different sources have shown promising potential in global climate research studies. In this section literature relevant to the National Center for Environmental Prediction and National Center for Atmospheric Research (NCEP/ NCAR) global reanalysis - NNGR (Kalnay et al., 1996) and the North American Regional Reanalysis - NARR (Mesinger et al., 2006) data is discussed. Several studies have compared the global reanalysis precipitation and temperature data with other available databases at different locations. Neito et al. (2004) compared the NNGR data with ECHAM4/OPYC3 and HadCAM3 models to analyze the correspondences and/or the discrepancies within the observed winter precipitation data during 1949-2000 for the

Iberian Peninsula. NNGR precipitation data effectively captured the spatial and temporal variability and showed a good agreement with the observed precipitation.

Ruiz-Barradas and Nigam (2006) found a correlation coefficient of 0.99 when the NNGR data were compared with the observed summer precipitation to analyze the inter-annual precipitation variability over the Great Plains, United States.

However, while Tolika et al. (2006) found an inferior agreement between NNGR and observations, they also found a closer inter-annual variability when NNGR was compared with the GCMHadAM3P data for examining the suitability of the averaged distributions and the spatial and temporal variability of the winter precipitation in Greece.

In many applications, the NNGR resolution appeared to be less satisfactory than the observed temperature and precipitation, especially in regions with complex topographies, (Choi et al 2009; Tolika et al, 2006; Rusticucci and Kousky, 2002; Haberlandt and Kite, 1998) due to coarse resolution (250 km X 250 km) and physical parameterizations (Castro et al 2007).

The recently released North American Regional Reanalysis (NARR) dataset, developed by Mesinger et al. (2006), designed to be "a long term, dynamically consistent, high-resolution, high frequency, atmospheric and land surface hydrology dataset for the North American domain", is a major improvement upon the global reanalysis datasets in both resolution and accuracy. However, due to the fact that the NARR is a recent product, it has not been widely evaluated.

Nigam and Ruiz-Barradas (2006) have made an inter-comparison between two global [40 yr- ECMWF Re-Analysis (ERA 40) and NCEP] and regional (NARR) datasets to

analyze the hydro-climatic variability over the Eastern United States and found that the NARR data provided a realistic spatial variation of summer and winter precipitation.

Most of the studies focused on the spatial distributions of the seasonal and/or inter-annual variability of hydro-meteorological data. There have been only a few studies relevant to hydrologic modeling. Woo and Thorne (2006) used temperature and precipitation data from the ERA 40, NNGR and NARR as input to a macro-scale hydrologic model for estimating the contribution of snowmelt to discharge in the Liard basin in the Subarctic Canada. They found (i) a cold bias resulting in later snowmelt peaks and (ii) that NARR provides a better representation of the relative flow contribution from different sections of the basin.

Thorne and Woo (2006) also applied three sets of climate data: (i) in-situ data from weather stations, (ii) NCEP/NCAR Global reanalysis data, and (iii) weather forecast data produced by the Canadian Meteorological Centre (CMC) as inputs to a Semi-distributed Land Use-Based Runoff Processes (SLURP) model. It was used to both simulate stream flow and to examine how the simulated flow for different parts of the basin relates to the measured discharge available for several sub-basins within the Liard sub-catchment.

Choi et al. (2007, 2009) evaluated the monthly and daily reanalysis datasets to examine their potential as an alternative data source for hydrologic modeling in Manitoba. Their study revealed a satisfactory performance of the temperature data; but a weaker performance of the precipitation data was noticed. The study also found a superior performance of the NARR precipitation values when compared to that of their NNGR counterparts.

Castro et al. (2007) applied 53 years of NNGR data with dynamic downscaling using the Regional Atmospheric Modeling System (RAMS) to generate regional climate model (RCM) climatology of the contiguous US and Mexico. They compared the RAMS simulated data with that of the NARR, the observed precipitation and temperature data, and found a good agreement of the NARR data in some parts of the Great Plains. The literature cited above clearly indicates the potential of the reanalysis dataset for use in hydrologic modeling and/or climate change for studies to replicate the current climate regime.

2.2 Downscaling AOGCM Outputs

The global climate models are generally designed to simulate present climate and predict future climate change with forcing by greenhouse gases and aerosols. Estimation of hydrological processes at a regional or watershed scale based on these global scale models does not provide satisfactory outputs. Limitations of the AOGCMs in regional studies include the following:

- Accuracy of the AOGCMs decreases at finer spatial and temporal scales; typical resolution of a global climate model varies between 250 km to 600 km which is still coarse for any watershed impact studies.

- Accuracy of AOGCMs decrease from large scale climate variables (wind, temperature, humidity, sea level pressure) to the smaller scale hydrologic variables (precipitation, evaporation, evapotranspiration, soil moisture, discharge) due to simplified approximation of radiant-energy transfer and sub-grid scale parameterizations, such as cloud formations and dissipation, cumulous convections

22

(thunderstorms and fair-weather cumulous clouds) and turbulence and sub-grid scale mixing processes.

Outputs from climate models are, thus scaled down to a suitable level for developing future climate scenarios. Statistical and dynamic downscaling represent two common methods used for this purpose. The dynamic downscaling approaches involve (i) running a regional scale limited area model with coarse GCM data as geographical or spectral boundary conditions, (ii) performing global-scale experiments with high resolution Atmosphere-GCM (AGCM), with coarse GCM data as initial (as partially and boundary) conditions; and (iii) the use of a variable-resolution global model with the highest resolution over the area of interest (Rummukainen, 1997). The most common technique for dynamic downscaling involves utilizing Regional Climate Models (RCMs), at a much higher resolution (Brissette et al., 2006). AOGCM output variables are used as boundary inputs for the RCMs, and provide a more accurate representation of the local climate than the coarsely gridded AOGCM data alone. The works of Vidal and Wade (2008), Wood et al. (2004) and Schmidli et al. (2006) compared dynamic downscaling to other methods. A limitation of the dynamic approach is the scale of RCM's (approximately 40 km x 40 km according to Brissette et al., 2006), which is still too coarse for application to smaller basins. The computational effort required for the dynamic approach makes it impractical where several AOGCMs and emissions scenarios are used (Maurer, 2007). Furthermore, RCMs have only been produced for selected areas; moving to a slightly different region requires repeating the experiment (Kay and Davies, 2008).

The second approach, namely statistical downscaling, is more popular in climate change impact assessments due to its computational ease and its ability to produce

synthetic datasets of any desired length. In this approach statistical relationships are developed to transfer large-scale features of the predictors (AOGCM) to regional scale predictands (variables). Hewitson and Crane (1992) pointed out to three underlying assumptions related to statistical downscaling: (i) the predictors are variables of relevance and are realistically modeled by the host AOGCM; (ii) the empirical relationship is also valid under altered climate conditions; and (iii) the predictors employed fully represent the climate change signal.

Several methods of statistical downscaling can be broadly divided into three categories: transfer function, weather typing and weather generator. Transfer functions rely on the direct quantitative relationship between the global large scale and local small scale variables obtained from different choices of mathematical transfer functions, predictors or statistical fitting processes. Applications of neural networks, regression based methods, least square methods, support vector machines, empirical orthogonal functions (Zorita and von Storch, 1999), etc., fall in this category. Von Storch (1999) and Burger (1996), however, have indicated the issue of under-prediction of the variance related to regression methods for daily precipitation downscaling because of relatively low predictability of local amounts by large-scale forcing alone.

Weather typing involves grouping local meteorological variables with respect to different classes of atmospheric circulation. Future regional climate scenarios are constructed either by resampling from the observed variable distribution or by first generating synthetic sequences of weather patterns using Monte Carlo techniques and resampling from the generated data. The relative frequencies of the weather classes are weighted to derive the mean or frequency distribution of the local climate. Climate

change is then determined from the changes of the frequency of the weather classes. Weather states are defined by applying cluster analysis to atmospheric fields (Heweitson and Crane, 1992; Huth, 2000, Kidson, 2000) or using subjective circulation classification schemes (Bardossy and Caspary, 1990; Jones et al, 1995). The similar weather patterns are grouped according to their nearest neighbours or a reference set (Wilby et al, 2004). The predictand is then assigned to the prevailing weather state and replicated under changed climate conditions by resampling or regression functions (Wilby et al, 2004; Corte-Real et al, 1995).

Stochastic weather generators simulate weather data to assist in the formulation of water resource management policies. They are essentially complex random number generators, which can be used to produce a synthetic series of data. This allows the researcher to account for natural variability when predicting the effects of climate change. Table 2.1 presents a summary of the relative advantages and limitations of different statistical downscaling models. Weather generators have an advantage over other downscaling methods because by producing long duration rainfall series, it is possible to examine rare events and extremes in the river basin (Brissette et al., 2007; Diaz-Nieto and Wilby, 2005; Wilks and Wilby, 1999). The underlying assumption of weather generator is that the past (control experiment) would be a representative of the future. It is, however, difficult to guarantee that the statistical relationship derived from current climate will remain same for future in the presence of climate change (Hewitson and Crane, 1996; Schulze, 1997; Joubert and Hewitson, 1997). Weather generators are believed to have difficulty in representing low frequency variances; however, this issue can be alleviated to some extent by conditioning the parameters on the large –scale state.

Table 2.1: Summary of Statistical Downscaling Approaches (Wilby et al., 2004)

Method	Advantages	Limitations
Transfer function	• Straightforward to apply • Employs full range of available predictor variables • Availability of software and solutions	• Poor representation of observed variance • May assume linearity and/or normality of data
Weather typing	• Provides physically interpretable link to the surface climate • Versatility • Composite for analysis of extreme events	• Requires additional task of weather classification • Circulation-based schemes can be insensitive to future climate forcing • May not capture intra-type variations in surface climate
Weather generator	• Production of large ensembles for uncertainty analysis or long simulations for extremes • Spatial interpolation of model parameters using landscape in regions with sparse data • Capability of generating sub-daily information • Ability to alter the parameters in accordance with scenarios of future climate changes- changes in variability as well as mean changes	• Arbitrary adjustment of parameters for future climate • Unanticipated effects to secondary variables of changing precipitation parameters • Most are designed for use independently at individual locations and few of them account for the spatial correlation of climate

Parametric, empirical or semi-parametric, and non-parametric (Brissette et al., 2007) weather generators are commonly used by the scientific community. In most parametric weather generators, a Markov chain is used to determine the probability of a wet or dry day and a probability distribution is assumed to determine the amount of precipitation (Kuchar, 2004; Hanson and Johnson, 1998). Most of the parametric weather generators are extensions of Richardson's WGEN, which was developed in 1981 (Richardson,

1981). Some examples of the parametric weather generators successfully employed using the Richardson approach are CLIGEN, WGENK, GEM, WXGEN, and SIMMENTO (Kuchar, 2004; Schoof et al., 2005; Hanson and Johnson, 1998; Soltani and Hoogenboom, 2003). Hanson and Johnson (1998) compared outputs from GEM to historical data using the means and standard deviations. Results showed that simulated total precipitation values were significantly underestimated for some months, and annual precipitation values were considerably smaller than the historical record (Hanson and Johnson, 1998). A study employing the SIMMENTO weather generator found that the variability (standard deviations) of wet fractions and amounts were significantly overestimated by the synthetic historical series (Elshamy et al., 2006). A major drawback of the parametric approach is that the Markov chain takes into account only the previous days' weather, not the subsequent past observations. As a result of this, the rare events, such as droughts or wet spells are not adequately produced (Sharif and Burn, 2007; Semenov and Barrow, 1997; Dibike and Coulibaly, 2005). Another limitation of the parametric weather generators is that an assumption must be made about the probability distribution of precipitation amounts, and different distributions do not give similar results (Sharif and Burn, 2007). Furthermore, the weather generators cannot be easily transferred to other basins as their underlying probability assumptions would change (Sharif and Burn, 2006). The computational effort is also significantly higher than other methods since many parameters must be estimated and statistically verified (Mehrotra et al., 2006). Parametric weather generators are less easily applied to multiple sites as simulations occur independently and thus spatial correlations would have to be assumed.

Semi-Parametric or Empirical weather generators include LARS-WG and the Wilks model, SDSM (Semenov and Barrow, 1997; Wilks and Wilby, 1999). LARS-WG differs from the parametric approaches described above because it employs a series-approach in which the wet and dry spells are determined by taking into account the observed values and assuming mixed-exponential distributions for dry/wet series as well as precipitation amounts (Semenov and Barrow, 1997). The wet/dry day status is first chosen, and then the amount is chosen conditional on the status. As such, the LARS-WG is able to satisfactorily reproduce wet and dry spells, unlike the parametric weather generators (Dibike and Coulibaly, 2005). Wilks (1998) improved the parametric models of Richardson (1981) by introducing Markov-chains of higher order that have a better "memory" of the preceding weather. The Richardson (1981) model was further extended for multi-site applications by using a collection of single site models in which a conditional probability distribution is specified and thus spatially correlated random numbers can be generated (Mehrotra, 2006; Wilks, 1998). A drawback to these empirical approaches is that there is still a subjective assumption about the type of probability distribution for precipitation amounts and spell lengths, and the spatial correlation structure is empirically estimated for use with multiple sites.

Non-parametric weather generators are computationally simple and do not require any statistical assumptions to be made. They work by using a nearest-neighbor resampling procedure known as the K-NN approach (Sharif and Burn, 2007; Brandsma and Buishand, 1998; Beersma et al., 2002; Yates et al., 2003). The nearest neighbor algorithm works by searching the days in the historical record that have similar characteristics to those of the previously simulated day, and then randomly selecting one of these as the

simulated value for the next day (Beersma et al., 2002). This approach is easily used in multi-site studies because the values are simulated concurrently, thus spatial correlation is preserved (Mehrotra et al. 2006). The K-NN algorithm has been successfully used for multi-site hydrological impact assessments in the Rhine Basin, accurately preserving spatial correlation and climatic variability (Beersma et al., 2002; Brandsma and Buishand, 1998). Apipattanavis et al. (2007) compared a K-NN to a semi-parametric weather generator. Box plots of wet-spell lengths showed that for some months the semi-parametric model could not reproduce maximum wet spell lengths, and average spell lengths were underestimated for the traditional K-NN model. A major limitation to the K-NN approach is that the values are merely reshuffled, thus no new values are produced (Sharif and Burn, 2007). Climatic extremes are essential in predicting flooding events in response to climate change, thus Sharif and Burn (2007) modified the K-NN algorithm to produce unprecedented precipitation amounts by introducing a perturbation component in which a random component is added to the resampled data points (Sharif and Burn, 2007). Monthly total precipitation and total monthly wet day box plots were used to evaluate the performance of the Modified K-NN algorithm. The algorithm was able to satisfactorily reproduce the statistics of the original dataset while adding variability, which is crucial in hydrologic impact assessments (Sharif and Burn, 2007). Prodanovic and Simonovic (2006) altered the modified K-NN algorithm of Sharif and Burn (2007) to account for the leap year. In order to allow for more variables for an improved selection of nearest neighbor, principal components are added in the weather generator (WG-PCA) (Eum et al., 2009). With the inclusion of more variables and perturbations, the updated

model is expected to more accurately define both present day climate conditions and also to produce estimates of future climate scenarios.

However, studies have indicated that the task of downscaling can sometimes become challenging due to the absence of proper station measurements. Gridded databases, such as the National Center for Environmental Prediction – National Center for Atmospheric Research (NCEP-NCAR) Global Reanalysis – NNGR (Kalnay et al., 1996) and the North American Regional Reanalysis – NARR (Mesinger et al., 2006) can be viable alternatives for alleviating these limitations of missing data and spatial bias resulting from uneven and unrepresentative spatial modelling (Robeson and Ensor, 2006; Ensor and Robeson, 2008). The reanalysis data are advantageous in impact studies because they are based on the AOGCMs with a fixed dynamic core, physical parameterizations and data assimilation systems (Castro et al., 2007).

Global (NNGR) and regional (NARR) reanalysis databases are also gaining use in uncertainty assessment studies. In many of their applications, however, the NNGR resolution (250 km $\times$ 250 km) is not satisfactory, especially in regions with a complex topography (Choi et al., 2009; Tolika et al, 2006; Rusticucci and Kousky, 2002; Haberlandt and Kite, 1998; Castro et al., 2007). The NARR dataset (Mesinger et al., 2006) is a major improvement upon the global reanalysis datasets in both resolution and accuracy. Literature related to an inter-comparison between the global and regional datasets (Nigam and Ruiz-Barradas, 2006; Woo and Thorne, 2006; Castro et al., 2007; Choi et al., 2007 and 2009) shows better agreement of NARR data.

2.3 Multi-Model Ensembles in Uncertainty Research

In recent years, quantifying uncertainties from AOGCM choice and scenario selections used for impact assessments has been identified as critical for climate change and adaptation research. Climate change impact studies derived from AOGCM outputs are associated with uncertainties due to 'incomplete' knowledge originating from insufficient information or understanding of the relevant biophysical processes, or a lack of analytical resources. Examples of uncertainty include the simplification of complex processes involved in atmospheric and oceanographic transfers, inaccurate assumptions about climatic processes, limited spatial and temporal resolution resulting in a disagreement between AOGCMs over regional climate change, etc. Uncertainties also emerge due to 'unknowable' knowledge, which arises from the inherent complexity of the Earth system and from our inability to forecast future socio-economic and human behavioral patterns in a deterministic manner (New and Hulme, 2000; Allan and Ingram, 2002; Proudhomme et al., 2003; Wilby and Harris, 2006; Stainforth et al., 2007; IPCC, 2007, Buytaert et al, 2009). Selection of the most appropriate AOGCM for the realization of future climate depends on user's ability to assess the model's strengths and weaknesses, the inability of which is recognized as one of the major sources of uncertainty (Wilby and Harris, 2006, Ghosh and Mujumdar, 2007; Tebaldi and Smith, 2010).

In most of the climate change impact assessment studies, single AOGCMs have been used for predicting future climate. It is well understood that in the current context of huge uncertainties, the utilization of a single AOGCM may only represent a single realization out of a multiplicity of possible realizations, and therefore cannot be representative of the future. So, for a comprehensive assessment of future changes in climate conditions, it is

important to use collective information by utilizing all available models and by synthesizing the projections and uncertainties in a probabilistic manner.

Studies that used multiple climate model information, however, cannot be found in abundance. Of the literatures available, one of the common approaches is the use of reliability estimates to multi-model ensembles. New and Hulme (2000) presented quantified uncertainties associated with climate change within a probabilistic framework. A hierarchical impact model based on Bayesian Monte Carlo simulations was developed to define posterior probability distributions for addressing uncertainty about future greenhouse gas emissions, the climate sensitivity and limitations and unpredictability in global climate models.

Raisanen and Palmer (2001) treated the AOGCM outputs as equally probable realizations and determined probabilities of climate change by computing the fraction of ensemble members in which the differential properties of models, such as bias and rate of convergence was disregarded. Probabilities of temperature and precipitation related to events defined for 20 year seasonal means of climate were studied. A cross verification exercise was used to obtain an upper estimate of the quality of the probability forcing in terms of skill score, reliability diagram and potential economic value.

Giorgi and Mearns (2003) confronted the approach undertaken in Raisanen and Palmer by introducing the 'Reliability Ensemble Averaging (REA)' technique, which considered the reliability-based likelihood of realization by models to calculate the probability of regional temperature and precipitation change. The method was applied to a set of transient experiments for the A2 and B2 IPCC emission scenarios with nine different

AOGCMs. Probabilities of surface air temperatures and precipitation were calculated for 10 regions on a sub-continental scale. REA was proved to be more flexible in assessment of risk and cost in regional climate change studies.

Tebaldi et al., (2004, 2005) used Bayesian statistics to estimate a distribution of future climates through the combination of past observational data and the corresponding AOGCM simulated climates. This technique was motivated by the assumption that an AOGCM ensemble represents a 'sample of the full potential climate model space compatible with the observed climate using probability distributions (PDFs)' at a regional scale. The method used two major criteria: bias and convergence that the REA method of Giorgi and Mearns (2003) quantified to assess model reliability. The ensembles of AOGCMs thus combined by their performances based on current climate and a measure of each model's agreement with the majority of ensemble. Tebaldi et al. (2005) further applied the same method using surface mean temperatures from nine AOGCMs, each run under A2 scenario aggregated over 22 regions and two 30 year average corresponding to current and future climate conditions to account for seasonal variations. Probabilistic approach thus appeared to be an important platform for estimating uncertainties from multi-model outputs.

Recently, Smith et al. (2009) extended the work of Tebaldi et al. by introducing the univariate approach to consider one region at a time. They are still using a multivariate approach, including cross validation, to confirm the resemblance of the Bayesian predictive distributions. Other literature on Bayesian methods in multi-model ensembles includes work from Allan et al. (2000), Benestad (2004), Stone and Allan (2005), and Jackson et al. (2004).

Another class of new but promising uncertainty estimation methods incorporates the downscaling of AOGCM scenarios and quantifying uncertainties by separately weighting outputs from different AOGCMs at every time step based on their performances. The results can be presented in a probabilistic framework. Wilby and Harris (2006) developed a probabilistic framework to combine information from four AOGCMs, two greenhouse scenarios where the AOGCMs were weighted to an index of reliability for downscaled effective rainfall. A Monte Carlo approach was adopted to explore components of uncertainty affecting projections for the river Thames for 2080s. The resulting cumulative distribution functions appeared to be most sensitive to uncertainty in (i) the selection of climate change scenarios, and (ii) the downscaling of different AOGCMs. Ghosh and Mujumdar (2007) used NNGR to develop a methodology to assess AOGCM uncertainty for examining future drought scenarios in a nonparametric manner using orthonormal method. The results showed promising aspects in comparison to other parametric/semi-parametric methods.

2.4 Intensity-Duration-Frequency Analysis

Literature related to intensity-duration-frequency (IDF) curves concentrates on developing appropriate distribution of fit, comparison of sampling techniques and generation of IDF information under climate change.

Interesting research is emerging on the development of alternative methods, other than the distribution fit, for developing IDF values. Huard et al. (2010) applied a Bayesian analysis to the estimation of IDF curves. Comparison of the Bayesian and classical approach using GEV distribution using peak over threshold (POT) method indicated the

34

extent of uncertainties in the IDF curves. Svensson et al. (2007) made an experimental comparison of methods for estimating rainfall IDF from fragmented records for Eskdalemuir, Scotland. Three different methods were applied to cope with the missing data in the annual and monthly series: (i) using only years/months with complete records; (ii) using only years/months with complete records with not more than 20% missing data; and (iii) using censored data from months where records are incomplete. The result recommends the use of monthly maxima for calculating return period rainfall allowing up to 20% of missing data in each month. Despite the fact that over a decade long research have been investigating for alternate methods for IDF development, studies related to developing IDF curves incorporating climate change are limited.

Estimations of future modifications in rainfall due to increase in greenhouse gas concentrations depend on response from global climate models. Studies have related statistical downscaling with outputs from global and regional climate model outputs. Nguyen et al. (2007a, b) and Desramaut (2008) presented a spatial-temporal downscaling method based on scale invariance technique for constructing IDF relations using outputs from two GCMs (HadCM3 A2 and CGCM2 A2) for future climate. The spatial downscaling methodology based on SDSM was used to generate daily precipitation data. The temporal scaling was performed for extreme value distribution factors based on current historical rainfall distribution. The studies found large differences in future IDF values between two the models.

Prodanovic and Simonovic (2007) developed IDF curves for current and future climate for city of London using a K-NN based weather generator. Future rainfall derived for the wet (CCSRNIES B21) scenario projected 30% increase in rainfall magnitude for a range

of durations and return periods. More recently Simonovic and Peck (2009) used all the available rainfall data for different durations for developing IDF information under the wet climate change scenario. The 24 hr duration rainfall was modified by applying moving window procedure to recreate maximum 24 hour rainfall events crossing the calendar day boundary. Their study indicated 10.7% to 34.9% change in IDF information for 2050s.

Coulibaly and Shi (2005) used outputs from CGCM2 B2 to develop IDF curves for Grand River and Kenora Rainy River regions in Ontario using statistical SDSM downscaling methodology. Their study found an increase in the range of 24-35% in the rainfall intensity for 24 hour and sub-daily durations for all stations of interest for 2050s and 2080s with decreases in 2020s.

Mailhot et al. (2006, 2007) used outputs from Regional Climate Models (RCMs) (CRCM A2) for developing IDF for different durations for May-October over Southern Quebec using regional frequency analysis. The results were obtained for the RCM grid-box scale ranging over 45 km distances in between the two grids. Projected rainfall showed 50% decrease by 2050s for 2 and 6 hour durations and 32% decrease for 12 and 24 hour durations than the base climate (1961-1990). The results indicated limitation of using grid box scale and acknowledged that the results may be improved by using point estimates.

Onof and Arnbjeg-Nielsen (2009) used an hourly weather generator approach with disaggregation to derive IDF values from hourly rainfall data. Future hourly data was obtained from RCM A2 scenario with a 10 KM x 10 KM resolution for 2050s. The

limitation of the study includes the stationarity assumption that the ratio of areal to the point estimates will remain unchanged with any changes in the climate.

Literature related to developing IDF values incorporating climate change from AOGCM models suffers from:

(i) *Limitations of statistical downscaling approaches:* Downscaling approaches such as SDSM or most of the weather generators assumed to have stationary climate. One possible way to overcome such issue is to perturb the model to generate values to achieve outputs beyond the range of inputs, which can be easily included in the weather generator.

(ii) *Application of sub-daily scaling factors to daily precipitation data and uncertainties:* Use of historical hourly data can prevent this issue.

(iii) *Use of single AOGCM response:* In all the literature listed above, single AOGCMs have been used for predicting future climate. It is well understood that in the presence of significant uncertainties, utilization of a single AOGCM may represent one of all possible outcomes and cannot be representative of the future. So, for a comprehensive assessment of the future changes, it is important to use collective information by utilizing all available AOGCM models, synthesizing the projections and uncertainties in a probabilistic manner.

(iv) *Appropriate distribution fit for the future:* In presence of human induced warming trends added to Earth's natural variability, it is unlikely that the present precipitation or rainfall pattern will comply with the future. Differences in the initializations and parameterizations of different climate model responses make it more complex to assume a specific distribution for all possible outcomes.

CHAPTER THREE

METHODOLOGY

This chapter details with theoretical frameworks for developing the models and algorithms used in the study. They are divided into three major sections: (i) assessment of hydro-climatic reanalysis data for climate change and hydrologic modeling; (ii) estimations of AOGCM and scenario uncertainties using fixed weight (Bayesian reliability ensemble average) and variable weight (weather generator, kernel density estimator, extended kernel density estimators) methods; and (iii) development of probability based intensity-duration-frequency curves under climate change (weather generator, disaggregation algorithms, weighted kernel estimator).

3.1 Assessment of Reanalysis Data

In mountainous, remote regions, or even at stations with large amounts of missing data, the task of hydrologic modeling is a major challenge due to the lack of observed information. Hydrologic impact studies dealing with climate change also require a data base long enough to be used as a supplement or addition with the historical data. With their more refined spatial and temporal coverage, the NCEP reanalysis data may be used effectively in data scarce regions (Reid et al., 2001).

Hydrologic models are conceptual representations of a part of the hydrologic cycle used for prediction and understanding of hydrologic processes operating within a basin. Detail

analysis of hydrologic exposure requires use of a calibrated hydrologic model to transform meteorological input (temperature, precipitation) into hydrological input (stream flow). Hydro-climate data from NCEP are thus applied as input to a continuous hydrologic model to generate stream flow for selected locations within the study area of interest. The following section explains different modules of the hydrologic model considered in this study.

3.1.1 Hydrologic Modeling

The continuous based hydrologic model captures land based physical processes of the hydrologic cycle (Bennett, 1988). It takes the soil moisture balance into consideration over a long term period and is useful mostly for simulating the daily, monthly and seasonal rainfall runoff processes for the basins with a large amount of pervious lands (Ponce, 1989). The continuous model needs detailed information of long term moisture losses due to evaporation and evapotranspiration. A typical continuous hydrologic model constitutes a combination of methods to describe conversion of excess rainfall into direct runoff, baseflow, channel/reservoir routing, together with losses due to movement of water through vegetation, surface, soil and ground water (Ponce, 1989). The continuous hydrologic model component used in this study is based on the United States Army Corps of Engineers, Hydrologic Engineering Center's Hydrologic Modeling System (HEC-HMS).

The HEC-HMS is designed for rainfall-runoff modeling for solving a wide range of problems at diverse geographic locations, although most of its applications have been limited to the North American basins. HEC-HMS has been successfully used for around

three decades and is recognized by the hydrologic community (Prodanovic, 2008). The model consists of three modules (Figure 3.1): (i) meteorologic module (which includes methods describing precipitation and/or evaporation); (ii) basin module (consisting of methods describing the physical properties of a catchment); and (iii) control module (where start and end times of a simulation are specified). The meteorologic and basin modules consist of a collection of methods allowing the user to specify and describe climatic and physical properties of the basin. For example, different loss methods (i.e., representing evaporation and/or evapotranspiration) are available depending on whether the user wishes to study the short (event) or long (continuous) term hydrologic characteristics of the basin. Detailed information about the structure of the model is available in USACE (2006).

The snow module: Precipitation and temperature from various sources are used as inputs in the hydrologic model. The regularly spaced reanalysis database is interpolated to the irregularly spaced sub-catchments within the basin that take precipitation as input. In this study, the Inverse Distance Weighting (IDW) method has been used for interpolating precipitation and temperature reanalysis data from their respective grids to sub-catchment grids. This method is widely used and recommended by the United States Army Corps of Engineers (Prodanovic and Simonovic 2007). For estimating the variable of interest using observed data, input for each weather station is separately considered with its coordinates (latitudes and longitudes). A search algorithm finds four closest stations containing data for each sub-catchment. In order to calculate the value at any location i, the distance is calculated between station i and its four nearest neighbors (denoted by d_1, d_2, d_3, d_4).
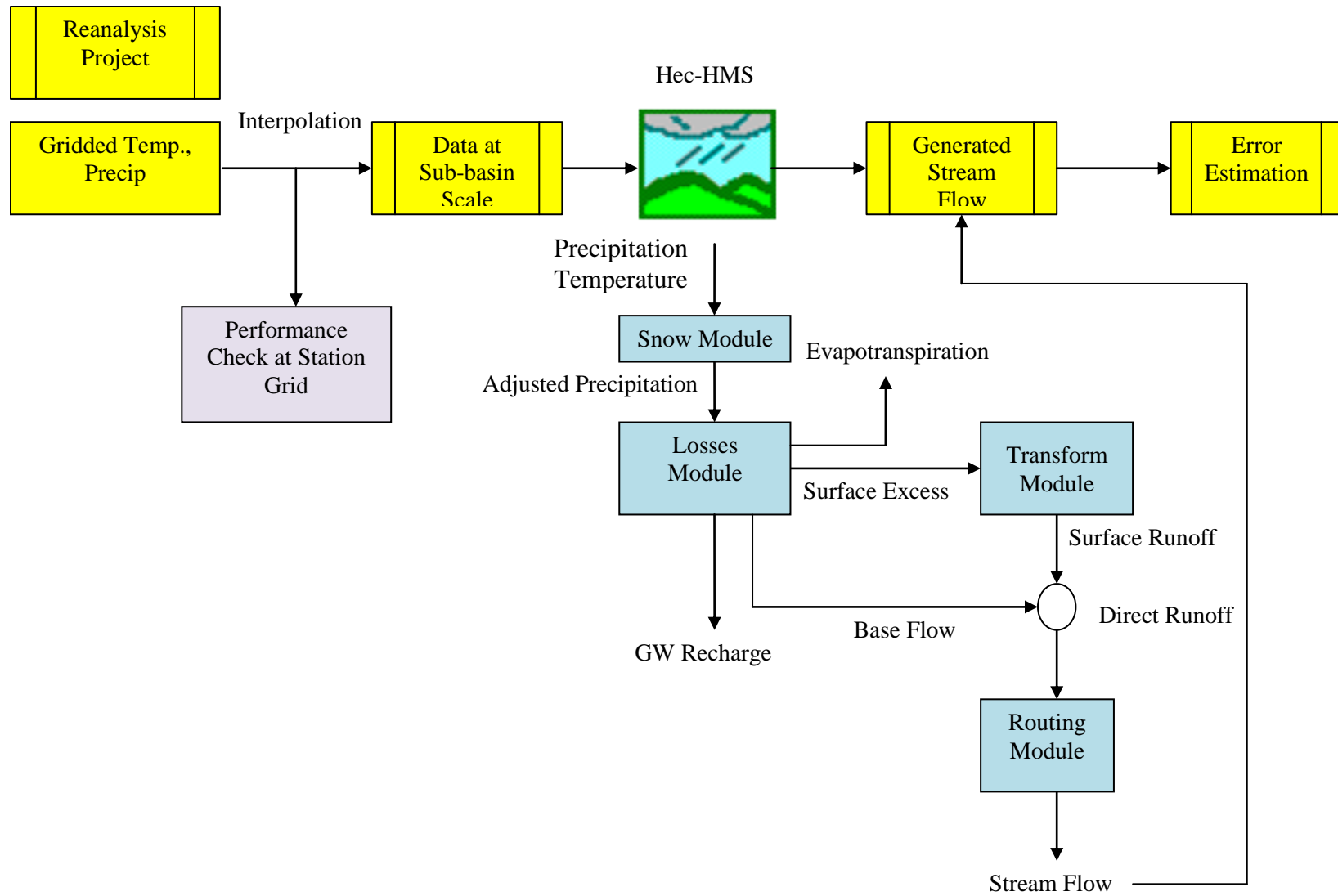
Figure 3.1: Flow Chart of Continuous Hydrologic Modeling using Reanalyses Data

41

Next, weights are computed for each of the closest neighbors and are assigned in inverse proportion to the square distance from i. Thus the closer the neighbor to the node j, the greater the weight it gets in the calculation. The weight of the closest station in the first quadrant is calculated by the following equation:

$$w_1 = \frac{\frac{1}{d_1^2}}{\frac{1}{d_1^2} + \frac{1}{d_2^2} + \frac{1}{d_3^2} + \frac{1}{d_4^2}} \tag{3.1}$$

where,

w_1 is the weight for neighbour in the first quadrant in relation to station i.

Similar calculations are performed for all other quadrants. After all weights are obtained, the values at station i for each time step are estimated by:

$$p_1(t) = \sum_{j=1}^{4} w_j p_j(t) \tag{3.2}$$

where,

j represents each node in a quadrant around station i; and

p represents the data value being interpolated.

At the time of the development of current continuous hydrologic model by Cunderlik and Simonovic (2004), the snow module was not included in the original HEC-HMS model structure. So, the interpolated precipitation and temperature data were integrated into the snow module outside the HEC-HMS model to separate the solid (snow) and liquid (rainfall) forms of precipitation. The same approach is used in this study. The snow module uses the meteorological data to compute snow accumulation and melt by degree-

day method (Cunderlik and Simonovic, 2004). The interpolated sub-basin precipitation and temperature values are separated into their solid and liquid forms of precipitation in the snow module. The snowfall is subjected to an accumulation and melt algorithm and produces snowmelt. It is then added to the liquid precipitation (or rainfall) and thus produces a new variable: 'adjusted precipitation'. The following sets of equations are used in this process:

Precipitation (mm/day) P_i is categorized as rain and snow by the following equations:

$$\left.\begin{matrix} S_i = P_i \\ R_i = 0 \end{matrix}\right\}, T_i < T_{min} \tag{3.3}$$

$$\left.\begin{matrix} S_i = P_i \cdot \left[\frac{T_{max} - T_i}{T_{max} - T_{min}}\right] \\ R_i = P_i - S_i \end{matrix}\right\}, T_{min} < T_i < T_{max} \tag{3.4}$$

$$\left.\begin{matrix} S_i = 0 \\ R_i = P_i \end{matrix}\right\}, T_i > T_{max} \tag{3.5}$$

where,

$S_i and R_i$ represent the measured amount of snow and rain, respectively (mm/day);

$i = 1, 2, 3, \ldots \ldots n$ represents number of days with precipitation;

$T_{min} = -4^0C$ and $T_{max} = -2^0C$ refer to the minimum and maximum temperature for below and above which snowfall and snowmelt will occur, respectively.

The solid precipitation is then subjected to an accumulation and melt algorithm and is eventually converted into snowmelt. The daily amount of snow melt is calculated as:

$$M_i = MR. (T_i - T_c) \tag{3.6}$$

where,

MR represents a parameter for snowmelt rate (mm/^{0}C/day) set to 4.0; and

T_c is a critical temperature for which snowmelt process can occur and is set to zero.

Previously obtained snowmelt is then accumulated with the converted snowmelt by the following equation:

$$S_i = S_i + S_{i-1} \qquad (3.7)$$

If snowmelt occurs (i.e. if $M_i > 0$) and if the accumulated snowmelt $S_i > M_i$, implying that only a portion of the accumulated snow is melted. It is represented by:

$$S_i = S_i - M_i \qquad (3.8)$$

$$P_a = R_i + M_i \qquad (3.9)$$

where,

P_a represents adjusted precipitation (mm/day).

If all accumulated snow melts,

$$P_a = R_i + S_i \qquad (3.10)$$

Lastly, if no snowmelt takes place,

$$P_a = R_i \qquad (3.11)$$

The loss module: The adjusted precipitation is further used as input into the precipitation loss module to obtain losses. Among the different methods of calculating losses available in HEC-HMS, the five layer soil moisture accounting (SMA) algorithm, developed by Leavesley et al. (1983), is chosen for continuous modeling of complex infiltration and evapotranspiration environments. The loss module is the most

complicated component as it simultaneously takes a large number of processes into consideration.

The losses module (Figure 3.1) implements several conceptual reservoirs to represent the storage and movement of water in each sub-catchment of the basin. The storage reservoirs include: (i) canopy interception; (ii) surface interception; (iii) soil profile; and (iv) a number of ground water layers. The amount of water stored in each conceptual reservoir is regulated by the inflow and outflow rates between the reservoirs. These include evapotranspiration, infiltration, percolation, surface runoff and ground water flow. The canopy storage layer consists of precipitation captured by vegetation such as trees, shrubs, bushes, grasses, etc; Precipitation is the only inflow that can fill this storage volume. The storage layer is filled first until it reaches to the maximum capacity. Moisture from this layer can only be removed by evapotranspiration. Once the canopy layer is filled, precipitation begins to fill the surface storage, and/or to infiltrate into the soil. The surface storage layer corresponds to the volume of water held by shallow depressions and cracks on the ground surface. The storage of water infiltrates into the soil, as long as the soil is unsaturated. The inflow to the surface storage layer is a combination of the precipitation excess from the canopy layer, and its own volume that is left over after infiltration.

The outflow from this layer consists of evaporation and surface runoff. Surface runoff refers to the flow produced when the surface storage layer exceeds its capacity, and cannot absorb water that has not already been infiltrated. During large precipitation events, the canopy and surface storage layer fill quickly and produce high amounts of

surface excess (as infiltration alone is not usually sufficient for absorbing all surplus precipitation). The soil profile storage refers to the top layer of the soil. Infiltrated water is the only inflow to this layer. Outflows represent percolation to the lower ground water layer and evapotranspiration. The soil storage is further divided into two zones: the upper zone and the tension zone. The upper zone can lose water to both percolation and evapotranspiration, while the tension zone loses water only through evaporation, but not percolation (Bennett, 1998). This is because the upper zone represents water held in the pores of the soil (which can freely percolate and/or evaporate), while the tension zone constitutes water held by capillary tension, thus making it difficult to flow and move but can evaporate. It should be mentioned that evapotranspiration rates from the soil vary, as it is more difficult to remove water held by capillary tension than water held between the pores of the soil. Evapotranspiration removes moisture from canopy, surface, and soil profile storage. In the Soil Moisture Accounting algorithm, evapotranspiration can only occur during periods free of precipitation. Potential evapotranspiration is calculated based on maximum regional monthly evapotranspiration rates, multiplied by a pan coefficient. Actual evapotranspiration rates are realized through a loss of moisture, first from the canopy, second from the surface, and lastly from the soil storage. However, actual evapotranspiration rates can never exceed their potential value. The water that percolates from the soil profile storage is used as an input to the ground water layer immediately beneath it. The outflows from this layer represent the ground water flow (one that is returned to the stream channel as baseflow), and a further percolation to either another ground water layer or as deep percolation representing water entering a deep aquifer.

The equations for the Soil Moisture Algorithm are well documented and can be found in Bennett (1998).

Transform and Routing Modules: The transform module uses Clark's Method (USACE 2006) to convert the surface excess obtained from the SMA algorithm into the direct runoff. The resultant surface runoff is joined with the baseflow to produce direct runoff. The direct runoff is then added into the flood routing module to calculate the generation of a flood wave by using modified puls method ultimately producing channel stream flow (USACE 2006). A series of linear reservoir method is used to transform lateral ground water flow (obtained from SMA algorithm) into baseflow.

3.2 Uncertainty Estimation Methods

Two approaches based on fundamentally different assumptions are applied to estimate uncertainty in climate model projections of future precipitation under different forcing scenarios. First, a Bayesian based reliability ensemble average (BA-REA) approach is used to estimate a distribution of future climates from the combination of past observed and corresponding AOGCM-simulated data. Next, a methodology combining statistical downscaling using a principal component analysis (PCA) based weather generator approach and nonparametric kernel density estimation technique is developed to quantify the uncertainties from AOGCMs. The difference between these two approaches lies in the fact that the BA-REA method combines uncertainties from different AOGCMs based on its mean bias, so a single weight for different models is present; whereas the

nonparametric kernel estimator is capable of providing weights for each time step based on the performance of different AOGCMs.

3.2.1 Fixed Weight Method

Bayesian Reliability Ensemble Average

The methodology developed by Tebaldi et al. (2004; 2005) consists of a formal Bayesian implementation and extension of the reliability ensemble averaging (REA) approach of Giorgi and Mearns (2002; 2003). It combines observed historical data and a multi-model ensemble of AOGCMs to compute probability density functions (PDFs) of future temperature and precipitation change over large regions under different forcing scenarios. Three components constitute the model structure: prior, likelihood, and posterior. The assumption is that the variability of present and future climate from different AOGCMs are random quantities and have different variances which are priori unknown. Although uninformative prior distribution has been chosen, both model-generated and observational data are applied for calculating meaningful posterior distributions. The choice of an uninformative prior distribution has the advantage of selecting parameter estimates similar to non-Bayesian approaches, such as maximum likelihood. In cases where there is lack of sufficient agreement between experts to determine a specific prior and no data from previous studies could be incorporated, (a situation similar to wide range of future climate scenarios), selection of an uninformative prior is justified. The choice of the likelihood or distribution of the data as a function of any random parameters constitutes the second parameter. The AOGCM responses are assumed to have a symmetric distribution whose center is the 'true value' of the variable

of interest, but maintains an individual variability to be a measure of how well each AOGCM depicts the natural variability. The prior and posterior distributions are combined into a joint posterior distribution using the Bayes' theorem. The empirical estimate of the posterior distribution is obtained using the Markov Chain Monte Carlo (MCMC) simulation by simulating samples from the posterior distribution.

Likelihoods

The likelihoods for the observations of current mean precipitation (X_0), simulations of present (X_j) and future (Y_j) mean precipitation by the ith model can be written as:

$X_0 \sim N[\mu, (\lambda_0)^{-1}]$, the likelihood of the observations of current climate

or alternately,

$X_o = \mu + \epsilon_o$

$X_i \sim N[\mu, (\lambda_i)^{-1}]$ \hfill (3.12)

or alternately,

$X_i = \mu + \eta_i$ (assuming a common Gaussian distribution for the error terms)

$Y_i \sim N[\nu + (\theta\lambda_i)^{-1}]$

or alternately,

$Y_i = \nu + \beta_x(X_i - \mu) + \dfrac{\xi_i}{\sqrt{\theta}}$ (assuming a common Gaussian distribution for the

error terms)

where,

μ and ν are random variables presenting the (unknown) true present and future mean precipitations respectively;

$(\lambda_0)^{-1}$ and $(\lambda_i)^{-1}$ are considered as a measure of ith AOGCM precision, and the estimates of natural observed variability which depends on the season, region and time average of the observation.

The parameter λ_0 is fixed as the reciprocal of the squared value of the standard deviation of the observations.

Random variable θ, also known as the inflation/deflation parameter allows for the possibility of the future and the present precipitation having different variances by a multiplicative factor and is common to all AOGCMs.

The alternate forms of equation 3.12 links X_i and Y_i through a linear regression equation equivalent to assuming that (X_i, Y_i) are jointly normal when parameter values are given and the correlation coefficient is relaxed to vary between -1 and + 1. For $\beta_x \neq 0,$ the modified equation for Y_i will create a direct (if positive) or inverse (if negative) relation between $X_i - \mu$ and $Y_i - \nu$. The value of β_x is also significant for representing the correlation: a value of 1 denotes the conditional independence of the signal of precipitation change produced by any AOGCM and $X_i - \mu$, the model bias for current precipitation. Values greater or smaller than 1 imply positive or negative correlation between them.

Prior Distribution

The prior distributions are chosen for the following precision parameters:

$\lambda_i = 1, 2, 3, \ldots .6$ have Gamma prior densities $(Ga(a, b))$:

$$\frac{b^a}{\Gamma(a)} \lambda_i^{a-1} exp^{-bx} \tag{3.13}$$

where,

a and b are known.

Similarly for θ, c and d are assumed to be known. For the model, $a = b = c = b = 0.001$ are chosen. The true climate means μ and ν for present and future precipitation have uniform prior densities so that even in the case of improper priors (do not integrate to one) they are assumed to have a proper posterior density function.

Posterior Distribution

Bayes' theorem is applied to the likelihood and priors. The resulting joint posterior distribution is given by:

$$\prod_{i=1}^{n} \left[\lambda_i^{a-1} e^{-b\lambda_i} \lambda_i \theta^{1/2} exp\left\{ -\frac{\lambda_i}{2}(X_i - \mu)^2 + \theta(Y_i - \nu)^2 \right\} \right] . \theta^{c-1} e^{-d\theta} . exp\left\{ -\frac{\lambda_0}{2}(X_0 - \mu)^2 \right\} \tag{3.14}$$

The above distribution does not represent any specific known parameter family. The posterior distribution fixes the parameters and considers a conditional posterior for others

to synthesize the data and the prior assumptions. For example, the distribution of μ for fixing all other parameters is Gaussian with:

Mean:

$$\tilde{\mu} = \left(\sum_{i=0}^{n} \lambda_i X_i\right) \Big/ \left(\sum_{i=0}^{15} \lambda_i\right) \tag{3.15}$$

Variance:

$$\left(\sum_{i=0}^{n} \lambda_i\right)^{-1} \tag{3.16}$$

Similarly, the conditional distribution of ν is Gaussian with

Mean:

$$\tilde{\nu} = \left(\sum_{i=0}^{n} \lambda_i Y_i\right) \Big/ \left(\sum_{i=0}^{15} \lambda_i\right) \tag{3.17}$$

Variance:

$$\left(\theta \sum_{i=0}^{n} \lambda_i\right)^{-1} \tag{3.18}$$

Equations 3.15 and 3.17 are comparable to the REA results as the weighted means of the 15 different AOGCMs with their scenarios and the observation with weights $\lambda_1, \dots \dots \lambda_n, \lambda_0$, respectively. These weights are derived by assuming parameters with random quantities and hence can be used for uncertainty estimation. This uncertainty will inflate the width of the posterior distributions of ν, μ and also the precipitation change, ΔP.

The mean of the posterior distribution of λ_i for $i = 1, 2, \dots n$ is approximated as:

$$E(\lambda_i | \{X_0, X_1, \ldots \ldots X_n, Y_1, \ldots \ldots, Y_n\}) \approx \frac{a+1}{b + \frac{1}{2}((X_i - \tilde{\mu})^2 + \theta(Y_i - \tilde{v})^2)} \tag{3.19}$$

Equation 3.19 expresses how the bias and convergence criteria are built into the model implicitly since the precision parameter or the weights λ_i for each AOGCM are large provided that both $|X_i - \mu|$ and $|Y_i - v|$ are small. $|Y_i - v|$ measures the distance of the ith model future response from the overall average response. So the results are strictly constrained by their convergence into future projections determined by the weighted ensemble of mean. For this study, $a = b = 0.001$ is chosen as per Tebaldi et al. (2004, 2005) to ensure that the contribution of the prior assumption to equation 3.19 is negligible.

Using the approximation similar to equation 3.19 the posterior mean can be written as:

$$E(\lambda_i | \{X_0, X_1, \ldots \ldots X_n, Y_1, \ldots \ldots, Y_n\})$$

$$\approx \frac{a+1}{b + \frac{1}{2}\left((X_i - \tilde{\mu})^2 + \theta\left(Y_i - \tilde{v} - \beta_x(X_i - \tilde{\mu})\right)^2\right)} \tag{3.20}$$

Next, the marginal posterior distribution is derived next using the MCMC approach. A large number of sample values are generated by applying the Gibbs Sampler using equation 3.14 for all parameters.

MCMC Approach: The Gibbs Sampler

The joint posterior distribution derived from assuming different distributions such as Gaussian, Uniform and Gamma in different stages does not represent any known

parametric family of distributions. Because they are conjugate, they allow for a closed-form deviation of all full conditional distributions.

Auxiliary randomization parameters s_i and t_i, $i = 1,2,3, \dots \dots . n$ are used to ensure an efficient simulation from student's t distribution within the Gibbs sampler. Fixing $s_i = t_i = 1$, $\beta_x = 0$, returns the full conditionals to the prior parameters.

$$\lambda_i| \dots \dots \dots \dots \dots . \sim Ga\left(a + 1, b + \frac{s_i}{2}(X_i - \mu)^2 + \frac{\theta t_i}{2}\{Y_i - v - \beta_x(X_i - \mu)\}^2\right) \qquad (3.21)$$

$$s_i| \dots \dots \dots \dots \dots . \sim Ga\left(\frac{\phi + 1}{2}, \frac{\phi + \lambda_i(X_i - \mu)^2}{2}\right) \qquad (3.22)$$

$$t_i| \dots \dots \dots \dots \dots . \sim Ga\left(\frac{\phi + 1}{2}, \frac{\phi + \theta\lambda_i\{Y_i - v - \beta_x(X_i - \mu)\}^2}{2}\right) \qquad (3.23)$$

$$\mu| \dots \dots \dots \dots \dots . \sim N\left(\tilde{\mu}, \left(\sum s_i\lambda_i + \theta\beta_x^2 \sum t_i\lambda_i + \lambda_0\right)^{-1}\right) \qquad (3.24)$$

$$v| \dots \dots \dots \dots \dots . \sim N\left(\tilde{v}, \left(\theta \sum t_i\lambda_i\right)^{-1}\right) \qquad (3.25)$$

$$\beta_x| \dots \dots \dots \dots \dots . \sim N\left(\widetilde{\beta_x}, \left(\theta \sum t_i\lambda_i + (X_i - \mu)^2\right)^{-1}\right) \qquad (3.26)$$

$$\theta| \dots \dots \dots \dots \dots . \sim Ga(c + \frac{N}{2}, d + \frac{1}{2}\sum t_i\lambda_i \{Y_i - v - \beta_x(X_i - \mu)\}^2) \qquad (3.27)$$

Simplifying,

$$\tilde{\mu} = \frac{\sum s_i\lambda_i X_i - \theta\beta_x \sum \lambda_i t_i(Y_i - v - \beta_x X_i) + \lambda_0 X_0}{\sum s_i\lambda_i + \theta\beta_x^2 \sum \lambda_i t_i + \lambda_0} \qquad (3.28)$$

$$\tilde{v} = \frac{\sum t_i\lambda_i\{Y_i - \beta_x(X_i - \mu)\}}{\sum t_i\lambda_i} \qquad (3.29)$$

$$\hat{\beta}_x = \frac{\sum t_i \lambda_i (Y_i - v)(X_i - \mu)}{\sum t_i \lambda_i (X_i - \mu)^2} \qquad\qquad (3.30)$$

From this sequence of full conditional distributions, the Gibbs sampler is coded to simulate iteratively. After a series of iterations, the MCMC process ignores the arbitrary set of initial values for parameters. Values sampled at each iteration represent a draw from the joint posterior distribution of interest, and any summary statistic can be computed to a degree of approximation that is a direct function of the number of the sampled values available, and an inverse function of the correlation between successive samples.

The reliability of any AOGCM is measured by two criteria to form the shape of the posterior distribution as a consequence of assumptions formulated in the statistical model: mean bias of present climate and rate of convergence of the future climate models to weighted ensemble mean.

3.2.2 Variable Weight Method

The variable weight method is developed by combining the principal component analysis based k-nearest neighbor weather generator and non parametric kernel estimators. An overview of the methodology proposed in the work is presented in Figure 3.2.

Downscaling

Stochastic weather generators simulate weather data to assist in the formulation of water resource management policies. The basic assumption for producing synthetic

sequences is that the past would be representative of the future. These sequences are essentially complex random number generators, which can be used to produce a synthetic series of data. This allows the researcher to account for natural variability when predicting the effects of climate change. The K-nearest neighbor based weather generator used in this study is developed based on Sharif and Burn (2007) and Yates et al. (2003). Nearest neighbor algorithms are capable of modeling non-linear dynamics of geophysical processes. They do not require any previous knowledge on the probability distribution of the input to be used. Furthermore, the temporal and spatial correlations of the input are preserved well in the generated data. In addition to preserving the correlation structure of the input data, perturbation mechanism is included to generate climate information beyond the limit of the historical information.

In order to reduce multi-dimensionality and collinearity associated with the large number of input variables, a principal component analysis (Appendix B) has been integrated within the weather generator. The process requires selecting the appropriate principal components (PCs) that will adequately represent most of the information of the original dataset.
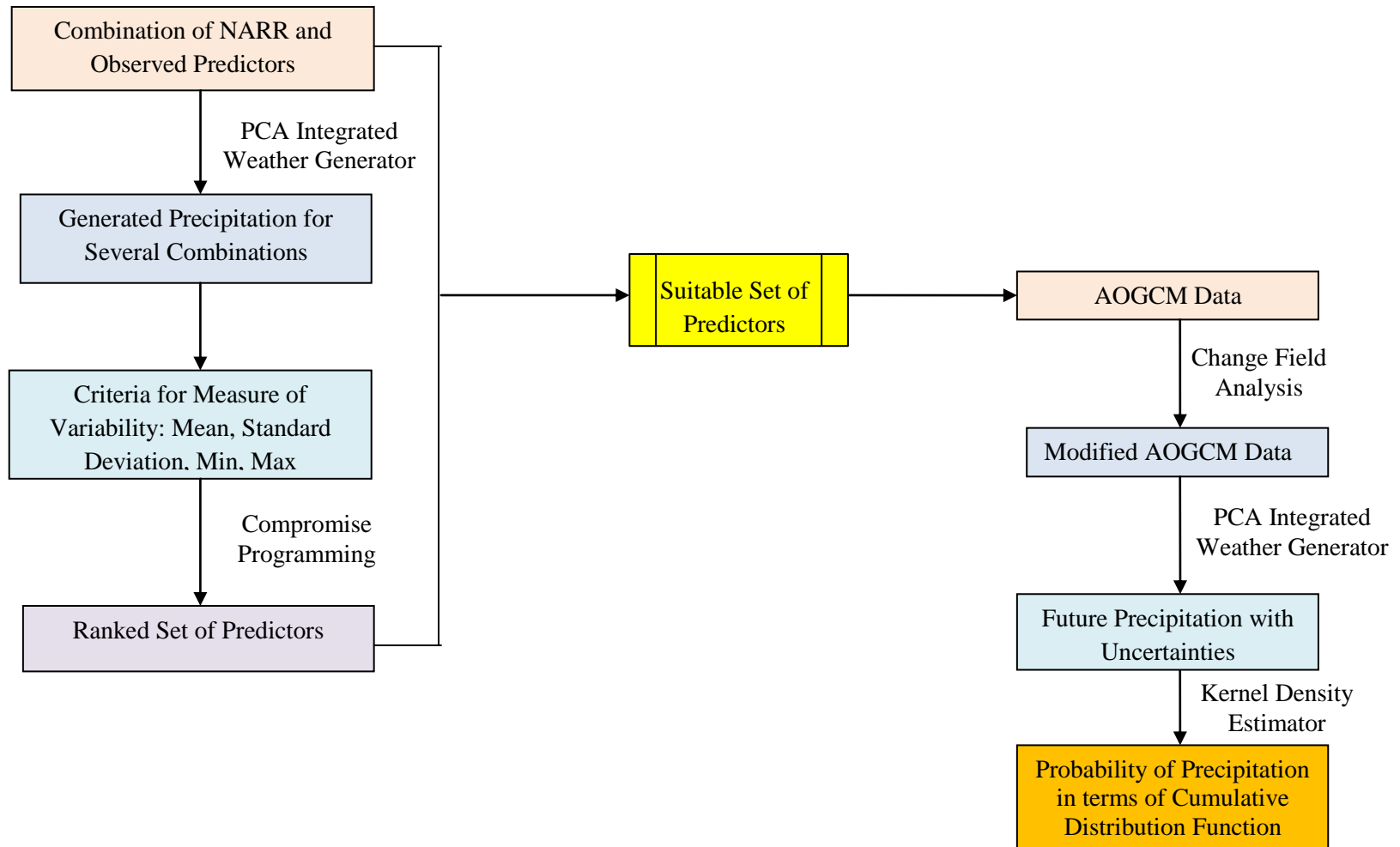
Figure 3.2: Flow Chart of Uncertainty Estimation using Nonparametric Method

The WG-PCA algorithm with p variables and q stations works through the following steps (Sharif and Burn, 2007):

1) Regional means of p variables for all q stations are calculated for each day of the observed data:

$$\bar{X}_t = \left[\bar{x}_{1,t}, \bar{x}_{2,t}, \ldots \ldots \bar{x}_{p,t} \right] \qquad \forall t = \{1,2, \ldots \ldots T\} \qquad (3.31)$$

Where,

$$\bar{x}_{i,t} = \frac{1}{q} \sum_{j=1}^{q} x_{i,t}^{j} \qquad \forall i = \{1,2, \ldots \ldots p\} \qquad (3.32)$$

2) The user-set parameters are as follows: potential neighbors, L days long where $L = (w + 1) \times N - 1$ for each of p individual variable with N years of historic record, and a temporal window of size w. The days within the given window are all potential neighbors to the feature vector. N data which correspond to the current day are deleted from the potential neighbors so the value of the current day is not repeated.

3) Regional means of the potential neighbors are calculated for each day at all q stations.

4) A covariance matrix, C_t of size $L \times p$ is computed for day t.

5) The first time step value is randomly selected for each of p variables from all current day values in the historic record.

6) Next, using the variance explained by the first principal component, Mahalanobis distance is calculated with equation 3.33.

$$d_k = \sqrt{(PC_t - PC_k)^2 \Big/ Var(PC)} \qquad \forall k = \{1,2,.....K\} \qquad\qquad (3.33)$$

$$PC_t = \overline{X_t}E \text{ and } PC_k = \overline{X_k}E$$

where,

PC_t is the value of the current day;

PC_k is the nearest neighbor transferred by the Eigen vector;

E is the eigen vector related to the largest eigen value.

$Var(PC)$ is the variance of the first principle component for all K nearest neighbors.

7) The selection of the number of nearest neighbors, K, out of L potential values using $K = \sqrt{L}$.

8) The Mahalanobis distance d_k is put in order of smallest to largest, and the first K neighbors in the sorted list are selected (the K Nearest Neighbors). A discrete probability distribution is used that weights closer neighbors highest in order to resample out the set of K neighbors. Using equations 3.34 and 3.35, the weights w, are calculated for each of these i neighbor.

$$w_k = \frac{\frac{1}{k}}{\sum_{i=1}^{K} \frac{1}{i}} \qquad\qquad \forall i = \{1, 2, ..., K\} \qquad\qquad (3.34)$$

Cumulative probabilities, p_j, are given by:

$$p_j = \sum_{i=1}^{j} w_i \qquad (3.35)$$

9) A random number $u(0,1)$ is generated and compared to the cumulative probability calculated above in order to select the current day's nearest neighbor. If $p_1 < u < p_K$, the day j for which u is closest to p_j is selected. However, if $p_1 \geq u$, then the day that corresponds to d_1, is chosen. For $u = p_K$, the day that corresponds to day d_K is selected. Upon selecting the nearest neighbor, the K-NN algorithm chooses the weather of the selected day for all stations in order to preserve spatial correlation in the data (Eum et al, 2009).

10) In order to generate values outside the observed range, perturbation is used. A conditional standard deviation $\sigma\,\sigma$ of variable i for j station from K nearest neighbors is estimated. For choosing the optimal bandwidth of a Gaussian distribution function that minimizes the asymptotic mean integrated square error (AMISE), Sharma et al. (1997) reduced Silverman's (Silverman 1986, pp. 86-87) equation of optimal bandwidth into the following form for a univariate case:

$$\lambda = 1.06\sigma K^{-\frac{1}{5}} \qquad (3.36)$$

Using the mean value of the weather variable $x_{i,t}^{j}$ obtained in step 9 and variance$(\lambda \sigma_i^{j})^2$, a new value $y_{i,t}^{j}$ can be achieved through perturbation (Sharma et al. 1997).

$$y_{i,t}^{j} = x_{i,t}^{j} + \lambda \sigma_i^{j} z_t \qquad (3.37)$$

where,

z_t is a random variable, distributed normally (zero mean, unit variance) for day t. Negative values are prevented from being produced for precipitation by employing a largest acceptable bandwidth (Sharma and O'Neil, 2002):

$$\lambda_a = \left. x_{*,t}^{j} \middle/ 1.55\sigma_*^{j} \right.$$ (3.38)

where,

* refers to precipitation.

If again a negative value is returned, a new value for z_t is generated (Sharif and Burn, 2006).

Nonparametric Kernel Estimators

A practical approach to deal with AOGCM and scenario uncertainties originating from inadequate information and incomplete knowledge should: (1) be robust with respect to model choice; (2) be statistically consistent in a uniform application across different area scales such as global, regional or local/watershed scales; (3) be flexible enough to deal with the variety of data; (4) obtain the maximum information from the sample; and (5) lead to consistent results. Most parametric methods do not meet all these requirements.

The Probability Density Function (PDF) is commonly used to describe the nature of data (Figure 3.3). In applications an estimate of the unknown $PDF = f(\ )$ based on random sample $x_1, x_2, \ldots \ldots x_n$ from $f(\ )$ is calculated in the form of $\widehat{PDF} = \hat{f}(\ )$.

Probability density functions estimated by any nonparametric method without prior assumptions are suitable for quantifying AOGCM and scenario uncertainties. Several approaches, such as kernel methods, orthogonal series methods, penalized-likelihood methods, k-nearest neighbor methods, Bayesian-spline methods, and maximum-likelihood or histogram like methods, are used throughout the relevant literature (Adamowski, 1985).
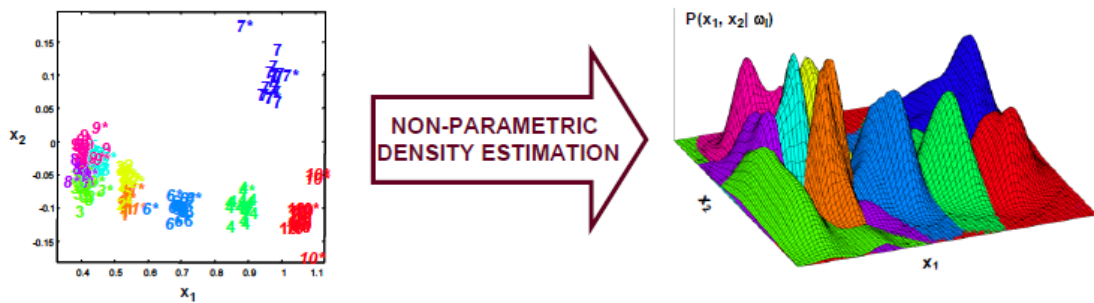
Figure 3.3: Non-parametric Density Estimation

(Source: http://research.cs.tamu.edu/prism/lectures/pr/pr_l7.pdf, Retrieved on 3/16/2011)

A Kernel density estimation method has been widely used as a viable and flexible alternative to parametric methods in hydrology (Sharma et al., 1997; Lall, 1995), flood frequency analysis (Lall et al., 1996; Adamowski, 1985), and precipitation resampling (Lall et al., 1996) for estimating a probability density function.

A kernel density estimate is formed through the convolution of kernels or weight functions centered at the empirical frequency distribution of the data (Figure 3.4). A kernel density estimator involves the use of the kernel function ($K(x)$) defined by:

$$\int_{-\infty}^{\infty} K(x)dx = 1 \tag{3.39}$$

A PDF can thus be used as a kernel function. The Parzen-Rosenbalt kernel density estimate $f_n(x)$ at x, from a sample of $\{x_1, \ldots, x_i, \ldots, x_n\}$ of sample size n is given by:

$$\widehat{f_h}(x) = \frac{1}{n}\sum_{i=1}^{n}\frac{1}{h}K_h\left(\frac{x - x_i}{h}\right) \tag{3.40}$$

where,

$t = \left(\frac{x-x_i}{h}\right)$ and $k_h(t)$ is a weight or kernel function required to satisfy criteria such as symmetry, finite variance, and integrates to unity.
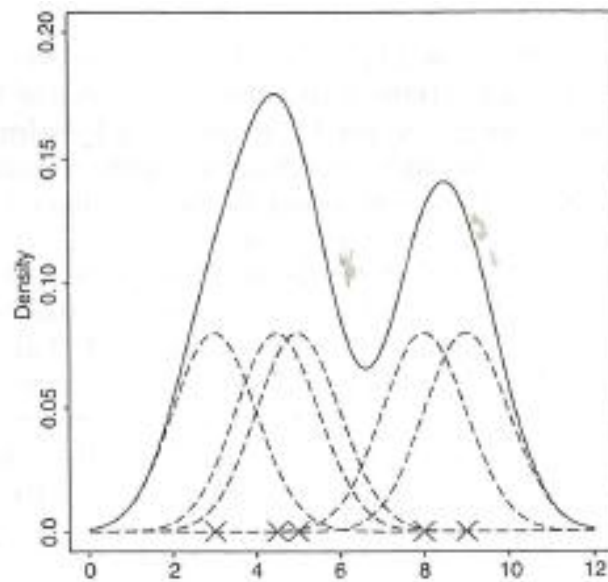
Figure 3.4: Kernel Density Estimate based on Observations (Wand and Jones, 1995)

Successful application of any kernel density estimation depends more on the choice of the smoothing parameter or bandwidth (h) and the type of kernel function $K(.)$, to a lesser extent.

The bandwidth for kernel estimation may be evaluated by minimizing the deviation of the estimated PDF from the actual one. Assuming a normal distribution for the bandwidth estimation, the optimal bandwidth for a normal kernel can be given by (Polansky and Baker, 2000):

$$h_n = (1.587)\hat{\sigma} n^{-\frac{1}{3}}$$ (3.41)

where,

$\hat{\sigma}$ is the sample standard deviation measured by Silverman (1986):

$$\hat{\sigma} = min\left\{S, {IQR}/{1.349}\right\}$$ (3.42)

where,

S is the sample standard deviation; and

IQR is the interquartile range.

This methodology is applied to derive the PDF of the mean monthly precipitation at different time steps.

3.2.3 Extreme Precipitation Indices

Simulation of extreme precipitation is dependent on resolution, parameterization and the selected thresholds. Sun et al. (2006) found that most AOGCM models tend to produce light precipitation (<10mm day^{-1}) more often than observed, too few heavy precipitation events and much less precipitation during heavy events (>10 mm day^{-1}) (Randall et al., 2007). The situation gets worse in the absence of any extreme

precipitation indices. In the IPCC (2007), several indices explaining extreme temperature and precipitation are proposed but most reports in the literature investigate percent change in the occurrence of such indices without previously accepted definition of their severity level.

Three precipitation indices have been used in this study for comparing the performance of the AOGCMs in generating extreme precipitation amounts. These indices describe precipitation frequency, intensity and extremes. The highest five day precipitation, the number of very wet days and the number of heavy precipitation days express extreme features of precipitation. For very wet days, the 95th percentile reference value has been obtained from all non-zero total precipitation events for the base climate. Heavy precipitation days are those days that experience more than 10 mm of precipitation.

For Canada, due to large variation of precipitation intensities in various regions, a fixed threshold may not be good to assess the severity level (Vincent and Mekis, 2006). Accordingly, in this study the severity of these indices is classified based on percentile values. A percentile indicates the relative standing of data value when data are sorted into a numerical order, from smallest to largest. Low percentiles always correspond to the lower data values while higher percentiles refer to higher data values. Classification by percentile method offer several advantages: it is simple and computationally inexpensive; and it is completely data driven (does not follow any specific distribution), therefore can be used at any location with different precipitation patterns.

3.2.4 Extended Kernel Estimators

The kernel estimator explained in section 3.2.2 is assumed to follow a normal distribution. This section provides an extensive evaluation of the extended kernel estimators based on the various methods of bandwidths selection.

Nonparametric estimators are erroneously considered to be less accurate with small sample sizes (Lall et al., 1993). With the increase in sample size, the choice of estimator selection (parametric or nonparametric) can only be made more accurately. Nonparametric kernel estimators based on (i) normal kernel estimator (Silverman, 1986), and (ii) the orthonormal method (Efromovich, 1999) have been applied by Ghosh and Mujumder (2007) for assessing AOGCM and scenario uncertainties of future droughts. In the present study, the application of a normal kernel estimator is extended with the commonly used bandwidth selection methods for estimating densities and addressing model choice and scenario choice uncertainties.

Definition

The nonparametric kernel density estimation described in section 3.2.2 is based on the conventional method of assuming a normal distribution function for unknown PDFs. Because of an uncertain future climate, it is not justifiable to assume a normal distribution of the PDFs. Allowing an extension for the kernel estimator by replacing the normal bandwidth for a data-driven procedure can better quantify the inherent uncertainties arising from different AOGCMs.

The behavior of the estimator (equation 3.40) may be analyzed mathematically under the assumption that the data sets represent independent realizations from a probability

density $f(x)$). The basic methodology of the theoretical treatment aims to discuss the closeness of estimator $\hat{f}$ to the true density, f. Successful application of the estimator depends mostly on the choice of a kernel and a smoothing parameter or bandwidth. Figure 3.5 presents a comparison of the degree of smoothing based on a specific bandwidth value. A change in kernel bandwidth can dramatically change the shape of the kernel estimate (Efromovich, 1999).
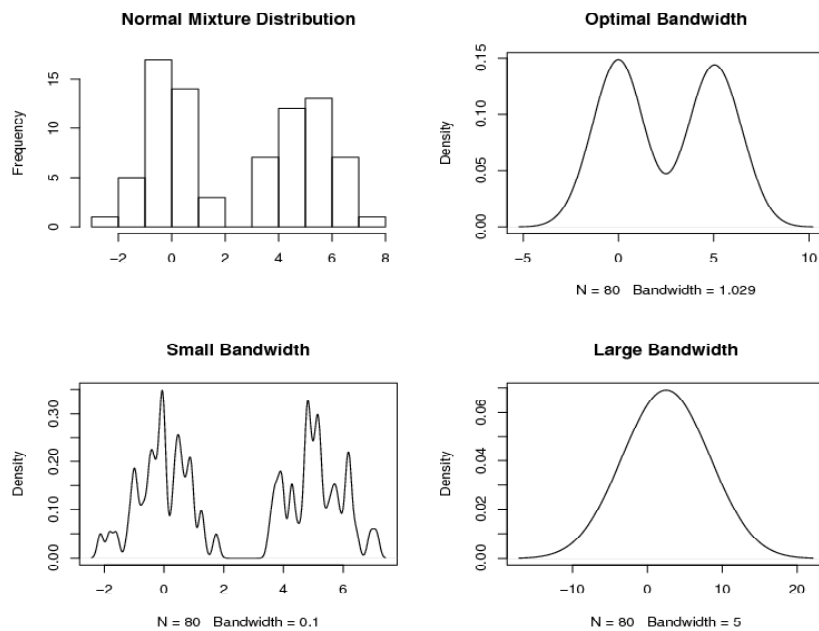
Figure 3.5: Kernel Smoothing

(Source: userwww.service.emory.edu/~cmagnan/.../Kuruwita.ppt, Accessed on: 3/16/2011)

For each x, $\hat{f}(x)$ can be thought as a random variable because of it's dependence on $X_1, X_2, \ldots \ldots X_n$. Except otherwise stated, $\sum$ will refer to a sum for $i = 1 \; to \; n$ and $\int$ to an integral over the range $(-\infty, \infty)$.

The discrepancy of the density estimator $\hat{f}$ from it's true density f can be measured by mean square error (MSE):

$$MSE_x(\hat{f}) = E[(\hat{f}(x) - f(x)]^2 \tag{3.43}$$

By standard elementary properties of mean and variance, equation 3.44 presents the mean square error as a sum of the squared bias and the variance at x.

$$MSE_x(\hat{f}) = \{E[(\hat{f}(x) - f(x)]^2\} + var\ \hat{f}(x) \tag{3.44}$$

In many applications a trade-off is applied between the bias and the variance; the bias can be reduced by increasing the variance and vice versa by adjusting the degree of smoothing. It can be obtained by minimizing the mean integrated squared error (MISE), a widely used measure of global accuracy of $\hat{f}$ as an estimator of f (Rosenblatt, 1956; Adamowski, 1985; Scott et al., 1981, Jones et al., 1996) and defined as:

$$MISE\ (\hat{f}) = E \int [(\hat{f}(x) - f(x)]^2 dx \tag{3.45}$$

Or in alternative form,

$$MISE(\hat{f}) = \int MSE_x(\hat{f}) dx$$

$$= E \int [(\hat{f}(x) - f(x)]^2 dx + \int var\ (\hat{f}) dx \tag{3.46}$$

which gives the $MISE$ as the sum of the integrated square bias and the integrated variance.

Asymptotic analysis provides a simple way of quantifying how the bandwidth h works as a smoothing parameter. Under standard assumptions, MISE is approximated by the asymptotic mean integrated squared error (AMISE) (Jones et al., 1996):

$$AMISE(h) = n^{-1}h^{-1}R(K) + h^4R(f^{''})\left(\int x^2\,K/_2\right)^2 \tag{3.47}$$

where,

$R(\varphi) = \int \varphi^2(x)dx$;

$\int x^2\,K = \int x^2\,K(x)dx$;

n is sample size;

h is bandwidth.

The first term (integrated variance) is large when h is too small, and the second term (integrated squared bias) is large when h is too large.

The minimizer of $AMISE(h)$ is calculated as:

$$AMISE(h) = \left[\frac{R(k)}{nR(f^{''})(\int x^2K)^2}\right]^{\frac{1}{5}} \tag{3.48}$$

Methods for Bandwidth Selection

Data driven estimation methods are broadly classified as first generation and second generation methods by Jones et al (1996).

First Generation Methods

First generation methods used for the selection of smoothing parameter include those proposed before 1990. These include the rule of thumbs, least square cross validation and biased cross validation methods.

The most basic method is the 'rule of thumb' used by Silverman (1986). The idea involves replacing the unknown part of h_{AMISE}, $R(f'')$ in equation 3.48 with an estimated value based on a parametric family such as a normal distribution $N(0, \sigma^2)$. However, this method is known to provide an over-smoothed function (Terrell and Scott, 1985; Terrell, 1990) and has been proven to be unrealistic in many applications. In the present study, h_{ROT} is used to denote the bandwidth based on the standard deviation in Silverman (1986).

The idea of 'least squared cross validation', first used by Bowman (1984) and Rudemo (1982) incorporates integrated squared error (ISE) as

$$ISE(h) = \int (\hat{f}_h - f)^2 = \int \hat{f}_h^2 - 2 \int \hat{f}_h f + \int f^2 \qquad (3.49)$$

The minimizer of the ISE is the same as the minimizer of the first two terms of the final form. The first term is known while the second term can be estimated by $2n^{-1} \sum_{i=1}^{n} \hat{f}_h(X_i)$, where $\hat{f}_i$ is the leave-out kernel density estimator with X_i removed. The largest minimizer is denoted by h_{CV} (Hall and Marron, 1991).

The biased cross validation (BLCV) proposed by Scott and Terrell (1987) seeks to directly minimize the AMISE by estimating the unknown $R(f'')$ in equation 3.48. It proceeds by selecting another bandwidth treated as the dummy variable of minimization. The smallest local minimizer of

$$BLCV(h) = n^{-1}h^{-1}R(K) + h^4 \times \left[R\left(\hat{f}_a'' - \frac{R(K'')}{mh} \right) \right] \left(\int x^2 K/2 \right)^2 \qquad (3.50)$$

is denoted by h_{BCV}.

Second Generation Method

Second generation methods comply with those developed after 1990 such as the solve-the-equation-plug-in approach, the smoothed bootstrap approach, etc. In this study only the solve-the-equation-plug-in approach is used, and hence it is described below.

The main thought behind the 'solve the equation plug in' approach is to plug an estimate of the unknown $R(f'')$ in the equation 3.48. The major challenge is to estimate a pilot bandwidth. The 'solve the equation' approach proposed by Hall (1980), Sheather (1983, 1986) and later refined by Sheather and Jones (1991) is used in this study. The smallest bandwidth, h_{SJPI} is considered as the solution of the fixed point equation

$$h = \left[\frac{R(K)}{nR(\hat{f}''_{g(h)})(\int x^2 K)^2} \right]^{\frac{1}{5}} \tag{3.51}$$

The major difference between the *BLCV* and *SJPI* approaches lies in the expression of the form $g(h)$ which provides a better representation of $R(f'')$. It is done by estimating an analogue of h_{AMISE} for estimating $R(f'')$ by $R(\hat{f}''_g)$.

The minimizer of the asymptotic mean squared error (AMSE) is expressed as:

$$g_{AMSE} = C_1\{R(f''')\}C_2(K)n^{-\frac{1}{7}} \tag{3.52}$$

for suitable functional C_1 and C_2. The expression of g in terms of h comes from solving the representation of h_{AIMSE} for n and substituting to get

$$g(h) = C_3\{R(f''), R(f''')\}C_4(K)h^{\frac{5}{7}} \tag{3.53}$$

for appropriate functionals C_3, C_4. The unknowns $R(f'')$ and $R(f''')$ are estimated by $R(\hat{f}'')$ and $R(\hat{f}''')$, with bandwidths chosen by reference to a parametric family, as for h_{ROT}.

While many variations have been tested for the treatment of $R(\hat{f}'')$ and $R(\hat{f}''')$, the major literature contribution has been to try to reduce the influence of the normal parametric family even further by using pilot kernel estimates instead of normal interference (Jones et al., 1996). Park and Marron (1990) has shown the improvements in terms of the asymptotic rate of convergence up to a certain point.

Figure 3.6 presents a comparison of mean square error (MISE) and density estimates using different types of bandwidths on a log_{10} scale taken from randomly generated 500 Monte Carlo replications of samples of size from two different distributions: (a) $N(0,1)$ and (b) $0.5N(-1, {}^4\!/_9) + 0.5N(1, {}^4\!/_9)$. It is seen that although the cross validation h_{LCV} is capable of providing the least MISE, it has a tendency of providing substantial skewness at the tail and h_{BCV} suffers oversmoothing problem. The plug-in (PI) estimate h_{SJPI} accounts for an acceptable error and adequate density estimates of the sample. Furthermore, unlike the cross validation bandwidths, the plug in estimate does not provide the minimizer value outside of the acceptable range $[{}^{h_{MISE}}\!/_3, 3h_{MISE}]$ and is free of generating multiple local minima (Park and Marron, 1990).
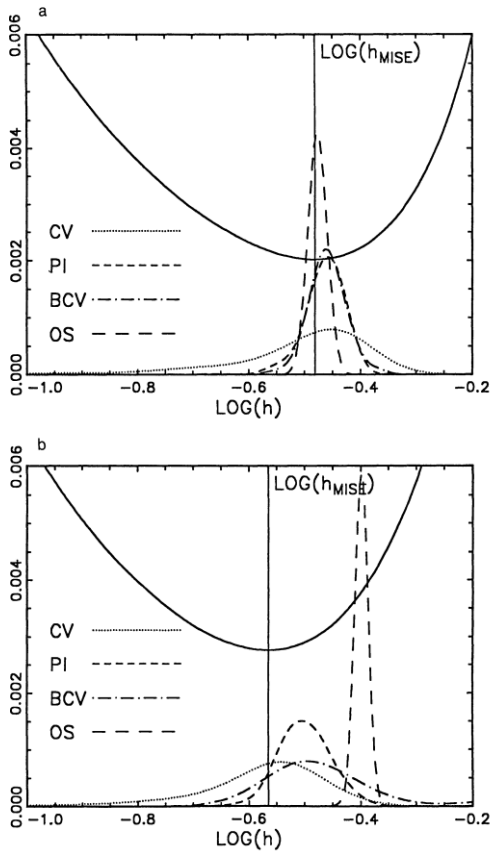
Figure 3.6: MISE(h) and Kernel Density Estimates of the Various Bandwidths (Park and Marron, 1990)

3.3 Intensity-Duration-Frequency Analysis under Climate Change

Intensity duration frequency analysis provides a convenient tool to summarize regional rainfall information by capturing essential characteristics of point rainfall for shorter durations. The methodology of developing of IDF curves for future (Figure 3.7) combines the use of long sequences of rainfall data from the weather generator, disaggregation of the daily climate data into hourly values and development of annual maximum precipitation using Annual Maxima Series method and fitting them into an appropriate distribution to calculate annual extremes for different returns periods.

73

3.3.1 Bias Correction of Downscaled Outputs

The weather generator developed in section 3.2.2 is used to generate long sequences of daily rainfall for different climate signals. The downscaling process scales down coarse grid outputs of AOGCMs into the scale of interest. However, significant simulation bias still may exist from the initializations of atmospheric-oceanic processes. Hence, employing coarse resolution global model output for regional and local climate studies requires an additional bias correction step based on the ability of the AOGCMs to reproduce the past climate. In this study, bias from the downscaled outputs is corrected by the following equations:

Bias in the AOGCMs is calculated by:

$$b_i = \frac{x_i - y_i}{x_i} * 100 \qquad (3.54)$$

where,

b_i is the bias from different AOGCMs;

x_i is the monthly mean of observed precipitation for 1965-1990; and

y_i is the monthly mean from different AOGCMs for 1965-1990.

The correction factor for the AOGCMs is then calculated using,

$$c_i = \frac{b_i}{100} + 1 \qquad (3.55)$$
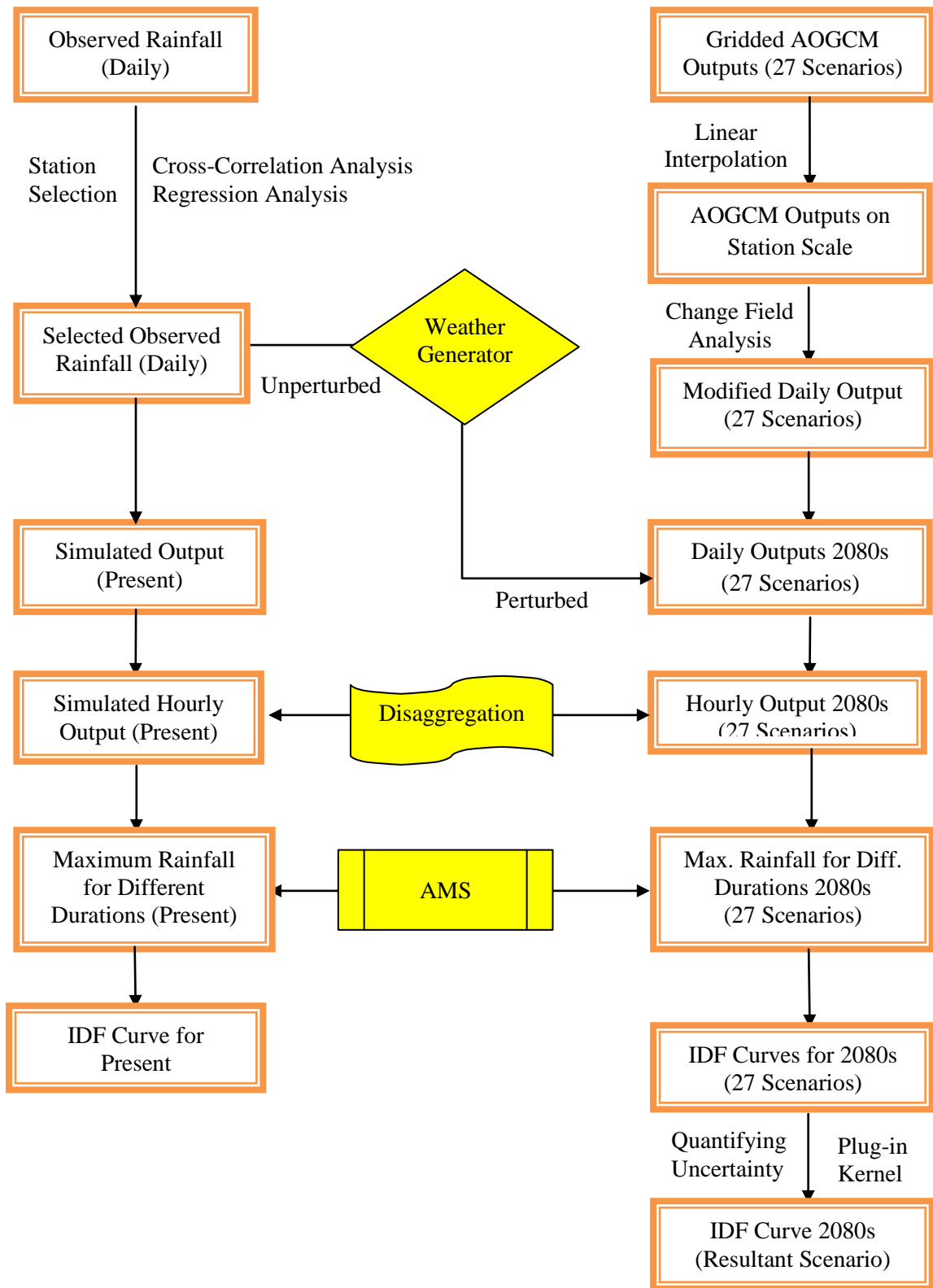
Figure 3.7: Schematic Diagram of Developing IDF Curve

So, the treated downscaled rainfall for 2080s becomes:

$$p_j = c_i * p_i \qquad\qquad (3.56)$$

where,

p_i is the untreated daily downscaled rainfall for 2080s.

3.3.2 Hourly Disaggregation

The weather generator used in this work is set to produce climate variable on a daily time scale. However, examination of short duration rainfall extremes requires the input data to be on a finer temporal scale such as, hourly or even smaller intervals. The disaggregation mechanism is thus developed to produce time series of hourly rainfall data which will be next used for frequency analysis and generating IDF information.

The disaggregation scheme works by extracting rainfall event records from the hourly observed data. A rainfall event can be defined as a period of non-zero rainfall for two or more days where the total amount of rainfall during the consecutive days is considered as the event rainfall value. Once the rainfall events are extracted from the historic record, they are disaggregated by a K-nearest neighbor approach. The algorithm considers daily rainfall produced by the weather generator for day t, for each station. A set of potential events are selected from the observed record. Once such event is chosen, the daily output is disaggregated into hourly values.

The selection of neighboring events from the observed record follows a simple rule: only events within a moving window of w_h days are selected to account for the

seasonally varied temporal distribution of rainfall. Events are selected from the prescribed moving window from all years in the historic record of events as a potential set of neighbors. The daily totals from downscaled outputs are compared with the set of neighboring event totals to assure that only disaggregation of similar events is considered.

Observed hourly data is used as a template on how the hourly values of the generated outputs would look like. A specific number of days are considered to compare with the present day value. The best match is determined by (Mansour and Burn, 2010):

$$z_i = \sqrt{(w_1 * (y_i - x_i)^2) + (w_2 * (e_y - e_x)^2)} \qquad (3.57)$$

where, y_i is the daily rainfall output from weather generator, x_i is the historical observed daily rainfall, e_y and e_x are the events calculated from WG outputs and historical (observed) data respectively. The weights w_1, w_2 are used to identify the best historical hourly ratio for the data.

The combination of the weights, which provide the lowest z_i for each value within the window, is considered as the daily ratio of historical hourly values used to disaggregate the WG's daily data into hourly values. The ratio of the hourly values found within the chosen day is applied to the daily value to create a plausible hourly set-up for the given daily data. This is done based on the methods of fragments (Svanidze, 1977; Sharif et al., 2007). The fragments represent the fraction of daily rainfall that occur during each hour of the day summing to unity and can be expressed as:

$$f_i = \frac{h_i}{\sum_{i=1}^{n} h_i} \qquad\qquad (3.58)$$

where,

f_i represents the fragments calculated for hour i;

h_i is the chosen hourly data from observations; and

n is the number of hours in a day equal to 24.

The fragments are then multiplied with the daily data to produce data for each hour:

$$h_i' = f_i \times d \qquad\qquad (3.59)$$

where,

d is the daily rainfall (mm).

This program has been sent daily data that already had known hourly values and the results have been compared in an attempt to verify that the model works correctly.

This approach utilizes locally observed data using a non-parametric method avoiding the chance of errors that might occur from the parametric methods due to theoretical distribution fits, parameter estimations and calibration. Additionally, there is high possibility that the statistical characteristics of the disaggregated rainfall are stored by applying the resampling algorithm.

3.3.3 Intensity-Duration-Frequency Analysis

Sampling of rainfall data for estimating rainfall extremes is commonly done using one of the two approaches: the annual maximam series (AMS) or block maxima and peak over threshold (POT), or partial duration series (PDS) (Coles, 2001). Literature identifies limitations and advantages of both methods. Madsen et al. (1997), Buishand et al. (1990), and Rasmussen et al. (1994) found POT to be a better approach than AMS. While Kartz et al. (2002), Smith (2003), de Michele and Salvadori (2005) suggested use of both methods. By definition, AMS approach includes the yearly peaks in the observational period while the POT involves all the peak events that exceed a given threshold value. The AMS method is more straightforward. If the number of annual maxima is small (<100), the obtained estimates may be sensitive to outliers. It is an asymptotic method that works well if the number of inputs from which a maximum is considered, is large. Jeruskova et al. (2006) showed that convergence to limit any distribution fit can be slow. For determining annual maxima, the maxima of 365 daily values are considered. The seasonal effect may also play a role. Application of POT is somewhat difficult than the AMS because of its selection of an appropriate threshold. For a satisfactory stability of the obtained results, testing of several threshold values such as 90%, 95% and 98% is recommended. Jeruskova et al. (2006) have shown that the POT method may work well for short memory series only. For longer data series, the series should be split into several more homogeneous groups. Both methods however, have their own disadvantages too; the AMS may neglect certain high values, while the POT may suffer from serial correlation problem (Jervis et al., 1936; Langbein, 1949; Taesombat and Yevjevich, 1978).

Rainfall intensity-duration-frequency (IDF) curves are derived from the statistical analysis of rainfall events for a period over time and used to capture important characteristics of point rainfall for shorter durations. It is considered as a convenient tool for gathering regional rainfall information required for municipal storm water management works. Site specific curves represent intensity-time relationship for a specific return period from a series of storms. Information is summarized by plotting the durations on the horizontal axis, the rate of rainfall (intensity in depth per unit of time) on the vertical axis and the curves for each design storm return period. Frequency is expressed in terms of return period, T, the average length of time between rainfall events that equals or exceed any given magnitude. For each selected duration, annual maximum rainfall is extracted from the rainfall data and frequency analysis is performed to the annual maximum rainfall to fit a probability distribution for standardizing the characteristics of rainfall for each station with varying rainfall record.

In Canada, Environment Canada is responsible (a) for collection and quality control of rainfall data and (b) for providing the rainfall extreme information in the form of IDF curves. Gumbel Extreme Value distribution is normally used to fit the annual extremes of rainfall using AMS method. It is acknowledged here that due to changes in future precipitation extremes the future rainfall may not follow the conventionally used Gumbel distribution. It would be adequate to consider a generalized extreme value (GEV) distribution. But the inherent uncertainties in the responses of AOGCM outputs do not guarantee GEV as the best fit for all AOGCMs. For simplicity, and compliance with Environment Canada's procedure, use of Extreme Value (EV) type 1 which is Gumbel distribution is adopted in this study.

The Gumbel probability distribution is expressed (Watt et al., 1989):

$$x_t = \mu_z + K_T\,\sigma_z \qquad\qquad\qquad (3.60)$$

where,

x_t represents the magnitude of the T year event;

μ_z is the mean of the annual maximum series;

σ_z is the standard deviation of the annual maximum series; and

K_T is a frequency factor depending on the return period T.

The frequency factor K_T is obtained using the following equation:

$$K_T = \frac{-\sqrt{6}}{\pi}\left[0.5772 + \ln\left(\ln\left(\frac{T}{T+1}\right)\right)\right] \qquad\qquad (3.61)$$

Meteorological Service of Canada (MSC) uses the above method to calculate rainfall frequency for durations of 5, 10, 30 minutes and 1, 2, 6, 12, 24 hours. Since most of the stations do not have observed sub-hourly data, the calculation of the frequencies for periods shorter than 1 hour may be based on the ratios provided by the World Meteorological Organization (Ministry of Transport of Ontario, 1997):

Duration (min)	5	10	15	30
Ratio (n-min to 60-min)	0.29	0.45	0.57	0.79

However, in the present study, durations shorter than 1 hour are not considered.

The IDF data is next fitted to a continuous function in order to make the process of IDF data interpolation more efficient i.e. if the ratio of any duration is not available, the IDF data is fitted to the following three parameter function:

$$i = \frac{A}{(t_d + B)^C}$$

(3.62)

where,

i presents the rainfall intensity in mm/hr;

t_d is the duration of rainfall in minute;

$A, B, and\ C$ are the constants.

To obtain optimal values for these three parameters, a reasonable value of B is assumed and the values of A and C are estimated by the least square method. The process is repeated to achieve the closest fit of the data (MTO, 1997). Plots of rainfall intensity vs. duration for each return period is then produced from the fitted IDF data to equation 3.60.

CHAPTER FOUR

APPLICATION OF METHODOLOGY

4.1 Study Area: Upper Thames River Basin

The Upper Thames River (UTR) basin (Figure 4.1) ($42^035'24''$N, $81^08'24''$W), located in Southwestern Ontario, Canada, is a 3,500 km^2 area nested between the Great Lakes Huron and Erie. The basin often experiences major hydrologic hazards, such as floods and droughts.
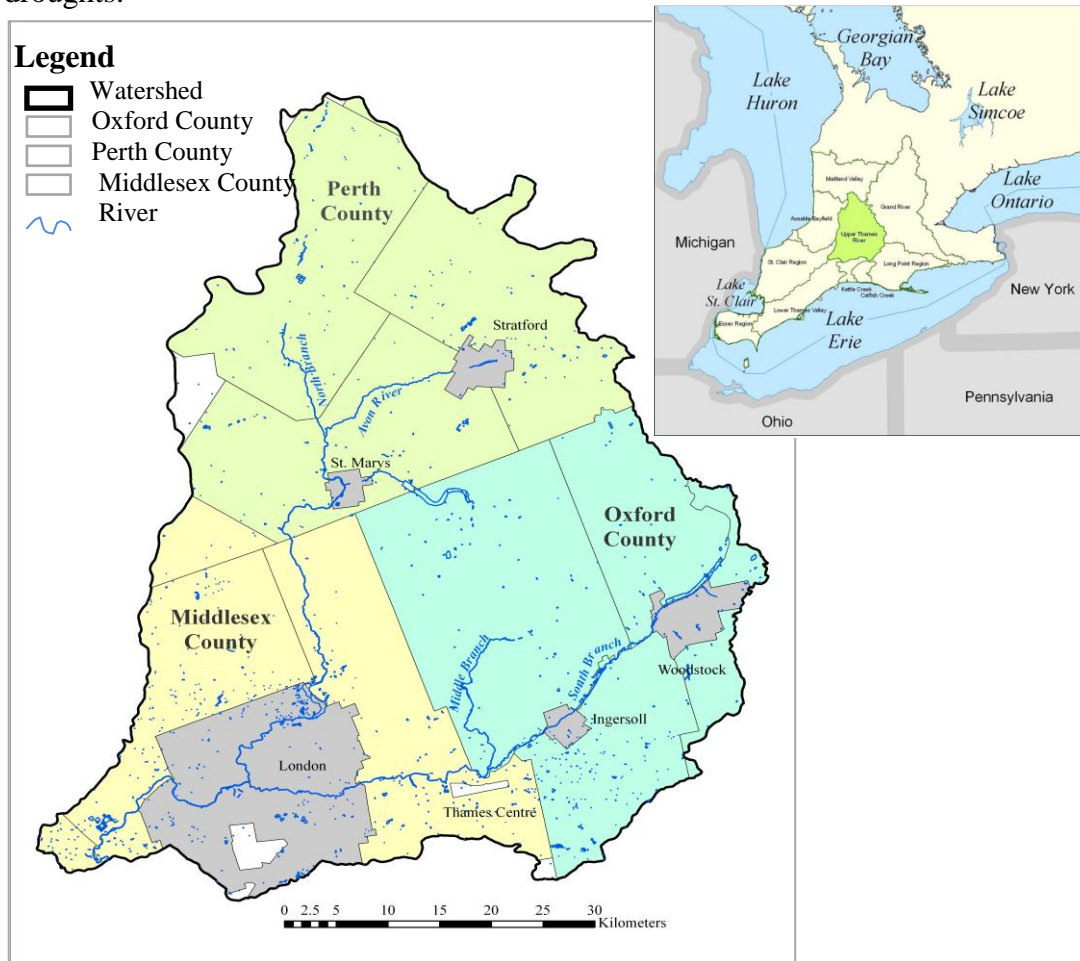
Figure 4.1: Map of the Upper Thames River Basin

The population of the basin is 450,000 (2006), of which 350,000 are the residents of the City of London. The length of the Thames River is 273 km (from Tavistock to its mouth at Lake St. Clair) and average annual discharge is about 36 m^3/sec. The basin consists of two majors tributaries of the river Thames: the North Branch (1,750 km^2), flowing southward through Mitchell, St. Mary's, and eventually into London, and the South Branch (1,360 km^2), flowing through Woodstock, Ingersoll, and east London. The Upper Thames River basin receives about 1,000 mm of annual precipitation, 60% of which is lost through evaporation and/or evapotranspiration, stored in ponds and wetlands, or recharged as groundwater (Prodanovic and Simonovic, 2006). Several weather stations around the basin provide point measurements of weather variables including daily temperature and precipitation. The basin has a well documented history of flooding events dating back to the 1700s (Prodanovic and Simonovic, 2006). High flows occur mostly in early March after snowmelt, and then again in July and August as a result of summer storms. Khaliq et al. (2008) reported that in the Canadian regime, low flow conditions show a seasonal behaviour: summer low flow from June to November and winter low flow from December to May. The UTR basin experiences frequent low flow conditions between June and September (Prodanovic and Simonovic, 2006).

4.2 Assessment of Reanalysis Data

As part of the present research, Solaiman and Simonovic (2010) performed a rigorous comparison of the two different reanalysis datasets for climate change impact studies and hydrologic modeling in the Upper Thames River basin. The data description, the

hydrologic model setup process and criteria used for evaluating model performances are presented next.

4.2.1 Data Description

For comparison, the following data sources were taken into account:

Observation

Daily observed precipitation and temperature data covering the UTR basin (Table 4.1 and Figure 4.2) for the period of 1980 – 2005 is collected from Environment Canada (http://climate.weatheroffice.ec.gc.ca/climateData/canada_e.html).

Table 4.1: Weather Stations in Upper Thames River Basin

Serial	Station Name	Location			Variables
		Latitude (^{0}N)	Longitude (^{0}W)	Elevation (m)	
1	Blyth	43.72	81.38	350.50	Prec, Tmax, Tmin, Tmean
2	Dorchester	43.00	81.03	271.30	Prec
3	Exeter	43.35	81.50	262.10	Prec, Tmax, Tmin, Tmean
4	Folden	43.02	80.78	328.00	Prec, Tmax, Tmin, Tmean
5	Glen Allan	43.68	80.71	400.00	Prec, Tmax, Tmin, Tmean
6	London A	43.03	80.15	278.00	Prec
7	St. Thomas	42.78	81.17	209.10	Prec, Tmin, Tmean
8	Stratford	43.37	81.00	345.00	Prec, Tmax, Tmin, Tmean
9	Waterloo A	43.46	81.38	317.00	Prec, Tmax, Tmean
10	Woodstock	43.14	80.77	281.90	Prec, Tmax, Tmin, Tmean
11	Wroxeter	43.86	81.15	335.00	Prec

(Data source: National Climate Data and Information Archive of Environment Canada
http://climate.weatheroffice.ec.gc.ca/climateData/canada_e.html, Retrieved on 14/11/2007)

Unfortunately, over the years only a few studies have been conducted for the purpose of making a reliable database and providing an adequate spatial coverage of variable climatic conditions within the basin. The spatial distribution of the weather stations is also sparse, especially in the west side of the basin, and does not cover the entire basin (Figure 4.2).
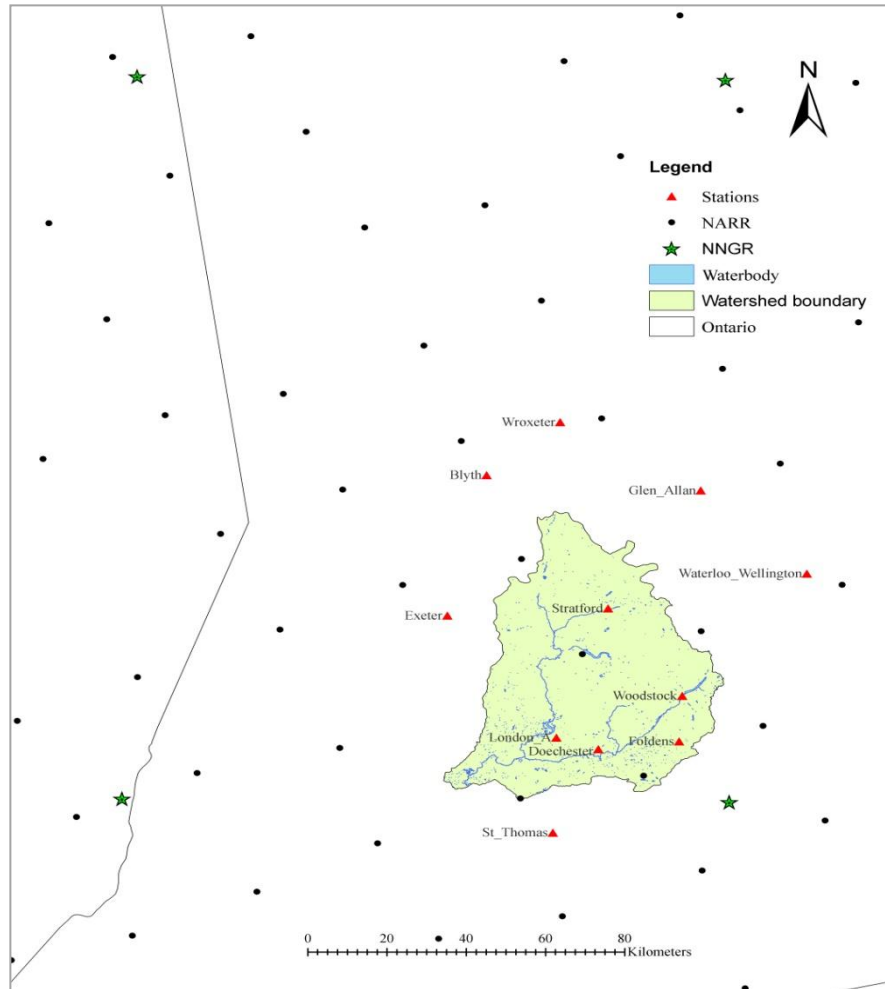
Figure 4.2: Location of the Observations and Grid Points

NCEP-NCAR Global Reanalysis (NNGR)

The NCEP-NCAR Global Reanalysis (NNGR) is 'an assimilated dataset using a state-of-the-art analysis/forecast system and past data since 1948' (Kalnay et al. 1996). One

interesting feature of the data set is that there are no precipitation estimates of sufficient spatial resolution or length, and hence no station precipitation data are assimilated directly into the model (Reid et al. 2001). It is provided 4 times daily at 6 hour interval, daily and monthly values of over 80 climatic variables on $2.5° \times 2.5°$ grid. The global reanalysis data for this project is made available through the Physical Sciences Division of the Earth System Research Laboratory of the National Oceanic and Atmospheric Administration (NOAA) (More information can be found from the NOAA website (http://www.cdc.noaa.gov/cdc/data.ncep.reanalysis.html, Retrieved on 4/7/2008).

North American Regional Reanalysis (NARR)

The NARR is an extension of the global reanalysis, that uses a very high resolution Eta model ($0.3° \times 0.3°$, 32 km grid spacing, 45 layers spatially) with the Regional Data Assimilation System (RDAS). Most of the variables are collected 8 times daily; daily and monthly means are also available at 29 pressure levels. Unlike its global counterpart, the NARR dataset has been developed by assimilating high quality and detailed precipitation observations into the atmospheric analysis, which consequently made the forcing to the land surface model component of the system more accurate. As such, a much improved analysis of land hydrology and land-atmosphere interaction has become possible (Nigam and Ruiz-Barradas, 2006). However, one significant weakness of the NARR data when applied in the Canadian regions is that the daily gauge-based data it uses for assimilation is sparse (1 degree grid), which may be insufficient for the model to perform as expected (NCEP website: www.emc.ncep.noaa.gov/mmb/rreanl/narr.ppt, Retrieved on 9/11/2009). NARR data for this study has been made available through the Data Access Integration of

the Canadian Climate Change Scenarios Network of Environment Canada. In order to assess the reanalysis data, the daily accumulated precipitation rate and the daily maximum, minimum and mean temperatures are considered. Data for each variable is collected for the period 1980–2005. The NNGR and NARR precipitation rate (kg m^{-2} s^{-1}) data is converted to the daily total (mm day^{-1}). As suggested by Reid et al. (2001) and Choi et al. (2007), precipitation values less than 0.5 mm/day^{-1} is considered zero in order to comply with the observed precipitation. Figure 4.2 and Table 4.1 present the details of 11 stations located within and around the Upper Thames river basin. Some parts of the basin are poorly covered due to the lack of weather stations in those areas. In some cases, stations are missing records over several months of the entire study period. For any station with more than 15% of missing records for a specific month, that month has been eliminated from both station and reanalysis datasets in order to maintain consistency.

4.2.2 Hydrologic Model Setup

The hydrologic model applied to the Upper Thames River basin is described in Cunderlik and Simonovic (2004, 2005). The model has been properly calibrated and verified with sensitivity analyses. The model consists of thirty-two special units, twenty one river reaches and three flood control reservoirs (Wildwood, Fanshawe and Pittock) (Figure 4.3). Each sub-basin is represented by rectangles and is provided with interpolated reanalysis data. The outputs of each sub basin are flow hydrographs joined by junctions (circles) where the flows are added together. River reaches represent the major rivers and streams in the basin and are shown as thick lines connected between two

junctions. The routing module described in section 3.1.1 is applied to each river reach, and thus acts as a passage of a flood wave as it moves through the river system. Reservoirs are depicted as triangles and the same routing rules are applied here. The model is seasonal in nature with different set of parameters for the summer and winter seasons. The parameter sets for the summer and winter seasons are presented in Cunderlik and Simonovic (2004) and Prodanovic and Simonovic (2007).
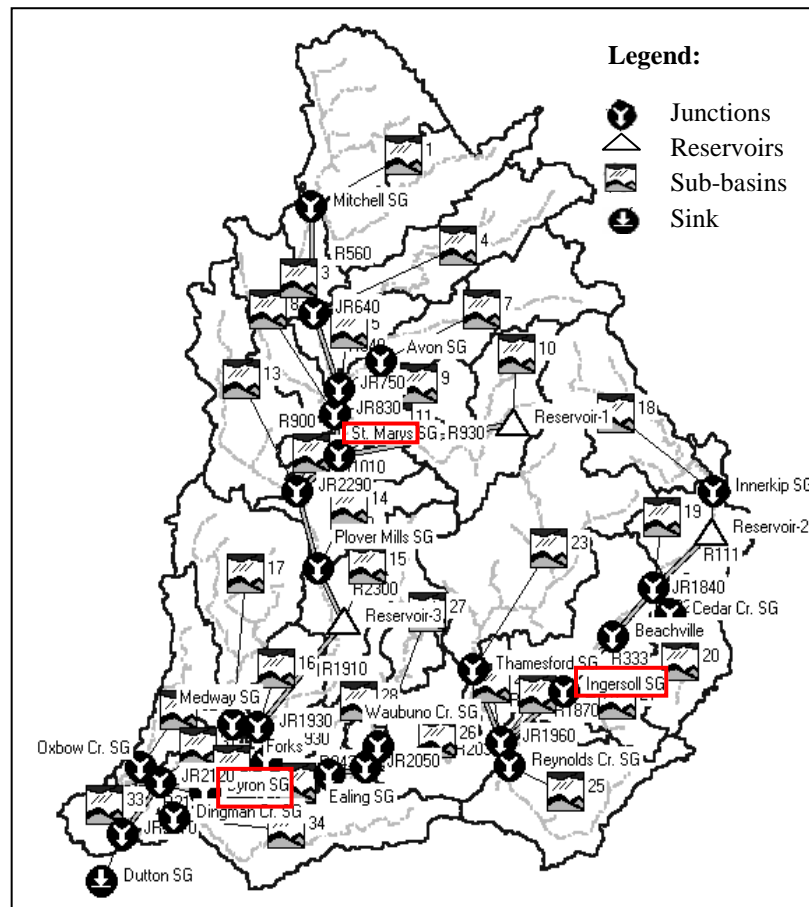
Figure 4.3: HEC-HMS Continuous Hydrologic Model at Upper Thames River Basin

4.2.3 Performance Evaluation and Error Estimation of Simulated Stream Flow

Quantitative assessments of the degree to which the simulated data match the observed data are used to provide an evaluation of the model's predictive abilities. It utilizes numerous statistics (t and F test statistic) and techniques. Goodness–of-fit (correlation coefficient, r and coefficient of determination, R^2) or relative error measurements are mostly used to assess the ability of the model. Unfortunately, they only describe the degree of collinearity between the observed and predicted values and provide a biased presentation of the efficiency of the model (Willmott 1981; Willmott et al. 1985; Kessler and Neas 1994; Legates and Davis 1997). Furthermore, they are oversensitive to extreme values and insensitive to additive and proportional differences between predicted and observed values (Legates and McCabe 1999). As a result, other statistics such as absolute error measures (root mean square, RMSE or mean absolute error, MAE) in terms of the units of the variables are developed to examine the association between observed and simulated data. In order for a complete assessment of the model performance, it is important to include at least one goodness-of-fit measure (r or R^2) and at least one absolute error measures (RMSE or MAE) along with additional supplemental information such as a comparison between the observed and simulated mean and standard deviations (Legates and McCabe 1999; Willmott et al. 1985). In this study, apart from RMSE, MAE and r, normalized mean square (NMSE) and relative bias have also been used to assess the accuracy of the estimates. The NMSE measures the average magnitude of the errors in the predicted dataset without considering their direction, whereas the relative bias provides the deviation of the simulations from observations.

90

Because of the existing model and data errors, it is necessary to use appropriate criteria for estimating the relevant uncertainties (Sorooshian et al. 1993). In this study, only data uncertainty arising from the (i) inconsistency and non-homogeneity and (ii) inadequate representation of the reanalysis data due to space and time limitations, are assessed. The probability density function (PDF) provides the most complete and ideal description of uncertainty. However, in most practical problems such a probability function cannot be derived precisely (Tung 1996). Another well known approach to characterize uncertainties is to express it in terms of a reliability domain, such as the confidence interval or quartile plot with some specific level of probabilistic confidence. The estimation of uncertainties in terms of the model errors and quartiles around the mean and variances has been conducted by several authors for the purpose of analysis (Khan et al. 2006). However, the confidence interval has inherent limitation due to it's inability to directly combine the confidence intervals of individual contributing random components to provide an overall confidence interval of the system (Tung 1996). Hence, an alternative is used by calculating the variance and mean, as a measure of the dispersion of the variable of interest. In this study, the uncertainty in the simulated discharges is assessed in terms of model errors and percentile plots in the estimates of mean and variances. The process consists of several steps. Twenty six years of daily discharge during May-November obtained from the observed, NNGR and NARR hydro-climatic data are taken into consideration. At first, the presentation of the uncertainties is plotted using box and whisker plots where the bottom and top end of the box indicate the 1st quartile (25th percentile) and 3rd quartile (75th percentile) of the dataset for the low flows during May-November, with their median in between. This is a common approach for

assessing the data quality and model capability and has been used by Prodanovic (2008) and Sharif and Burn (2006). Next, errors in the estimates of means and variances of low flows have been evaluated using a non-parametric statistical hypothesis test at a 95% confidence interval. The following sections provide the equations used to calculate the performance statistics and statistical tests conducted.

Performance Evaluation Criteria

Many model performance statistics are available in order to assess the accuracy of the estimates. For this particular work, the model performance and forecasting results are compared by a set of five statistics. A brief description of these statistics is given below.

The Root mean square error (RMSE) which is the square root of the differences between the observations C_O and predicted values C_P:

$$RMSE = \left(\frac{1}{N} \sum_{i=1}^{N} \left(C_{P_i} - C_{O_i} \right)^2 \right)^{\frac{1}{2}} \tag{4.1}$$

where,

N is the number of observations;

C_{O_i} and C_{P_i} are observed and predicted values respectively.

The mean square errors provide a general illustration of the relevancy of the simulated values by giving a global goodness to fit by including errors and biases in the calculation. The lower the RMSE value, the better the model. RMSE, however, doesn't necessarily reflect whether the two sets of data move in the same direction. For instance, by simply

scaling the network output, we can change the MSE without changing the directionality of the data. This limitation can be overcome by introducing a second index, correlation coefficient, r.

The correlation coefficient (r) between an observed value C_{O_i} and a desired model output C_{P_i} is defined by:

$$r = \frac{\frac{1}{N}\sum_{i=1}^{N}\left[\left(C_{P_i} - \bar{C}_{P_i}\right)\left(C_{O_i} - \bar{C}_{O_i}\right)\right]}{\sqrt{\frac{1}{N}\sum_{i=1}^{N}\left(C_{P_i} - \bar{C}_{P_i}\right)^2} \sqrt{\frac{1}{N}\sum_{i=1}^{N}\left(C_{O_i} - \bar{C}_{O_i}\right)^2}} \tag{4.2}$$

where,

N is the number of observations; and

$\bar{C}_{O_i}$ and C_{P_i} are the mean observed and predicted values respectively.

This statistic provides a measure of the prediction ability of a model and it is an important tool for comparing two models as it is independent of the scale of data. The r value can range from -1 (perfect negative correlation) to 1 (perfect positive correlation) through 0 where 0 means no correlation. An r value of 0.9 and above is very satisfactory, 0.8 to 0.9 presents a fairly good model but below 0.7 is considered unsatisfactory.

The normalized mean squared error (NMSE) is another version of the mean square error which is normalized to provide for comparisons among different models (Agirre-Basurko et al, 2006).

$$NMSE = \frac{\frac{1}{N}\sum_{i=1}^{N}\left(C_{P_i} - C_{O_i}\right)^2}{\frac{1}{N}\sum_{i=1}^{N}\left(C_{O_i} - \bar{C}_{O_i}\right)^2} \tag{4.3}$$

The mean absolute error (MAE) is a linear score which means that all the individual differences are weighted equally in the average. In short, it measures the average magnitude of the errors in predicted dataset without considering their direction. It can be expressed as:

$$MAE = \frac{1}{N}\sum_{i=1}^{N}|C_{O_i} - C_{P_i}| \tag{4.4}$$

For a perfect fit, C_{O_i} should be equal to C_{P_i} so that MAE becomes zero.

The relative bias (RB) provides a measure of the magnitude of bias between the observed and target data. It can be expressed as:

$$RB = \frac{\frac{1}{N}\sum_{i=1}^{N}(C_{P_i} - C_{O_i})}{\bar{C}_O} \tag{4.5}$$

t and F Test Statistics

The statistical t test is performed for investigating the means of two samples. If the test indicates a rejection of the null hypothesis at the $p = 0.05$ level, then the means or variances are considered to be statistically different. This procedure uses the null hypothesis that the difference between two population means is equal to a hypothesized value $H_0: \mu_1 - \mu_2 = \mu_0$.

For the purpose of the test, the following hypotheses are established:

$H_0: \mu_1 - \mu_2 = 0$ (the mean of the two samples are same)

$H_0: \mu_1 - \mu_2 \neq 0$ (the mean of the two samples are different)

The *t* test performed assumes equal variances for all datasets to be tested. It is more powerful than the unequal variance assumptions, but can result in serious errors if the variances are not equal. Therefore, it is important to test whether the variances of all datasets are equal. Accordingly *F* tests are subsequently performed to determine whether the variances of two different datasets are significantly different. This procedure uses the null hypothesis that the two variances are equal, i.e.

$$H_0: \sigma_1^2 = \sigma_2^2$$

The following hypotheses are thus established:

$H_0: \sigma_o^2 = \sigma_{G/R}^2$ (the observations and the NNGR (G) or NARR (R) have equal

variances)

$H_0: \sigma_o^2 < \sigma_{G/R}^2$ (the observations have variances smaller than the NNGR (G) or NARR

(R))

The *t* and *F* test statistics for this research are calculated using Minitab statistical software (Minitab Inc., 2007).

Wilcoxon Rank Sum Test and Levene's Test

One of the best non-parametric methods for constructing a hypothesis test *p* value for the difference of two population means is the Wilcoxon rank-sum test (Khan et al. 2006). It is used to check the differences of mean from two sets of samples. For hypothesis testing, both samples are combined into a single ordered sample and ranks are then assigned to the sample values from smallest to the largest, irrespective of the source of the samples. The test statistic can be the sum of the ranks assigned to those values from one of the populations.

Given two random samples $X_{1,\dots\dots\dots\dots}, X_m$ and $Y_1, \dots\dots\dots\dots Y_n$, the Wilcoxon rank

sum statistic is defined by computing the ranks R_i, $i = 1, 2, \dots N$ for the combined sample

$\{X_1, \dots\dots, X_n, Y_1, \dots\dots, Y_n\}$, where $N = n + m$. Then

$$W_x = \sum_{i=1}^{m} R_i \qquad (4.6)$$

A smaller sum of the samples provides the indication that the values of that specific

population tend to be smaller than the other population and hence, the null hypothesis of

no differences between populations may be rejected (Conover, 1980). In terms of the

hypothesis testing, the p value corresponds to the level of significance for which the

observed test statistic lies on the boundary between acceptance and rejection of the null

hypothesis (Khan et al, 2006). Detail description of method can be found in Conover

(1980). The Wilcoxon rank sum test for this research is performed using statistical

software S-plus (TIBCO, 2008).

The second test to be applied is the modified version of Levene's test (Levene 1980) for

testing the equality of two sample population variances as proposed by Brown and

Forsythe (1974). This method considers the distances of the observations from their

sample median rather than their sample mean, which makes the test more robust with

data following a skewed distribution. For performing the test, a variable X with sample

size N is divided into K subgroups, N_i is the sample size of the ith subgroup. Using the

above definitions, the Levene's test statistic is expressed as:

$$W = \frac{(N - K) \sum_{i=1}^{K} N_i (Z_i - Z)^2}{(K - 1) \sum_{i=1}^{n} \sum_{j=1}^{N_i} (Z_{ij} - Z_i)^2} \qquad (4.7)$$

where,

Z_{ij} is defined by:

$$Z_{ij} = |X_{ij} - \tilde{X}_\iota| \qquad (4.8)$$

where,

$\tilde{X}_\iota$ is the median of the ith subgroup;

X_{ij} is the value of the jth sample from the ith group;

$Z = \frac{1}{N}\sum_{i=1}^{k}\sum_{j=1}^{N_i} Z_{ij}$ is the group mean of all Z_{ij}; and

$Z_i = \frac{1}{N}\sum_{j=1}^{N_i} Z_{ij}$ is the overall mean of Z_{ij} for group i.

The Levene's test rejects the hypothesis that the variances are equal if

$$W > F(\alpha, K - 1, N - K) \qquad (4.9)$$

where,

$F(\alpha, K - 1, N - K)$ is the upper critical value of the F distribution with $K - 1$ and $N - K$ degrees of freedom at a significance level of α.

The Levene's test has been performed using the statistical software (Minitab Inc, 2007).

4.3 Uncertainty Estimation Methods

4.3.1 Data and Model Setup: Fixed Weight Approach

The fixed weight approach involves Bayesian reliability ensemble average (BA-REA) method described in section 3.2.1. For this study, area averaged precipitation response from all 15 AOGCMs and scenarios (Table 4.2), averaged for the London station is considered to compare with the PDFs generated by the methodology presented in Section 3.2.2.

Table 4.2: AOGCM Models and Emission Scenarios used for Uncertainty Estimation

GCM Models	Sponsors, Country	SRES Scenarios	Atmospheric Resolution	
			Lat	Long
CGCM3T47, 2005	Canadian Centre for Climate Modelling and Analysis, Canada	A1B, A2, B1	3.75°	3.75°
CGCM3T63, 2005		A1B, A2, B1	2.81°	2.81°
CSIROMK3.5, 2001	Commonwealth Scientific and Industrial Research Organization (CISRO) Atmospheric Research, Australia	A2, B1	1.875°	1.875°
GISSAOM, 2004	National Aeronautics and Space Administration (NASA)/ Goddard Institute for Space Studies (GISS), USA	A1B, B1	3°	4°
MIROC3.2HIRES, 2004	Centre for Climate System Research (University of Tokyo), National Institute for Environmental Studies, and Frontier Research Centre for Global Change (JAMSTEC), Japan	A1B, B1	1.125°	1.125°
MIROC3.2MEDRES, 2004		A1B, A2, B1	2.8°	2.8°

Data source: Canadian Climate Change Scenario Network Website, (http://cccsn.ca/?page=dd-gcm, Retrieved 9/20/2008)

To generate PDF of precipitation affected by the climate change, simulated present

(1961-1990) and future (2041-2070) precipitation (X_i, Y_i) are considered for winter (December-January-February) and summer (June-July-August) seasons. The outputs from 15 different sets of experiments from six AOGCMs for the two time slices, (1961-1990, 2041-2070) are extracted for the 22 stations and averaged for the London station using inverse distance approach. The natural variability is expressed as the inverse of the variance of observed precipitation for 1961-1990 (X_0). It is calculated as the inter-annual variance on the basis of the observed record (X_0). The computer codes for developing the BA-REA method used in this study can be downloaded from National Centre for Atmospheric Research website (*http://www.image.ucar.edu/~nychka/REA/*, Retrieved on 8/04/2010).

4.3.2 Application of Variable Weight Approach

Data Description and Selection of Predictors

Daily precipitation and temperature are the most important atmospheric forcing parameters required for any hydrologic impact study for a larger river basin (Salathe Jr., 2003). Climate models, however, suffer from missing important mesoscale and surface features that control precipitation. Sole use of precipitation data from such models directly into climate change impact studies may not reflect the proper spatial and temporal characteristics of the area's original precipitation pattern. Additional climate variables from large scale atmospheric circulation pattern are commonly used to predict precipitation in an area. The choice of appropriate predictors is thus one of the most important steps in downscaling process. Rainfall can be related to air mass transport and thus related to atmospheric circulation, which is a consequence of pressure differences

and anomalies (Bardossy, 1997). Mean sea level pressure is the basis of derived variables such as surface vorticity, airflow strength, meridional and zonal flow components and divergence (Wilby and Wigley, 2000). Specific humidity is reported to have significance to AOGCM precipitation schemes (Hennessy et al., 1997). Considering all the above factors, predictor variables mentioned in Table 4.3 are initially chosen to generate precipitation in this study.

Table 4.3: Definition of Predictor Variables

Predictors	Abbreviations
Precipitation (mm/day)	P
Maximum temperature (^{0}C)	Tmax
Minimum temperature (^{0}C)	Tmin
Mean sea level pressure (Pa)	PRMSL
Specific humidity (Kg/ Kg)	SPFH
Zonal (eastward) wind velocity component (m/s) at 10 m	UGRD
Meridional (northward) wind velocity component (m/s) at 10 m	VGRD

Daily observed precipitation (precip), maximum and minimum temperature (Tmax and Tmin) data from 22 stations covering the UTR basin for the period of 1979-2005 is collected from the Environment Canada (Table 4.4). The rest of the atmospheric variables are collected from NARR reanalysis dataset for a period of 1979 – 2005. Precipitation values less than 0.5 mm day^{-1} are considered zero as suggested by Reid et al. (2001) and Choi et al. (2007). NARR data for this study has been made available through the Data Access Integration of Environment Canada (DAI, 2009).

Table 4.4: Weather Stations used for Uncertainty Estimation

| Serial | Station Name | Location | | | Correlation |
		Latitude (^{0}N)	Longitude (^{0}W)	Elevation (m)	
1	Blyth	43.72	81.38	350.50	0.42
2	Brantford	43.72	81.38	196.00	0.65
3	Chatham	42.38	82.20	180.00	0.49
4	Delhi	42.87	80.55	231.70	0.66
5	Dorchester	43.00	81.03	271.30	0.79
6	Embro	43.25	80.93	358.10	0.70
7	Exeter	43.35	81.50	262.10	0.57
8	Fergus	43.73	80.33	417.60	0.56
9	Foldens	43.02	80.78	328.00	0.73
10	Glen Allan	43.68	80.71	400.00	0.57
11	Hamilton A	43.17	79.93	237.70	0.67
12	Ilderton	43.05	81.43	266.70	0.70
13	London A	43.03	80.15	278.00	0.56
14	Petrolia Town	42.86	82.17	201.20	0.52
15	Ridge Town	42.45	81.88	205.70	0.68
16	Sarnia	43.00	82.32	180.60	0.63
17	Stratford	43.37	81.00	345.00	0.61
18	St. Thomas	42.78	81.17	209.10	0.68
19	Tilsonburg	42.86	80.72	213.40	0.73
20	Waterloo A	43.46	81.38	317.00	0.72
21	Woodstock	43.14	80.77	281.90	0.49
22	Wroxeter	43.86	81.15	335.00	0.42

Data source: National Climate Data and Information Archive of Environment Canada

(http://climate.weatheroffice.ec.gc.ca/climateData/canada_e.html, Retrieved 14/11/2007)

While the direct downscaling of minimum and maximum temperature has produced good results, precipitation values are not well reproduced directly from AOGCM data

(Brissette et al., 2006). For selection of appropriate conditioning variables, several combinations of predictors are used to generate synthetic versions of the historic dataset. A multi-objective compromise programming tool (Simonovic, 2009) is then used to find an optimal set of predictors. Assessment of trade-offs between different combinations of variables (considered as alternatives) is done according to four variability measures (considered as criteria): mean, standard deviation, maximum and minimum values for each month. The rank of each combination is measured by the compromise programming distance metric which is calculated as the distance from the ideal solution for each alternative. More Information about the compromise programming method can be found in Appendix C. Table 4.5 presents the ranks obtained for each combination of predictors. It is clearly seen that a combination of all seven predictors is the closest to the ideal solution in most months and hence, is selected for further analysis.

Table 4.5: Rank Table of Different Combinations of Predictors

Cases	Months					
	1 2	3 4	5 6	7 8	9 10	11	12
P, Tmax, Tmin, PRMSL	7 6	5 6	3 1	1 5	7 4	6	1
P, Tmax, Tmin, PRMSL, SPFH	4 1	7 5	4 2	7 7	6 1	3	7
P, Tmax, Tmin, PRMSL, SPFH, UGRD, VGRD	**5 2**	**2 4**	**2 4**	**3 3**	**1 6**	**4**	**2**
P,Tmax,Tmin,PRMSL,UGRD,VGRD	6 4	1 7	7 5	2 1	4 2	5	6
P, Tmax, Tmin, SPFH	3 7	4 1	5 3	6 2	5 3	7	4
P, Tmax, Tmin, SPFH, UGRD, VGRD	2 3	6 3	1 7	5 6	3 5	2	5
P, Tmax, Tmin, UGRD, VGRD	1 5	3 2	6 6	4 4	2 7	1	3

* P: Precipitation, Tmax: Maximum temperature, Tmin: Minimum temperature, PRMSL: Mean sea level pressure, SPFH: Specific humidity, UGRD: Eastward wind component, VGRD: Northward wind component

Generation of Future Climate Change Scenarios

For developing future climate change scenarios, climate outputs from 15 different AOGCM models and scenarios (Table 4.2) are extracted from CCCSN website. Four time slices: 1960-1990 (baseline), 2011-2040 (2020's), 2041-2070 (2050s) and 2071-2100 (2080s) are selected for extracting data for seven variables (minimum temperature, maximum temperature, precipitation, specific humidity, northward wind component, southward wind component and mean sea level pressure).

Six AOGCM models are collected, each with two to three emissions scenarios, as specified by the IPCC's Special Report on Emissions Scenarios (Nakicenovic et al, 2000). Full descriptions of the AOGCMs and emissions scenarios used in the study can be found in Appendices D and E. Both NARR and the AOGCM datasets are processed to conform to the station's grid points.

Monthly information from each of the AOGCM emission scenarios is collected for four time slices: 1961-1990, 2011-2040 (2020s), 2041-2070 (2050s) and 2071-2100 (2080s). Because of the limited quality and unavailability of daily inputs from many AOGCMs, monthly inputs should be used. Climate variables from nearest grid points are interpolated to provide a dataset for each of the stations of interest in the same way as the NARRs. In order to generate future climate data, the difference between the base climate and the AOGCM outputs (2020s, 2050s, 2080s) are computed for all predictors. The change factors are then used to modify the historic datasets collected for each station to create future datasets. The differences between current and future climate are used to calculate monthly change factor and added with the predictors to generate a modified

103

time series. These modified datasets are used as input into the weather generator to produce synthetic datasets of any length for the time period of interest.

Weather Generator Performance Evaluation

In order to reduce multi-dimensionality and collinearity associated with the large number of input variables, principal component analysis is integrated with the weather generator. The process requires selection of appropriate principal components (PCs) that will adequately represent most information in the original dataset. It is found that the first PC is able to explain over 95% of the variations associated with the inputs. Hence, only first PC is considered for the weather generator.

The weather generator model described in section 3.2.2 is used to simulate climatic input for different climate scenarios. This study uses 22 stations for the period of 1979-2005 (N=27) to simulate precipitation scenarios using seven meteorological variables. Employing the temporal window of 14 days (w=14) and 27 years of historic data (N=27), 404 days are considered as potential neighbors *(L=(w+1) x N-1=404)* for each variable. 12 different runs, each comprising of 27 years of daily precipitation are generated. Errors in the estimates of mean and variance of generated precipitation are evaluated using statistical hypothesis test at 95% confidence level. The performances of the weather generator outputs are evaluated using Wilcoxon Rank test and Levene's test described in section 4.2.3. Frequency distributions of the wet and dry spells are compared to examine its ability to reproduce the historic information. Downscaled outputs from AOGCM may still contain bias from the initialization of different climate models. So the monthly mean of the AOGCM outputs are replaced with the historical observed mean in the downscaled

outputs. Using the kernel density estimators described in section 3.2.2 bandwidths are calculated for each time step. Density functions derived for the summer and winter seasons are compared. The generated daily data downscaled using WG-PCA are averaged to monthly value to draw PDF for the comparison with the BA-REA approach. The average monthly total values for winter (DJF) and summer (JJA) for each scenario are considered. Values from each AOGCM for any specific year are considered as an independent set of realization and are used to draw PDFs.

4.3.3 Uncertainty Estimation of Extreme Precipitation Indices

Most efforts related to climate change impact on precipitation are focused on studying the changes in means, although extremes usually have the greatest and most direct impact on the environment. Study on the detection of changes in extremes is limited and hence needs further investigation. For investigating the severity of extreme precipitation events, the indices described in section 3.2.3 are divided into five different categories. Table 4.6 presents the classification scheme of the severity level.

Table 4.6: Classification of Extreme Precipitation Indices based on Percentile Approach

Serial	Description
1	<= 25th percentile of 1961-1990 observed precipitation
2	25th – 50th percentile of 1961-1990 observed precipitation
3	50th –75th percentile of 1961-1990 observed precipitation
4	75th – 95th percentile of 1961-1990 observed precipitation
5	>95th percentile of 1961-1990 observed precipitation

Performance Evaluation

In presence of uncertainties from different AOGCMs and scenarios, it is possible that the future distribution of extremes will be different than historical extremes. Furthermore, because each model provides different realizations of future climate, it is also possible that their distribution will differ in between different scenarios of the same model. The extreme indices data calculated from the downscaled AOGCM outputs are compared using different distributions to search for an optimal distribution of fit. The performances of the distribution fits are ranked using three goodness-of-fit test results: Kolmogorov-Smirnov test, Anderson-Darling Estimate and Chi-Squared Test.

Kolmogorov-Smirnov Test

The Kolmogorov-Smirnov test is used to decide whether the sample comes from a hypothesized continuous distribution. The samples $x_1, x_2, \ldots \ldots, x_n$ are assumed to be random, originating from some distribution with Cumulative Distribution Function (CDF) $F(x)$. The Kolmogorov-Smirnov statistic (D) is based on the largest vertical difference between the theoretical and the empirical CDF:

$$D = \max_{1 \leq i \leq n} \left(F(x_i) - \frac{i-1}{n}, \frac{i}{n} - F(x_i) \right) \tag{4.10}$$

Anderson-Darling Estimate

The Anderson-Darling procedure compares the fit of an observed CDF to an expected CDF. The method provides greater weight to the tail distribution than the Kolmogorov-Smirnov test. The Anderson-Darling statistic A^2 is expressed as:

$$A^2 = -n - \frac{1}{n} \sum_{i=1}^{n} (2i - 1) . \left[lnF(X_i) + \ln\left(1 - F(X_{n-i+1})\right)\right]$$ (4.11)

Chi Squared Test

The Chi–squared test is used to determine if a sample comes from a specific distribution. The test statistic is expressed as:

$$\chi^2 = \sum_{i=1}^{k} \frac{(O_i - E_i)^2}{E_i}$$ (4.12)

where,

O_i is the observed frequency;

E_i is the expected frequency calculated by:

$$E_i = F(x_2) - F(x_1)$$

Where,

F is the CDF of the probability distribution being tested; and

$x_1 \ and \ x_2$ are the limits of the ith bin.

In terms of hypothesis tests, the distributional form is rejected at the chosen significance level α if the test statistic is greater than the critical value defined as: $\chi^2_{1-\alpha,k-1}$, representing the Chi-squared inverse CDF with $k - 1$ degrees of freedom and a significant level of α.

Selection of Bandwidths

Several bandwidth selection methods are applied on the precipitation indices for investigating an appropriate bandwidth to be used in the kernel estimation process. To measure how well the bandwidth selection methods perform, this section proceeds with

the comparison of various bandwidth selectors by applying them in the assessment of extreme precipitation indices. Figure 4.4 present kernel density estimates with statistics constructed using several bandwidth selectors: (i) the rule of thumb (ROT; by Silverman, 1986) as explained in section 3.2.2), (ii) Least square cross validation (LCV) which searches for bandwidth based on likelihood (by Terrell and Hall, 1990, as explained in section 3.2.4) and (iii) the plug in estimator that selects the bandwidth using the pilot estimator of the derivatives refined by Sheather and Jones, 1991 (SJPI; named after Sheather-Jones plug in estimator (section 3.2.4)). The choice of kernel is strictly limited to examining two of the most widely used types: Gaussian and Epanechnikov kernels, the functions of which are expressed as:

$$\text{Gaussian:} \qquad K(u) = \frac{1}{\sqrt{2\pi}} e^{-\frac{1}{2}u^2}$$

$$\text{Epanechnikov:} \qquad K(u) = \frac{3}{4}(1 - u^2)$$

The 'original' estimate is created by mixing the inputs and 1000 samples are generated from the mixtures without any estimation of bandwidth. This estimate is created for assessing how different techniques respond to the original data type. By comparing the generated estimators it can be seen that the density estimate using ROT is highly over-smoothed which may have missed important features of the generated data. For both kernel types, it failed to capture the multimodality. In the case of LCVs, there are suggestions of multiple modes in the density curve. However, it is still severely under-smoothed; the small bumps occurring from the uncertainties of different AOGCM types make it harder to understand the structure of real data. The bandwidth by
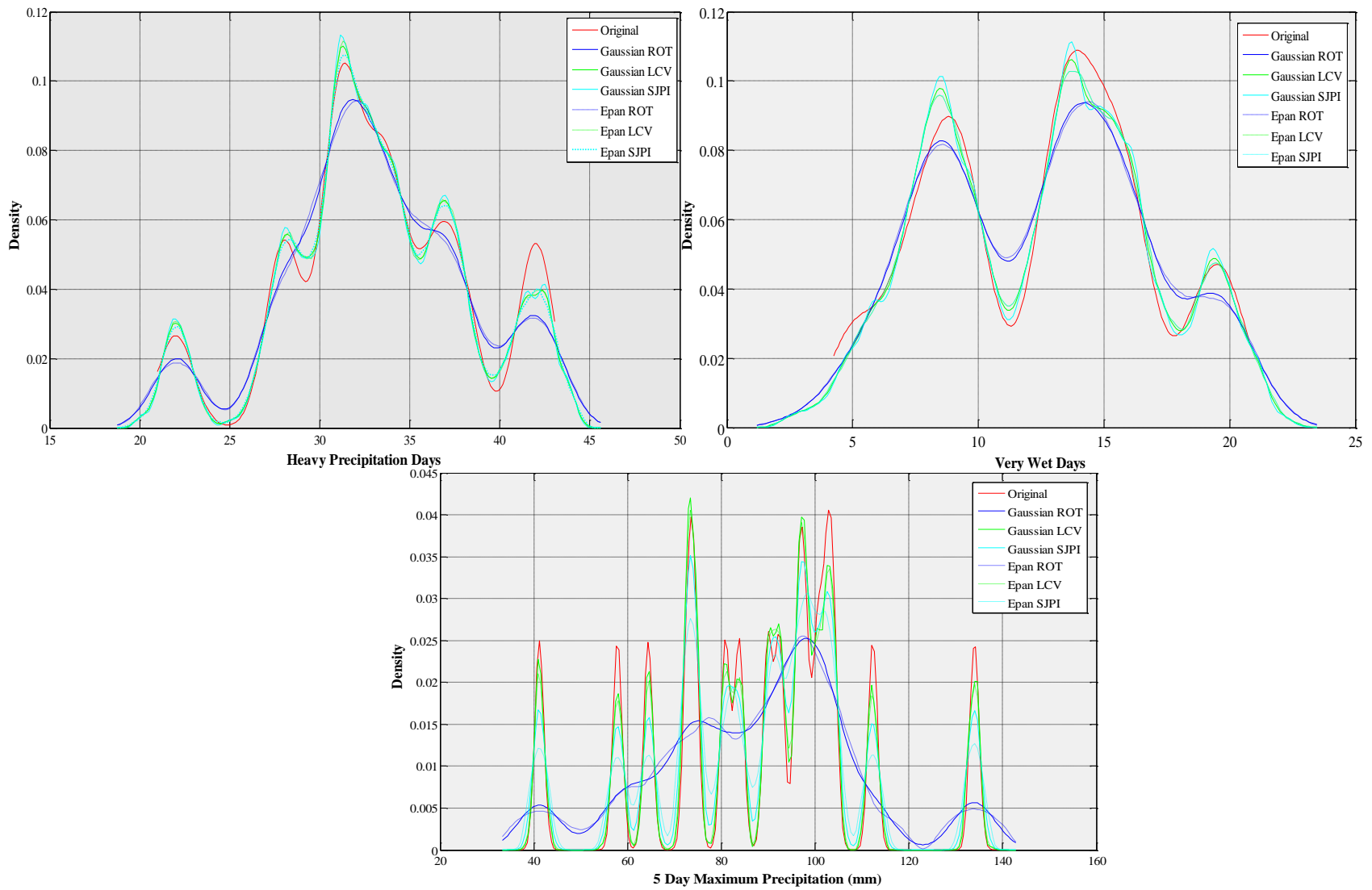
Figure 4.4: Comparison of Various Bandwidths of Extreme Precipitation Indices

SJPI seems to be in a better agreement with the 'original' estimate and provides a strong indication of multimodal distribution. From Figure 4.4, it is also evident that the choice of kernel merely plays a role in the estimation of density. So for the present study, the Gaussian kernel with a Sheather-Jones plug in (SJPI) estimator is used to calculate the bandwidth for estimating density of the extreme precipitation indices.

4.4 Intensity-Duration-Frequency Analysis

The major focus of the development of intensity-duration-frequency design curves for future climate involves analyzing changes in extreme rainfall at local level. Any change in the rainfall pattern may demand revision of design standards or new regulations in storm water management strategies, guidelines and design practices. Most of the design standards used for the municipal water management infrastructure depends on rainfall. Present research thus uses rainfall as input to examine the changes in the annual extreme rainfall with the expected changes in climate. This section describes the selection and processing of rainfall data and methods applied for generating IDF curves for the city of London.

4.4.1 Data Selections

Hourly rainfall data covering stations around London for the period of 1965-2003 (Figure 4.5) has been extracted from the Data Access Integration Network (DAI, 2009). Daily rainfall data for the same stations and same time period is obtained from

Environment Canada (http://climate.weatheroffice.ec.gc.ca/climateData/canada_e.html, Retrieved on 10/08/2010).
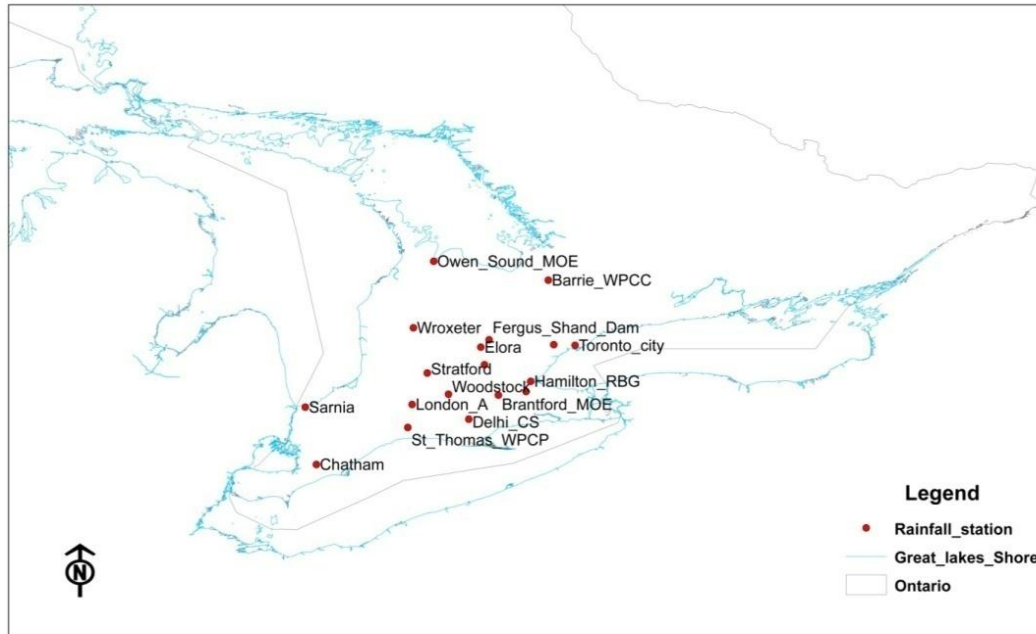
Figure 4.5: Meteorological Stations used for IDF Analysis

The station selection process is highly dependent on the availability of hourly data of adequate length. This is an important step in running nearest neighbor based weather generator used in the present study. The number of stations used in the K-NN algorithm influences computation of regional means and the Mahalanobis distance (see section 3.2.2 for details), which affects the choice of the nearest neighbor. Data of shorter durations are available only for a handful of stations. So stations closer to London but with shorter record have not been considered in this study. At first, all hourly stations within 200 km radius of London are considered. Next, stations with data going back to 1965 with a record till 2003 are selected. Figure 4.5 and Table 4.7 present the details of stations used initially for IDF analysis.

Table 4.7: Rain Gauge Station Details

Climate ID	Station Name	Latitude (deg)	Longitude (deg)	Elevation (m)	Distance from London (km)
6110557	Barrie WPCC	44.3758	-79.6897	221	190
6140954	Brantford MOE	43.1333	-80.2333	196	75
6131415/6	Chatham WPCP	42.39	-82.2153	180	113
6131982/3	Delhi	42.8667	-80.55	232	52
6142285/6	Elora	43.65	-80.4167	376	91
6142400	Fergus	43.7347	-80.3303	418	102
6153194	Hamilton A	43.1717	-79.9342	238	100
6153300/1	Hamilton RBG	43.2833	-79.8833	102	106
6144475/8	London Int'l A	43.0331	-81.1511	278	0
6116132	Owen Sound MOE	44.5833	-80.9333	179	173
6127519	Sarnia	43	-82.3	181	93
6137361/2	St. Thomas	42.7833	-81.1667	236	28
6148105	Stratford MOE	43.3689	-81.0047	345	39
6158350	Toronto	43.6667	-79.4	113	158
6158733	Toronto Int'l A	43.6772	-79.6306	173	142
6149387	Waterloo A	43.45	-80.3833	317	78
6119500	Wiarton A	44.7458	-81.1072	222	190
6149625	Woodstock	43.1361	-80.7706	282	33

The number of stations used to generate long sequence of rainfall series influence outputs of weather generator. Stations surrounding the station of interest help to capture the spatial and temporal characteristics in the region. In cases where only limited data are available, surrounding stations may help to add spatial and temporal characteristics of the rainfall values. Conversely, use of too many stations can be computationally expensive and unnecessary; especially for short duration rainfall where convective storms are highly

localized weather patterns, operating on relatively small spatial scales. Stations located too far may affect the performance of the weather generator. So regression and cross correlation analysis are performed for identifying important stations for London. For regression analysis, the stations are grouped based on selected distances from London (Table 4.8). Regression results for each group are provided in the Appendix F. The results are expressed in terms of t-test statistics, p values and the coefficient of determination.

Table 4.8: Groups for Regression Analysis based on Distances

Stations	Groups based on Distances (km)						
	0-200	0-175	0-150	0-125	0-100	0-75	0-50
Barrie WPCC	√						
Brantford MOE	√	√	√	√	√	√	
Chatham WPCP	√	√	√	√			
Delhi	√	√	√	√	√	√	
Elora	√	√	√	√	√		
Fergus	√	√	√	√			
Hamilton A	√	√	√	√	√		
Hamilton RBG	√	√	√	√			
London Int'l A	√	√	√	√	√	√	√
Owen Sound MOE	√	√					
Sarnia	√	√	√	√	√		
St. Thomas WPCP	√	√	√	√	√	√	√
Stratford MOE	√	√	√	√	√	√	√
Toronto	√	√					
Toronto Int'l A	√	√	√				
Waterloo A	√	√	√	√	√		
Wiarton A	√						
Woodstock	√	√	√	√	√	√	√
Total	18	16	14	13	10	6	4

Results from the Appendix F show significant t-test statistic for all predictors reducing the possibility of over-fitting by an insignificant predictor. The term 'probability value' *(p)* denotes the results of the testing of hypothesis that the regression coefficient is equal

to zero which in turn quantifies the importance of the regressor. The null hypothesis says that the coefficient of the predictor is equal to zero and the alternate hypothesis says the coefficient of predictor is different than zero. So the *p* value below the cut off level (0.05) denotes that the coefficient of that particular predictor is not zero and can be an important addition to the model. Low or near zero value is desirable as it is inversely related to the importance of a predictor (Minitab Inc., 2007). The t-statistics for the independent variables are equal to their coefficient estimates divided by their respective standard errors. In theory, the t-statistic of any one variable may be used to test the hypothesis that the true value of the coefficient is zero (which is to say, the variable should not be included in the model). In a standard normal distribution, only 5% of the values fall outside the range plus-or-minus 2. Low t-statistic (or equivalently, a moderate-to-large exceedance probability) of a variable suggests that the standard error would not be adversely affected by its removal. The rule-of-thumb in this regard is to remove the least important variable if its t-statistic is less than 2 in absolute value, and/or the exceedance probability is greater than .05 (Minitab Inc, 2007). From the t-statistic results it is seen that stations within 100 km distance appear to be the best option for London. This can also be clearly seen from the coefficient of determination plot in Figure 4.6
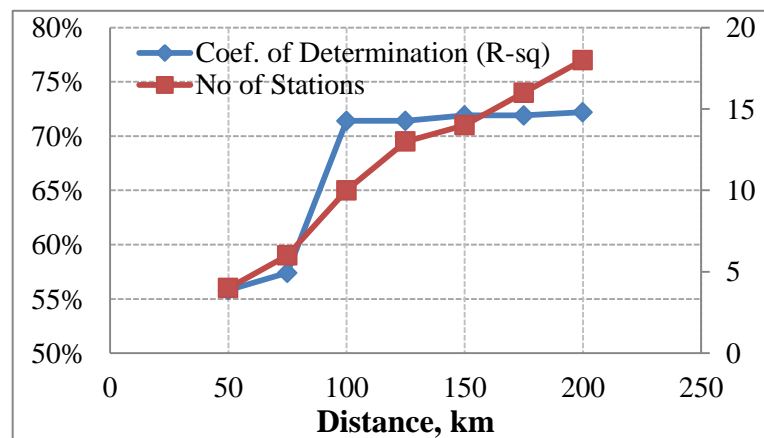
Figure 4.6: Performances of Stations based on Distance

114

where addition of more stations, beyond 100 km distance apparently cannot improve the model performance.

Next, the cross correlation analysis is performed to identify the correlation between the stations (Table 4.9). Results show that stations within 100 km radius are correlated well, with correlation greater than 60% for all stations but Elora. However, the regression test shows that inclusion of Elora may provide important information to the spatial and temporal pattern for London and therefore it is included in the IDF analysis. Finally, nine stations with hourly and daily rainfall data from 1965-2003, located within 100 km radius of London station have been selected for further analysis.

Table 4.9: Cross-Correlation Results for Stations Within 200 km Distance from London

Stations	Distance (km)	Lag				
		-2	-1	0	1	2
London A	0	-0.004	0.094	1.000	0.094	-0.004
Waterloo A	78	-0.004	0.063	0.729	0.097	0.000
Woodstock	33	0.003	0.273	0.723	0.022	-0.012
Sarnia	93	0.018	0.131	0.676	0.054	-0.014
Hamilton A	100	0.003	0.050	0.670	0.136	-0.008
Delhi CS	52	-0.004	0.236	0.657	0.020	-0.014
Brantford MOE	75	0.000	0.249	0.645	0.026	-0.019
Stratford MOE	39	-0.005	0.263	0.633	0.028	-0.004
Hamilton RBG	106	0.002	0.214	0.618	0.037	-0.008
Toronto Int'l A	142	-0.002	0.043	0.610	0.125	0.000
St. Thomas WPCP	28	-0.009	0.344	0.609	0.030	-0.008
Fergus	102	-0.005	0.203	0.564	0.033	-0.009
Toronto	158	-0.005	0.158	0.564	0.028	-0.012
Elora	91	-0.002	0.199	0.550	0.066	0.002
Chatham WPCP	113	-0.006	0.278	0.488	0.008	-0.013
Barrie	190	-0.010	0.122	0.461	0.062	-0.007

Wiarton A	190	-0.021	0.049	0.454	0.101	-0.009
Owen Sound	173	-0.024	0.146	0.373	0.047	-0.005

Both historical daily and hourly data contains missing values. Inverse distance weighted method is applied to the daily data to fill the missing values.

4.4.2 Development of Climate Change Scenarios

For this study, precipitation data for two time slices: 1960-1990 (baseline) and 2071-2100 (2080s) are collected. It is important to note here that the AOGCMs provide only precipitation data which includes both snow and rainfall, especially during winter. They do not count for rainfall change information. Hence for this study, change in the precipitation between different AOGCM scenarios and historical observed precipitation are used to calculate the change fields and are applied to the historical daily rainfall data to develop modified rainfall series for input in the weather generator. A total of 27 scenarios from 11 AOGCMs, each with two to three emission scenarios (Nakicenovic et al, 2000) are selected for developing future scenarios. Full descriptions of the emissions scenarios and AOGCMs can be found in Appendices D and E. Table 4.10 provides a complete list of the details of the AOGCM scenarios used in this study.

Climate change scenarios from AOGCM outputs are used to condition the input data using the weather generator. Outputs from AOGCMs for 1961-1990 represent baseline climate against which the future climate change scenarios for 2071-2099 (2080s) are computed. Based on the AOGCM data, change fields for each scenario are calculated as the difference between the monthly mean precipitation from their 1961-1990 mean. This

difference is then multiplied with the locally observed station data to generate climate

change scenarios appropriate for the City of London at a daily time scale.

Table 4.10: List of AOGCM Models and Emission Scenarios

GCM models	Sponsors, Country	SRES scenarios	Atmospheric resolution	
			Lat	Long
CGCM3T47, 2005	Canadian Centre for Climate Modelling and Analysis, Canada	A1B, A2, B1	3.75°	3.75°
CGCM3T63, 2005		A1B, A2, B1	2.81°	2.81°
CSIROMK3.5, 2001	Commonwealth Scientific and Industrial Research Organization (CISRO) Atmospheric Research, Australia	A1B, A2, B1	1.875°	1.875°
ECHAM5AOM, 2005	Max Planck Institute for Meteorology, Germany	A1B, B1, A2	1.875°	1.875°
ECHO-G, 1999	Meteorological Institute of the University of Bonn, Meteorological Research Institute of the Korea Meteorological Administration (KMA), and Model and Data Group, Germany/Korea	A1B, B1, A2	3.9°	3.9°
GFDLCM2.1, 2005	U.S. Department of Commerce/ National Oceanic and Atmospheric Administration (NOAA)/Geophysical Fluid Dynamics Laboratory (GFDL), USA	A1B, B1, A2	2°	2.5°
GISSAOM, 2004	National Aeronautics and Space Administration (NASA)/ Goddard Institute for Space Studies (GISS), USA	A1B, B1	3°	4°
MIROC3.2HIRES, 2004	Centre for Climate System Research (University of Tokyo), National Institute for Environmental Studies, and Frontier Research Centre for Global Change (JAMSTEC), Japan	A1B, B1	1.125°	1.125°
MIROC3.2MEDRES, 2004		A1B, A2, B1	2.8°	2.8°
CCSR/NIES B21, 1999	Centre for Climate System Research, University of Tokyo and National Institute for Environmental Studies, Japan	B21	5.6°	5.6°
CSIROMK2b, 1997	Commonwealth Scientific and Industrial Research Organization (CISRO) Atmospheric Research, Australia	B11	5.6°	3.2°

As an example, if the change field for the month of July and August are 10% and -5%, all daily July and August rainfall values are multiplied by a factor of 1.05 and 0.95, respectively. This newly modified data is then used with the weather generator to generate daily time series of any preferred length for different scenarios. For this study, 27 different climate scenarios are developed which represent different realizations of future.

4.4.3 Development of Methodology

Once preparation of data is complete, daily weather generator described in section 3.2.2 is used to simulate a sequence of rainfall for all stations. For the verification purpose, the perturbation of the weather generator is kept off in order to replicate the exact scenario as the historical observed one. This study uses 10 stations for the period of 1965-2003 (N=39) to simulate different rainfall scenarios. Employing the temporal window of 14 days (w=14) and 39 years of historic data (N=39), 584 days are considered as potential neighbors *(L=(w+1) x N-1=584)*. Each case is simulated three times thus generating 117 years of output sequences. It is expected that such length of output is sufficient enough to estimate event with return period of 100 years. Following this, the hourly disaggregation algorithm is applied to the generated data on an hourly time scale. Important parameters for the disaggregation model include:

Events: Any event for which rainfall continued for two or more days are considered as events.

Moving window: Any specific number of days in which the current daily rainfall will be compared to search for similar (nearest neighbour) events is called moving window which is fixed as 50 days here.

Weights: Weights used in the process determine which historical hourly ratio would be the best for the data. Comparison of different combinations of weights have projected that the value of $w_1 = 0.2$ and $w_2 = 0.8$ in equation 3.57 provides the closest fit and are selected in this research.

For analyzing the performance of the methodology combining the daily weather generation and hourly disaggregation method, one additional scenario called 'historical unperturbed' is created by keeping the perturbation module off in the weather generator. This scenario just reproduces the historical daily information and the results are used in the disaggregation model to generate hourly values. The performance of the weather generator and disaggregation model to reproduce historical data is evaluated using box-whiskers plot and the frequency plots, respectively.

The perturbation process inside the weather generator is next applied to generate IDF information using the historical observed rainfall. This scenario called 'historical perturbed' assumes that the future climate will remain the same ignoring any change in the future climate due to enhanced green house gas emissions. The daily downscaled outputs from different climate scenarios, prior to disaggregation are tested for bias correction. Comparison of 1961-1990 mean historical observed rainfall with those developed from different scenarios for base climate reveal that significant bias still exit in the base climate which is used to initialize the future climate; which means the bias might be carried out in the downscaled output.

The IDF curves generated using the 'historical unperturbed' scenario is compared with the IDF information available from Environment Canada. The relative differences between the two cases are compared by the following relation:

$$Relative\ difference = \frac{|x_1 - x_2|}{\dfrac{x_1 + x_2}{2}} \times 100 \qquad\qquad (4.13)$$

The IDF values generated from different climate scenarios represent wide range of uncertainties. The kernel estimator based plug-in approach is thus applied to combine information at each yearly time step. Weights are produced from the intensities of different durations of rainfalls for different return periods. Once the weighted plot is derived, probabilities for the IDF values at 1, 2, 6, 12 and 24 hours durations are presented for 2, 5, 10, 25, 50 and 100 year return periods in terms of cumulative distribution plots.

CHAPTER FIVE

RESULTS AND DISCUSSION

This chapter presents simulated results for the models, methods and algorithms developed in Chapter 3 and 4 and applied for the Upper Thames River basin. The results are divided into the following categories: First, the comparative performances of the reanalysis datasets are presented. Performances of the PCA integrated weather generator are next evaluated for deriving future climate signals. A total of 15 different scenarios are developed. They are used to estimate uncertainties using non-parametric kernel estimators. The results obtained are compared with Bayesian based reliability ensemble average (BA-REA), a second multi-model uncertainty estimation method. Selection of appropriate kernel method is further examined for extreme precipitation events. The results are presented in terms of probability density estimates. Finally, results for developing a probability based rainfall intensity-duration-frequency (IDF) curves using 27 different climate signals are presented.

5.1 Assessment of Reanalysis Data

The analyses of the results are evaluated for climate change and hydrologic modeling studies. First, the performance of the temperature and precipitation from NNGR and NARR datasets, interpolated to the stations around the Upper Thames River basin are examined. A trend analysis is performed to see whether the reanalysis dataset is capable

of capturing the yearly temperature trend in the observations. Student's t and F tests are performed to check for the similarity of the means and variances for both data types with respect to observations. Next, changes in temperature anomalies over the years are compared. For precipitation, the performance of both datasets is analyzed in terms of goodness-of-fit measure. The cumulative precipitation of selected stations during the year of 2000 is computed. The second part of the analysis contains an evaluation and comparison of the daily discharge generated by the HEC-HMS model. The results for three stream gauges within the basin: Byron, Ingersoll and St. Mary's are presented. Performances of the NNGR and NARR generated discharges are compared with the historical simulated flow using statistical goodness-of-fit measure: the root mean square error (RMSE), correlation coefficient (r), normalized mean squared error (NMSE), mean absolute error (MAE) and relative bias (RB). The output (daily discharge) is assessed by comparison graphs, scatter plots and confidence interval plots. Because of the existing model and data errors, it is necessary to use appropriate criteria for estimating the relevant uncertainties (Sorooshian, 1993). In this study, only data uncertainty arising from (i) the inconsistency and non-homogeneity, and (ii) the inadequate representation of the reanalysis data due to space and time limitations, are assessed. The error arising from the data source is evaluated by estimating the mean and variance.

5.1.1 Reanalysis Data Performance Results

The abilities of the NNGR and NARR to capture the inter-annual variability of temperature and precipitation are presented in this section on a station-by-station basis. These stations are situated within and around the Upper Thames River basin.

Temperature

Table 5.1 presents the quality of daily temperature data from NNGR and NARR with respect to the observations in terms of bias and correlation. Correlations are above 0.95 in the case of both datasets, which indicates that the values are closer to the observations in terms of goodness-of-fit. For all stations, the biases between the datasets are within 25%.

Table 5.1: Comparison of Mean Daily Temperature during 1980-2005

Stations	Mean			Mean Bias		Correlation	
	Observed	NNGR	NARR	NNGR	NARR	NNGR	NARR
Exeter	7.76	8.18	9.25	5.46	19.25	0.98	0.97
Foldens	7.93	8.43	9.21	6.42	16.15	0.98	0.98
Glen Allan	6.70	7.97	7.72	19.00	15.31	0.98	0.98
St. Thomas WPCP	8.60	8.59	9.32	-0.18	8.33	0.98	0.97
Stratford MOE	7.42	8.26	8.48	11.39	14.30	0.98	0.98
Waterloo A	6.96	8.13	8.62	16.87	23.81	0.98	0.98
Woodstock	7.77	8.37	8.70	7.69	11.96	0.98	0.98

Figure 5.1 presents mean monthly temperature at selected stations in the basin. Both reanalysis datasets demonstrate a tendency to over-estimate the observed values, especially during summer. NNGR has repeatedly under-predicted temperature during early spring and winter, thereby indicating higher biases. Except spring and summer, they seem to be in fairly close agreement with observed temperature. NNGR shows a comparatively higher degree of consistency during late spring and fall. Although NARR overestimates throughout the year, it has been able to capture the monthly trend for all stations within 20% bias, except for March where the deviation is very high. Except for
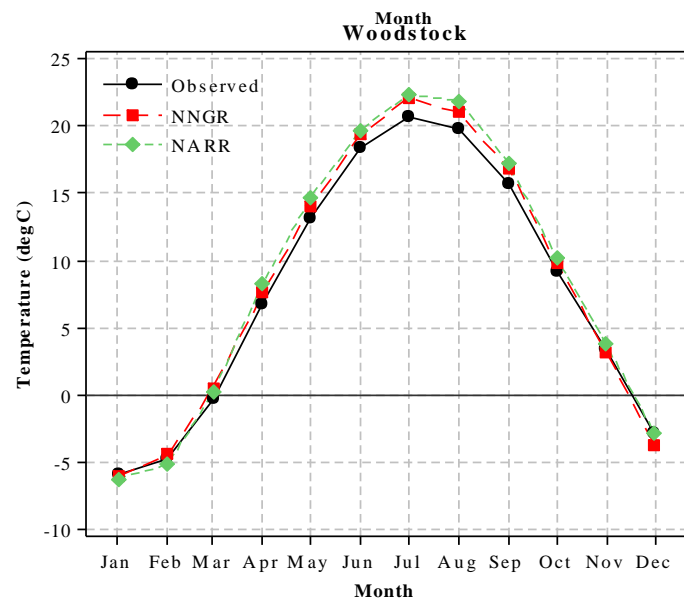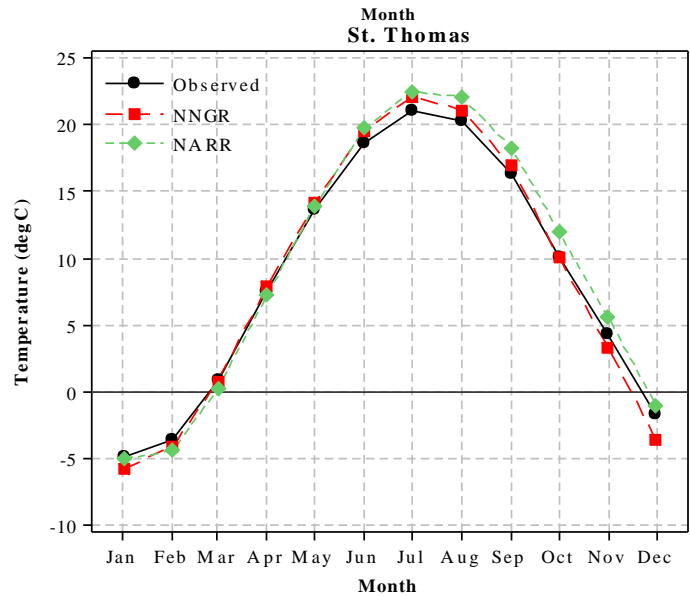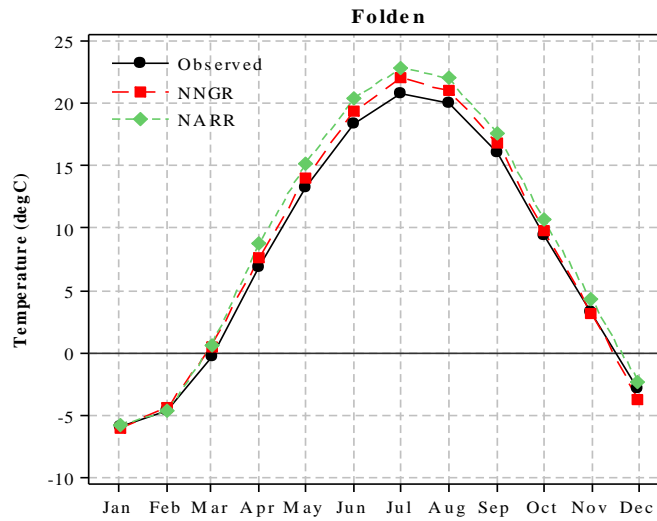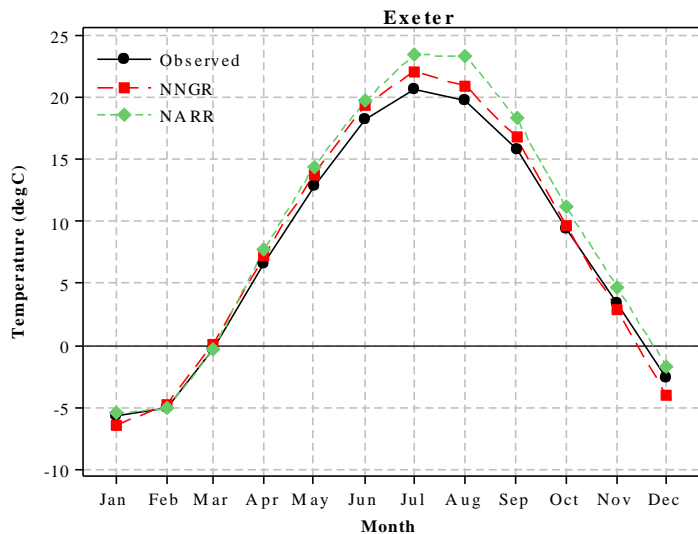
Figure 5.1: Mean Monthly Temperature between Observed (EC) and NNGR/NARR

the above discrepancies, the agreement confirms the findings from previous studies and shows that both NNGR and NARR satisfactorily capture the observed intra-seasonal and annual fluctuations (Kalnay and Cai, 2003, Kalnay et al., 2006, Pielke et al., 2007).

Next, statistical tests are performed on the monthly temperature to determine whether the reanalysis data produces monthly climatological data that are representative of the true climatology. To test the null hypothesis that the reanalysis and observations render consistent monthly means and variances, student's t test and the F test are performed. Table 5.2 (a) presents the student's t test static results for the similarity of means, assuming equal variances for all three datasets.

Table 5.2 (a): t -Test Statistic for Mean Monthly Temperature during 1980-2005

Station	Modified t-Test Static							
	Diff.	95% CI Diff.	t	p	Diff.	95% CI Diff.	t	p
		NNGR				NARR		
Woodstock	-0.59	(-2.15, 0.96)	-0.75	0.45	-0.59	(-2.15,0.96)	-0.75	0.45
St. Thomas	0.02	(-1.51, 1.54)	0.02	0.98	-0.71	(-2.23, 0.81)	-0.92	0.36
Folden	-0.51	(-2.07, 1.05)	-0.64	0.52	-1.27	(-2.85, 0.30)	-1.59	0.11
Exeter	-0.42	(-1.99, 1.14)	-0.53	0.59	-1.48	(-3.07, 0.11)	-1.83	0.07
Glen Allan	-1.27	(-2.86, 0.31)	-1.58	0.11	-1.02	(-2.62, 0.58)	-1.25	0.21
Stratford	-0.84	(-2.4, 0.71)	-1.07	0.28	-1.05	(-2.64, 0.53)	-1.3	0.19
Waterloo A	-1.17	(-2.74, 0.39)	-1.47	0.14	-1.65	(-3.24, -0.1)	-2.03	0.04

The results are presented in terms of the estimates of differences between the observed and NNGR/NARR means, the 95% confidence interval for the differences and the hypothesis results (*t* and *p* values). Confidence intervals are calculated for the selected stations. The range includes 0 values suggesting that there are no differences in means. The probability *(p)* values for all cases are greater than the chosen α level (0.05), which

indicates that there is no evidence of a different mean in the three datasets, except for Waterloo A. Table 5.2 (b) presents the hypothesis test results of the F test for both reanalysis datasets. The p values for the F test also appear to be greater than 0.05, which fails to reject the null hypothesis of the variances being equal. Thus, it is reasonable to assume that the observations and NNGR/NARR have equal variances in F test.

Table 5.2 (b): F Test Static Results for Mean Monthly Temperature during 1980-2005

| Station | F test static | | | |
| | Test static | P value | Test static | P value |
	NNGR		NARR	
Woodstock	1.71	0.191	2.74	0.099
St. Thomas	3.49	0.062	3.36	0.067
Folden	1.05	0.437	2.01	0.157
Exeter	2.54	0.112	4.17	0.052
Glen Allan	1.45	0.23	1.63	0.203
Stratford	2.85	0.092	4.98	0.06
Waterloo A	2.97	0.085	4.97	0.06

A trend analysis has also been tested to determine whether the reanalysis database is consistent with the true trend based on the observations. It is important to note that the reanalysis trends cannot provide reliable estimates of the true atmospheric trends. However, it can be used to check whether the distribution of the reanalysis trends provide a reasonable representation of the expected range of atmospheric trends. Comparison of yearly temperature trends in Table 5.3 shows that in case of NNGR, for all stations but Exeter, a weak negatively inclined trend per year (-0.0085 to -0.1577) is prominent. It suggests a slow cooling drift whereas the observed trend shows a warming trend. NARR,

on other hand, has been able to capture the increased temperature trend with less than 25% error except for Exeter.

Table 5.3: Comparison of Trend Analysis Results during1980-2005

Station	Trends				
	Observed	NNGR	NARR	% Bias NNGR	% Bias NARR
Folden	0.0452	-0.0085	0.0525	-118.81	16.15
Glen Allan	0.0356	-0.0059	0.0443	-116.78	24.44
Exeter	0.0543	0.0011	0.0334	-97.97	-38.49
Stratford	0.0611	-0.0070	0.0495	-111.54	-18.99
St. Thomas	0.0456	-0.0063	0.0556	-113.92	21.93
Waterloo A	0.0341	-0.0035	0.0361	-110.40	5.87
Woodstock	0.0428	-0.0157	0.0407	-136.85	-4.91

Next, temperature anomaly charts are compared in Figures 5.2 (a) through (c) for the summer (June-July-August) and winter (December-January-February) months to check the yearly differences during the period of 1980-2005. The values below 0 represent the years when the mean temperature was underestimated by the reanalysis data; whereas the values above 0 represent the years in which the temperatures were over-estimated. Anomaly charts are particularly useful to assess the magnitudes of temperature changes. The results from different stations are consistent with the evaluated performance of an over-prediction during summer months and variable predictions during winter.
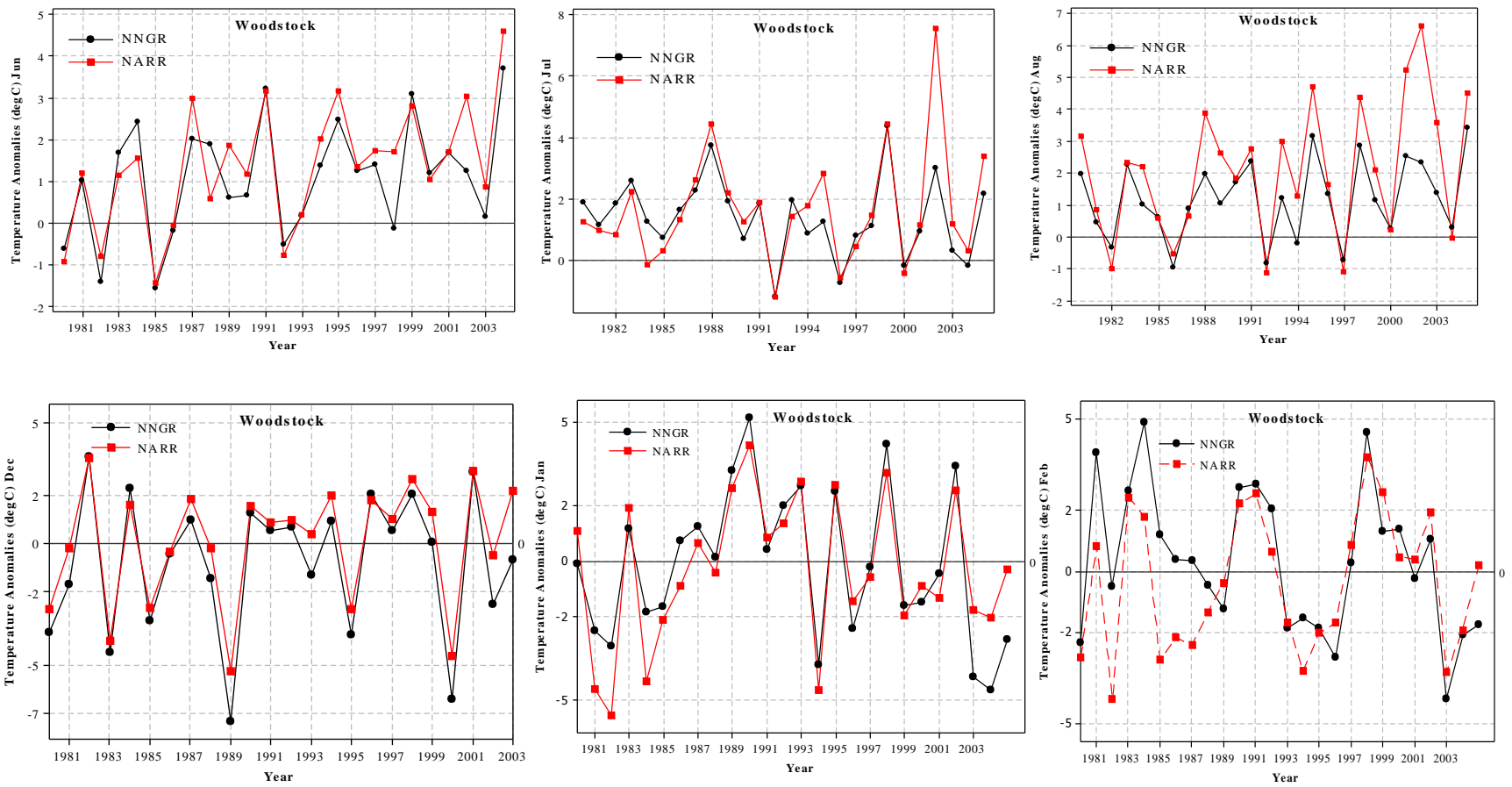
Figure 5.2 (a): Changes in Temperature Anomalies over Woodstock during June-August and December-February (1980-2005)

128
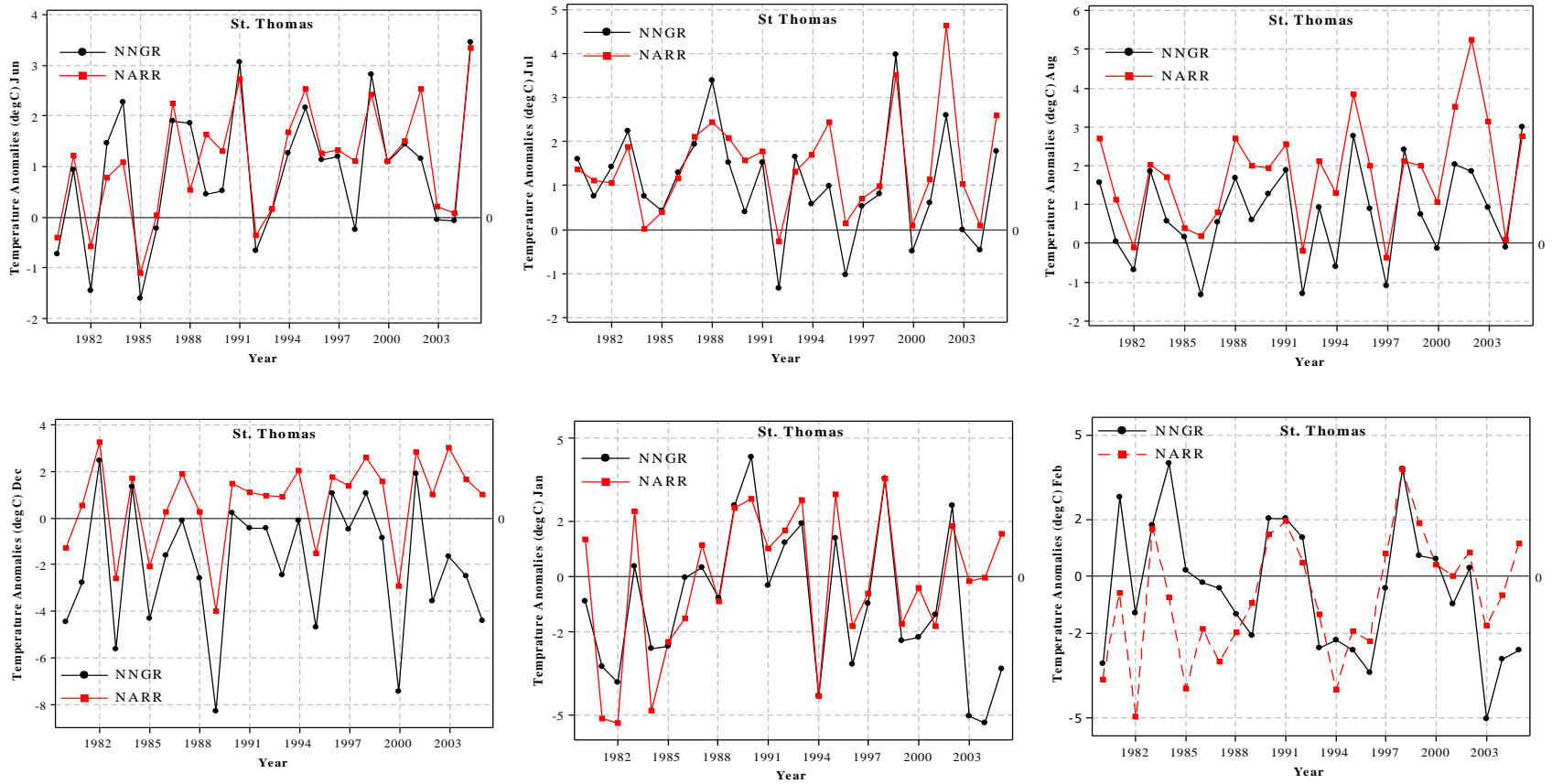
Figure 5.2 (b): Changes in Temperature Anomalies over St. Thomas during June-August and December-February during 1980-2005
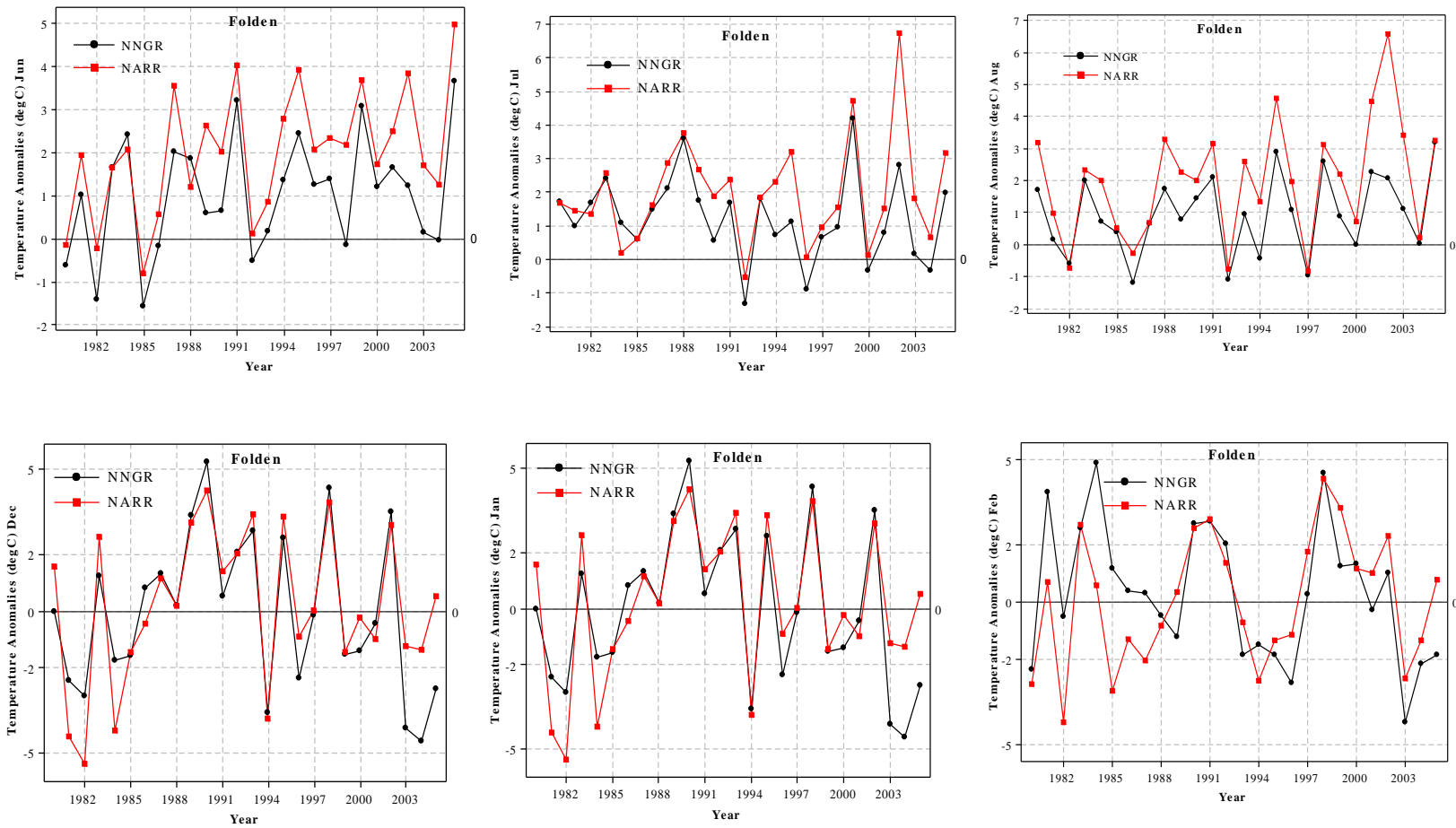
Figure 5.2 (c): Changes in Temperature Anomalies over Folden during June-August and December-February during 1980-2005

130

Precipitation

Precipitation, generally have higher variances than temperature and is more difficult to simulate. Table 5.4 presents the statistics of mean daily precipitation calculated for selected stations around the basin. The variance within the observed precipitation ranges from 64.48 to 78.03, while the variance of NNGR varies from 24.67 to 45.79. The mean bias from NNGR varies between -15.81% and -32.10% with respect to observations, suggesting that it is not able to capture the variability of the precipitation in the region. For NARR, the variance is much higher with values ranging between 29.47 and 71.33 and a mean bias of -5.75 to -31.64%.

Table 5.4: Comparison of Mean Daily Precipitation during 1980-2005

Station	Variance ((mm/day)^2)			Mean Bias (mm/day)		Correlation	
	Obs	NNGR	NARR	NNGR	NARR	NNGR	NARR
Dorchester	75.00	30.00	67.68	-15.81	-7.64	0.36	0.48
Blyth	73.91	24.67	43.43	-32.10	-31.64	0.33	0.40
London A	78.03	45.79	29.47	-24.52	-18.71	0.50	0.50
Exeter	65.60	25.73	46.17	-23.25	-21.73	0.35	0.42
Foldens	75.28	31.83	62.92	-16.28	-13.22	0.36	0.51
Glen Allan	64.48	25.54	56.06	-16.07	-6.11	0.37	0.46
St. Thomas	77.21	29.68	44.33	-21.89	-27.23	0.32	0.48
Stratford	59.81	27.35	71.33	-18.98	-5.75	0.37	0.45
Woodstock	76.65	31.03	68.13	-19.22	-12.78	0.37	0.51

The correlation values are much lower than the temperature, and they also show greater variability by station. The correlation values between observation and NNGR are also below 0.4 except for London station. While for NARR, the correlation appeared higher than the NNGR which implies a higher station-to-station correlation around the grid

points in terms of the goodness-of-fit measure. The inter-station variability in the mean bias and correlation may be related to the individual station locations with respect to local geographic features.

Figure 5.3 (a), (b), and Appendix G present the cumulative daily precipitation graphs of NARR and NNGR at different stations for the year 2000. In Stratford, Woodstock and Waterloo-Wellington, NARR is fairly close to the observed precipitation. In London, however, NNGR data perform slightly better. Interestingly, the gap between the observed and estimated data widens from summer for London, Stratford, St. Thomas, Wroxeter while for Folden, Waterloo-Wellington and Woodstock the datasets followed the observed values closely throughout the year.
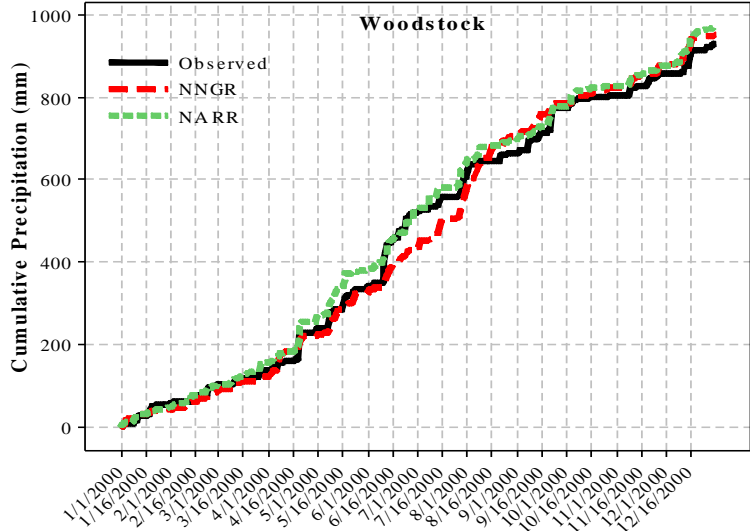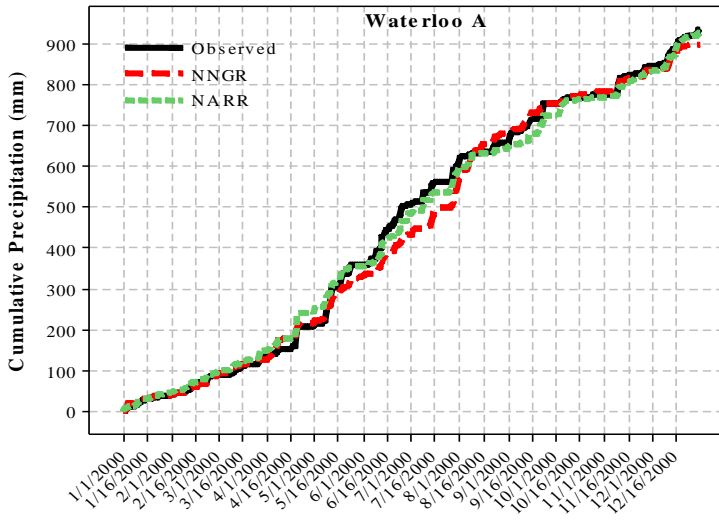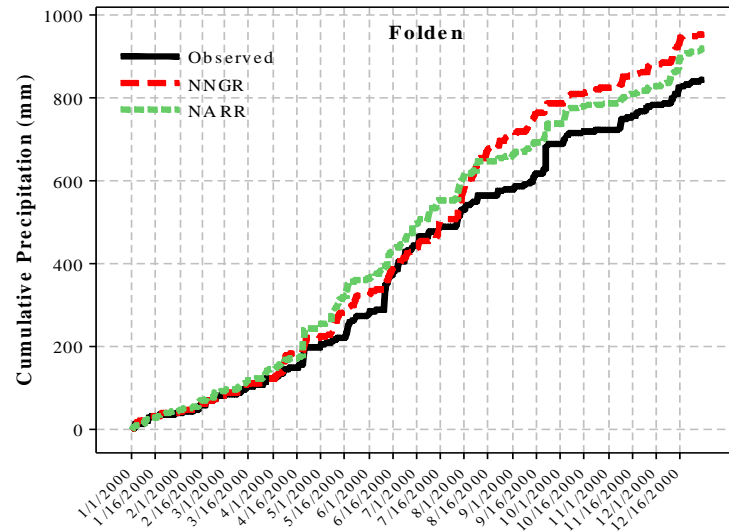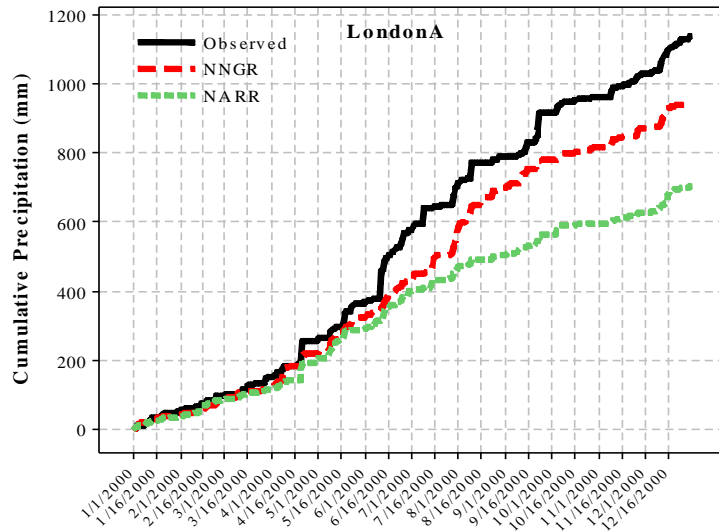
Figure 5.3: Comparison of Cumulative Daily Precipitation in 2000

133

5.1.2 Hydrologic Model Results

Performance Evaluation

Table 5.5 compares the statistical performance measures of the daily flow obtained during January 1980 - December 2005 for evaluating the performance of the reanalysis data. The root-mean-square-error for both NNGR and NARR varies considerably, from 4.00 m^3/s (NNGR) and 3.44 m^3/s (NARR) at Ingersoll to 28.1 m^3/s (NNGR) and 24.37 m^3/s (NARR) at Byron. .

Table 5.5: Comparison of Performance Statistics at Selected Locations within the Basin

Location	NNGR					NARR				
	RMSE (m^3/s)	r	NMSE	MAE (m^3/s)	RBias (%)	RMSE (m^3/s)	r	NMSE	MAE (m^3/s)	RBias (%)
Byron	28.09	0.44	1.03	15.73	31	24.37	0.65	0.77	9.95	-12
Ingersoll	4.29	0.41	1.25	2.62	45	3.44	0.63	0.80	1.57	-7
St. Marys	10.08	0.44	0.97	5.23	26	10.04	0.59	0.97	3.72	-9

The correlation coefficients produced by NARR (0.59-0.65) are significantly higher than those produced by NNGR (0.41-0.44). The normalized mean square error is also slightly higher in the case of NNGR. The absolute mean error is differentiable both in terms of the data types and locations. NNGR produces higher errors. It also appears that the MAE measure is lowest at locations where more than one sub-basin is contributing to the total runoff. The values of the relative bias differ greatly at the selected locations, with the NARR, unlike NNGR, producing a negative bias. The bias produced by the

NNGR data is much higher, ranging from 26% to 45% to that of -12% to -7% from NARR. At Byron, the outlet of the basin, with a contributing area of 3,110 km^2 (Cunderlik and Simonovic, 2004) and with 32 sub-basins the model results are poor. Such performance at Byron can be attributed to the fact that this suffers from inadequate meteorological data, which may have restricted a more satisfactory representation of the daily flow.

Flow Comparison Plots

Figures 5.4 and 5.5 present flow comparison graphs during June-August, 2001-2005. The modeled hydrograph from the reanalysis data does not provide a good fit to the observed simulated data. Peaks are not captured by either NNGR or NARR; moreover, some biased peaks are generated by NNGR during the low flow periods.
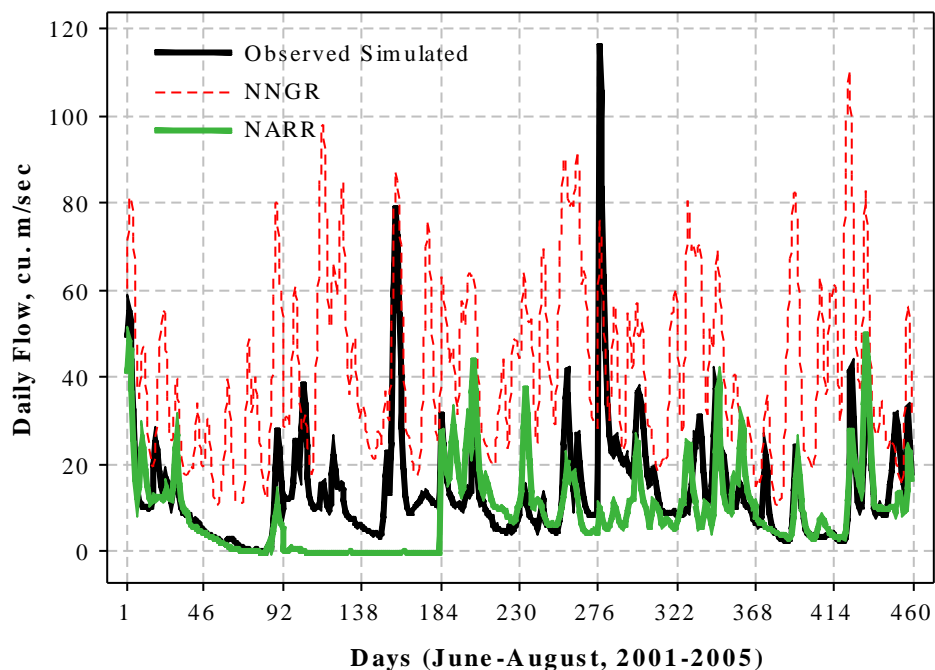
Figure 5.4: Daily Hydrographs at Byron during June-August, 2001-2005
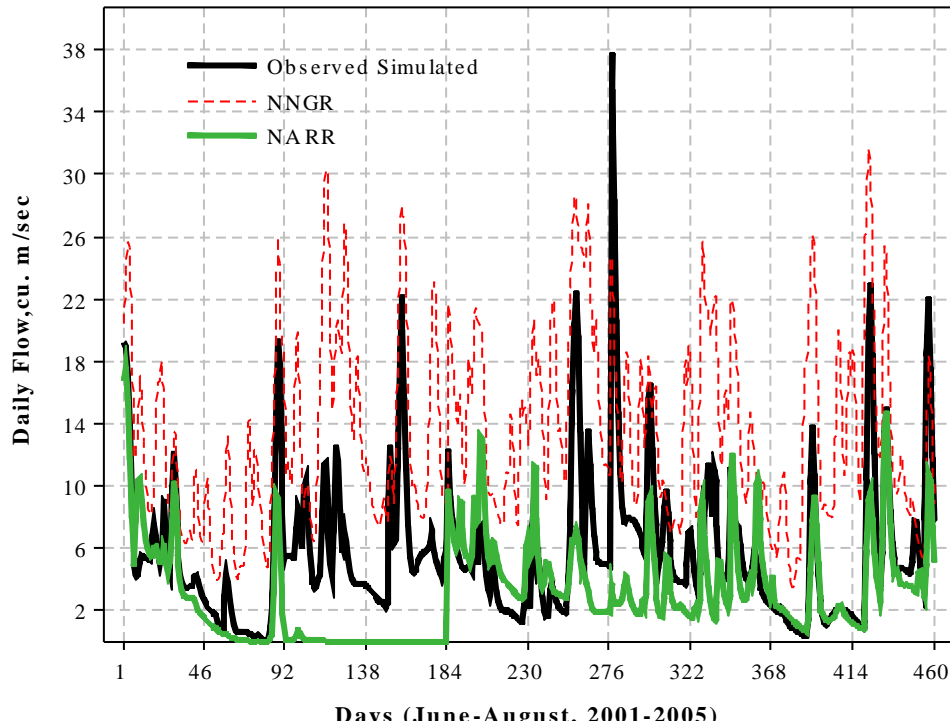
Figure 5.5: Daily Hydrographs at St. Marys during June-August, 2001-2005

The hydrographs generated by the NARR data for the low flows are better than the NNGR data. The model performance for low flow improves with the increase of contributing area. NNGR has systematically overestimated the peaks during summer; NARR has not shown systematic bias in most of the periods except for the year 2002.

Figures 5.6 (a), (b), and Appendix H present a comparison of the scatter plots between precipitation and associated flows during May-August, 1980-2005 at Byron, Ingersoll and St. Mary's. The higher flows show significantly scattered patterns; low flows are in better agreement with precipitation because the low flows are more directly linked with the deficit of precipitation. NNGR generated flows, however, show relatively less concurrence than NARR. This may be explained by the level of bias present in the dataset.
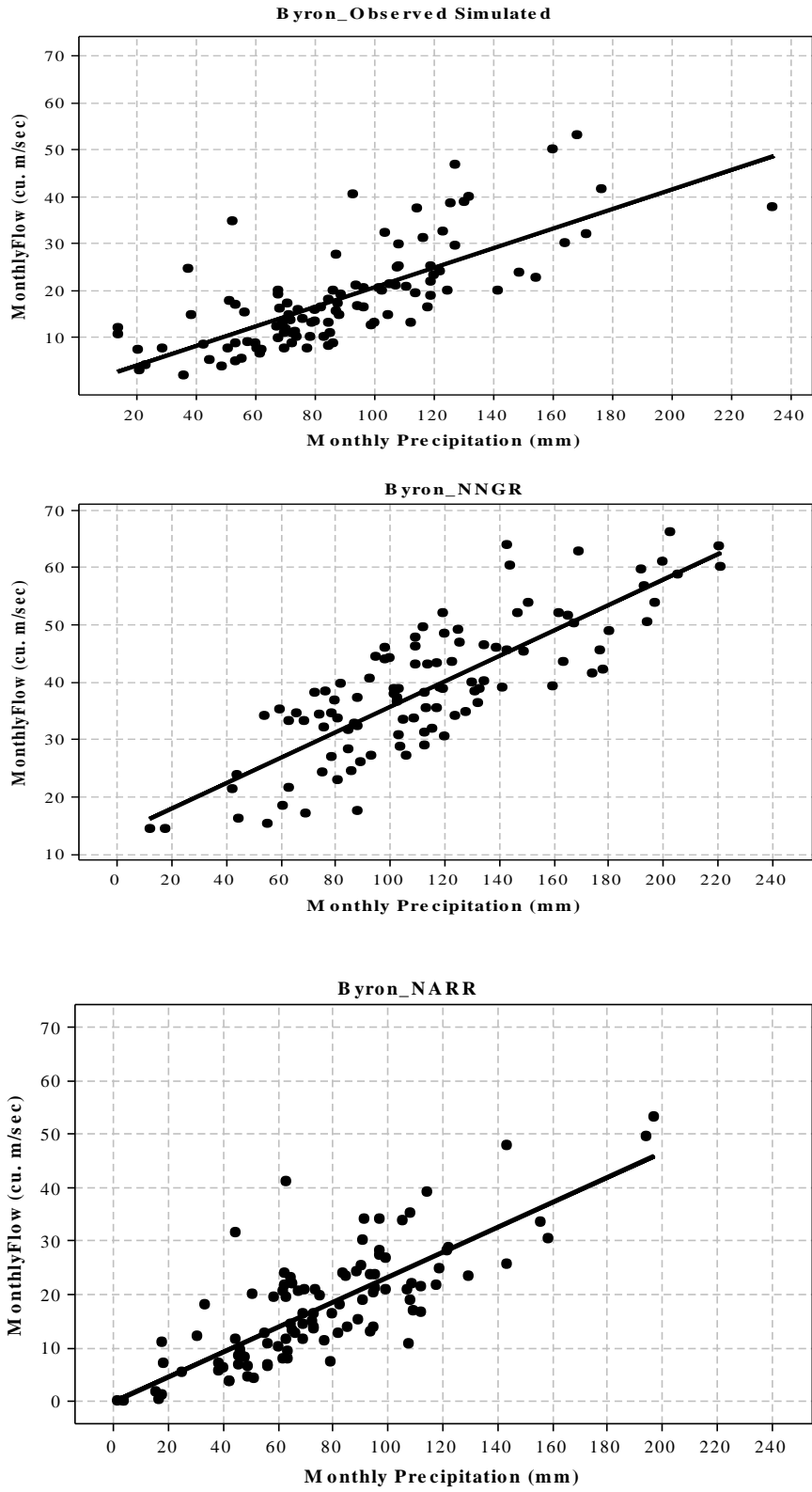
Figure 5.6 (a): Scatter Plots of Precipitation and Flow (May-August, 1980-2005) at Byron

St. Mary_Observed Simulated

St. Mary_NNGR

St. Marys_NARR
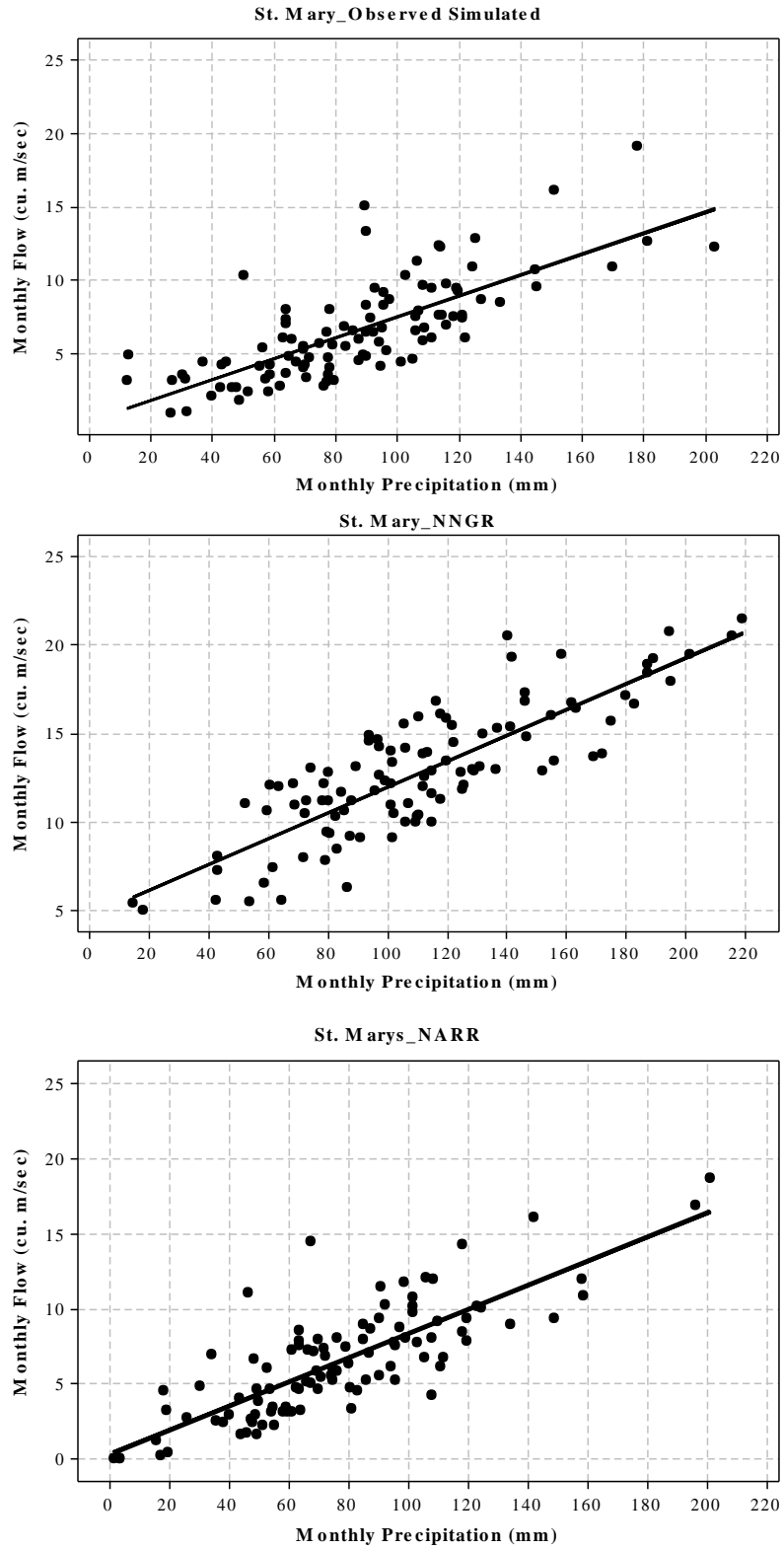
Figure 5.6 (b): Scatter Plots of Precipitation and Flow (May-August, 1980-2005) at St. Marys

Error Evaluation in terms of Box and Whiskers Plot

Figures 5.7 (a) and (b) present the box plots of the monthly flow at Byron and St. Mary's during May-November, 1980-2005. Although the model is applied on daily data, the statistics from the daily data are aggregated into a monthly scale to facilitate the presentation of results. Summer values show variability in the estimated means.
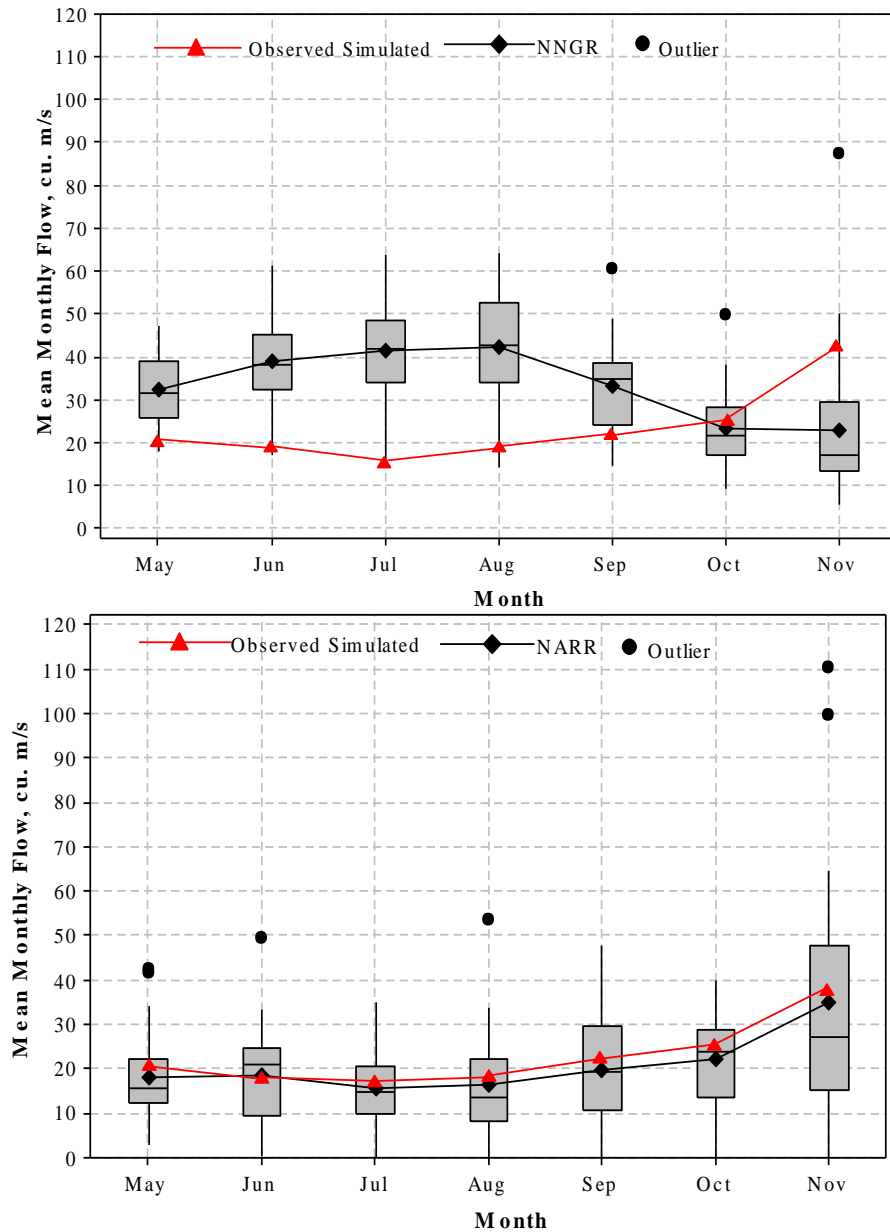
Figure 5.7 (a): Box Plots of Monthly Flow during May-November, 1980-2005 at Byron
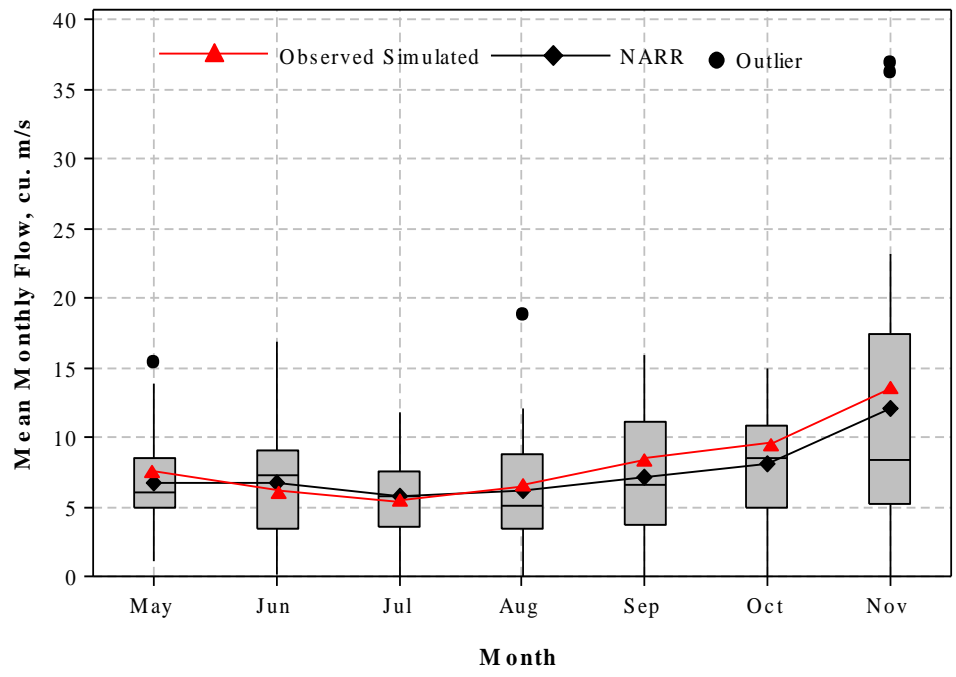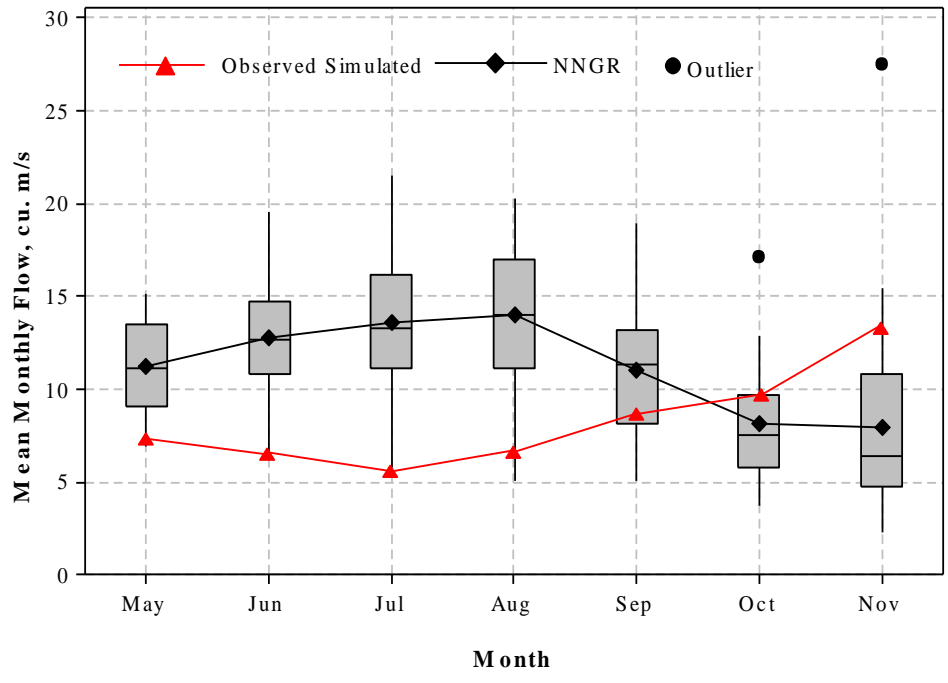
Figure 5.7 (b): Box Plots of Monthly Flow during May-November, 1980-2005 at St. Marys

The bottom and top ends of the box indicate the 1st quartile (25th percentile) and 3rd quartile (75th percentile) of the flows, with their median in between. From the plots for

140

Byron, it can be seen that the historical mean of the simulated stream flow deviates significantly from the mean for NNGR except for the month of October. While NARR is consistent and is able to adequately present the observed simulated discharge. NNGR, however, has suffered from a significant overestimation during most of the months considered in the study (excluding October and November). Some values during September through November are above the top whiskers, i.e., considered as outliers. In most months, the monthly average discharge from the observed simulated dataset falls below the 25th percentile value of NNGR flows. The performance of NARR is, however, very satisfactory and suffers from only minor underestimations. In most cases, the mean observed simulated discharge is close to the NARR median (except in October). Although in few years the NARR discharge appeared outside the top whisker's range (outliers), those are, however, very few compared to the entire dataset.

Error Evaluation in terms of Mean and Variance

Table 5.6 presents the results of the non-parametric Wilcoxon rank-sum test performed for evaluating errors in the estimation of the mean daily flow values for May-November, 1980-2005. The statistical significance test results (p values) reveal that at a 95% confidence level, errors at the Byron location are higher in NNGR for all months ($p<0.05$) except October, and in NARR the errors are significant during only three months. Similar results can be seen at St. Mary's as well, where NARR produced higher errors in three months while NNGR errors were high in all seven months.

Table 5.6: Test Results (p values) of the Wilcoxon Rank Test at 95% Confidence Level

Month	Byron		St. Marys	
	NARR	NNGR	NARR	NNGR
May	0.08	0.00	0.76	0.00
Jun	0.87	0.00	0.23	0.00
Jul	0.53	0.00	0.13	0.00
Aug	0.00	0.00	0.02	0.00
Sep	0.76	0.00	0.31	0.00
Oct	0.01	0.95	0.00	0.00
Nov	0.00	0.00	0.00	0.00

Next, Levene's test is used at Byron and St. Mary's to evaluate the quality of the variance of the simulated flows at a 95% confidence level. The results are presented in Table 5.7. In the case of Byron, the variance test results of NNGR reveal that for all months except two, all the p values fall below 0.05; the case is even worse at St. Mary's, with only one month above the threshold p level (>0.05), suggesting that the observed simulated and NNGR generated flow variance is statistically different.

Table 5.7: Test Results (p values) of the Levene's Test at 95% Confidence Level

Month	Byron		St. Marys	
	NARR	NNGR	NARR	NNGR
May	0.04	0.77	0.04	0.09
Jun	0.10	0.00	0.02	0.00
Jul	0.44	0.00	0.47	0.00
Aug	0.65	0.00	0.10	0.00
Sep	0.08	0.91	0.02	0.02
Oct	0.00	0.00	0.00	0.00
Nov	0.99	0.00	0.91	0.00

For NARR, however, the *p* values for five months are found to be above 0.05, indicating the equality of variance for those months. These test results confirm that the variability of the NARR generated flows can be considered equal to the observed simulated flows in general, but NNGR generated flows cannot be considered equal at the 95% confidence level.

5.2 Quantifying AOGCM and Emission Scenario Uncertainties

The performance of all methods and comparison results for estimating uncertainties are presented here. First, the BA-REA method and non-parametric weather generator are evaluated. The indices for estimating the severity of extreme precipitation events are developed and compared with the future climate. Finally, the probabilities of extreme precipitation events are assessed with associated AOGCM and scenario uncertainties. Results are presented for London station.

5.2.1 Fixed Weight (BA-REA) Method

The performance of the Bayesian reliability method can be assessed by model bias and convergence. Table 5.8 presents bias from six different AOGCMs during the summer (June-July-August) and winter (December-January-February) months. Bias is calculated as the difference of each AOGCM's response, X_i (1961-1990) from the mean of the posterior distribution, μ generated from the analysis.

Table 5.8: Biases from AOGCM Responses to Present Climate (1961-1990) in London

	Model Bias (%)					
Season	CGCM3 T47	CGCM3 T63	CSIRO MK3.5	GISS AOM	MIROC 3.2HIRES	MIROC 3.2MEDRES
Summer	-22.50	2.12	-6.50	-12.07	14.92	14.10
Winter	-2.18	1.68	-11.46	0.04	26.24	5.64

Figure 5.8 presents posterior distribution of precipitation change ΔP for London during the winter and summer seasons. The solid line shows the fitted curve. The points along the base of the densities mark predicted precipitation change from the 15 AOGCM scenarios for 2050s.
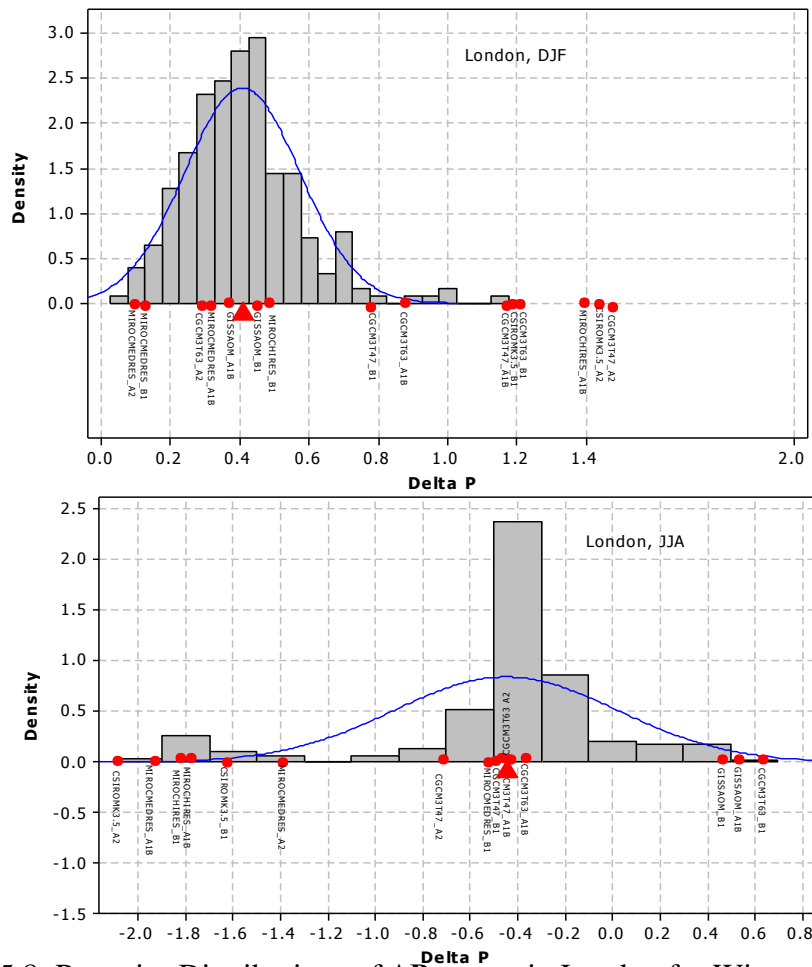
Figure 5.8: Posterior Distributions of $\Delta P = \nu - \mu$ in London for Winter and Summer

The triangle indicates the REA estimate of the changes in mean precipitation. The change in precipitation (climate response) [$Y_i - X_i$, for $i = 1, 2, ..., 15$] computed from 15 models and the scenarios' are plotted along the x axis (dots). The triangles represent the REA estimate of the mean change. A measure of convergence can be assessed using the relative position of the individual responses. The relative position is used to identify the outlier models and the models that reinforce each other. The comparison of multi-model densities in Figure 5.8 and the bias measure in Table 5.8 identify the models with higher biases (Table 5.8) and the models that act as outliers (Figure 5.8). The models with smaller biases receive larger weights. The cases that respect both criteria are the ones where the probability density is concentrated.

Figures 5.9 (a) and (b) summarize the posterior distributions for the precision parameters λ_i.
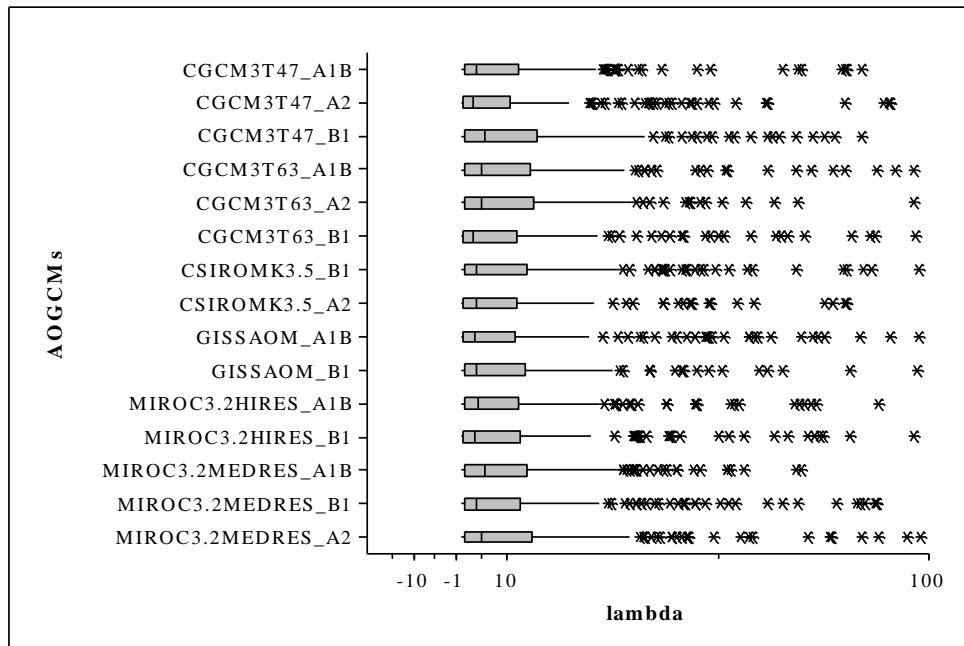
Figure 5.9 (a): Posterior Distributions of Model Specific Precision Parameter, λ_i during Winter
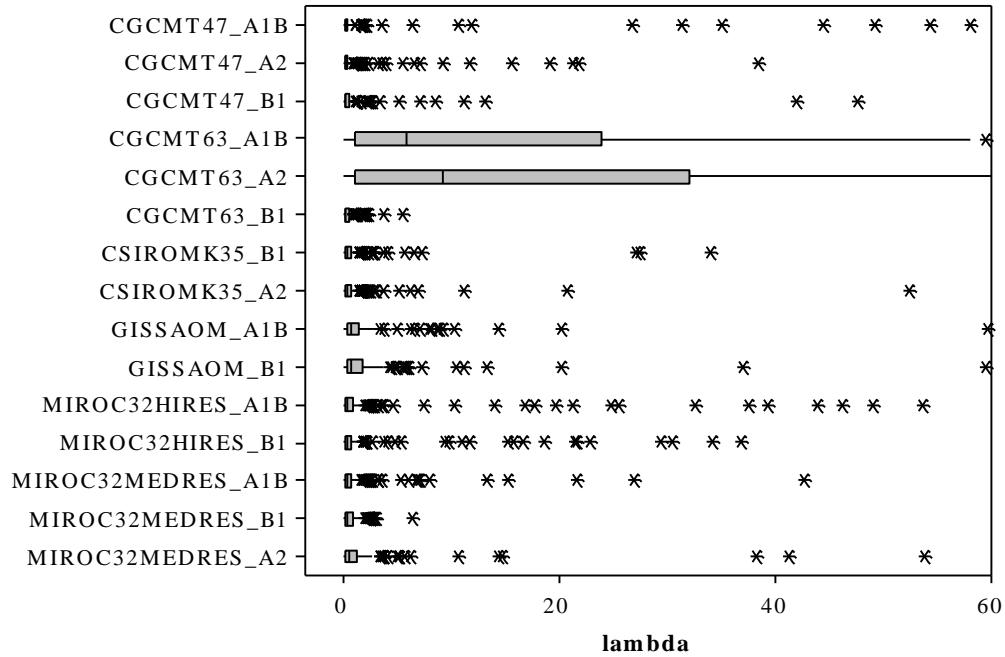
Figure 5.9 (b): Posterior Distribution of λ_i , the Precision Parameter for Summer

The scoring of the AOGCM scenarios should be evaluated through the relative position of the boxplots with respect to each other, rather than by comparing point estimates. Large λ_i values indicate that the distributions of the AOGCM responses are more concentrated to the true climate response. The posterior distributions, shifted towards right indicate AOGCM's better performances than those shifted to the left. Overlaps among these distributions indicate uncertainty in the relative weighting of the models. Table 5.9 presents an overall measure of reliability for the AOGCMs by summing up the weights from each model through relative weighting. The values are computed as $100 \times \lambda_i^* / \sum_{i=1}^{15} \lambda_i$ where λ_i^* are the means of the posterior distributions derived from MCMC simulation of AOGCM outputs. The results are ranked based on performances for summer (June, July and August) and winter (December, January and February) seasons separately.

146

Table 5.9: Relative Weighting of the 15 AOGCM Scenarios (2050s) for London

Models/Scenarios	DJF	JJA
CGCMT47_A1B	2.22	4.07
CGCMT47_A2	1.11	1.09
CGCMT47_B1	7.76	2.80
CGCMT63_A1B	4.30	31.83
CGCMT63_A2	11.06	36.56
CGCMT63_B1	1.32	0.41
CSIROMK35_B1	2.46	1.10
CSIROMK35_A2	3.37	2.77
GISSAOM_A1B	18.21	2.66
GISSAOM_B1	24.25	4.10
MIROC32HIRES_A1B	0.07	4.28
MIROC32HIRES_B1	0.09	4.51
MIROC32MEDRES_A1B	8.75	1.26
MIROC32MEDRES_B1	8.44	0.69
MIROC32MEDRES_A2	6.57	1.86

The Tables 5.8 and 5.9 clearly indicate the varying degree of the model performances for different seasons thereby suggesting a deviating skill in reproducing present day climate and a different level of agreement among the models for different signals of precipitation change. Next, the posterior distribution of the inflation/deflation parameter θ is shown to compare the simulations of the present day to future climate scenarios.

Figure 5.10 presents the posterior distribution of θ, the inflation/deflation parameter for comparing present climate to the future, common to all six AOGCMs for both summer and winter seasons. A θ value less than 1 indicates the deterioration in the degree of precision (Tebaldi et al., 2004).
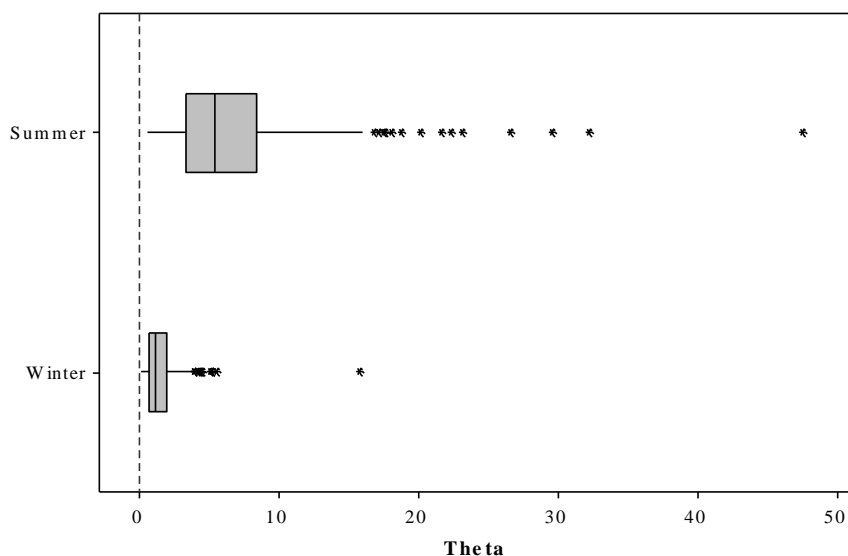
Figure 5.10: Posterior Distribution of θ, the Inflation/Deflation Parameter

The figure provides an overall degree of performance for the REA method, by considering a common value for all AOGCMs. For summer and winter, the models overall show improved performances, however with varying degree. Agreements are better represented during summer than winter.

5.2.2 Variable Weight (Kernel Estimator) Method

The variable weight method involves downscaling of AOGCM responses for future climate scenarios and estimating the uncertainties using nonparametric density estimator by considering different weights at each time intervals. This study uses 22 stations for the period of 1979-2005 (N=27) to simulate precipitation scenarios using seven meteorological variables. Employing the temporal window of 14 days (w=14) and 27

years of historic data (N=27), 404 days are considered as potential neighbors $(L=(w+1)$ x

$N-1=404)$ for each variable. 12 different runs, each comprising 27 years of daily

precipitation are generated. Errors in the estimates of mean and variance of generated

precipitation are evaluated using a statistical hypothesis test at 95% confidence level. The

performance of WG in representing the present climate is tested by using the

nonparametric Wilcoxon-rank test and Levene's test (Levene, 1980). Table 5.10 presents

statistical significance test results (p values) for the differences of means and equality of

variances of the observed and simulated daily precipitation for summer and winter for

London. The p values at 95% confidence level for all runs are above the threshold (0.05)

which clearly indicates that there is no evidence of different means between the observed

and generated precipitations. The results of the Levene's test for the equality of variances

of observed and simulated precipitation at 95% confidence level are presented next.

Table 5.10: Test Results (p values) of the Wilcoxon Rank Test and Levene's Test

Runs	Wilcoxon Rank Test		Levene's Test	
	Summer	Winter	Summer	Winter
1	0.46	0.48	0.61	0.55
2	0.76	0.61	0.72	0.58
3	0.64	0.67	0.56	0.99
4	0.93	0.37	0.98	0.18
5	0.60	0.98	0.87	0.59
6	0.59	0.53	0.96	0.99
7	0.91	0.95	0.64	0.20
8	0.91	0.95	0.64	0.20
9	0.76	0.67	0.98	0.84
10	0.48	0.63	0.91	0.19
11	0.77	0.80	0.41	0.66
12	0.76	0.29	0.76	0.30

The *p* values appear above 0.05 thresholds, indicating similar variability of the simulated precipitation with the observed precipitation. So, the observed and the simulated precipitation can be assumed to have equal variances.

Frequency distributions of wet-spell lengths for winter and summer months are plotted in Figure 5.11. A comparison of observed and simulated values for wet-spell lengths shows very close agreement between the frequency distributions.
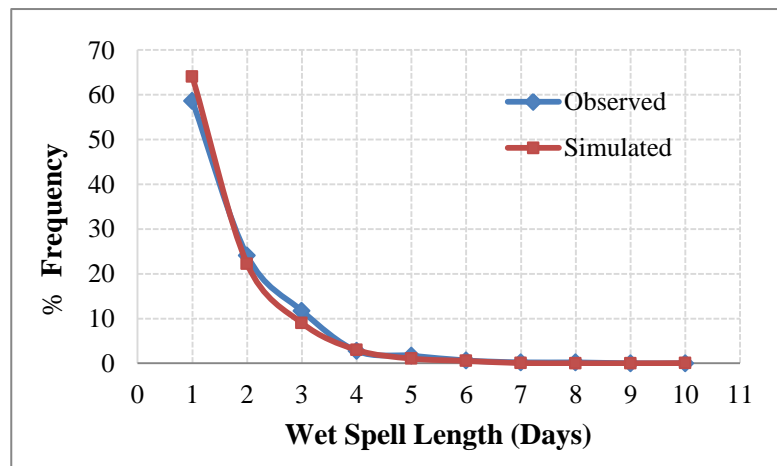
Figure 5.11 (a): Frequency Plots of Wet Spell Lengths for Summer
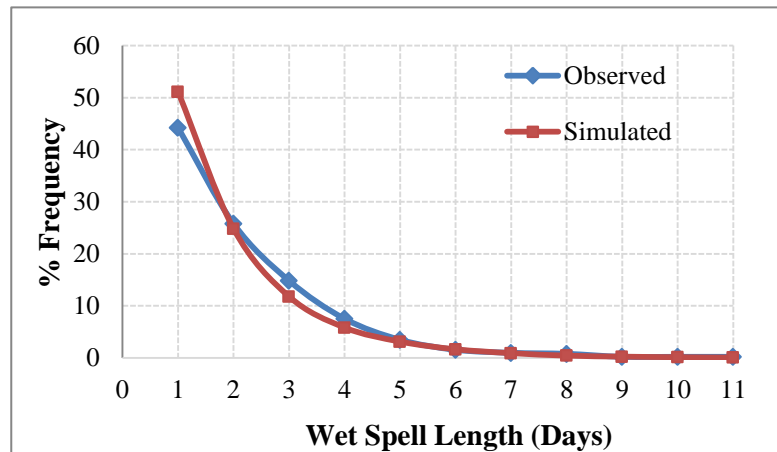
Figure 5.11 (b): Frequency Plots of Wet Spell Lengths for Winter

The frequency of wet-spell lengths in the simulated data for summer is almost

identical to the observed values, except for the one day lengths where the simulated data show a slight overestimation. The same is the case for the winter months. The performance of the weather generator in reproducing wet-spell lengths is very good.

The modified data for generating climate change scenarios from 15 different AOGCMs and emission scenarios contain 27 years of daily data created using the monthly change fields. By running each model 12 times, 324 (12x27=324) years of synthetic data are generated. In order to investigate the intensity of wet spells for future climate, bar charts are made showing the percent change in wet spell intensity from the historical values to the future values. Intensities are calculated using the total amount of precipitation that fell during the spell over the length of the spell. The percent changes in wet spell intensities are determined for 3, 5 and 7 day wet spells. The plots are made for summer (June, July, August) and winter (December, January February) in both time periods. Figures 5.12 (a) through (c) show the bar charts for the summer months of the 2050s.
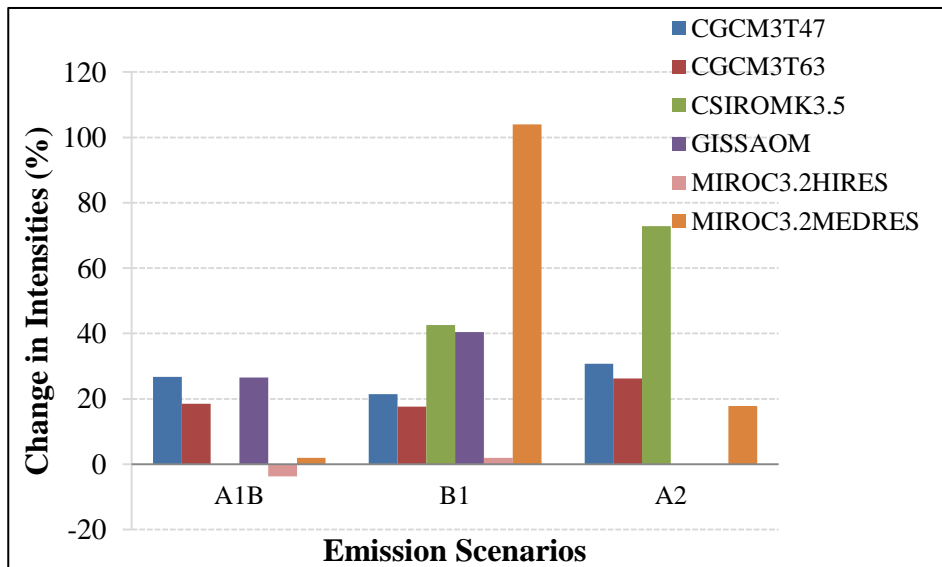
Figure 5.12 (a): Change in 3-Day-Spell Intensities for Summer, 2041-2070
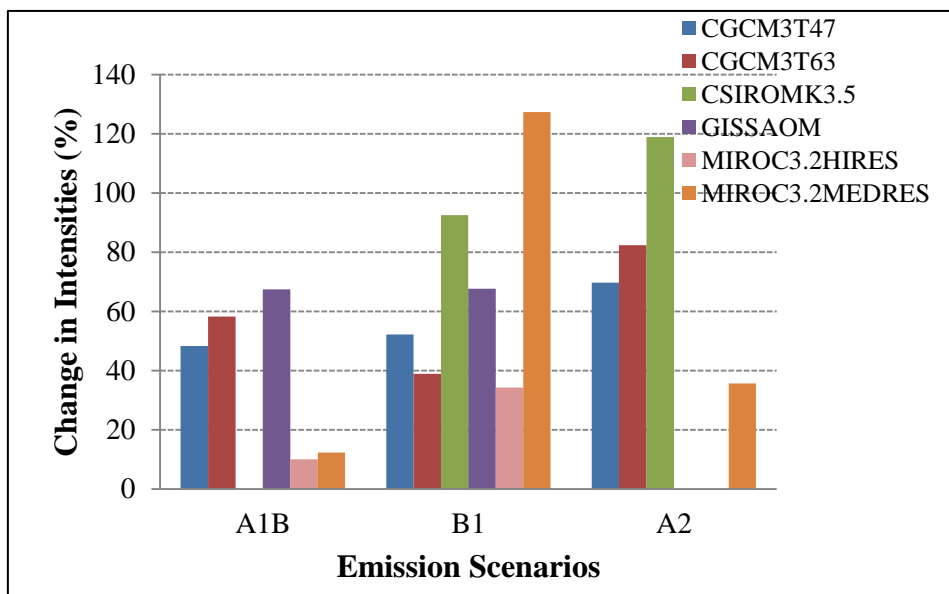
Figure 5.12 (b): Change in 5-Day-Spell Intensities for Summer, 2041-2070

For summer wet spells, all models except the MIROC3.2HIRES A1B, show an increase in 3-day intensities. The most significant increase in intensity is predicted by MIROC3MEDRES A2 (100%) and CSIROMK3.5 A2 (47%). For 5-day wet spells, all models predict an increase with CSIROMK3.5 A2 and MIROC3MEDRES B1 predicting the highest intensities over 100%. The smallest increase is predicted by MIROC3.2MEDRES A1B and MIROC3HIRES A1B with below 20% of changes. The average change from all the models and scenarios is between 35 -70%, indicating high uncertainties among the AOGCMs and their scenarios. For a 7 day spell, CGCM3T63 B1, CGCM3T47 B1 and A2, and MIROC3MEDRES B1 show 6-25% increase in precipitation intensity; however, the rest of the models predict a 7-38% decrease in intensity for 7-day spells during summer. The highest decrease is predicted by the GISSAOM B1 scenario. Overall, the general trend for summer precipitation in the 2050s

as predicted by several AOGCM's suggests that precipitation intensities for shorter spells will increase with a decrease in longer wet-spells intensities.
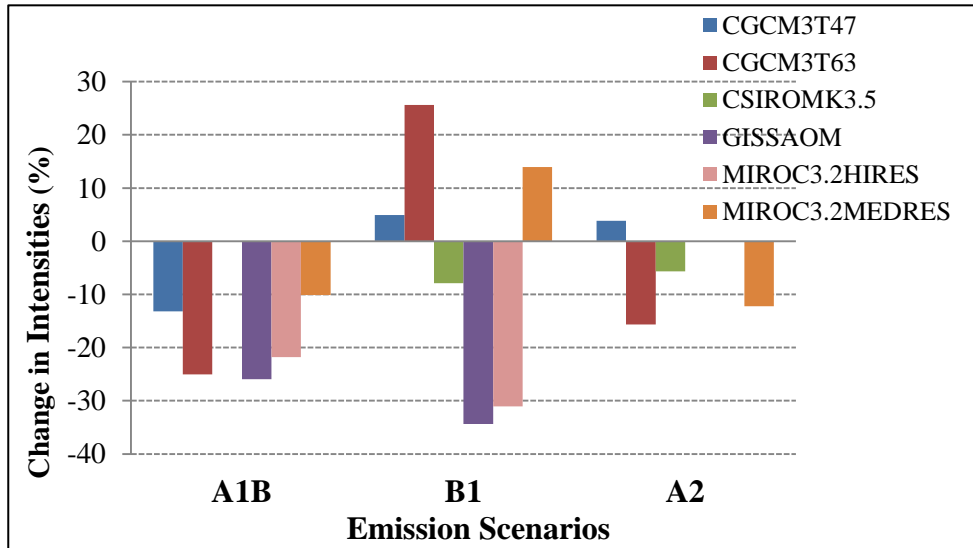
Figure 5.12 (c): Change in 7-Day-Spell Intensities for Summer, 2041-2070

In the next section, a comparison between both uncertainty estimation methods is presented. The mean precipitation obtained from each AOGCM and emission scenario is assumed to be an independent realization of future climate. Using this concept, climate density curves are generated by combining the information from all AOGCMs for the 2050s, the results of which are presented in section 5.2.3.

5.2.3 Fixed vs. Variable Weight Method

This section presents a comparison of the uncertainty estimation methods explained in sections 3.2.1 and 3.2.2 using density estimators. Figures 5.13 (a) and (b) present density estimates of precipitation change for the winter and summer seasons with the results

obtained from the WG combined kernel density estimates and the BA-REA method for London station using 2050s (2041-2070) time slice. The density estimate of the posterior distribution of the precipitation change from BA-REA method provides an under-smoothed curve during summer. Many spurious bumps, especially at the tails, for both winter and summer can be seen which make it harder to understand the structure of the data. The estimates using a kernel estimator show evidence of a smoothed structure.
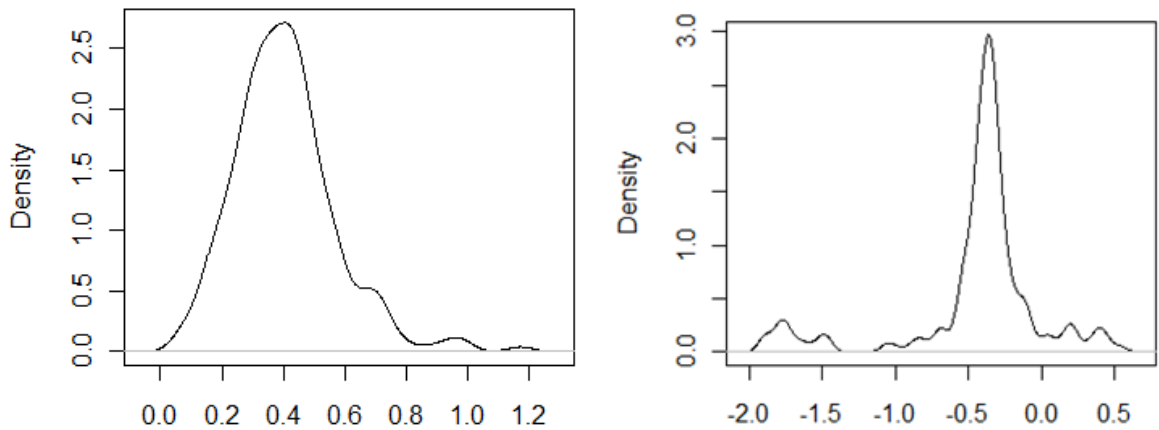
Figure 5.13 (a): Density Estimate of the Mean Precipitation Change in London using BA-REA Method for Winter and Summer

The extended benefit of the kernel estimators is that unlike BA-REA, the generated outputs can be processed further and converted to the indices of interest. The probabilities can then be calculated for any frequency of data, either monthly, or daily, or yearly, while the BA-REA method provides the mean change by combining the AOGCM scenarios. Moreover, the weight/kernel function (*K(.)*), in equation 3.40 can be calculated at any point of interest within the range of data.

.
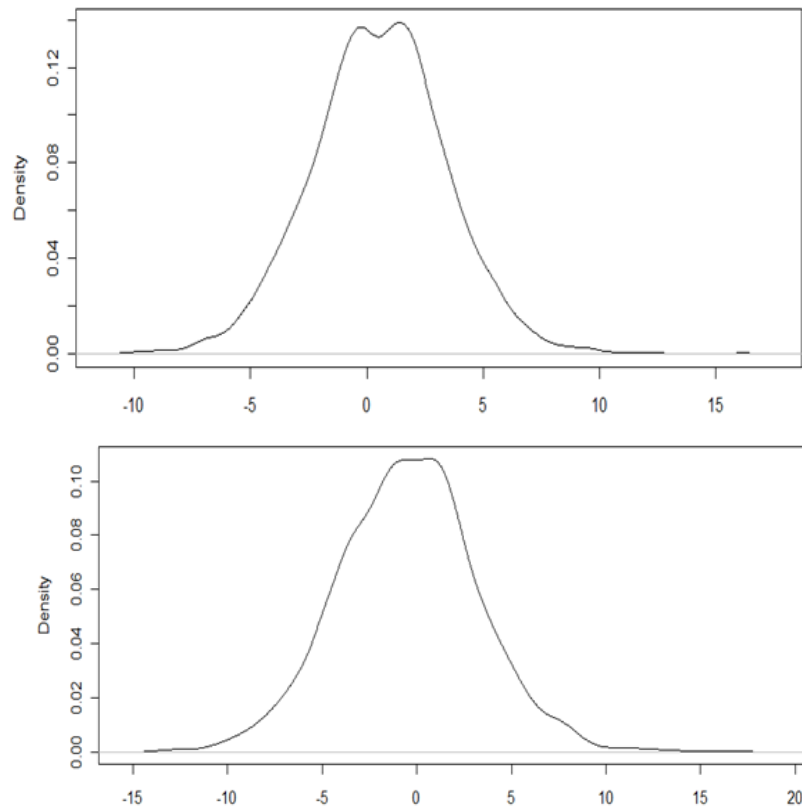
Figure 5.12 (b): Density Estimate of the Mean Precipitation Change using Kernel
Estimator for Winter (top) and Summer (bottom)

5.2.4 Uncertainty Estimation of Extreme Precipitation Events

Changes in Future Extreme Precipitation Events

Changes in the precipitation indices compared to the historic observed 1979-2005 values
are computed from the downscaled precipitation for three time slices (2020s, 2050s, and
2080s) and presented in Table 5.11. Both summer and winter show different changing
patterns. For summer, half of the scenarios show a decrease in number of heavy
precipitation and very wet days for all three time slices, while most models show an
increase in 5 day maximum precipitation amount. This clearly indicates a higher intensity

of precipitation during extreme precipitation events. However, ranges of change are very high, indicating higher uncertainties in model projections during summer. For winter, most of the models are in agreement over the increasing trend of extreme precipitation indices for three time slices. In this case also, the uncertainty range is high.

Distribution Fitting

In the presence of uncertainties in AOGCM models, there is still concern over the choice of a unique distribution for the future climate responses. The comparison of the optimal distribution of different AOGCM data based on probability plots and goodness of fit test provides an insight into the level of inherent uncertainties. The performances of different distributions during summer and winter are evaluated using three goodness-of – fit-tests: Kolmogorov-Smirnov test, Anderson-Darling estimate, and Chi-Squared test. The performance of any specific distribution is ranked based on the goodness of fit values. The optimum parameters for the best fitted distribution function are summarized in Appendix I. From the tabulated results it can be observed that for extreme precipitation events, most models are fitted with the Generalized Extreme Value distribution with varying value of the shape (k), location (μ) and scale (σ) parameters. However, the distribution of wet days with >95th percentile precipitation during the summer season fits a well defined Frechet distribution, indicating a distribution different than the historical perturbed/no change scenario.

Table 5.11: Percent Changes in Extreme Precipitation Events for 2020s, 2050s and 2080s

Models/Scenarios	Heavy Precip Days			Very Wet Days			5 Day Precip		
	2020	2050	2080	2020	2050	2080	2020	2050	2080
Summer									
CGCM3T47_A1B	3.89	2.86	1.37	8.19	5.96	1.87	5.64	0.75	2.49
CGCM3T47_A2	1.87	3.45	-2.51	5.34	5.07	-1.33	5.88	3.03	-0.55
CGCM3T47_B1	7.26	-2.93	-1.56	13.97	0.44	5.87	8.27	1.96	2.45
CGCM3T63_A1B	-2.38	-6.56	-1.18	6.23	-3.91	2.05	12.17	-2.54	1.16
CGCM3T63_A2	-10.78	3.30	-1.56	-11.57	9.70	-0.71	-4.73	6.70	5.25
CGCM3T63_B1	-7.51	-6.85	-7.50	-5.60	-6.85	-7.12	-2.80	2.83	-4.70
CSIROMK3.5_A2	18.44	29.73	26.84	39.68	57.92	52.05	26.98	37.51	35.18
CSIROMK3.5_B1	5.61	19.57	16.37	14.77	39.68	29.00	9.81	30.38	18.45
GISSAOM_A1B	1.03	6.38	15.91	3.56	14.59	32.38	3.64	9.59	20.15
GISSAOM_B1	5.06	5.57	8.15	11.92	16.01	22.42	8.76	9.19	16.53
MIROC3HIRES_A1B	-25.84	-24.38	-26.72	-35.32	-38.26	-39.59	-19.41	-23.08	-26.93
MIROC3HIRES_B1	-14.55	-25.70	-16.82	-18.68	-31.94	-24.82	-11.64	-19.30	-15.91
MIROC3MEDRES_A1B	-13.31	-23.24	-33.12	-16.28	-31.58	-41.28	-12.08	-20.45	-27.70
MIROC3MEDRES_A2	-13.09	-12.50	-40.01	-15.75	-16.81	-56.41	-14.01	-9.18	-38.89
MIROC3MEDRES_B1	-14.85	-20.38	-15.57	-17.53	-27.05	-20.82	-10.23	-17.58	-13.58
Winter									
CGCM3T47_A1B	26.15	38.60	47.13	40.00	59.88	76.66	19.40	27.09	29.02
CGCM3T47_A2	28.88	32.80	60.11	43.08	48.13	91.86	23.07	20.54	38.96
CGCM3T47_B1	25.31	48.85	45.16	33.38	73.36	66.94	21.49	27.87	25.75
CGCM3T63_A1B	19.57	23.31	35.05	22.77	26.50	54.55	10.54	9.52	20.76
CGCM3T63_A2	10.07	26.04	33.66	12.77	40.45	47.66	9.82	15.14	20.14
CGCM3T63_B1	20.32	7.21	19.52	16.62	5.65	29.00	11.21	1.30	10.26
CSIROMK3.5_A2	22.44	31.12	38.55	30.00	40.45	62.55	12.24	24.71	26.66
CSIROMK3.5_B1	20.04	39.51	21.30	23.54	60.51	21.17	12.65	25.41	12.75
GISSAOM_A1B	6.87	10.70	27.38	6.31	4.08	41.54	5.80	-0.94	15.45
GISSAOM_B1	17.03	11.66	18.71	19.23	16.62	23.05	12.55	5.30	6.26
MIROC3HIRES_A1B	-4.80	6.73	6.10	-9.38	7.22	11.76	-0.15	2.02	-2.13
MIROC3HIRES_B1	-4.09	-2.91	18.66	-18.92	-5.64	18.97	-7.27	-7.47	2.61
MIROC3MEDRES_A1B	-7.67	0.64	-0.41	-14.77	-11.12	-2.35	-9.68	-7.52	-1.02
MIROC3MEDRES_A2	-6.26	-1.61	5.58	-12.31	-7.67	10.35	-8.40	-5.01	-0.84
MIROC3MEDRES_B1	-9.64	-2.95	6.63	-16.92	-11.91	-0.15	-5.64	-10.02	-3.02

The GEV distribution unites the type I, type II and type III extreme value distributions into a single family, thereby allowing a continuous range of possible shapes. For $k < 0$, the GEV is equivalent to the type III extreme value (reversed Weibull). For $k > 0$, the GEV is equivalent to type II distribution (Frechet). As k approaches 0, the GEV becomes the type I (Gumbel). Although most of the models and scenarios show the best fit with extreme value distributions, to be more precise, with the Type II (Frechet) and Type III (reversed Weibull) distributions with shape parameters greater and smaller than 0 respectively, the shape parameter values (k) appear close to 0. However, the differences in the k values show extent of the variations among the distributions for each index. The tables further point out the limitations of the parametric methods for quantification of uncertainties assuming any specific distribution and parameter values.

Non-parametric Uncertainty Estimation by Plug-in Estimate

To examine uncertainties in future extreme precipitation events, the yearly values of the indices from each AOGCMs and emission scenario are considered as random and as a set of independent realizations. This set is then used at each time step to establish a PDF by applying the bandwidth values presented in section 3.2.4. The cumulative distribution function (CDF) values at the upper and lower ranges of each severity class are calculated by numerical integration. The difference between the upper and lower value can thus be considered as the probability of that specific class of extreme precipitation indices for future. Figures 5.14 through 5.16 present the probability of the heavy precipitation days, the very wet days, and 5 day precipitation for three time slices. Both indices show somewhat similar results for the summer and winter seasons. For $<25^{th}$ percentile values, heavy precipitation days show an increase in probability for the later part of the century.

158

For the 25th-50th and 50-75th percentile ranges, probabilities decrease slightly while approaching 2100. However, the higher probability of precipitation days over the time is observed for >75th and >90th percentile range. This trend is supported by the probabilities of very wet day and 5 day precipitation for the summer season. In summary, the increased probability of the high end extreme precipitation events indicates larger chance of high intensity events during the later part of the century.
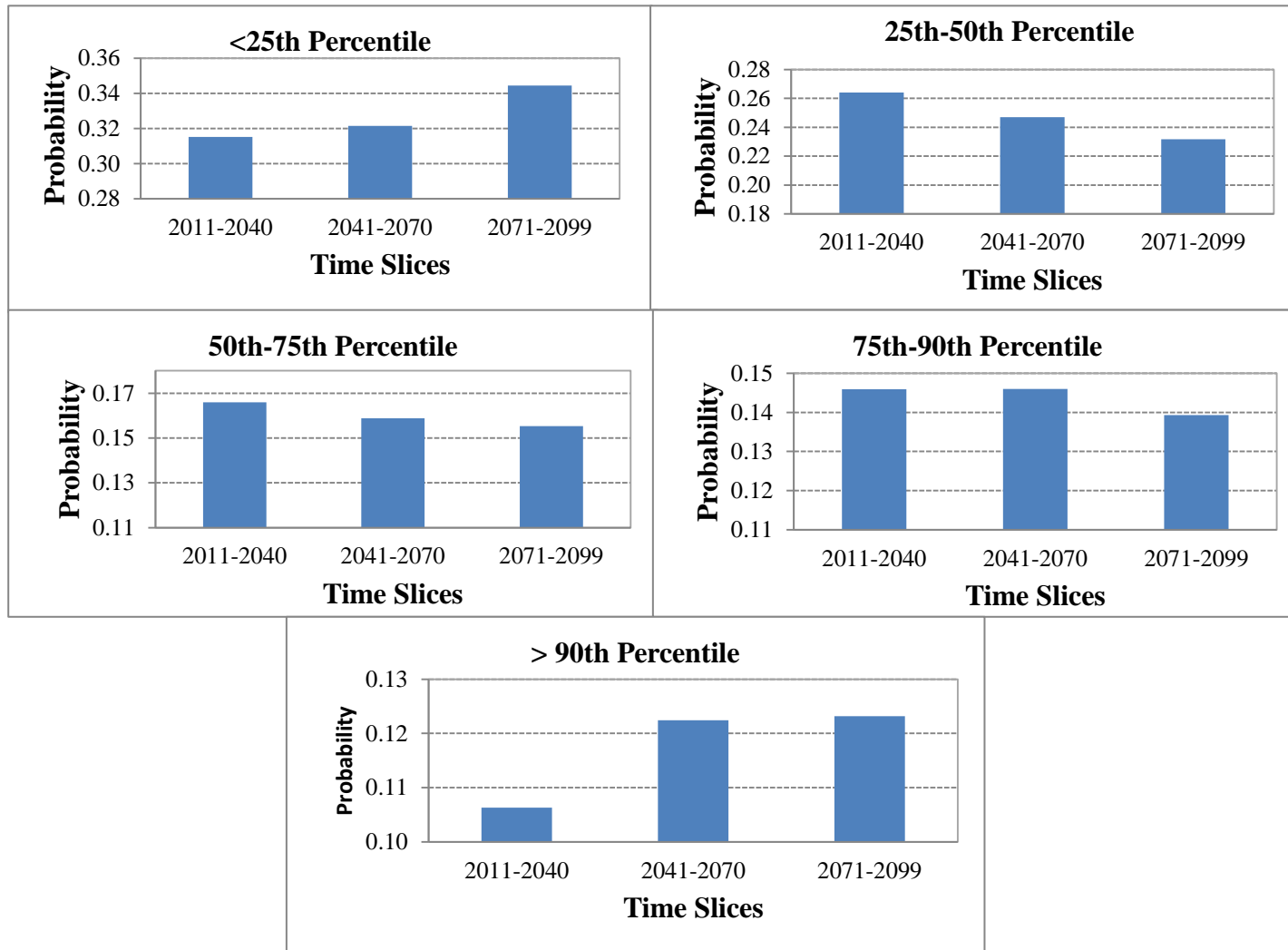
Figure 5.14 (a): Probability of Heavy Precipitation Days during Summer
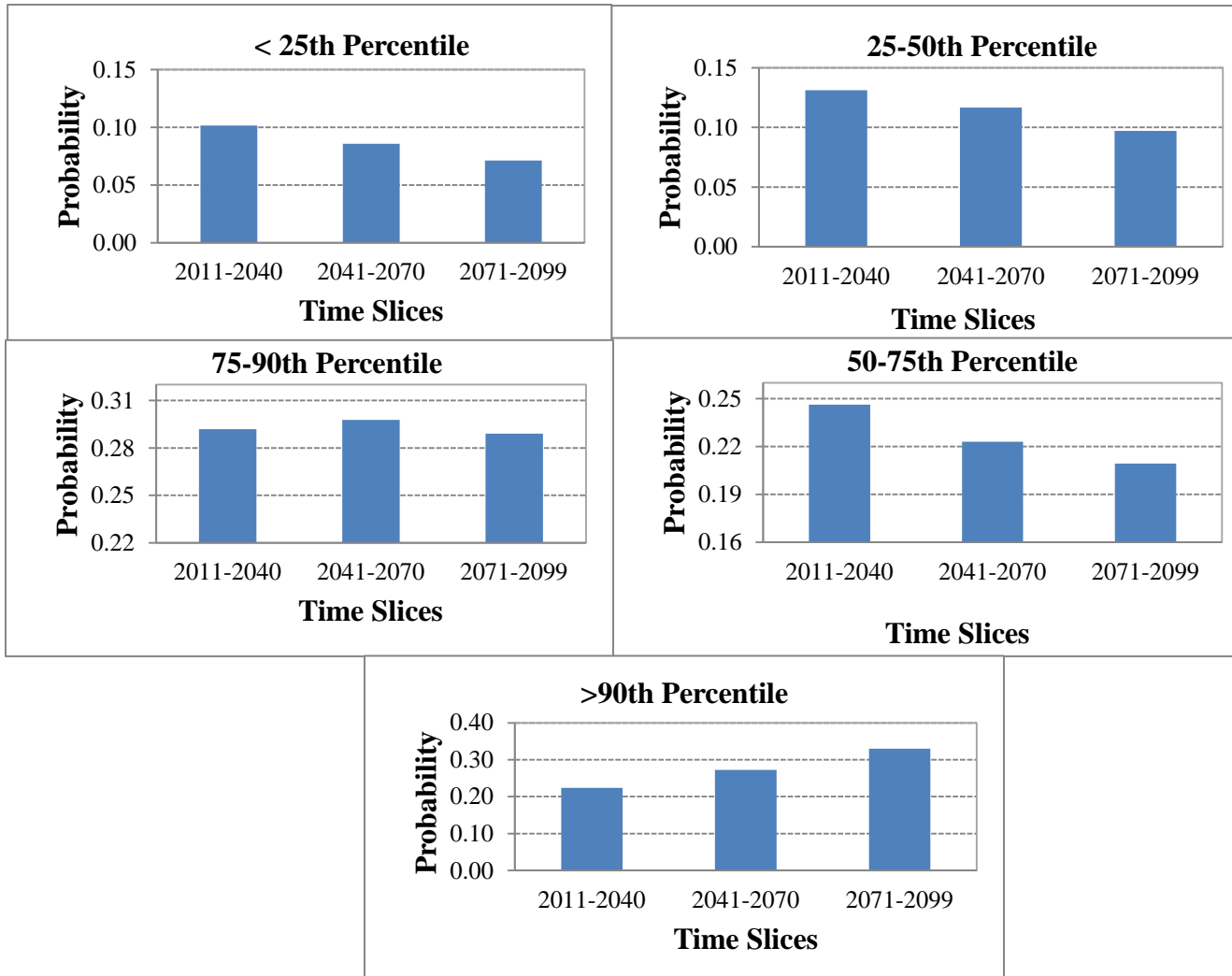
Figure 5.14 (b): Probability of Heavy Precipitation Days during Winter
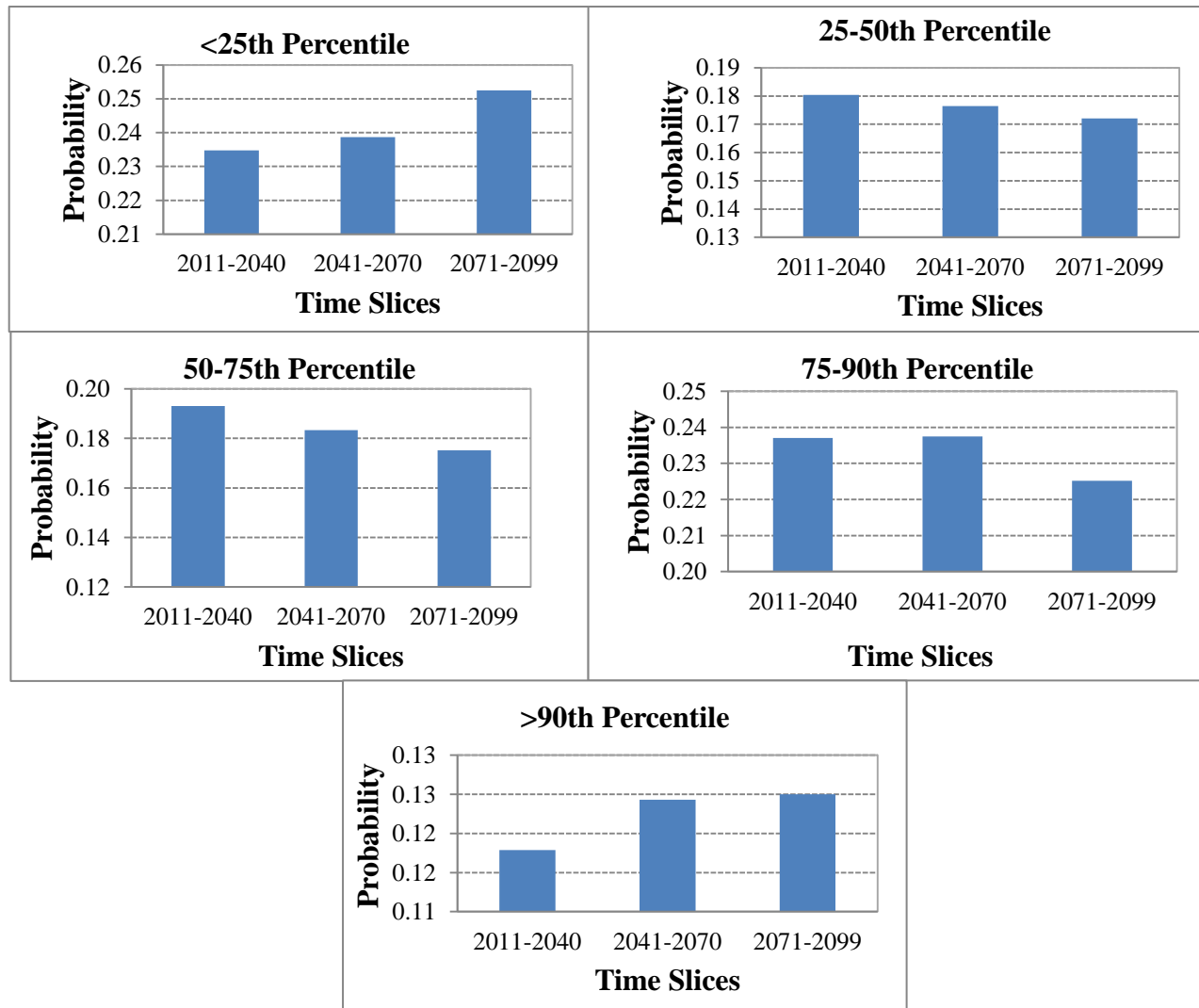
Figure 5.15 (a): Probability of Very Wet Days during Summer
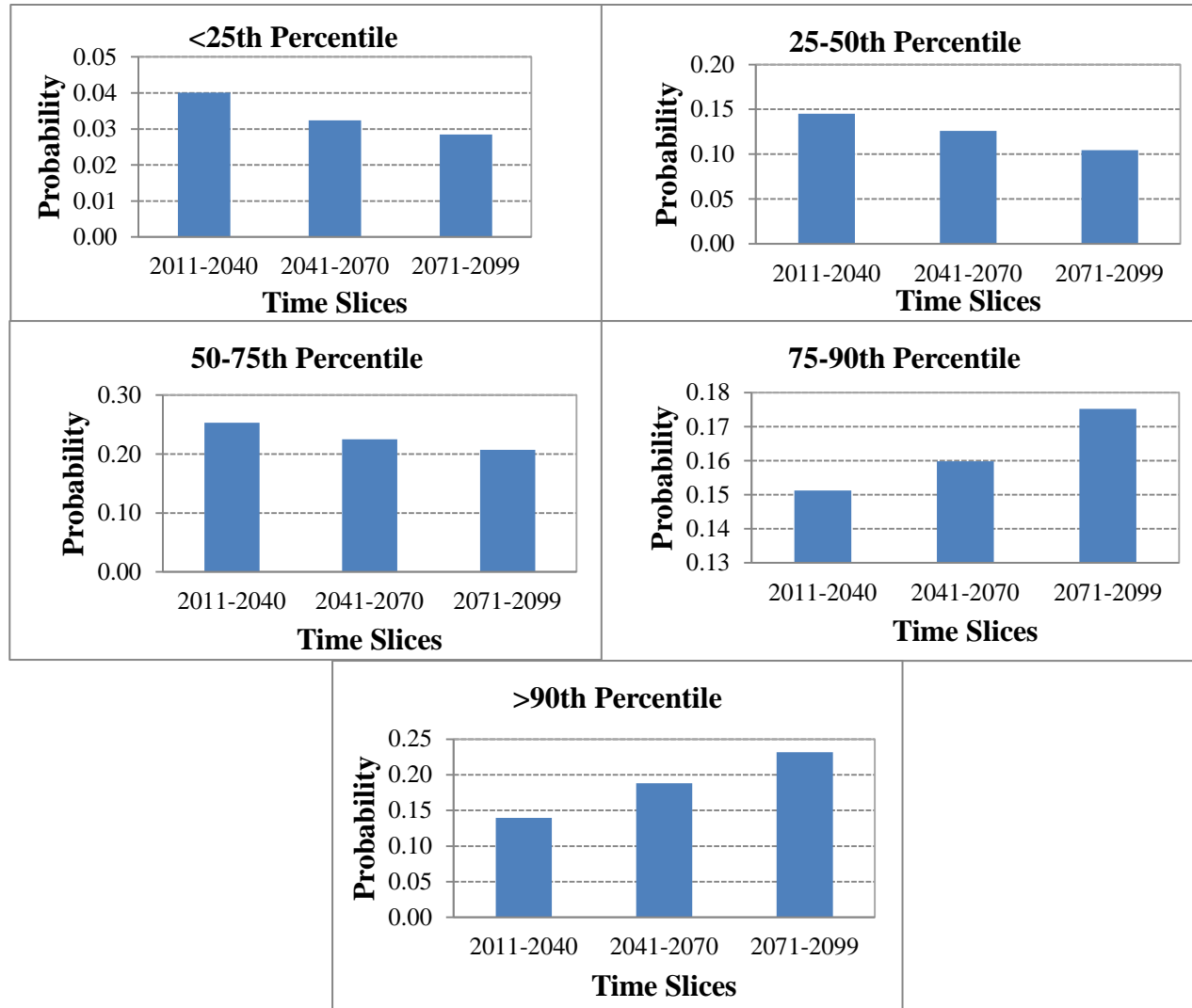
Figure 5.15 (b): Probability of Very Wet Days during Winter

163
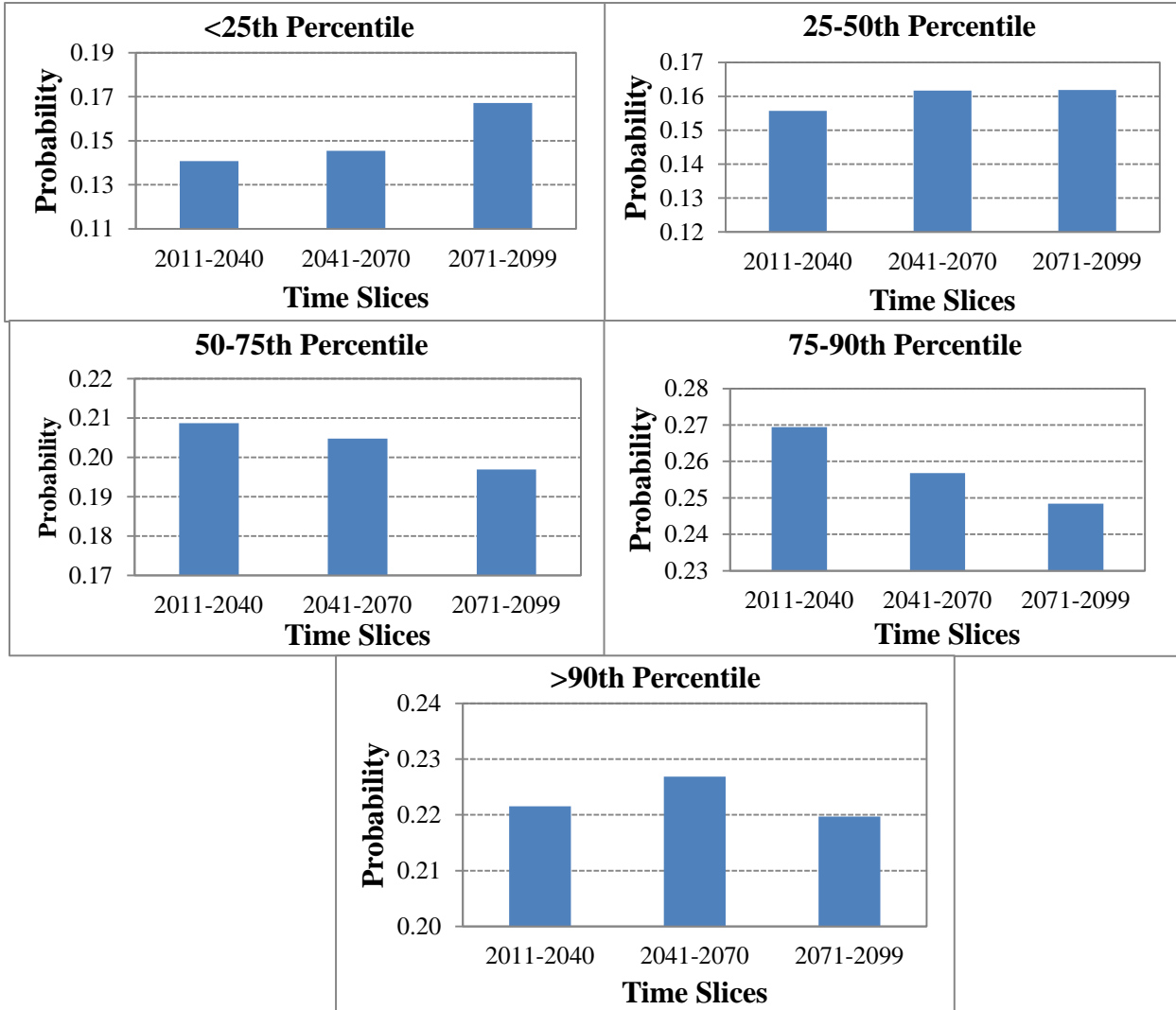
Figure 5.16 (a): Probability of 5 Day Precipitation during Summer
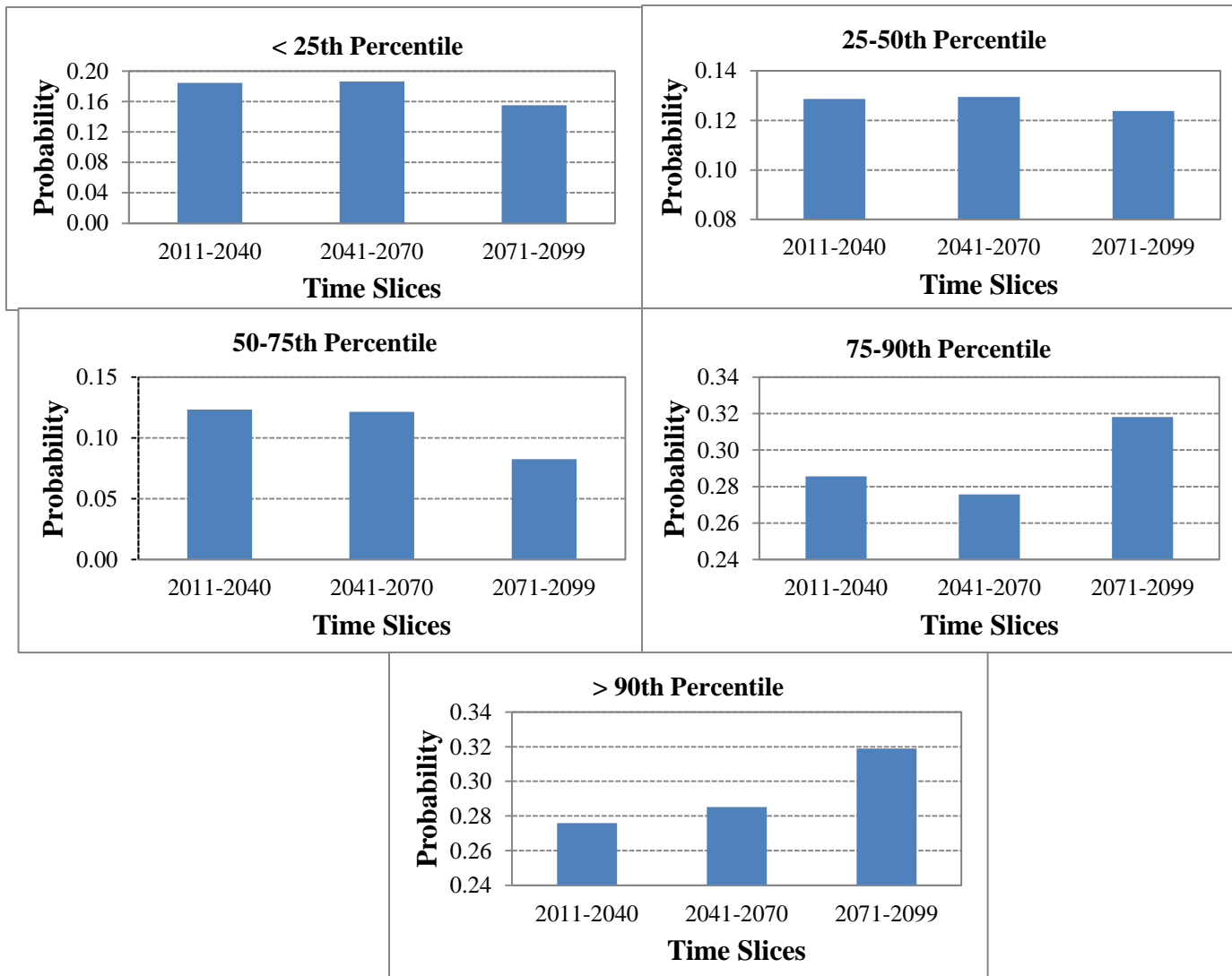
Figure 5.16 (b): Probability of 5 Day Precipitation during Winter

The method explained in this section can be seen as a major improvement over the 'normal' kernel (Silverman, 1986) method applied in other AOGCM and scenario uncertainty studies. The Sheather-Jones plug-in (SJPI) kernel estimation method proposed here overcomes the limitations associated with the assumptions of normality in the case of unknown densities/distributions. It is completely data driven; hence, more robust, flexible, and independent. The methodology has also been extensively revised by the statisticians.

The orthomornal method (Efromovich, 1999) used by Ghosh and Mujumdar (2007) to estimate uncertainties of future droughts provides another important step in the development of nonparametric uncertainty estimation techniques. However, one major limitation of the orthonormal method is the use of a subset of the Fourier series which consists of cosine functions without proper justification.

The additional benefit of kernel density estimators for the assessment of AOGCM and scenario uncertainties derives from the fact that the scientific community is now highly confident that the trends in the precipitation over future periods are not going to follow the same distribution as in the past. It still remains true, for any statistical method, that larger sample provides better estimate of data distribution. It is our expectation that with the advance of more sophisticated global climate models, the kernel method will be applied with more confidence for uncertainty estimation problems.

5.3 Developing Intensity-Duration-Frequency Curves under Climate Change

This section presents the results of the methodology introduced in section 3.3 for the development of IDF curves for 2080s. Results are presented for the City of London.

5.3.1 Verification of the IDF Generation Methods

As described in section 4.4.3, the daily weather generator is used to simulate a sequence of rainfall for all stations in the Upper Thames River basin. For the verification purpose, the perturbation functionality of the weather generator (section 3.2.2, step 10) is kept off in order to replicate the exact scenario as the historical observed one. In order to test the output of the weather generator, the box and whisker plots for monthly historical simulated rainfall are developed and presented in Figure 5.17.
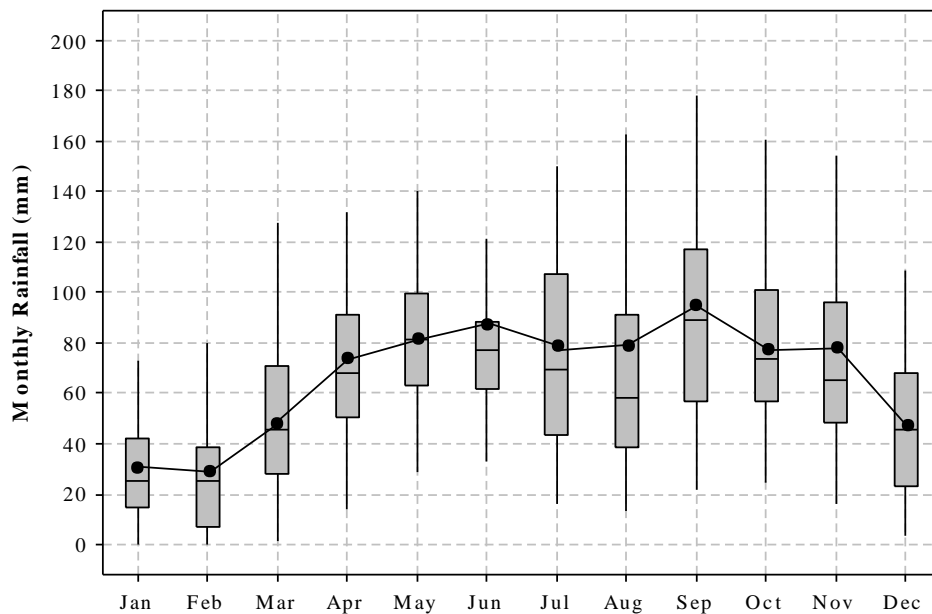
Figure 5.17: Box and Whiskers Plot of Simulated Monthly Rainfall in London

The boxes show the 25th percentile, 50 percentile and 75th percentile of data while the whiskers are plotted with 1.5 times the inter-quartile range from the boxes. Black line denotes the monthly mean rainfall from observations. For all cases the historic observed means are shown in terms of line plot to assess the ability of the weather generator to reproduce the temporal and spatial character of rainfall for the City of London. From the Figure 5.17, it is seen that the model has been able to replicate the historic observed pattern adequately.

Next, the daily rainfall is disaggregated into hourly values using the method described in section 3.3.2. The comparison of the performance of the historic simulated hourly values with the observed hourly data is presented in terms of frequency plots (Figure 5.18). The frequency of small range rainfall is slightly over-estimated and the mid range rainfall is slightly under-estimated by the disaggregation model. Overall, the frequency of the extreme rainfall is captured well.
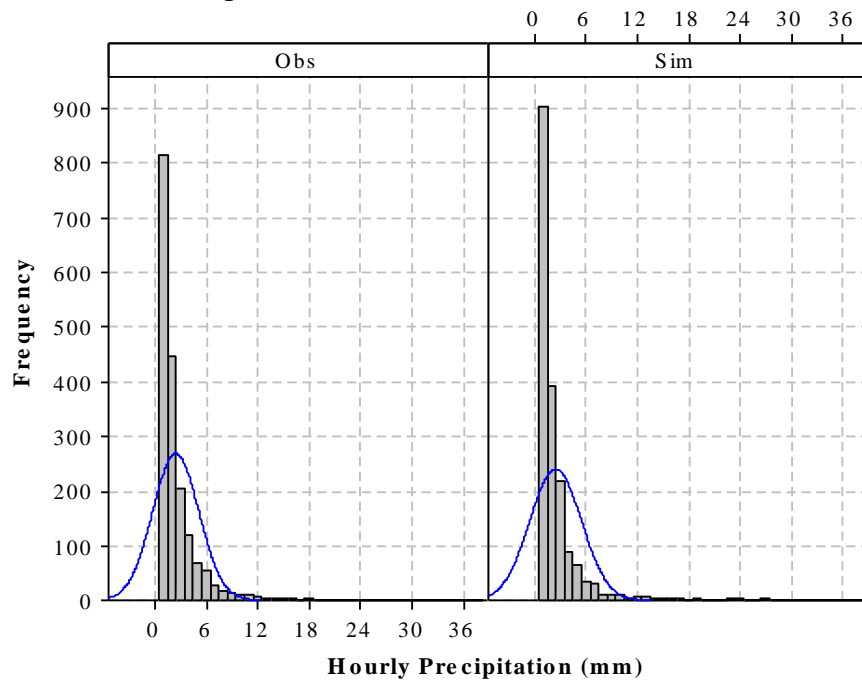
Figure 5.18: Frequency Plots of Observed (Obs) and Simulated (Sim) Hourly Rainfall

Finally, the annual maximum rainfall for 1, 2, 6, 12 and 24 hour durations is generated to fit Gumbel distribution for calculating return periods. These are then compared with the IDF information obtained from Environment Canada (EC) (Table 5.12).

Table 5.12 (a): Comparison of Extreme Rainfall in London in terms of Depth (mm)

Historic Unperturbed (1965-2003)	Return Period, T years					
Duration, hrs	2	5	10	25	50	100
1	21.80	30.38	36.06	43.24	48.56	53.85
2	28.05	40.11	48.09	58.18	65.66	73.09
6	36.41	49.90	58.83	70.11	78.49	86.80
12	42.61	56.33	65.41	76.89	85.40	93.86
24	49.70	64.63	74.52	87.01	96.28	105.48
EC (1943-2003)	Return Period, T years					
Duration, hrs	2	5	10	25	50	100
1	24.40	35.30	42.50	51.60	58.30	65.00
2	29.60	41.60	49.50	59.60	67.00	74.40
6	36.70	48.20	55.80	65.40	72.50	79.60
12	43.00	54.70	62.50	72.40	79.70	87.00
24	51.30	66.80	77.10	90.00	99.60	109.20

Table 5.12 (b): Relative Difference between EC IDF Information and Historic Unperturbed Scenario

Duration, min	Return Period, T years					
	2	5	10	25	50	100
60	11.25	14.98	16.39	17.63	18.22	18.76
120	5.38	3.66	2.89	2.42	2.02	1.78
360	0.80	3.46	5.29	6.96	7.93	8.65
720	0.91	2.94	4.56	6.02	6.91	7.58
1440	3.18	3.30	3.40	3.37	3.39	3.46

It should be noted that the Environment Canada uses rainfall data from 1943-2003 to develop IDF curves for London. However, hourly data is available only from 1961; data prior to 1961 may exist in paper form and are not available. For the present study, the hourly rainfall data for London is further reduced down to 1965 for matching rainfall data from other nearby stations to be used for multi-site weather generator. Table 5.12 (a) presents the intensity-duration-frequency data obtained from the historic unperturbed scenario together with the IDF data generated by EC. The results obtained are compared in terms of the relative differences (Equation 4.13).

Table 5.12 (b) presents the relative difference of rainfall intensity between the historic unperturbed and the EC data. The short duration rainfall (1 hr) is underestimated by the historic unperturbed scenario, while the intermediate (2, 6, 12 hrs) and longer (24 hrs) duration rainfalls are able to closely replicate the EC generated intensities for all return periods.

5.3.2 IDF Results for Future Climate

The perturbation process inside the weather generator is added to generate IDF information using the historical observed rainfall. This scenario called 'historical perturbed' assumes that the future climate will continue to change as the consequence of already altered green house gas concentrations in the atmosphere, ignoring any future change in green house gas emissions. Table 5.13 presents comparison between the monthly mean precipitation from different AOGCM scenarios and historical observed values. Mean monthly precipitation vary significantly between months for all models.

Table 5.13: Monthly Mean Precipitation (mm) from AOGCMs for 1965-1990

Scenarios/month	Jan	Feb	Mar	Apr	May	Jun	Jul	Aug	Sep	Oct	Nov	Dec
Observed	**2.28**	**2.21**	**2.51**	**2.65**	**2.48**	**2.80**	**2.46**	**2.79**	**3.04**	**2.66**	**3.17**	**3.16**
CGCM3T47	1.99	1.95	2.25	2.71	2.88	2.66	2.12	2.11	2.35	2.29	2.88	2.73
CGCM3T63	2.14	1.80	2.45	2.84	3.69	3.42	3.00	2.40	2.30	2.87	2.67	2.93
CSIROMK3	1.94	2.16	2.44	2.97	3.28	2.64	2.42	1.80	1.72	2.31	2.42	2.21
ECHAM5OM	3.01	3.63	3.62	4.11	4.33	4.41	3.58	3.47	3.32	2.47	2.99	3.09
ECHO-G	2.08	2.10	2.49	3.43	4.45	3.66	3.82	3.18	2.59	2.67	2.92	2.21
GFDLCM2.1	2.46	2.83	2.86	2.90	3.54	3.19	3.23	3.04	3.36	2.29	2.83	2.62
GISSAOM	2.04	2.22	2.51	2.79	2.54	2.21	2.59	2.91	3.18	3.04	2.57	2.56
MIROC3.2 HIRES	2.88	2.56	2.97	3.32	3.01	3.23	3.76	3.34	3.40	2.90	3.28	3.14
MIROC3.2 MEDRES	2.21	2.57	2.64	2.86	2.92	3.49	3.71	3.00	2.96	2.47	2.52	2.40
CCSRNIES B21	1.84	2.24	2.86	3.25	3.63	4.18	4.77	3.52	2.07	1.40	1.73	2.05
CSIROMk2b B11	1.51	1.53	1.74	2.34	2.50	3.21	3.26	2.20	1.71	1.88	1.79	1.64

So using the methods described in section 3.3.1 downscaled outputs are corrected for the bias from AOGCMs to contain same mean as the observed climate. The daily weather generator output, after being disaggregated into hourly rainfall, is next used to generate intensity duration frequency data for 27 different scenarios presented in Table 4.10 to create different realizations of future climate using different AOGCM responses. Figure 5.19 presents the IDF data obtained using climate scenarios in terms of depth. The ECHAM5AOM A1B and MIROC3MEDRES A2 models appear to be the wettest and the driest amongst all. The summarized results of the percent differences in the rainfall intensity between the wettest, the driest scenarios (Figure 5.19) and the historic perturbed scenarios are presented in Table 5.14.

Table 5.14: Percent Differences between Historic Perturbed, Wet and Dry Scenarios

ECHAM5AOM_A1B (Wet Scenario) and Historic Perturbed

Duration, min	Return Period, T years					
	2	5	10	25	50	100
60	62.68	69.56	72.42	75.00	76.44	77.60
120	60.64	65.84	67.98	69.91	70.99	71.86
360	65.13	77.09	82.29	87.12	89.88	92.13
720	66.03	77.77	83.09	88.17	91.13	93.57
1440	63.22	72.99	77.42	81.63	84.07	86.09

MIROC3MEDRES_A2 (Dry Scenario) and Historic Perturbed

Duration, min	Return Periods, T years					
	2	5	10	25	50	100
60	-6.79	-2.90	-1.28	0.18	0.99	1.65
120	-12.70	-15.09	-16.07	-16.96	-17.45	-17.85
360	-7.06	-6.60	-6.40	-6.21	-6.10	-6.02
720	-0.68	1.66	2.72	3.73	4.32	4.81
1440	-0.44	-0.10	0.05	0.20	0.28	0.35
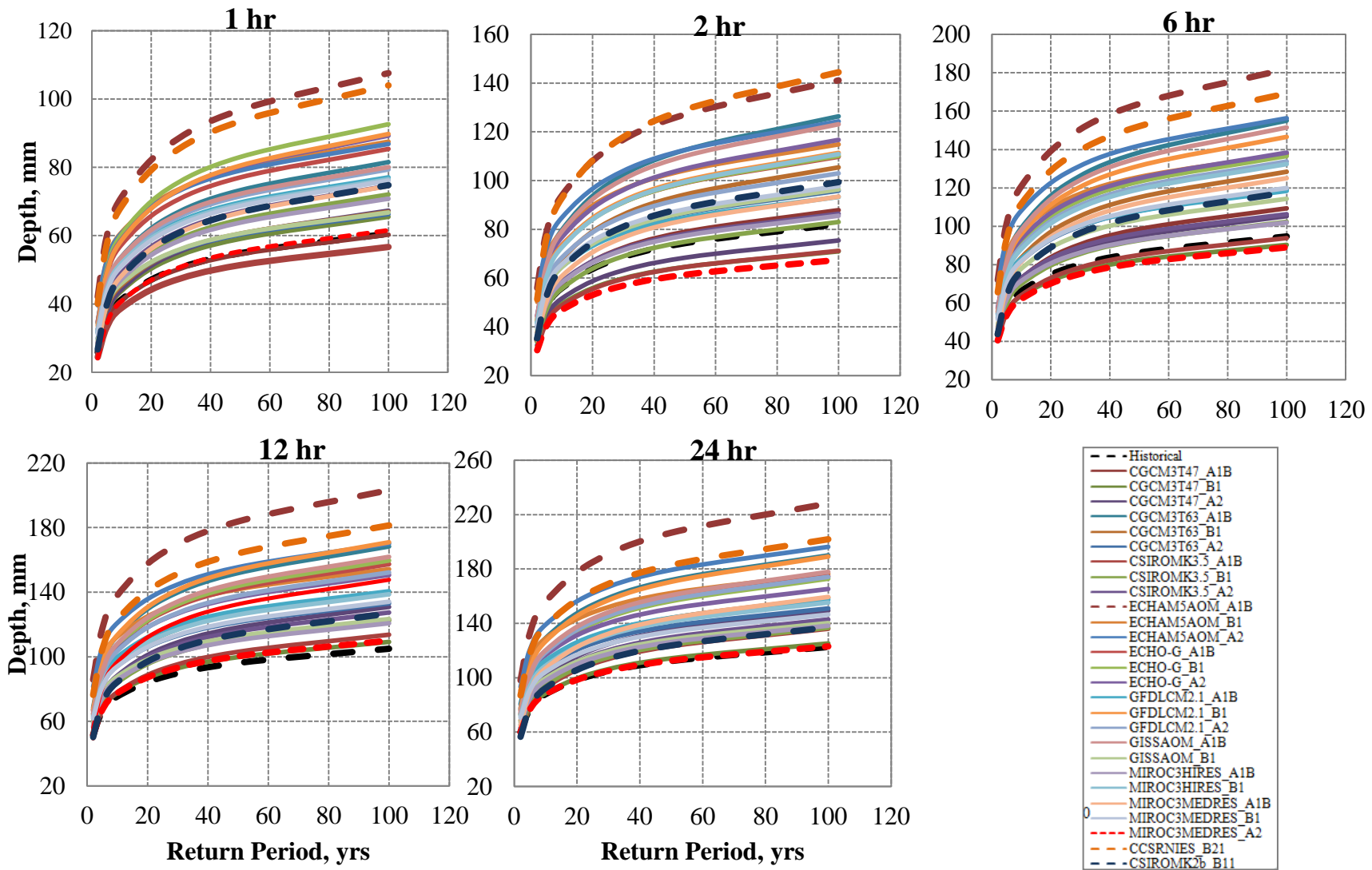
Figure 5.19: IDF Plots of AOGCM Scenarios for Different Durations

The wettest ECHAM5AOM A1B model shows an average of 80% increase in rainfall compared to the historic perturbed scenario. While the driest MIROC3.2 MEDRES A2 scenario shows slight decrease in precipitation intensity than the historic perturbed scenario.

5.3.3 Uncertainty Quantification of IDF Results

Because of the inherent uncertainties, the newly developed IDF curves from different AOGCMs are unable to provide an accurate estimate of future extreme rainfall, but they establish a significant fact: the future climate will not be the same as the historic one. Previous studies (Simonovic and Peck, 2009; Prodanovic and Simonovic, 2007) have generated updated IDF information for the City of London for 2050s (2041-2070) based on a single scenario (CCSRNIES B21) selected from the upper range of all scenarios presented in this study. In presence of uncertainties presented in section 5.3.2, adoption of one single scenario may suffer from under/over-estimation of the risks, which may have significant implications for the storm water management and design practice. So, a kernel estimator based on the data driven plug-in approach described in section 3.2.4 is applied next to quantify the uncertainty arising from different AOGCM scenarios. Due to the fact that unlike other uncertainty estimation methods, kernel estimator provides variable weights at each point of interest, weights are calculated from the mean of all AOGCM data for presentation purpose. The weight function is calculated by modifying Equation 3.40 as follows:

$$w(x, x_j, \lambda) = \frac{\frac{x - x_j}{\lambda}}{\sum_{j=1}^{27} \frac{x - x_j}{\lambda}} \tag{5.1}$$

where,

x represents any data point within the range of generated data for time period t for which kernel estimator is applied;

x_j is the AOGCM simulated data;

λ is the plug-in bandwidth; and

$j = 1,2, ….., 27$ is the number of AOGCM models and scenarios.

The mean of the total sample size x_{ij} is considered as the data point from which the distance will be measured, where $i = 1,2, ……… 117$ years of simulated IDF data.

Figure 5.20 and Appendix J present the IDF curves incorporating extreme rainfall information from the AOGCM scenarios. In this case, four scenarios are selected: the 'historical perturbed' scenario as future state ignoring climate change, 'ECHAM5AOM A1B' scenario as the wettest scenario, 'MIROC3MEDRES A2' as the driest and the 'resultant' scenario as the weighted scenario incorporating multi-model information. The IDF curves of these selected scenarios for all durations are presented in Appendix J. Table 5.15 presents the percent difference between the historical perturbed and resultant scenarios for 2080s. From the Table 5.15 it is seen that due to the changing climate, the intensity of rainfall is expected to increase by 20-40 % in 2071-2099.
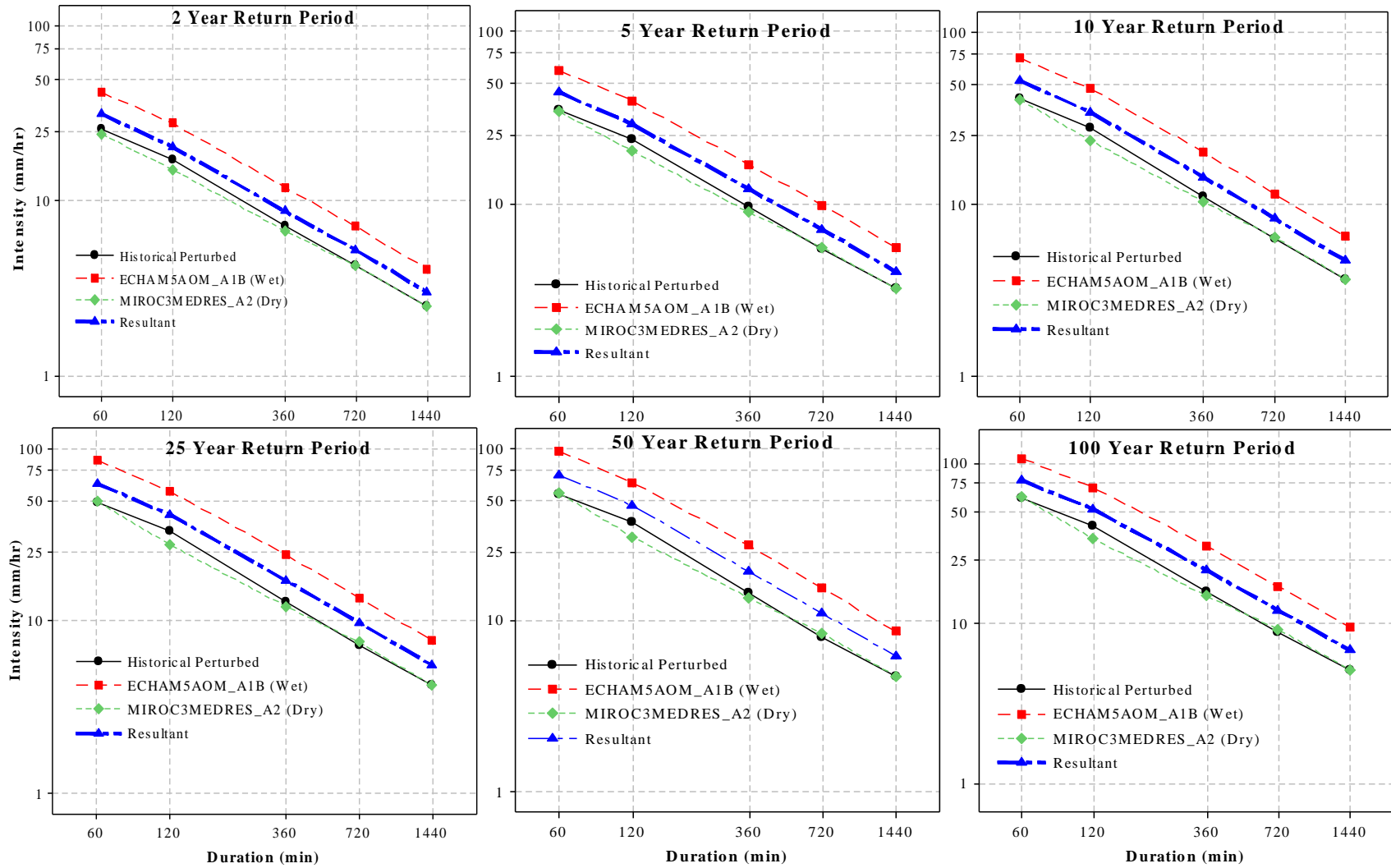
Figure 5.20: Comparison of IDF Plots for Different Scenarios

Table 5.15: Percentage Difference between Historical Perturbed and the 'Resultant'

Scenario for 2080s

Duration, min	Return Period, T years					
	2	5	10	25	50	100
60	21.76	25.29	26.76	28.08	28.82	29.42
120	17.40	21.41	23.06	24.55	25.38	26.04
360	20.85	27.32	30.14	32.75	34.25	35.47
720	22.20	28.94	31.99	34.91	36.61	38.01
1440	20.63	25.77	28.10	30.32	31.60	32.67

Finally, the probabilities of extreme rainfall for all return periods are presented in terms of cumulative distribution plots. First, IDF plot of the resultant scenario is created (Figure 5.21). The cumulative distribution plots using the IDF from the AOGCM scenarios are plotted for all return periods and are presented in Figures 5.22 (a) through (e).
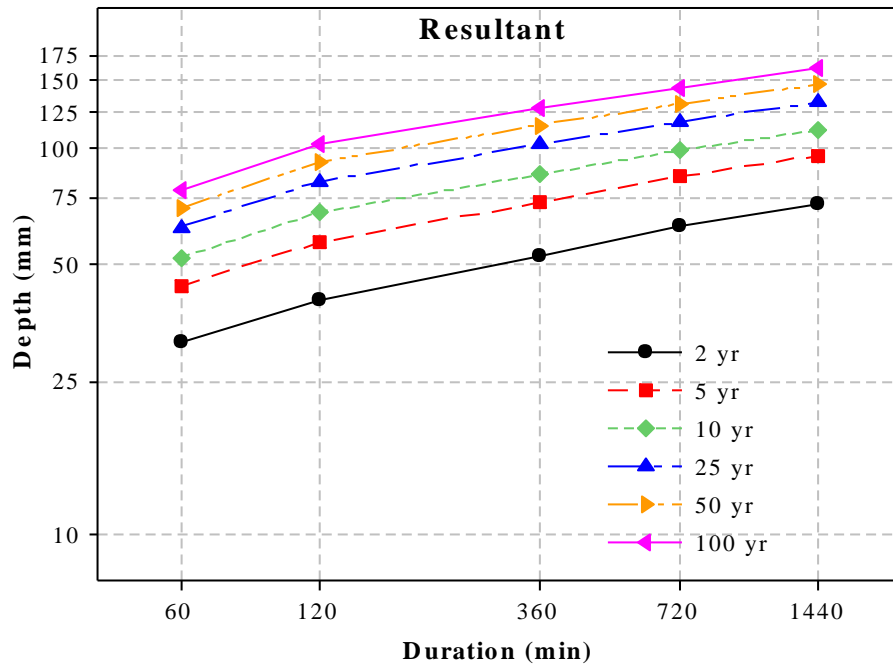
Figure 5.21: IDF Plot for Resultant Scenario

Information from Figures 5.21 and 5.22 are combined to gather probabilities for any specific storm for any specific return period. For example, if the depth of 6 hour (360 min) storm for 5 year return period is 75 mm (Figure 5.21), the maximum probability of this specific storm from Figure 5.22 (b) is obtained to be 0.66. This additional probability information will allow to the use of the updated IDF information with more confidence.
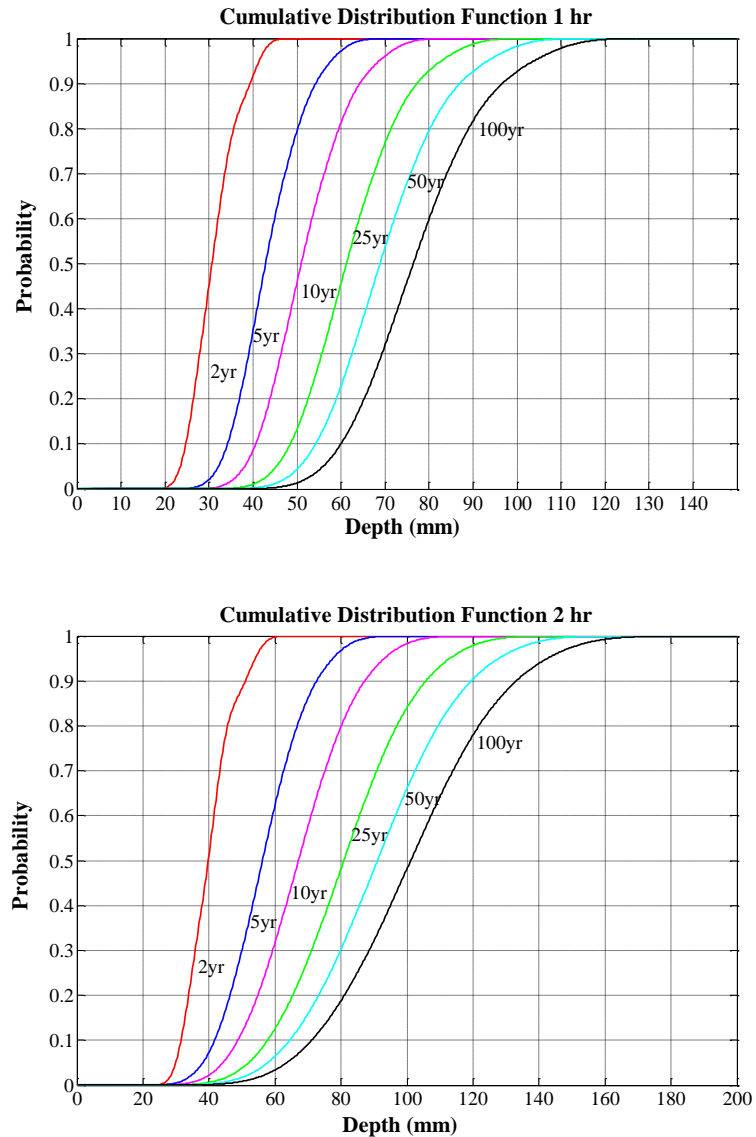
Figure 5.22 (a): Probability based IDF Curve of 1 and 2 Hour Duration
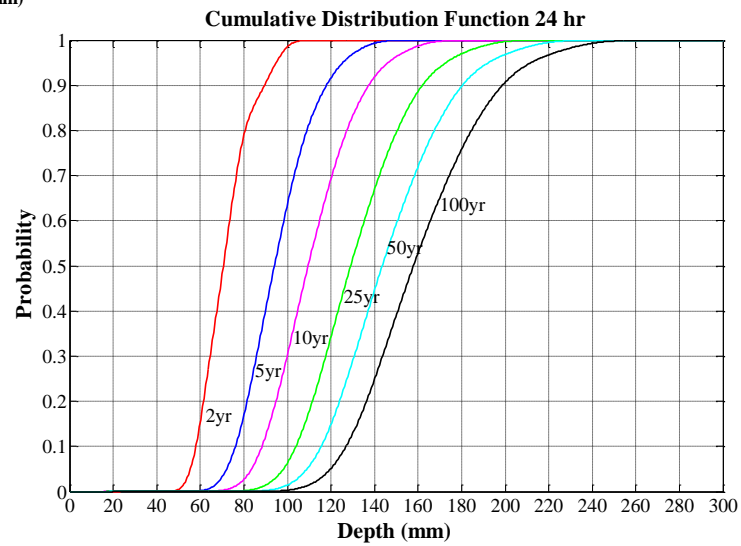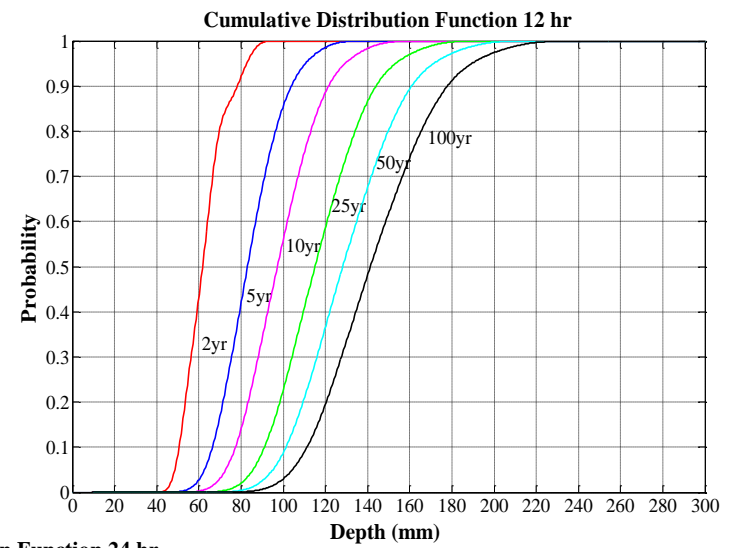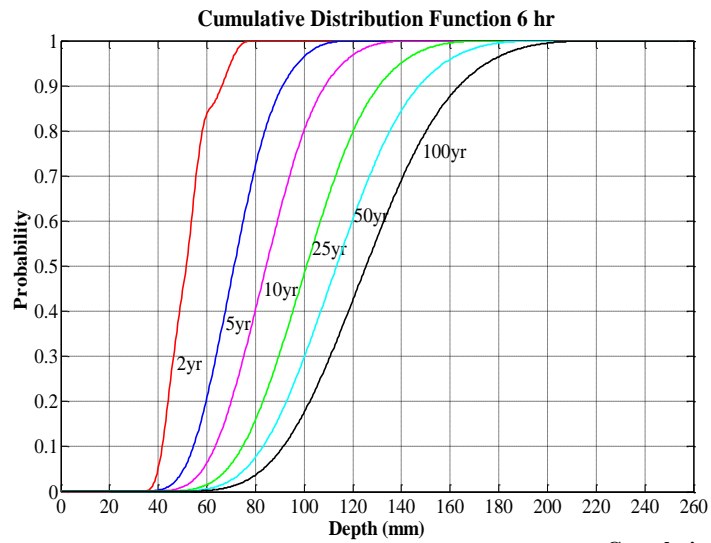
Figure 5.22 (b): Probability based IDF Curve of 6, 12, 24 Hour Duration

179

CHAPTER SIX

CONCLUSIONS

The work presented in this thesis has introduced three important questions related to the studies of climate extremes: (i) how should the AOGCM outputs from different global climate models and scenarios be selected to assess the severity of extreme climate events?; (ii) should climate change studies adopt equal weights from the global climate model information while modeling uncertainty?; and (iii) what are the chances for the future extreme precipitation events to be more severe?. In an attempt to answer these questions, the major findings of the three major themes of works are presented in the following sections. First, the applicability of reanalysis data for climate change and hydrological modeling studies are outlined. Second, remarks regarding parametric and nonparametric uncertainty estimation techniques for estimating multiple AOGCM and scenario uncertainties for extreme precipitation events are presented. Finally, the results for developing a probability based intensity-duration-frequency curves are summarized.

6.1 Major Findings

6.1.1 Assessment of Reanalysis Data

In mountainous, remote regions, or even for stations with large amount of missing data, the task of hydrologic modeling continues to be a major challenge due to the overall lack of information. In a rapidly changing climate, this is becoming a major concern. In order to investigate the hydrologic impacts of climate change it is important to model the present climate accurately. The global and regional reanalysis data from the National

Centre for Environmental Prediction (NCEP) with their more refined spatial and temporal coverage have the potential to be used effectively in data scarce regions. To take advantage of these synthetic data, there is, however, a need for accurate synopsis of the climate conditions. Because the reanalysis dataset is produced by assimilating observed weather information, including surface temperature into a numerical weather forecast system, it can be thought of as the product of an advanced interpolation scheme (numerical weather model) which takes into account important factors, such as topography and land cover (Choi et al. 2009). In this study, the performance of the NCEP global and regional reanalysis data under present climate conditions for precipitation and temperature are verified with selected stations around the Upper Thames River basin in the South-western Ontario, Canada. NARR dataset has been able to interpret a real scenario by capturing the temperature trends during 1980-2005, with some over-estimation during the summer months. The means and the variances of both datasets do appear to be similar when evaluated by t and F tests. The results for computing precipitation at several stations show variable results. While for some stations the reanalysis datasets performed well, for a couple of stations both of them appeared to suffer from under-estimation and over-estimation, thereby necessitating a careful check before their application. The overall goodness of fit results indicate better performance by NARR when compared to NNGR.

The present study has demonstrated that the NARR data can be a feasible substitute to the observed weather stations data. It is, however, important to keep in mind the limitation of NARR data: (i) the daily gauged data that is used for the assimilation of NARR, comes in 1 degree grid for the Canadian domain which may be insufficient for

the assimilating model to perform well; and (ii) the weather station data represent point information while NARR provides areal averages in 32 km x 32 km grid. A considerable variation of climate within the NARR grid cells is possible, which can be more prominent in complex topographies. The latter is, however, not considered a major drawback as in hydrologic modeling the areal representation of precipitation is more important than the point precipitation (Choi et al, 2009).

For this study, the meteorological inputs from the NCEP data sources are used with the semi-distributed continuous hydrologic model developed based on the computational engine of HEC-HMS for the period 1980-2005. The differences between the two datasets appear to be more prominent from the following analysis. First, the comparison of their relative bias shows that NNGR is associated with a more significant bias than its NARR counterpart. The NARR produced an insignificant negative bias at all locations, which may be due to insufficient meteorological inputs that have restricted the representation of the real basin conditions. Second, the flow hydrographs show that NNGR is associated with some biases that lead to time shifts of the peaks. This can be the result of (a) the continuous model calibration for low flow conditions, and/or (b) the sparse grid points, especially from NNGR. In the case of NARR, the model performance for low flow improves at downstream locations with the increase of the contributing basin area. Although there are under- and over-estimations, NARR has not shown any systematic bias. The comparisons of the precipitation and flow scatter plots support the above explanation: higher flows are scattered from their fitted lines while the precipitation and low flows appeared to be in better agreement. Third, the box plots present a clear distinction between the two reanalysis datasets: the NARR data have successfully

followed the trend, while the performance of NNGR data has been inferior. The errors associated with the generated flows that are derived from estimating means and variances have been further tested using the non-parametric Wilcoxon rank sum test and Levene's test. Both tests indicate that NARR dataset leads to smaller error. Its variability is also shown to be closer to the observed variability for most of the months at the 95% confidence level.

Based on the following observations, it can be concluded that the differences in simulating discharge using NARR and NNGR data sets lie in their inherent process of generating precipitation. The NARR data are produced by assimilating high quality and detailed precipitation observations into the atmospheric analysis. Therefore, they are making the forcing into the land surface model component of the system more accurate by enabling the interaction of the land hydrology and land-atmosphere. This interaction has not been considered in the NNGR. The coarser grid of NNGR may also have limited its performance. Considering the satisfactory performance of NARR, and also the drawbacks of NARR data over some parts of the Canadian landscape, it is suggested that a thorough investigation should be carried out for its application in both climate and hydrologic impact studies.

6.1.2 Uncertainty Estimation

This part of the thesis dealt with the approaches for quantifying AOGCM and scenario uncertainties from the modeled outputs of extreme precipitation events for London, Ontario, Canada. The work is strictly limited to the uncertainties of the outputs

from several AOGCMs and scenarios and does not consider the uncertainties due to parameterization or structure of the models. Two very different multi-model ensemble methods namely, the Bayesian reliability ensemble average (BA-REA) and the downscaling based kernel density estimator are used for uncertainty estimation. A comparison of these two methods reveals that while the BA-REA method can be a good alternative for predicting mean changes in precipitation in any region, it cannot be used in estimating uncertainties of different extreme events occurring at a daily time scale. The capability of the BA-REA method to analyze the climate responses is fairly limited; whereas the downscaled outputs can be obtained in any frequency according to the need of the user. The data-driven kernel estimator is capable of assuming data values at each time step as an independent realization, instead of calculating weights based on the means. It has a significant implication for estimating uncertainties of extreme precipitation events; calculating weights based on the mean can ignore the higher or lower values which may cause an unrealistic representation of climate extremes, such as floods, droughts, etc. However, the kernel estimator has its limitations too, from the extended chance of over or under-smoothing resulting from wrong selection of bandwidth. The comparison of the best fit curves for different AOGCM scenarios for extreme precipitation indices shows varying agreement and thereby the limited benefits of parametric distribution approach.

The choice of an appropriate bandwidth selection method is a significant step for kernel estimation. The shape of the distribution function is important in determining the performance of the bandwidth. The comparative results of different bandwidth selectors show that the rule of thumb (ROT) method assuming normal kernel suffers from over-

smoothing for both indices while the least square cross validation (LCV) method results in under-smoothed distributions. The Sheather Jones plug in (SJPI) estimator offered a useful compromise between the ROT and the LCV methods. This trade-off between the distributions of the bandwidths seems to be an intrinsic criterion for assessing the performance of data-driven bandwidth selectors. Using the SJPI bandwidths, the CDFs for different severity classes are calculated for the extreme precipitation indices. The analyses are based on the assumption that the outputs from different AOGCMs are independent realizations; hence, indices have a different PDF at each time step and are not limited to any specific type of distribution. The nonparametric methods can be seen as a major improvement over the parametric methods which assume specific distributions for estimating uncertainties. Considering the probabilities obtained, it can be said that the probability of severe and extreme events are going to increase for both summer and winter, due to the changes in climate over next century.

6.1.3 Intensity-Duration-Frequency Analysis

The methodology for updating of rainfall IDF curves for the City of London incorporating uncertainties associated with the use of different AOGCMs are presented in the final section. The analysis of the annual maximum rainfall for developing intensity-duration-frequency plots for the City of London under climate change has resulted in important findings. Overall, two objectives have been achieved by this study. First, an extensive investigation of the possible realizations of future climate from 29 scenarios

185

developed from AOGCM models and scenarios are performed using a downscaling based disaggregation approach. A nonparametric K-Nearest Neighbor (K-NN) multi-site weather generator operating on a daily time step is used to produce long sequence of rainfall data. The use of perturbation scheme eliminates the assumptions of data stationarity to some extent by generating data beyond the range of the input. The selection of appropriate stations using cross correlation and statistical regression analysis has strengthened the justification of using multi-site weather generator. Multiple stations better capture the surrounding spatial and temporal characteristics of rainfall for the station of interest. This has important implication for generating rainfall extremes for future due to the widely suspected inability of AOGCMs to simulate good quality precipitation data.

The disaggregation scheme used in this study is developed based on nonparametric K-NN algorithm. Since the scheme does not require any parameterization, it can be transferred to any area of interest with minimal adjustment. The downscaled daily outputs are disaggregated into hourly values. Annual maximum series of rainfall are fitted to Gumbel distribution to develop IDF curves for 1, 2, 6, 12 and 24 hour durations for 2, 5, 10, 25, 50 and 100 years return periods. The associated uncertainties are estimated using non-parametric kernel estimation approach and the resultant IDF curve is developed based on a probabilistic way.

The basic findings from the study are presented as follows:

- The rainfall patterns in the City of London will most certainly change in future due to climate change.

186

- Generation of future IDF information based on single site is limited. Incorporating a multi-site weather generator to produce sequences of future rainfall offers a more reliable approach for providing better spatial and temporal characteristics of rainfall patterns.

- Adoption of a single scenario for developing IDF information only provides a single realization of the future; application of a multi-model approach can provide more realistic information about the future climate.

- Use of the wettest or the driest scenario may be useful to capture the upper and lower bound scenario of the future climate change; however, single use of any of these scenarios may suffer from over/underestimation of the rainfall extremes with serious implications on storm water management practice and the development of design standards.

- Although the results derived from different scenarios indicate large uncertainty associated with the global climate models, all of them indicate increase in intensity of future rainfall with a varying degree.

- A kernel based plug-in estimation approach is able to incorporate the uncertainties arising from different AOGCM models and to provide a more acceptable change in future rainfall extremes. The resultant scenario combining information from all AOGCMs and emission scenario responses indicates approximately 20-40% change in different duration rainfall for all return periods.

- Use of a probability based intensity-duration-frequency curve is encouraged in order to apply the updated IDF information with higher level of confidence.

6.2 Conclusion

The research findings presented in section 6.1 has added important information to the studies of extreme events. Assessment of regional reanalysis hydro-climatic has shown a promising potential as an addition or alternate to the observed data in the mountainous, data scarce regions or even regions with higher missing values. The generated future climate scenarios represent the nature and progression of uncertainties from several global climate models and their emission scenarios. The comparison of two different multi-model uncertainty ensemble models has provided useful information. The variable weight method combining downscaling based on a principal component integrated weather generator and data driven kernel density estimator is capable of considering the AOGCM outputs as individual realization at each time step, rather than depending on their performances based on the mean or bias values. The prevalent conception of the increased intensity of extreme precipitation indices resulting from climate change are quantified with probability information. Classifying these indices based on their severity level has added useful insight to the occurrence of those extreme rare events (events with $>75^{th}$ percentile values). The intensity-duration-frequency curves for future climate are also integrated with probability information. Overall, the presented research is expected to broaden our existing knowledge on the nature of the extreme precipitation events and the propagation and quantification of uncertainties arising from the global climate models and emission scenarios.

6.3 Recommendations for Future Research

Present work offers a framework for estimating uncertainties from the modeled outputs of multiple AOGCMs and scenarios. This section provides some recommendations for further research:

- In the first section of the study, only global and regional reanalysis data are investigated for their application in the climate change and hydrologic modeling studies. Based on the analysis, the NARR data is further used as additional input with the observed data in the statistical downscaling method based weather generator for generating long sequences of climate data. As stated earlier, the NARR suffers from limitation due to its relatively coarse grid. A comparison of its performances with the recently developed finer grid data (10 km), such as the Canadian daily dataset (Hutchison et al, 2009) may help towards the search for a more accurate source of alternative database.

- The uncertainty estimation methodology introduced in this research does not consider uncertainties arising from the use of different downscaling approaches. It is possible that uncertainty may also arise from the use different parameters within the same downscaling approach. Future research thus may include uncertainty investigation of the downscaling approaches. The Principal Component based K- Nearest Neighbour weather generator used for downscaling purpose considers only the first principal component for calculating Mahalanobis distance. Addition of more principal components is expected to improve the downscaling results. The weather generator used in the study is set that it can

be applied to daily data only. Modification of the algorithm for a finer temporal scale is recommended.

- The yearly maximum rainfall generated for developing the probability based intensity-duration-frequency curve in this work considers utilization of the annual maximum series (AMS) method only. A comparison of peak over threshold (POT) and AMS may help to provide more accurate IDF curves. The disaggregation scheme used in this study does not consider inter-station characteristics which may miss some important information from the neighbouring stations. In this study only duration over 1 hour is considered. Sub-hourly durations can have significant impact on the municipal storm water management practice. The generated IDF curves are based on yearly maximum values. Seasonal analysis of extremes and developing seasonal IDFs will be an interesting extension of the current research. Use of more comprehensive inputs other than daily rainfall is encouraged. Finally, application of the probable maximum precipitation (PMP) method should be carried out too.

REFERENCES

Adamowski, K., (1985). Nonparametric kernel estimation of flood frequencies. *Water Resources Research, 21 (11),* 1585-1590.

Agirre-Basurko, E., G. Ibarra-Berastegi and I. Madariagac, (2006). Regression and multilayer perceptron-based models to forecast hourly O_3 and NO_2 levels in the Bilbao area. *Environmental Modelling and Software, 21*, 430–446.

Allan, M. R., and W. J. Ingram, (2002). Constraints on future changes in climate and the hydrologic cycle, *Nature, 419,* 224– 232.

Allen, M. R., P. A. Stott, J. F. B. Mitchell, R. Schnur, and T. L. Delworth, (2000). Quantifying the uncertainty in forecasts of anthropogenic climate change. *Nature*, *407*, 617-620.

Apipattanavis, S., G. Podesta, P. Rajagopalan, and R. W. Katz, (2007). A semi-parametric multivariate and multisite weather generator. *Water Resources Research*, *43*, W11401, doi: 10.1029/2006WR005714.

Bardossy, A., (1997). Downscaling from GCM to local climate through stochastic linkages. *Journal of Environmental Management, 49,* 7-17.

Bárdossy A., and H. J. Caspary, (1990). Detection of climate change in Europe by analyzing European atmospheric circulation patterns from 1881 to 1989. *Theor. Appl. Climatol.,* 42, 155- 167.

Beersma, J. J., T. A. Buishand, and R. Wojcik, (2001). Rainfall generator for the Rhine basin: multi-site simulation of daily weather variables by nearest-neighbour resampling. In: Generation of Hydrometeorologicalreferenceconditionsfor the assessment of flood

hazard in largeriverbasins, P. Krahe and D. Herpertz (Eds.), CHR-Report No. I-20, Lelystad, 69-77.

Benestad, R. E., (2004). Tentative probabilistic temperature scenarios for northern Europe. *Tellus, Ser. A, 56,* 89– 101.

Bennett, T., (1998). Development and application of a continuous soil moisture accounting algorithm for the Hydrologic Engineering Center Hydrologic Modeling System (HEC-HMS). Masters Thesis, Department of Civil and Environmental Engineering, University of California, Davis, California.

Bowman, A. W., (1984). An alternative method of cross-validation for the smoothing of density estimates, *Biometrika, 71,* 353-360.

Brandsma, T., and T. A. Buishand, (1998). Simulation of extreme precipitation in the Rhine basin by nearest-neighbour resampling. *Hydrology and Earth System Sciences, 2(2-3),* 195-209.

Brissette, F., R. Leconte, M. Minville, and R. Roy, (2006). Can we adequately quantify the increase/decrease of flooding due to climate change?. *EIC Climate Change Technology, IEEE*. Doi: 10.1109/EICCCC.2006.277254.

Brown, M. B., and A. B. Forsythe, (1974). Robust tests for the equality of variances. *Journal of the American Statistical Association, 69,* 364-367.

Buishand, T. A. and G. R. Demare, (1990). Estimation of the annual maximum distribution from samples of maxima in separate seasons. *Stochastic Hydrol. Hydraul., 4,* 89-103.

Burger, G., (1996). Expanded downscaling for generating local weather scenarios. *Climate Research, 7,* 111-128.

Buytaert, W., R. Ceˊlleri, and L. Timbe, (2009). Predicting climate change impacts on water resources in the tropical Andes: effects of GCM uncertainty. *Geophysical Research Letters, 36*, L07406, doi:10.1029/2008GL037048.

Castro, C. L., R. A. Pielke Sr. and J. O. Adegoke, (2007). Investigation of the summer climate of the contiguous United States and Mexico using the Regional Atmospheric modeling System (RAMS). Part I: Model Climatology (1950 - 2002). *Journal of Climate, 20,* 3844–3864.

CCCSN (2011). Canadian Climate Change Scenarios Network. Retrieved on 3/01/2011 from http://cccsn.ca/downscaling.

Choi, W., A. Moore, and P. F. Rasmussen, (2007). Evaluation of temperature and precipitation data from NCEP-NCAR global and regional reanalysis for hydrological modeling in Manitoba. *In* Proceedings of the CSCE 18th Hydrotechnical Conference on Challenges for Water Resources Engineering in a Changing World, Winnipeg, Manitoba, 1-10.

Choi, W., S. K. Kin, P.F. Rasmussen, and A. R. Moore, (2009). Use of the North American regional reanalysis for hydrologic modelling in Manitoba. *Canadian Water Resources Journal, 34 (1),* 17-36.

Colglazier, E., (1991). Scientific uncertainties, public policy, and global warming: how sure is sure enough. *Policy Studies Journal, 19 (2)*, 61-72.

Conover, W. J., (1980). *Practical Nonparametric Statistics*. 2nd Edition. Wiley, New York.

Cortereal, J, X. B. Zhang, and X. L. Wang, (1995). Downscaling GCM information to regional scales - a nonparametric multivariate regression approach, *Clim Dynam*, *11* (7), 413-424.

Coles S., (2001). *An Introduction to Statistical Modeling of Extreme Values*. Springer, London.

Coulibaly, P. and X. Shi, (2005). Identification of the effect of climate change on future design standards of drainage infrastructure in Ontario. Report prepared by McMaster University with funding from the Ministry of Transportation of Ontario. 82 pp.

Crane, R. G., and B.C. Hewitson, (1998). Doubled CO_2 precipitation changes for the susquehanna basin: down-scaling from the genesis global climate model. *International Journal of Climatology*, *18*, 65-76.

CSA (2010). Development, interpretation and use of rainfall intensity- duration-frequency (IDF) information: A guideline for Canadian water resources practitioners. 1st Edn., Canadian Standards Association, CSA PLUS 4013-10.

Cubasch, U., G. A. Meehl, G. J. Boer, R. J. Stouffer, M. Dix, A. Noda, C. A. Senior, S. Raper, and K. S. Yap, (2001). The scientific basis. Contribution of working group 1 to the Third assessment report of the Intergovernmental Panel of Climate Change, Cambridge University Press, Cambridge, UK and New York, USA, 881 pp.

Cunderlik, J. M., and S. P. Simonovic, (2004). Assessment of water resources risk and vulnerability to changing climatic conditions: Calibration, verification and sensitivity analysis of the HEC-HMS hydrologic model. Report No. IV, Department of Civil and Environmental Engineering, The University of Western Ontario, London, Ontario, Canada.

Cunderlik, J. M. and S. P. Simonovic, (2005). Hydrological extremes in a southwestern Ontario river watershed under future climate conditions. *IAHS Hydrological Sciences Journal, 50(4)*, 631–654.

DAI Catalogue, (2009). Catalogue available datasets through DAI (Data Access and Integration), version 1.0, April 2009, Montreal, QC, Canada, 24 pp.

De Michele, and C., G. Salvadori, (2005). Some hydrological applications of small sample estimators of generalized Pareto and extreme value distributions. *Journal of Hydrology, 301,* 37–53.

Desramault, N., (2008). Estimation of intensity duration frequency curves for current and future climates. Thesis submitted to the Graduate and Postdoctoral Studies Office in partial fulfilments of requirements of the degree of Master of Engineering department, McGill University, Montreal, Québec, Canada. 75 pp.

Diaz-Neito, J., and R. L. Wilby, (2005). A comparison of statistical downscaling and climate change factor methods: Impacts on low flows in the River Thames, United Kingdom. *Climatic Change, 69*, 245-268.

Dibike Y. B. and P. Coulibaly, (2005). Hydrologic impact of climate change in the Saguenay watershed: Comparison of downscaling methods and hydrologic models. *Journal of Hydrology, 307(1-4)*, 145-163.

Efromovich, S., (1999). *Nonparametric Curve Estimation: Methods, Theory, and Applications*, Springer, New York.

Elshamy, M. E., H.S. Wheater, N. Gedney and C. Huntingford, (2006). Evaluation of the rainfall component of a weather generator for climate impact studies. *J. Hydrol., 326,* 1–24.

Ensor, L. A. and S. M. Robeson, (2008). Statistical characteristics of daily precipitation: comparisons of gridded and point datasets. *Journal of Applied Meteorology and Climatology, 47(9),* 2468- 2476.

Eum, H. I., V. Arunachalam, and S. P. Simonovic, (2009). Integrated reservoir management system for adaptation to climate change impacts in the Upper Thames River basin. Water Resources Research Report no. 062, Facility for Intelligent Decision Support, Department of Civil and Environmental Engineering, London, Ontario, Canada, 81 pages. ISBN: (print) 978-0-7714-2710-7; (online) 978-0-7714-2711-4.

Ghosh, S., and P. P. Majumdar, (2007). Nonparametric methods for modeling GCM and scenario uncertainty in drought assessment. *Water Resources Research, 43,* W07495, 19pp, doi:10.1029/2006WR005351.

Giorgi, F., and L. O. Mearns, (2003). Probability of regional climate change calculated using the reliability ensemble averaging (REA) method. *Geophysical Research Letters, 30(12)*, 1629, doi: 10.1029/2003GL017130.

Guo, S.L., R. K. Kachroo, and R. J. Mngodo, (1996). Nonparametric kernel estimation of low flow quantiles. *Journal of Hydrology, 185,* 335-348.

Haberlandt, U., and G. W. Kite, (1998). Estimation of daily space-time precipitation series for macroscale hydrologic modeling. *Hydrological Processes, 12,* 1419-1432.

Hall, P., and J. S. Marron, (1991). Lower bounds for bandwidth selection in density estimation. *Probability Theory and Related Fields, 90,* 149-173.

Hanson, C. L., and G. L. Johnson, (1998). GEM (Generation of weather Elements for Multiple applications): its application in areas of complex terrain. *Hydrology, Water Resources and Ecology in Headwaters IAHS, 248*, 27-32.

Hennessy, K. J., and J. F. B. Mitchell, (1997). Changes in daily precipitation under enhanced greenhouse conditions. *Climate Dynamics, 13,* 667-680.

Hewitson B. C, and R, G. Crane, (1992). Regional-scale climate prediction from the GISS GCM. *Global Planet Change Sec, 97*, 249-267.

Huard, D., A. Mailhot, and S. Duchesne, (2010). Bayesian estimation of intensity-duration-frequency curves and of the return period associated to a given rainfall event. *Stoch. Environ. Res. Risk. Assess., 2,* 337-347.

Hughes, J. P., and P. Guttorp, (1994). A class of stochastic models for relating synoptic atmospheric patterns to regional hydrologic phenomena. *Water Resources Research, 30(5),* 1535–1546.

Hutchinson, M. F., D. W. McKenney, K. Lawrence, J. H. Pedlar, R. F. Hopkinson, E. Milewska, and P. Papadopol, (2009). Development and testing of Canada-wide interpolated spatial models of daily minimum-maximum temperature and precipitation for 1961-2003. *Journal of Applied Meteorology and Climatology, 48 (4),* 725-741.

Huth, R, (2004). Sensitivity of local daily temperature change estimates to the selection of downscaling models and predictors, *Journal of Climate*, *17*, 640-651.

Intergovernmental Panel on Climate Change (IPCC) (2007). Climate change (2007). Impacts, adaptation and vulnerability. Contribution of working group II to the Fourth Assessment Report of the Intergovernmental Panel on Climate Change, edited by M. Parry et al., Cambridge University Press, UK.

IPCC (2007). Climate change (2007) The physical science basis. Contribution of working group 1 to the Fourth Assessment Report of the Intergovernmental Panel of Climate Change, Annexes [Baede, A.P.M. (ed.)]. Cambridge University Press, Cambridge UK and New York, USA, 48 pp.

Jackson, C., M. K. Sen, and P. L. Stoffa, (2004). An efficient stochastic Bayesian approach to optimal parameter and uncertainty estimation for climate model predictions. *J. Climate, 17,* 2828–2841.

Jaruskova, D. and M. Hanek, (2006). Peak over threshold method in comparison with block maxima method for estimating high return levels of several northern Moravia precipitation and discharges Series. *J. Hydrol. Hydromech, 4,* 309-319.

Jarvis, C.S. et al., (1936). Floods in the United States, Magnitudes and Frequency. USGS Water Supply Paper 771, Washington, DC.

Jolly, W. M., J. M. Graham, A. Michailis, R. Nemani, and S. W. Running, (2005). A flexible integrated system for generating meteorological surfaces derived from point sources across multiple geographic scales. *Environmental Modelling and Software, 20*, 873- 882.

Jones, M.C., J. S. Marron, and S. J. Sheather, (1996). A brief survey of bandwidth selection for density estimation. *Journal of the American Statistical Association, 91(433),* 401–407.

Joubert A. M, and B. C. Hewitson, (1997). Simulating present and future climates of southern Africa using general circulation models. *Prog Phys Geog., 21*, 51–78.

Jones, P. D., J.M. Murphy, and M. Noguer, (1995). Simulation of climate change over Europe using a nested regional-climate model, I: assessment of control climate, including sensitivity to location of lateral boundaries, *Q. J. R. Meteorological Society*, *121*, 1413-1449.

Kalnay, E., and M. Cai, (2003). Impact of urbanization and land use change on climate. *Nature, 423*, 528-531.

Kalnay, E., M. Kanamitsu, R. Kistler, W. Collins, D. Deaven, L. Gandin, M. Iredell, S. Saha, G. White, J. Woolen, Y. Zhu, M. Chelliah, W. Ebisuzaki, W Higgins, J. Janowiak, C. Mo, C. Ropelewski, J. Wang, A. Leetmaa, R. Reynolds, R. Jenne, and D. Joseph, (1996). The NCEP-NCAR Reanalysis Project. *Bulletin of the American Meteorological Society, 77 (3),* 437–471.

Katz, R. W., M. B. Parlange, and P. Naveau, (2002). Statistics of extremes in hydrology. *Advances in Water Resources, 25,* 1287-1304.

Kay, A. L., and H. N. Davies, (2008). Calculating potential evaporation from climate model data: A source of uncertainty for hydrological climate change impacts. *Journal of Hydrology, 358,* 221-239.

Kessler, E., and B. Neas, (1994). On correlation, with applications to the radar and raingage measurement of rainfall. *Atmos. Res., 34,* 217-229.

Khan, S., P. Coulibaly, and Y. Dibike, (2006). Uncertainty analysis of statistical downscaling methods using Canadian global climate model predictors. *Hydrologic Processes, 20*, 3085-3104.

Khaliq, M. N., T. B. Ouarda, P. Gachon, and L. Sushama, (2008). Temporal evolution of low-flow regimes in Canadian rivers. *Water Resources Research, 44,* W08436, doi:10.1029/2007WR006132.

Kidson, J. W., (2000). An analysis of New Zealand synoptic types and their use in defining weather regimes. *Int. J. Climatol, 20*, 299-316.

Kittel, T. G. F. and Coauthors, (2004). VEMAP Phase 2 bioclimatic database I. Gridded historical (20th century) climate for modeling ecosystem dynamics across the conterminous USA. *Climate Research, 27*, 151-170.

Kuchar, L., (2004). Using WGENK to generate synthetic daily weather data for modelling of agricultural processes. *Mathematics and Computers in Simulation, 65,* 69–75.

Lall, U., (1995). Nonparametric function estimation: recent hydrologic contributions. Reviews of Geophysics, Contributions in Hydrology, U.S. National Report to the IUGG 1991-1994, 1093-1099.

Lall, U., B. Rajagopalan and D. G. Tarboton, (1996). A nonparametric wet/dry spell model for daily precipitation. *Water Resources Research, 32(9),* 2803-2823.

Langbein, W.B., (1949). Annual floods and the partial duration flood series. *Transactions of AGU, 30,* 879–881.

Legates, D. R. and G. J. McCabe, (1999). Evaluating the use of goodness of fit measures in hydrologic and hydro-climatic model validation. *Water Resources Research, 35 (1),* 233-241.

Levene, H., (1980). *Contributions to Probability and Statistics*. Stanford University Press, USA.

Mehrotra, R., R. Srikanthan, and A. Sharma. (2006). A comparison of three stochastic multi-site precipitation occurrence generators. *Journal of Hydrology, 331,* 80-292.

Madsen, H., and D. Rosbjerg, (1997). Generalized least squares and empirical Bayes estimation in regional partial duration series index-flood modeling. *Water Resources Research, 33 (4),* 771–781.

Mailhot, A. and S. Duchesne, (2010). Design criteria of urban drainage infrastructures under climate change. *J Water Resour Plann Manage, 136,* 201–208.

Mailhot, A., S. Duchesne, G. .Rivard, E. Nantel, D. Caya, and J-P Villeneuve, (2006). Climate change impacts on the performance of urban drainage systems for Southern Québec. *Proceedings of EIC Climate Change Technology Conference*, Ottawa, Ontario, Canada.

Mansour, R. and D. H. Burn, (2010). Weather generator and hourly disaggregation model. Department of Civil Engineering, University of Waterloo, Waterloo, Ontario, Canada, April 2010.

Mesinger, F., G. DiMego, E. Kalnay, K. Mitchell, P. C. Shafran, W. Ebisuzaki, D. Jovic, J. Wollen, E. Rogers, E. H. Berbery, M. B. Ek, Y. Fan, R. Grumbine, W. Higgins, H. Ki, Y. Lin, G. Mankin, D. Parrish, and W. Shi, (2006). North American regional reanalysis. *Bulletin of the American Meteorological Society, 87(3),* 343-360.

NCAR (2010). National Centre for Atmospheric Research. Retrieved on 8/04/2010 from http://www.image.ucar.edu/~nychka/REA/.

Min, S.-K., X. Zhang, and F. W. Zwiers, (2011). Human contribution to more-intense precipitation extremes. *Nature, 470,* 378-381.

Minitab Inc., (2007). Minitab 15 Statistical Software. [Computer software]. State College, PA: Minitab, Inc. (www.minitab.com).

Minville, M., F. Brissette, and R. Leconte, (2008). Uncertainty of the impact of climate change on the hydrology of a Nordic watershed. *Journal of Hydrology, 358,* 70-83.

MTO (1997). Ministry of Transportation of Ontario drainage management manual. Drainage and Hydrology Section, Transportation Engineering Branch, and Quality Standards Division, Ministry of Transportation of Ontario, Ottawa, Ontario, Canada.

Murphy, J. M. et al., (2004). Quantifying uncertainties in climate change from a large ensemble of general circulation model predictions. *Nature, 430*, 768–772. (doi:10.1038/nature02771).

Muzik, I., (2001). Sensitivity of hydrologic systems to climate change. *Canadian Water Resources Journal, 26 (2),* 233–253.

Nakicenovic, N., J. Alcamo, G. Davis, B. de Vries, J. Fenhann, and co-authors, (2000). IPCC special report on emissions scenarios. *UNEP/GRID-Ardenal Publications*.

Neito, S., M. D. Frias, and C. Rodriguez-Puebla, (2004). Assessing two different climatic models and the NCEP-NCAR reanalysis data for the description of winter precipitation in the Iberian Peninsula. *International Journal of Climatology, 24*, 361-376.

New, M., and M. Hulme, (2000). Representing uncertainty in climate change scenarios: a Monte-Carlo approach. *Integrated Assessment, 1,* 203-213.

Nguyen, T-D., V-T-V. Nguyen, and P. Gachon, (2007*a*). A spatial-temporal downscaling approach for construction of intensity-duration-frequency curves in consideration of GCM-based climate change scenarios. *Advances in Geosciences*, *6,* 11-21.

Nguyen, V-T-V., T-D. Nguyen, and A. Cung, (2007*b*). A statistical approach to downscaling of sub-daily extreme rainfall processes for climate-related impacts studies in urban areas. *Water Science and Technology: Water Supply*, *7 (2),* 183-192.

Nigam, S. And A. Ruiz-Barradas, (2006). Seasonal hydroclimate variability over North American global and regional reanalysis and AMIP simulations: varied representation. *Journal of Climate, 19 (5)*, 815-837.

NOAA (2008). The National Oceanic and Atmospheric Administration. Retrieved on 4/7/2008 from http://www.cdc.noaa.gov/cdc/data.ncep.reanalysis.html.

Onof, C., and K. Arnbjerg-Nielsen, (2009). Quantification of anticipated future changes in high resolution design rainfall for urban areas. *Atmospheric Research, 92*, 350–363. doi:10.1016/j.atmosres.2009.01.014.

Pall, P., T. Aina, D. A. Stone, P. A. Stott, T. Nozawa, A. G. Hilberts, D. Lohmann, and M. R. Allen, (2011). Anthropogenic greenhouse gas contribution to flood risk in England and Wales in autumn 2000. *Nature, 370,* 382-385.

Pielke, R. A. Sr., (2002). *Mesoscale Meteorological Modeling*. 2nd ed. Academic Press, Orlando, Florida. 676 pp.

Polansky, A. M. and E. R. Baker (2000). Multistage plug-in bandwidth selection for kernel distribution function estimates. *Journal of Statistical Computation and Simulation*, *65*, 63-80.

Ponce, V. M., (1989). *Engineering Hydrology, Principles and Practices*. Prentice-Hall, Englewood Cliffs, New Jersey.

Prodanovic, P., (2008). Water resources systems under climate change: a simulation approach. PhD thesis, Faculty of Graduate Studies, The University of Western Ontario, London, Ontario, Canada.

Prodanovic, P. and S. P. Simonovic, (2006). Inverse drought risk modeling of the Upper Thames River Watershed. Water Resources Research Report no. 053, Facility for Intelligent Decision Support, Department of Civil and Environmental Engineering, London, Ontario, Canada, 252 pages. ISBN: (print) 978-0-7714-2636-0; (online) 978-0-7714-2637-7.

Prodanovic, P., and S. P. Simonovic, (2007). Development of rainfall intensity duration frequency curves for the city of London under the changing climate. Water Resources

Research Report no. 058, Facility for Intelligent Decision Support, Department of Civil and Environmental Engineering, London, Ontario, Canada, 51 pages. ISBN: (print) 978-0-7714-2667-4; (online) 978-0-7714-2668-1.

Proudhomme, C., D. Jakob, and C. Svensson, (2003). Uncertainty and climate change impact on the flood regime of small UK catchments, *Journal of Hydrology, 277,* 1 – 23.

Raisanen, J., and T. N. Palmer, (2001). A probability and decision-model analysis of a multimodel ensemble of climate change simulations. *J. Climate, 14,* 3212– 3226.

Randall, D.A., R.A. Wood, S. Bony, R. Colman, T. Fichefet, J. Fyfe, V. Kattsov, A. Pitman, J. Shukla, J. Srinivasan, R.J. Stouffer, A. Sumi and K.E. Taylor, (2007). Climate Models and Their Evaluation. In: Climate change 2007: The physical science basis. Contribution of Working Group I to the Fourth Assessment Report of the Intergovernmental Panel on Climate Change [Solomon, S., D. Qin, M. Manning, Z. Chen, M. Marquis, K.B. Averyt, M.Tignor and H.L. Miller (eds.)]. Cambridge University Press, Cambridge, United Kingdom and New York, NY, USA.

Rasmussen, P.F., F. Ashkar, D. Rosbjerg, and B. Bobee, (1994). The POT method for flood estimation: a review. In: Hipel, K.W. (Ed.), Stochastic and Statistical Methods in Hydrology and Environmental Engineering, Extreme Values: Floods and Droughts, vol. 1. Kluwer, Dordrecht, NL, pp. 15–26.

Reid, P. A., P. D. Jones, O. Brown, C. M. Goodess, and T. D. Davies, (2001). Assessments of the reliability of NCEP circulation data and relationships with surface climate by direct comparisons with station based data. *Climate Research, 17*, 247–261.

Richardson, C.W., (1981). Stochastic simulation of daily precipitation, temperature, and solar radiation. *Water Resources Research 17*, 182–90.

Rosenblatt, M., (1956). Remarks on some nonparametric estimates of a density function. *Ann. Math. Statist. 27(3),* 832-837.

Rudemo, M. (1982). Empirical Choice of Histograms and Kernel Density Estimators. *Scandinavian Journal of Statistics, 9,* 65-78.

Ruiz-Barradas, A., and S. Nigam, (2006). Great Plains hydroclimatic variability: The view from the North American regional reanalysis. *Journal of Climate, 19 (12),* 3004– 3010.

Rummukainen, M., (1997). Methods for statistical downscaling of GCM simulations. *RMK No. 80*, SMHI, Norrkping.

Rusticucci, M. M. and V. E. Kousky, (2002). A comparative study of maximum and minimum temperatures over Argentina: NCEP-NCAR Reanalysis versus station data. *Journal of Climate, 15 (15),* 2089-2101.

Salathe Jr., E. P., (2003). Comparison of various precipitation downscaling methods for the simulation of streamflow in a rainshadow river basin. *International Journal of Climatology, 23,* 887-901.

Schoof, J. T., A. Arguez, J. Brolley, J. J. O'Brien, (2005). A new weather generator based on spectral properties of surface air temperatures. *Agricultural and Forest Meteorology 135*, 241–251.

Schmidli, J., C. Frei, and P. L. Vidale, (2006). Downscaling from GCM precipitation: A benchmark for dynamical and statistical downscaling methods. *Int. J. Climatol., 26*, 679– 689.

Schulze, R. E., (1997). Impacts of global climate change in a hydrologically vulnerable region: challenges to South African hydrologists. *Progress in Physical Geography, 21*, 113-136.

Scott, D. W., and G. R. Terrell, (1987). Biased and Unbiased Cross- Validation in Density Estimation. *Journal of the American Statistical Association, 82,* 1131-1146.

Semenov, M. A, and E. M Barrow, (1997). Use of a stochastic weather generator in the development of climate change scenarios. *Climatic Change, 35,* 397-414.

Sharma, A., D. G. Tarbaton, and U. Lall, (1997). Streamflow simulation − a nonparametric approach. *Water Resources Research, 33 (2),* 291-308.

Sharif, M., and D. H. Burn, (2006). Simulating climate change scenarios using an improved K-nearest neighbor model. *Journal of hydrology, 325,* 179-196.

Sharif, M., D. H. Burn, and K. M. Wey, (2007). Daily and hourly weather generation using a K-nearest neighbor approach. 18th CSCE Hydrotechnical Conference, August 2007, Winnipeg, MB, 1 - 10.

Sharma, A., and R. O'Neill, (2002). A nonparametric approach for representing interannual dependence in monthly streamflow sequences. *Water Resources Research, 38(7),* doi 10.1029/2001 WR000953.

Sheather, S. J., (1983). A data-based algorithm for choosing the window width when estimating the density at a point. *Computational Statistics and Data Analysis, 1,* 229-238.

Sheather, S. J., (1986). An improved data-based algorithm for choosing the window width when estimating the density at a point. *Computational Statistics and Data Analysis, 4, 61-65.*

Sheather, S. J., and M. C. Jones, (1991). A reliable data-based bandwidth selection method for kernel density estimation. *Journal of the Royal Statistical Society, Ser. B, 53,* 683-690.

Silva, V. B. S., V. E. Kousky, W, Shi, and R. W. Higgins, (2007). An improved gridded historical daily precipitation analysis for Brazil. *Journal of Hydrometeorology, 8*, 847-861.

Silverman, B. W., (1986). *Density Estimation for Statistics and Data Analysis. Monographs on Statistics and Applied Probability*, Chapman & Hall/ CRC., Washington, D.C.

Simonovic, S.P, (2009). *Managing Water Resources: Methods and Tools for a Systems Approach*. Earthscan, London, Sterling, VA.

Simonovic, S. P., and A. Peck, (2009). Updated rainfall intensity duration frequency curves for the City of London under the changing climate. Water Resources Research Report no. 065, Facility for Intelligent Decision Support, Department of Civil and Environmental Engineering, London, Ontario, Canada, 64 pages. ISBN: (print) 978-0-7714-2819-7; (online) 978-0-7714-2820-3.

Smith, R. L., C. Tebaldi, D. Nychka, and L. Mearns, (2009). Bayesian modeling of uncertainty in ensembles of climate models. *Journal of the American Statistical Association, 104 (485),* 97-116., doi: 10.1198/jasa.2009.0007.

Solaiman, T. A., and S. P. Simonovic, (2010). NCEP-NCAR reanalysis data for hydrologic modelling on a basin scale. *Canadian Journal of Civil Engineering*, *37(4),* 611-623.

Soltani, A., and G. Hoogenboom, (2003). A statistical comparison of the stochastic weather generators WGEN and SIMMETEO. *Climate Research 24,* 215-230.

Sorooshian, S, Q. Duan, and V. Gupta, (1993). Calibration of rainfall-runoff models: application of global optimization to the Sacramento soil moisture accounting model. *Water Resources Research, 29(4)*, 1185-1194.

Srikanthan, R., and T. A. McMahon, (2001). Stochastic generation of annual, monthly and daily climate data: a review. *Hydrology and Earth Systems Sciences 5 (4),* 653–670.

Stainforth, D. A., T. E. Downing, R. W. A. Lopez, and M. New, (2007). Issues in the interpretation of climate model ensembles to inform decisions. *Philos. Trans. R. Soc., Ser. A, 365,* 2163–2177.

Sterl, A., (2004). On the (in)homogeneity of reanalysis products. *Journal of Climate, 17(19),* 3866-3873.

Stone, D. A., and M. R. Allan, (2005). The end-to-end attribution problem: from emissions to impacts, *Climate. Change, 77,* 303– 318.

Sun, Y., S. Solomon, A. Dai, and R. Portmann, (2006). How often does it rain? *Journal of Climate, 19*, 916–934.

Svanidze, G.G., (1977). *Mathematical Modeling of Hydrologic Series*, T. Guerchon, translator, Water Resources Publications, Littleton, Colorado.

Svensson, C., R. Clarke, D. Jones, (2007). An experimental comparison of methods for estimating rainfall intensity-duration-frequency relations from fragmantory methods. *Journal of Hydrology, 341*, 79-89.

Taesombat, V., V. Yevjevich, (1978). Use of partial flood series for estimating distribution of maximum annual flood peak. Hydrology Papers #97, Colorado State University, Fort Collins, CO.

Tebaldi, C., L. O. Mearns, D. Nychka, and R. L. Smith, (2004). Regional probabilities of precipitation change: A Bayesian analysis of multimodel simulations. *Geophysical Research Letters, 31*, L24213, doi: 10.1029/2004GL021276.

Tebaldi, C., R. L. Smith, D. Nychka and L.O. Mearns, (2005). Quantifying uncertainty in Projections of Regional Climate Change: a Bayesian Approach to the Analysis of Multimodel Ensembles. *Journal of Climate, 18 (10),* 1524-1540.

Tebaldi, C., and R. L. Smith, (2010). Characterizing uncertainty of climate change projections using hierarchical models. In The Oxford Handbook of Applied Bayesian Analysis [eds. O'Hagan, T. and West, M.], Oxford University Press, UK, 896 pp.

Terrell, G. R. (1990). The maximal smoothing principle in density estimation. *Journal of the American Statistical Association, 85,* 470-477.

Terrell, G. R., and D. W. Scott, (1985). Oversmoothed nonparametric density estimates. *Journal of the American Statistical Association, 80,* 209-214.

Thorne, R. and M. K. Woo, (2006). Efficacy of a hydrologic model in simulating discharge from a large mountainous basin. *Journal of Hydrology, 330*, 301-312.

TIBCO Software Inc., (2008). S-Plus 8.0 Statistical Software. [Computer software]. Somerville, MA. (http://spotfire.tibco.com/products/s-plus/statistical-analysis-software.aspx).

Tolika, K., P. Maheras, H. A. Flocas, and A. A.-P. Imitriou, (2006). An evaluation of a General Circulation Model (GCM) and the NCEP-NCAR Reanalysis data for winter precipitation in Greece. *International Journal of Climatology, 26*, 935–955.

Trenberth, K. E., A. Dai, R. M. Rasmussen, and D. B. Parsons, (2003). The changing character of precipitation. *Bulletin of American Meteorological Society, 84*, 1205–1217. (doi:10.1175/BAMS-84-9-1205)

Trigo, R.M. and J.P. Palutikof, (2001). Precipitation scenarios over Iberia: a comparison between direct GCM output and different downscaling techniques. *J. Climate 14*, 4422-4446.

Tung, Y. K., (1996). Uncertainty analysis in water resources engineering. Stochastic Hydraulics' 96, Tickle, Goulter, Xu, Wasimi & Bouchart (eds). 1996 Balkema, Rotterdam, ISBN 9054108177.

USACE, (2006). Hydrologic modelling system HEC–HMS, User's manual for version 3.0.1. United States Army Corps of Engineers, Hydrologic Engineering Center, Davis, California.

Vidal J.-P., and S. D. Wade, (2008). A framework for developing high-resolution multi-model climate projections: 21st century scenarios for the UK. *International Journal of Climatology, 28(7),* 843-858.

Vincent, L.A., and E. Mekis, (2006). Changes in daily and extreme temperature and precipitation indices for Canada over the twentieth century. *Atmosphere-Ocean, 44(2),* 177- 193.

von Storch, J.-S., (1999). What determines the spectrum of a climate variable at zero frequency. *Journal of Climate, 12*, 2124-2127.

Watt, W., K. Lathem, C. Neill, T. Richards, and J. Rousselle, (1989). Hydrology of Floods in Canada: A guide to Planning and Design. National Research of Canada, Ottawa, Ontario, Canada.

Whitfield, P. H., and A. J. Cannon, (2000). Recent variation in climate and hydrology in Canada. *Canadian Water Resources Journal, 25 (1),* 19–65.

Widmann M, C. S. Bretherton, and E. P. Salathe-Jr., (2003). Statistical precipitation downscaling over the North-western United States using numerically simulated precipitation as a predictor. *Journal of Climate, 16(5),* 799-816.

Wilby, R. L., and I. Harris (2006). A framework for assessing uncertainties in climate change impacts: Low-flow scenarios for the River Thames, UK, *Water Resources Research, 42,* W02419, doi: 10.1029/2005WR004065.

Wilby, R.L., S. P. Charles, E. Zorita, B. Timbal, P. Whetton, and L. O. Mearns, (2004). The guidelines for use of climate scenarios developed from statistical downscaling Methods. *Supporting material of the Intergovernmental Panel on Climate Change (IPCC), pre- pared on behalf of Task Group on Data and Scenario Support for Impacts and Climate Analysis (TGICA).(http : ==ipccddc:cru:uea:ac:uk=guidelines=StatDownGuide:pdf).*

Wilby, R. L., and T. M. L. Wigley, (2000). Precipitation predictors for downscaling: observed and general circulation model relationships. *International Journal of Climatology, 20,* 641-661.

Wilks D. S. and R. L. Wilby, (1999). The weather generation game: a review of stochastic weather models. *Progress in Physical Geography, 23(3),* 329-357.

Wilks, D.S., (1998). Multi-site generalization of a daily stochastic precipitation model. *Journal of Hydrology, 210*, 178–191.

Willmott, C. J., (1981). On the validation of models. *Phys. Geogr., 2,* 184-194.

Willmott, C. J., R. E. Ackleson, J. J. Davis, K. M. Feddema, D. R. Klink, L. Legates, J. O'Donnell, C. M. and Rowe, (1985). Statistics for the evaluation and comparison of models. *J. Geophys. Res., 90*, 8995-9005.

Woo, M-K, and R. Thorne, (2006). Snowmelt contribution to discharge from a large mountainous catchment in subarctic Canada. *Hydrologic Processes, 20,* 2129-2139.

Wood, A. W., L. Leung, V. Sridhar, and D. P. Lettenmaier, (2004). Hydrologic implications of dynamical and statistical approaches to downscaling climate model outputs. *Climatic Change, 62*, 189–216, 2004.

Xu, Chong-Yu, and V. P. Singh, (2004). Review on regional water resources assessment models under stationary and changing climate. *Water Resources Management, 18,* 591–612.

Yates D, S. Gangopadhyay, B. Rajagopalan, and K. Strzepek, (2003). A technique for generating regional climate scenarios using a nearest-neighbour algorithm, *Water Resources Research, 39(7),* 1199-1213.

Zhang, Q., C- Y Xu, Z. Zhang, Y-D. Chen, C-L. Liu, and H. Lin, (2008). Spatial and temporal variability of precipitation maxima during 1960 – 2005 in the Yangtze River basin and possible association with large scale circulation. *Journal of Hydrology, 353*, 215–217.

Zhang, X., L. A Vincent, W. D. Hogg, and A. Niitsoo, (2000). Temperature and precipitation trends in Canada during the 20th century. *Atmosphere-Ocean, 38,* 395-429.

Zorita, E. and H. von Storch, (1999). The analog method - a simple statistical downscaling technique: comparison with more complicated methods. *J. Climate, 12*, 2474-2489.

APPENDICES

APPENDIX A: Atmosphere-Ocean Global Climate Models

Criteria for Selecting Climate Scenarios

Five criteria that should be met by climate scenarios if they are to be useful for impact researchers and policy makers are suggested by IPCC (2007) and are quoted here:

- *Criterion 1: Consistency with global projections. They should be consistent with a broad range of global warming projections based on increased concentrations of greenhouse gases. This range is variously cited as 1.4°C to 5.8°C by 2100, or 1.5°C to 4.5°C for a doubling of atmospheric CO2 concentration (otherwise known as the "equilibrium climate sensitivity").*

- *Criterion 2: Physical plausibility. They should be physically plausible; that is, they should not violate the basic laws of physics. Hence, changes in one region should be physically consistent with those in another region and globally. In addition, the combination of changes in different variables (which are often correlated with each other) should be physically consistent.*

- *Criterion 3: Applicability in impact assessments. They should describe changes in a sufficient number of variables on a spatial and temporal scale that allows for impact assessment. For example, impact models may require input data on variables such as precipitation, solar radiation, temperature, humidity and wind speed at spatial scales ranging from global to site and at temporal scales ranging from annual means to daily or hourly values.*

- *Criterion 4: Representative. They should be representative of the potential range of future regional climate change. Only in this way can a realistic range of possible impacts be estimated.*

- *Criterion 5: Accessibility. They should be straightforward to obtain, interpret and apply for impact assessment. Many impact assessment projects include a separate scenario development component which specifically aims to address this last point. The DDC and this guidance document are also designed to help meet this need.*

Challenges in using AOGCMs

GCMs depict the climate using a three dimensional grid over the globe (Figure), typically having a horizontal resolution of between 250 and 600 km, 10 to 20 vertical layers in the atmosphere and sometimes as many as 30 layers in the oceans. Their resolution is thus quite coarse relative to the scale of exposure units in most impact assessments, hence only partially fulfilling criterion 3. Moreover, many physical processes, such as those related to clouds, also occur at smaller scales and cannot be properly modeled. Instead, their known properties must be averaged over the larger scale in a technique known as parameterization. This is one source of uncertainty in GCM-based simulations of future climate. Others relate to the simulation of various feedback mechanisms in models concerning, for example, water vapor and warming, clouds and radiation, ocean circulation and ice and snow albedo. For this reason, GCMs may simulate quite different responses to the same forcing, simply because of the way certain processes and feedbacks are modeled.

However, while these differences in response are usually consistent with the climate

215

sensitivity range described in criterion 1, they are unlikely to satisfy criterion 4 concerning the uncertainty range of regional projections. Even the selection of all the available GCM experiments would not guarantee a representative range, due to other uncertainties that GCMs do not fully address, especially the range in estimates of future atmospheric composition.
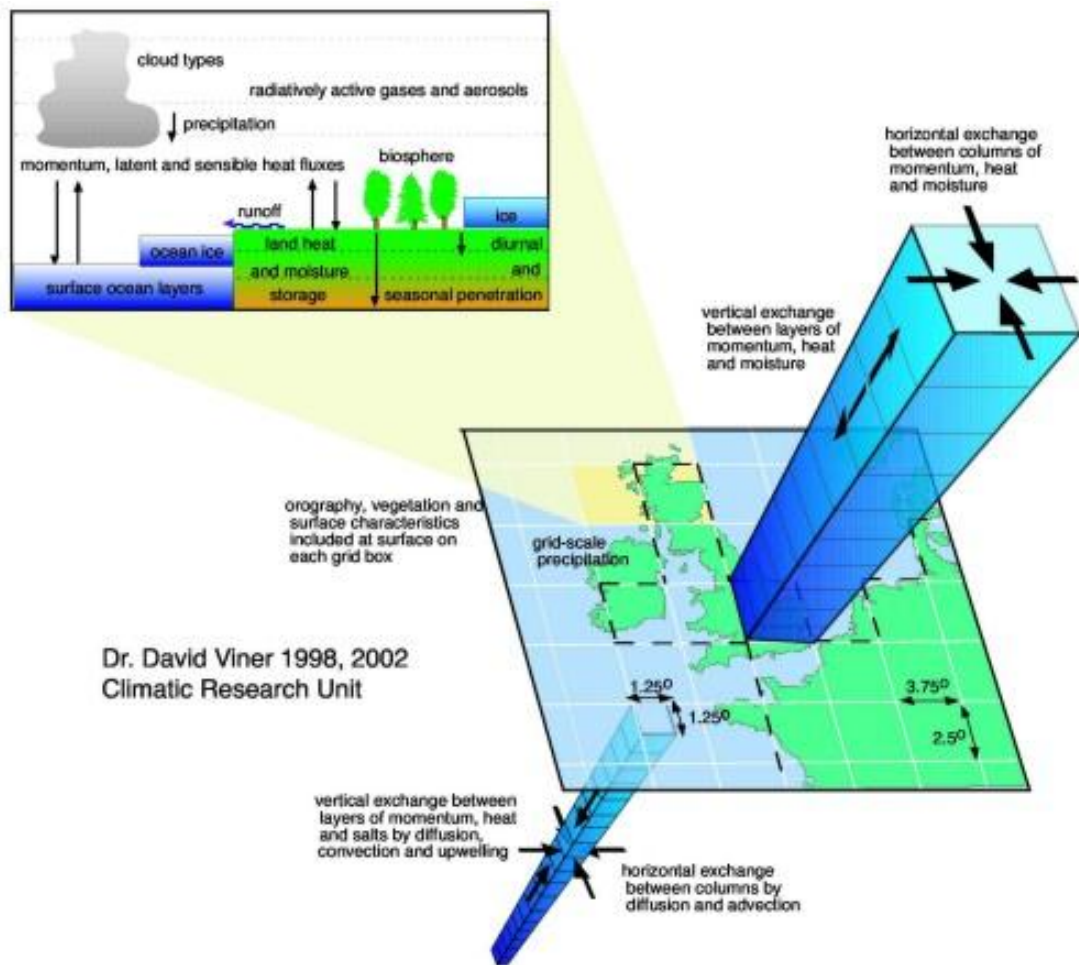
Figure: 3-Dimensional Representation of Climate Models (Climate Research Unit, 2011)

(from http://www.cru.uea.ac.uk/cru/info/modelcc/ retrieved on 3/01/2011)

APPENDIX B: COMPROMISE PROGRAMMING

Multi-objective analysis is the methodology for assessing trade-offs between set of alternative solutions based on using one or more objectives. First step of multi-objective analysis consists of identifying the set of non-dominated solutions (the subset of solutions, worthy of further consideration to determine the best solution) within the feasible region, X. So instead of seeking a single optimal solution, a set of non-dominated solutions is sought. For each solution outside the set of non-dominated ones, it is considered that there is a non-dominated solution for which all objective functions remain unchanged or improved and at least one is strictly improved (Simonovic, 2009).
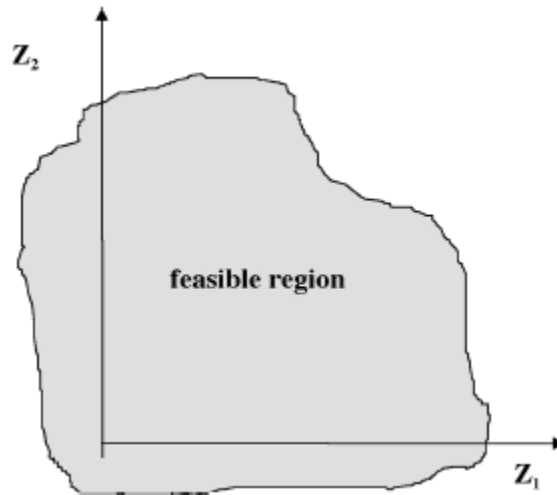
Figure B-1: Feasible region of a multi-objective problem presented in the objective space (Simonovic, 2009)

The preferred design for any problem is chosen from one of the non-dominated solutions. The non dominated solutions are grouped into two categories: the major alternatives and

the compromises. A compromise group lies somewhere in between the major alternatives (Figure X-2).

The remainder of the feasible region of solutions is categorized into dominated and excluded solutions. Dominated solutions are those that are inferior in all essential aspects to the other solutions. They can thus set aside for further consideration. Excluded solution re those that perform so badly on one or more objectives that they lie beneath the acceptability threshold. Thus they may be dropped from further consideration. There are many decision situations in which the decision maker must choose among a finite number of alternatives which are evaluated on a common set of non-commensurable multiple objectives or criteria.
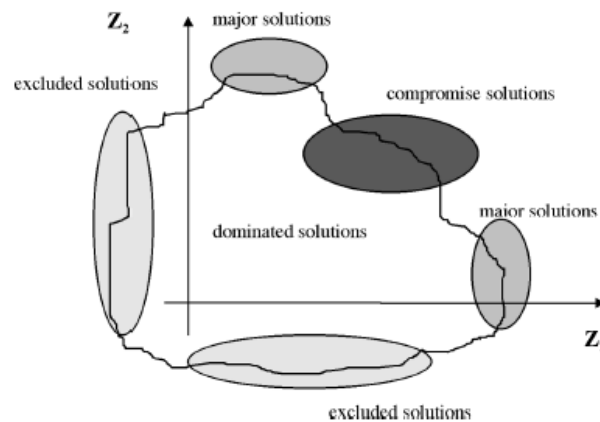
Figure B-2: Classification of feasible multi-objective alternative solutions (Simonovic, 2009)

The multi-objective analysis used in this study constitutes compromise programming which is a method for reducing the set of non-dominated solutions according to their

distance from the ideal solution. The distance from the ideal solution for each alternative is measured by a distance metric.

Compromise programming identifies solutions closest to the ideal solution, as determined by the distant metric. Due to it's simplicity, transparency and easy adaptation to both continuous and discrete settings, a compromise programming is recommended as the multi-objective analysis method of choice for application to water resources systems management. The process of evaluating the set of non-dominates solutions to measure how close the points come to the ideal solution.
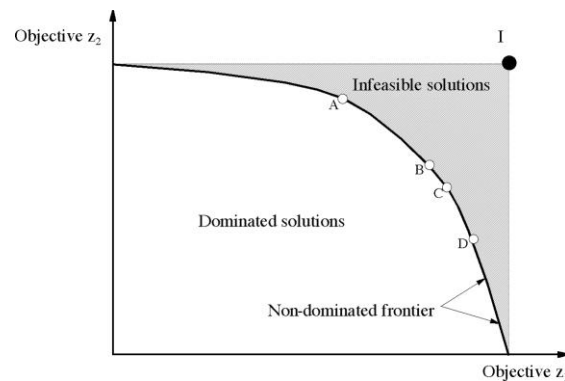
Figure B-3: Illustration of compromise solutions (Simonovic, 2009)

The case of input selection in the present study can be thought of as a four objective (or criteria) problem. The solution for which all objectives $z_i, i = 1, ...4$ are maximized is point I which is the solution obtained by maximizing the objectives, i. It is clear from Figure X-3, that the ideal solution represents the set of infeasible solutions. For this particular study, seven different combinations of inputs represent seven discrete solutions

of the problem. The solution identified as being the closest to the ideal solution are called compromise solution and constitute the compromise set.

For determining the closeness, assuming the decision maker views all alternatives as equally important, the distant matric L_p, is calculated as

$$min\left\{L_p(x) = \left[\sum_{i=1}^{4}\left\{\propto_i^p \left(\frac{z_i^* - z_i(x)}{z_i^* - z_i^{**}}\right)^p\right\}\right]^{1/p}\right\}$$

Where, $\frac{z_i^* - z_i(x)}{z_i^* - z_i^{**}}$ is a scaling function defined as

$$z_i^* = \max_{x \in X} z_i, \qquad\qquad i = 1,2,\ldots\ldots\ldots\ldots r$$

$$z_i^{**} = \min_{x \in X} z_i, \qquad\qquad i = 1,2,\ldots\ldots\ldots\ldots r$$

Where,

p is the distance parameter

$\propto_p$ is the weight

The choice of the value of p depends on the type of the problem and the desired solution. The larger the value of p, the greater the concern. For this study, p is assumed to be 2. Introducing $\propto_p$ allows the expression of the decision maker's feelings concerning the relative importance of the various objectives. In this study all four alternatives, the mean, standard deviation, maximum and minimum values from the seven different alternative combinations of the inputs are given equal weights assuming all alternatives to be equally important.

By introducing p and $\propto_p$, the compromise programming considers double weighting scheme. The parameter p reflects the importance of the maximal deviation and the parameter $\propto_p$ reflects the relative importance of the ith objective.

Once the distance metric L_p is calculated for each alternative, they are sorted in an ascending order. The sorted values are then ranked based on their values; the lower the distance metric, the higher the rank or the best compromise set.

APPENDIX C: PRINCIPAL COMPONENT ANALYSIS

The principal component analysis (PCA) is performed to reduce the dimensionality of any dataset of inter-related variables while preserving as much variation of the present data as possible.

The principal component analysis allows to compute a linear transformation that maps data from a high dimensional space to a lower one.

The best low-dimensional space can be determined by the best eigenvectors of the covariance matrix of x (i.e. the eigenvectors correcponding to the largest eigenvalues, also called the principal components).

If $x_1, x_2, \ldots \ldots, x_M, | x_M$ are $N \times 1$ vectors, The principal components are calculated as:

Step 1: Calculate the the mean: $\bar{x} = \frac{1}{M} \sum_{i=1}^{M} x_i$

Step 2: subtract the mean: $\phi_i = x_i - \bar{x}$

Step 3: for the matrix $A = \phi_1 \quad \phi_2 \quad \ldots \quad \phi_M \qquad (N \times M)$ matrix, then compute the covariance matrix:

$$C = \frac{1}{M} \sum_{n=1}^{M} \phi_n \phi_n^T = AA^T$$

Step 4: compute the eigenvalues of C: $\lambda_1 > \lambda_2 + \cdots > \lambda_N$

Step 5: compute the eigenvectors of C: $u_1, u_{2,} \ldots, u_N$

Since C is symmetric, $u_1, u_{2,} \ldots, u_N$ form a basis (i.e. aby vector x or actually $(x - \bar{x})$ can be written as a linear combination of the eigenvectors:

$$x - \bar{x} = b_1 u_1 + b_2 u_2 + \cdots + b_N u_N = \sum_{i=1}^{N} b_i u_i$$

Step 6: The dimensionality reduction step: keep only terms corresponding to the K nearest eigenvalues:

$$\hat{x} - \bar{x} = \sum_{i=1}^{K} b_i u_i \ \ where \ K \ll N$$

The representation of $\hat{x} - \bar{x}$ into the basis $u_1, u_2, \dots \dots \dots, u_K$ is this

$$\begin{bmatrix} b_1 \\ b_2 \\ .. \\ b_K \end{bmatrix}$$

In the PCA, it is assumed that the new variables (i.e. $b_i's$) are uncorrelated.

The covariance of $b_i's$ is:

$$U^T C U = \begin{bmatrix} \lambda_1 & 0 & 0 \\ 0 & \lambda_2 & 0 \\ . & . & . \\ . & . & . \\ 0 & 0 & \lambda_K \end{bmatrix}$$

The covariance matrix presents only second order statistics among the vector values. Since the new values are linear combinations of the original variables, it is difficult to interpret their meaning.

A principal component is defined as a linear combination of optimally-weighted observed varianles. In

In order to choose the principal components (K), the following criterion is used:

$$\frac{\sum_{i=1}^{K} \lambda_i}{\sum_{i=1}^{N} \lambda_i} > Threshold \ (e.g. 0.9 \ or \ 0.95)$$

Source: http://www.cse.unr.edu/~bebis/MathMethods/PCA/lecture.pdf

APPENDIX D: Atmosphere-Ocean Global Climate Models Used

Canadian Coupled Global Climate Model

The third generation Coupled Global Climate Model (CGCM3) was created in 2005 by the Canadian Centre for Climate Modelling and Analysis (CCCma) in Victoria, BC for use in the IPCC 4th assessment report to run complex mathematical equations which describe the earth's atmospheric and oceanic processes. The CGCM3 climate model includes four major components: an atmospheric global climate model, an ocean global climate model, a thermodynamic sea-ice model, and a land surface model (Hengeveld, 2000) and consists of two resolutions, T47 and T63. The T47 version has a surface grid whose spatial resolution is roughly 3.75 degrees lat/lon and 31 levels in the vertical. The ocean grid shares the same land mask as the atmosphere, but has four ocean grid cells underlying every atmospheric grid cell. The ocean resolution in this case is roughly 1.85 degrees, with 29 levels in the vertical.

The T63 version has a surface grid whose spatial resolution is roughly 2.8 degrees latitude/longitude and 31 levels in the vertical. As before the ocean grid shares the same land mask as the atmosphere, but in this case there are 6 ocean grids underlying every atmospheric grid cell. The ocean resolution is therefore approximately 1.4 degrees in longitude and 0.94 degrees in latitude. This provides slightly better resolution of zonal currents in the Tropics, more nearly isotropic resolution at mid latitudes, and somewhat reduced problems with converging meridians in the Arctic. (Compiled from http://www.ec.gc.ca/ccmac-cccma/default.asp?lang=En&n=1299529F-1)

Commonwealth Scientific and Industrial Research Organization's Mk3.5 Climate Systems Model

Australia's Commonwealth Scientific and Industrial Research Organization created the AOGCM CSIROMK3.5, which is an improved version of the MK climate systems model. The model consists of several components: atmosphere, land surface, ocean and polar ice. The dynamic framework of the atmospheric model is based upon the spectral method with the equations cast in the flux form that conservs predicted variables. The atmospheric moisture variables (vapour, water and ice) are advected by a Semi-Lagrangian Transport (SLT) algorithm (McGregor, 1993). The most recent version (MK3.5) has included a representation of the Great Lakes and changes in land surface scheme and it's representation of surface albedo under freezing than it's previous versions. The MK3.5 version provides improved information by including the spatially varying eddy transfer coefficients (Visbeck et al, 1997) and the Kraus-Turner mixed layer (1967) scheme. Improvements have also been done in it's oceanic behavior in the high latitude Southern ocean, where the stratification and circulation are generally more realistic than the prior models. The spatial resolution of the model is 1.875×1.875.

Compiled from (http://www.cawcr.gov.au/publications/technicalreports/CTR_021.pdf)

Max Planck Institute for Meteorology's ECHAM5AOM Model

ECHAM5 is the 5th generation of the ECHAM global climate model. Depending on the configuration the model resolves the atmosphere up to 10 hPa for tropospheric studies, or up to 0.01 hPa for middle atmosphere studies. The current version differ in the vertical extent of the atmosphere as well as the relevant processes than it's earlier

versions. It is capable of hosting sub-models (chemistry, aerosol and vegetation) going beyond the meteorological processes of a AOGCM. The model can be used as a part of a coupled ocean GCM, in assimilation by linear relaxation and as a standalone column model.

For integrations to start, the model requires several files. These file contain information for the description of the initial or re-start state of the atmosphere (boundary conditions at the surface, the ozone distribution and tables of constants of LW radiation schemes), the description of assumed conditions during the integration, e.g. sea surface temperature, or the initialization of parameterizations.

(Compiled from http://www.mpimet.mpg.de/en/science/models/echam/echam5.html)

Meteorological Institute, University of Bonn Meteorological Research Institute of KMA Model and Data Groupe at MPI-M's ECHO-G Model

The climate model ECHO-G (Legutke and Voss, 1999) is a coupled climate model consisting of the atmospheric model ECHAM4 (Roeckner et al., 1996) and the ocean model HOPE (Wolff et al., 1997).

The ECHAM4-model is based on primitive equations. The prognostic variables are vorticity, divergence, logarithm of surface pressure, temperature, specific humidity, mixing ratio of total cloud water and optionally a number of trace gases and aerosols.The vertical extension is up to a pressure level of 10 hPa, which corresponds to a height of approximately 30km. A hybrid sigma-pressure coordinate system is used with 19 irregularly ordered levels and with highest resolution in the atmospheric boundary layer.

The bottom level is placed at a height of about 30m above the surface corresponding approximately to the surface layer. In this study the ECHAM4 model has a horizontal resolution of about 3.75lat x 3.75lon.

The ocean model HOPE (Hamburg Ocean Primitive Equation) is an ocean global climate model (OGCM) based on primitive equations with the representation of thermodynamic processes. It is a non-eddy resolving circulation model. HOPE-G has a horizontal resolution of approximately 2.8lat x 2.8lon with a grid refinement in the tropical regions over a band from 10N to 10S. This meridional grid refinement reaches a value of 0.5 at the equator allowing for a more realistic representation of ENSO variability in the tropical Pacific Ocean . The ocean model has 20 vertical, irregularly ordered layers.

The coupling as well as the interpolation between the atmosphere and the ocean model is controlled by the coupling software OASIS (Terray et al., 1998). Concerning the coupling dynamics, at a distinct frequency the atmospheric component of the model passes heat, fresh water and momentum to the ocean and gets information about surface conditions of the ocean. This frequency is equal for all exchange fields and describes a 'coupled time step'. The fields that are exchanged are averaged over the last coupled time step. Further aspects of the exchange processes are flux corrections due to the interactive coupling between ocean and atmosphere in order to prevent climate drift. These heat- and freshwater fluxes were diagnosed in a coupled spin-up integration. Accordingly, the sea-surface-temperature and sea-surface salinity were restored to their climatological observed values. This flux adjustment is constant in time and its global average vanishes.

Quoted from (http://coast.gkss.de/staff/wagner/midhol/model/model_des.html)

Goddard Institute for Space Studies' Atmospheric Ocean Model

The North American Space Association and the Goddard Institute for Space Studies developed the GISS-AOM climate model, first in 1995 and then a revised version was created with smaller grids in 2004 for the IPCC 4th assessment report. The model requires two kinds of input, specified parameters and prognostic variables, and generates two kinds of output, climate diagnostics and prognostic variables. The specified input parameters include physical constants, the Earth's orbital parameters, the Earth's atmospheric constituents, the Earth's topography, the Earth's surface distribution of ocean, glacial ice, or vegetation, and many others. The time varying prognostic variables include fluid mass, horizontal velocity, heat, water vapor, salt, and subsurface mass and energy fields. The resolution for the model is 4° longitude by 3° latitude (PCMDI, 2005). The atmospheric grid has 12 vertical layers (PCMDI, 2005).

Model for Interdisciplinary Research on Climate version 3.2

The Japanese Model for Interdisciplinary Research on Climate version 3.2 (MIROC3.2) was developed in two resolutions: the high resolution (MIROC3.2HIRES) in $1.125° \times 1.125°$ grid and the medium resolution (MIROC3.2MEDRES) in $2.8° \times 2.8°$ grid. For present study, two emissions scenarios from MIROC3.2HIRES (A1B and B1) and three scenarios (A1B, A2 and B1) from MIROC3.2MEDRES were used.

APPENDIX E: SRES Emission Scenarios
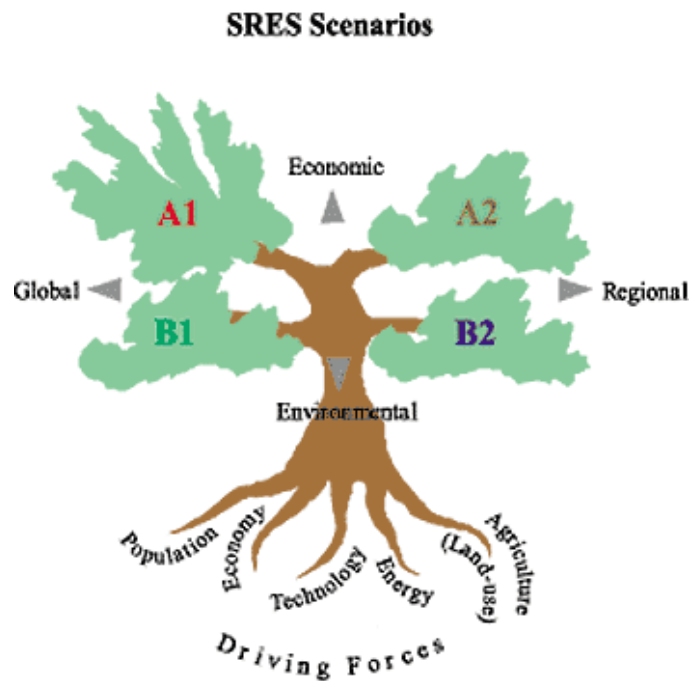
SRES Scenarios

Figure A1: SRES Emission Scenarios (Nakicenovic et al, 2000)

A1B: In scenario A1B, the storyline includes rapid economic expansion and globalization, a population peaking at 9 billion in 2050, and a balanced emphasis on a wide range of energy sources (Nakicenovic et al, 2000).

B1: The storyline for the B1 scenario is much like A1B in terms of population and globalization; however there are changes toward a service and information economy with more resource efficient and clean technologies. Emphasis is put on finding global solutions for sustainability (Nakicenovic et al, 2000).

A2: For scenario A2, the storyline consists of a world of independently operating nations with a constantly increasing population and economic development on a regional

level. Technological advances in this storyline occur more slowly due to the

divisions between nations (Nakicenovic et al, 2000).

APPENDIX F: Regression Test Results

Regression Results for Stations Within 0-200 km Radius Distance

Predictor	t-Statistic	Probability (p)
Hamilton RBG	-8.52	0.000
Hamilton A	20.54	0.000
Fergus	-3.91	0.000
Elora	-4.17	0.000
Delhi	10.71	0.000
Chatham WPCP	**0.27**	**0.791**
Brantford MOE	-6.15	0.000
Woodstock	26.58	0.000
Waterloo A	28.64	0.000
St. Thomas WPCP	10.53	0.000
Stratford MOE	8.06	0.000
Sarnia	25.15	0.000
Barrie	3.92	0.000
Owensound	**-2.82**	**0.005**
Wiarton	7.49	0.000
Toronto City	-4.75	0.000
Toronto Int'l A	4.69	0.000

Regression Results for Stations Within 0-175 km Radius Distance

Predictor	t-Statistic	Probability (p)
Woodstock	26.43	0.000
St. Thomas WPCP	9.97	0.000
Stratford MOE	8.34	0.000
Delhi	10.81	0.000
Brantford MOE	-6.42	0.000
Waterloo A	29.85	0.000
Sarnia	25.80	0.000
Elora	-4.05	0.000
Hamilton A	21.40	0.000
Hamilton RBG	-11.24	0.000
Fergus	-3.96	0.000
Chatham WPCP	**0.22**	**0.829**
Toronto Int'l A	4.29	0.000
Owensound	**2.38**	**0.017**

Regression Results for Stations Within 0-150 km Radius Distance

Predictor	t-Statistic	Probability (p)
Woodstock	26.36	0.000
St. Thomas WPCP	9.96	0.000
Stratford MOE	8.92	0.000
Delhi	10.83	0.000
Brantford MOE	-6.50	0.000
Waterloo A	29.82	0.000
Sarnia	25.97	0.000
Elora	-4.01	0.000
Hamilton A	21.43	0.000
Hamilton RBG	-11.26	0.000
Fergus	-3.62	0.000
Chatham WPCP	**0.33**	**0.743**
Toronto Int'l A	4.36	0.000

Regression Results for Stations Within 0-125 km Radius Distance

Predictor	t-Statistic	Probability (p)
Woodstock	26.30	0.000
St. Thomas WPCP	9.86	0.000
Stratford MOE	8.77	0.000
Delhi	10.63	0.000
Brantford MOE	-6.76	0.000
Waterloo A	34.25	0.000
Sarnia	26.30	0.000
Elora	-3.68	0.000
Hamilton A	23.70	0.000
Hamilton RBG	-10.81	0.000
Fergus	**-3.30**	**0.001**
Chatham WPCP	**0.19**	**0.853**

Regression Results for Stations Within 0-100 km Radius Distance

Predictor	t-Statistic	Probability (p)
Woodstock	25.76	0.000
St. Thomas WPCP	10.17	0.000
Stratford MOE	7.79	0.000
Delhi	9.41	0.000
Brantford MOE	-10.98	0.000
Waterloo A	34.39	0.000
Sarnia	25.85	0.000
Elora	-8.26	0.000
Hamilton A	21.60	0.000

Regression Results for Stations Within 0-75 km Radius Distance

Predictor	t-Statistic	Probability (p)
Woodstock	30.19	0.000
St. Thomas WPCP	10.22	0.000
Stratford MOE	13.99	0.000
Delhi	15.71	0.000
Brantford MOE	2.27	0.023

Regression Results for Stations Within 0-50 km Radius Distance

Predictor	t-Statistic	Probability (p)
Woodstock	40.28	0.000
St. Thomas WPCP	19.86	0.000
Stratford MOE	16.68	0.000

APPENDIX G: Cumulative Precipitation for 2000
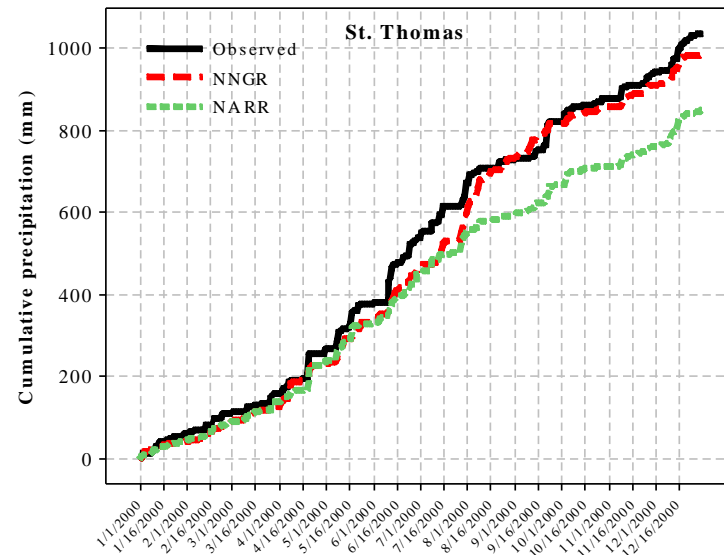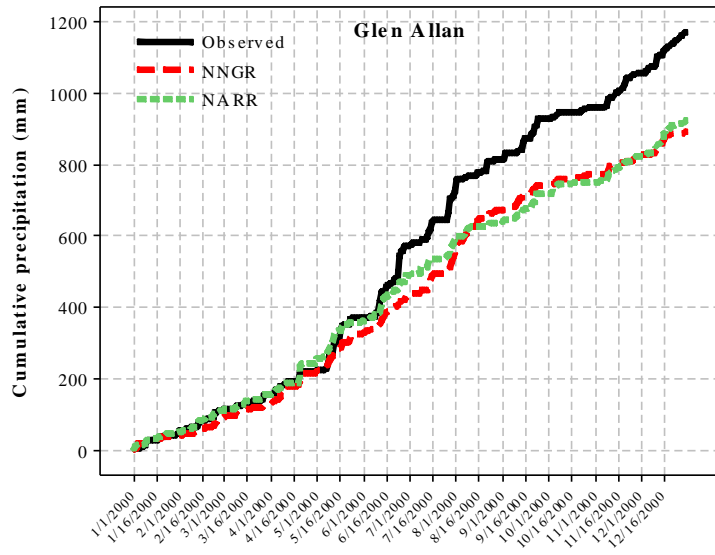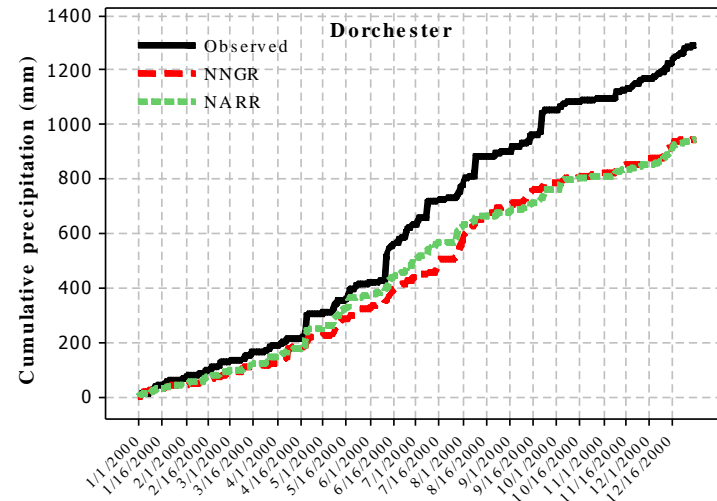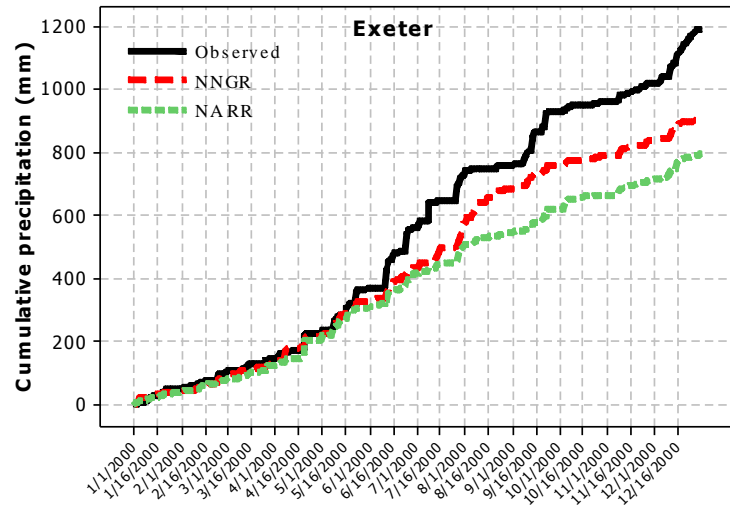
APPENDIX H: Scatter plots of Precipitation and Flow (May-August, 1980-2005) at Ingersoll

Ingersoll_Observed Simulated

Ingersoll_NNGR

Ingersoll_NARR
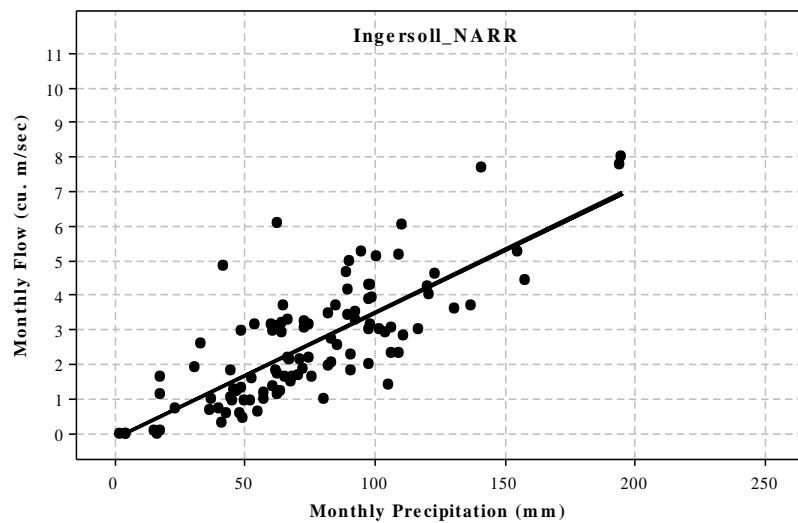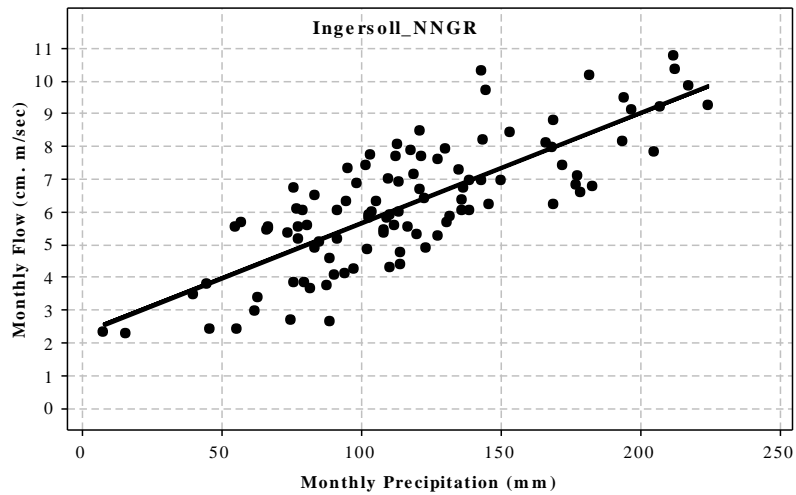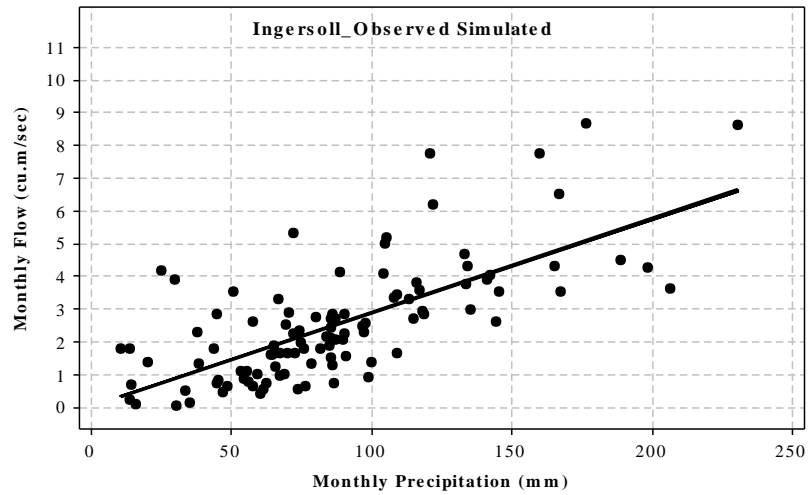
APPENDIX I: Distribution Fit of Extreme Precipitation Indices

Table I-1: Heavy Precipitation Days for 2050s Summer

AOGCM Models/Scenarios	Distribution Fit	Parameters					
		k	σ	μ	α	β	γ
Historical Perturbed	GEV III	0.14	2.48	7.511	-	-	-
CGCM3T47 A1B	GEV III	0.15	2.58	7.34	-	-	-
CGCM3T47 A2	GEV III	0.30	2.81	7.72	-	-	-
CGCM3T47 B1	GEV III	0.16	2.75	6.99	-	-	-
CGCM3T63 A1B	Gamma 3P	-	-	-	24.78	0.52	-4.94
CGCM3T63 A2	GEV III	0.32	2.84	7.75	-	-	-
CGCM3T63 B1	GEV III	-0.20	2.37	6.88	-	-	-
CSIROMK3.5 A2	Gamma	-	-	-	11.68	0.92	11.68
CSIROMK3.5 B1	GEV III	0.26	2.75	9.13	-	-	-
GISSAOM A1B	Gamma 3P	-	-	-	58.56	0.38	-13.51
GISSAOM B1	Log-Pearson 3	-	-	-	9.27	0.11	3.18
MIROC3HIRES A1B	GEV III	0.21	2.26	5.53	-	-	-
MIROC3HIRES B1	GEV III	0.24	2.23	5.41	-	-	-
MIROC3MEDRES A1B	Log-Pearson 3	-	-	-	8.72	0.14	2.97
MIROC3MEDRES A2	Gamma 3P	-	-	-	36.94	0.39	7.32
MIROC3MEDRES B1	GEV III	0.23	2.46	5.75	-	-	-

Table I-2: Heavy Precipitation Days for Winter

AOGCM Models/Scenarios	Distribution Fit	Parameters		
		k	σ	μ
Historical Perturbed	Normal	-	2.64	6.68
CGCM3T47 A1B	GEV Type II	0.62	4.46	8.19
CGCM3T47 A2	GEV Type II	0.59	4.58	7.85
CGCM3T47 B1	GEV Type II	0.60	4.81	8.86
CGCM3T63 A1B	GEV Type II	0.61	4.35	7.27
CGCM3T63 A2	GEV Type II	0.63	4.41	7.43
CGCM3T63 B1	GEV Type II	0.64	4.26	6.36
CSIROMK3.5 A2	GEV Type II	0.66	5.13	7.95
CSIROMK3.5 B1	GEV Type II	0.66	5.09	8.38
GISSAOM A1B	GEV Type II	0.64	4.40	6.58
GISSAOM B1	GEV Type II	0.67	4.58	6.59
MIROC3HIRES A1B	GEV Type II	0.60	3.84	6.06
MIROC3HIRES B1	GEV Type II	0.65	3.76	5.64
MIROC3MEDRES A1B	GEV Type II	0.58	3.91	5.71
MIROC3MEDRES A2	GEV Type II	0.63	3.83	5.68
MIROC3MEDRES B1	GEV Type II	0.62	3.63	5.64

Table I-3: Very Wet Days for Summer

AOGCM Models/Scenarios	Distribution Fit	Parameters				
		α	B	k	σ	μ
Historical Perturbed	GEV III			0.06	1.24	1.40
CGCM3T47 A1B	Frechet	0.99	2.57	-	-	-
CGCM3T47 A2	Frechet	0.92	2.14	-	-	-
CGCM3T47 B1	Frechet	0.99	2.74	-	-	-
CGCM3T63 A1B	Frechet	0.89	1.80	-	-	-
CGCM3T63 A2	Frechet	0.90	2.02	-	-	-
CGCM3T63 B1	Frechet	0.82	1.43	-	-	-
CSIROMK3.5 A2	Frechet	0.83	1.98	-	-	-
CSIROMK3.5 B1	Frechet	0.90	2.45	-	-	-
GISSAOM A1B	Frechet	0.81	1.43	-	-	-
GISSAOM B1	Frechet	0.84	1.66	-	-	-
MIROC3HIRES A1B	Gen. Pareto	-	-	0.63	3.52	-0.15
MIROC3HIRES B1	Gen. Pareto	-	-	0.68	3.41	-0.29
MIROC3MEDRES A1B	Gen. Pareto	-	-	0.64	3.33	-0.33
MIROC3MEDRES A2	Frechet	0.83	1.29	-	-	-
MIROC3MEDRES B1	Gen. Pateto	-	-	0.65	0.85	0.25

Table I-4: Very Wet Days for Winter

| AOGCM Models/Scenarios	Distribution Fit	Parameters				
		K	σ	μ	α	β
Historical Perturbed	GEV II	-0.070	1.52	2.59	-	-
CGCM3T47 A1B	Gumbel Max	-	2.17	3.40	-	-
CGCM3T47 A2	GEV II	0.10	2.04	3.34	-	-
CGCM3T47 B1	Gamma	-	-	-	2.61	1.81
CGCM3T63 A1B	GEV III	-0.14	1.58	2.61	-	-
CGCM3T63 A2	GEV III	0.14	1.72	2.99	-	-
CGCM3T63 B1	GEV III	0.15	1.53	2.55	-	-
CSIROMK3.5 A2	Weibull	-	-	-	2.57	6.09
CSIROMK3.5 B1	GEV III	-0.16	1.98	3.98	-	-
GISSAOM A1B	GEV III	-0.17	1.77	3.20	-	-
GISSAOM B1	GEV III	-0.22	1.82	3.32	-	-
MIROC3HIRES A1B	GEV III	-0.03	1.18	1.5	-	-
MIROC3HIRES B1	Gumbel Max	-	1.16	1.69	-	-
MIROC3MEDRES A1B	Gumbel Max	-	1.15	1.68	-	-
MIROC3MEDRES A2	GEV III	-0.20	1.46	2.30	-	-
MIROC3MEDRES B1	GEV III	-0.09	1.30	1.88	-	-

Table I-5: Maximum 5 Day Precipitation for Summer

AOGCM Models/Scenarios	Distribution Fit	Parameters		
		k	σ	μ
Historical Perturbed	GEV II	0.026	23.30	54.71
CGCM3T47 A1B	Gumbel Max	-	23.14	55.98
CGCM3T47 A2	GEV II	0.11	21.71	55.99
CGCM3T47 B1	GEV II	0.038	23.40	57.89
CGCM3T63 A1B	GEV II	0.036	21.57	54.43
CGCM3T63 A2	GEV II	0.07	24.55	57.71
CGCM3T63 B1	GEV II	0.061	21.66	57.58
CSIROMK3.5 A2	GEV II	0.093	30.01	75.01
CSIROMK3.5 B1	GEV II	0.097	27.75	70.83
GISSAOM A1B	GEV II	0.20	21.75	58.17
GISSAOM B1	GEV II	0.044	24.6	60.57
MIROC3HIRES A1B	GEV II	0.10	16.78	41.65
MIROC3HIRES B1	GEV II	0.09	19.07	42.95
MIROC3MEDRES A1B	GEV II	0.02	18.77	43.61
MIROC3MEDRES A2	GEV II	0.061	20.83	49.79
MIROC3MEDRES B1	GEV II	0.09	17.3	45.12

Table I-6: Maximum 5 Day Precipitation for Winter

AOGCM Models/Scenarios	Distribution Fit	Parameters					
		K	σ	μ	α	β	γ
Historical Perturbed	GEV II	0.07	15.85	42.45	-	-	-
CGCM3T47 A1B	GEV II	0.07	18.93	54.03	-	-	-
CGCM3T47 A2	GEV II	0.08	18.64	50.48	-	-	-
CGCM3T47 B1	GEV II	0.09	18.14	54.38	-	-	-
CGCM3T63 A1B	GEV II	0.04	17.46	46.26	-	-	-
CGCM3T63 A2	GEV II	0.05	18.58	48.35	-	-	-
CGCM3T63 B1	GEV II	0.05	15.65	43.05	-	-	-
CSIROMK3.5 A2	GEVII	0.098	21.17	50.56	-	-	-
CSIROMK3.5 B1	GEV II	0.13	18.57	52.01	-	-	-
GISSAOM A1B	GEV II	0.07	15.24	41.70	-	-	-
GISSAOM B1	Frechet 3P	-	-	-	6.25	97.63	-54.53
MIROC3HIRES A1B	Gamma 3P	-	-	-	3.01	13.28	13.23
MIROC3HIRES B1	GEV II	0.1	13.83	38.85	-	-	-
MIROC3MEDRES A1B	Gamma 3P	-	-	-	2.27	13.45	17.68
MIROC3MEDRES A2	Gamma 3P	-	-	-	3.26	10.843	14.15
MIROC3MEDRES B1	Gumbel Max	-	14.12	38.78	-	-	-

APEPNDIX J: IDF Plots of Selected Scenarios

243
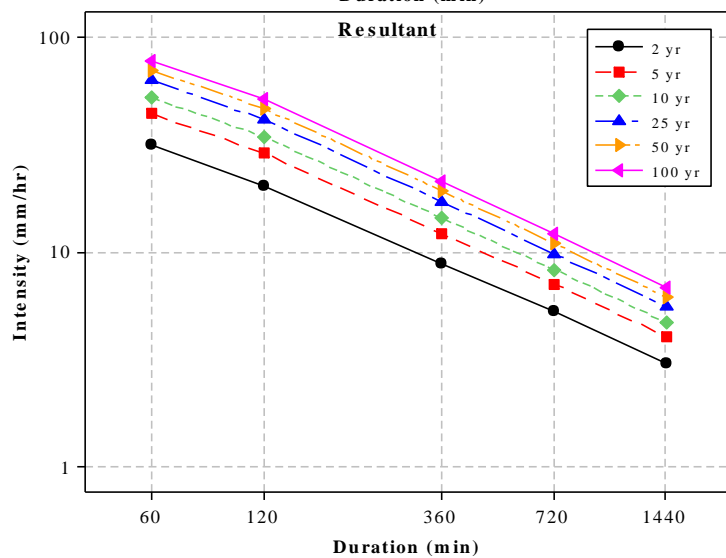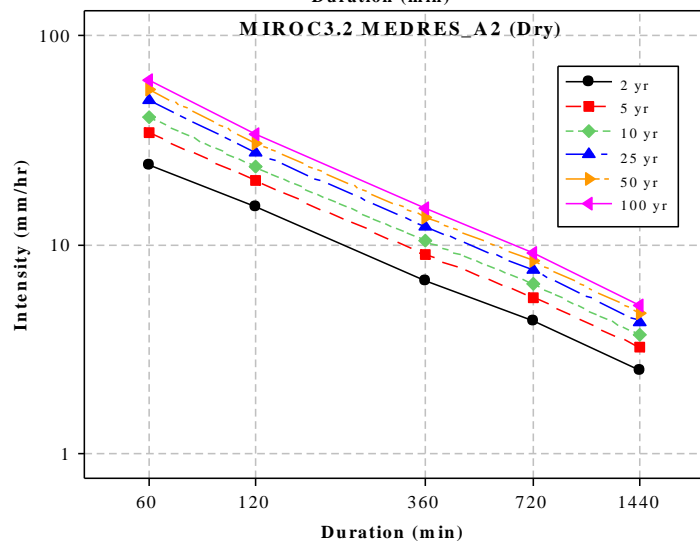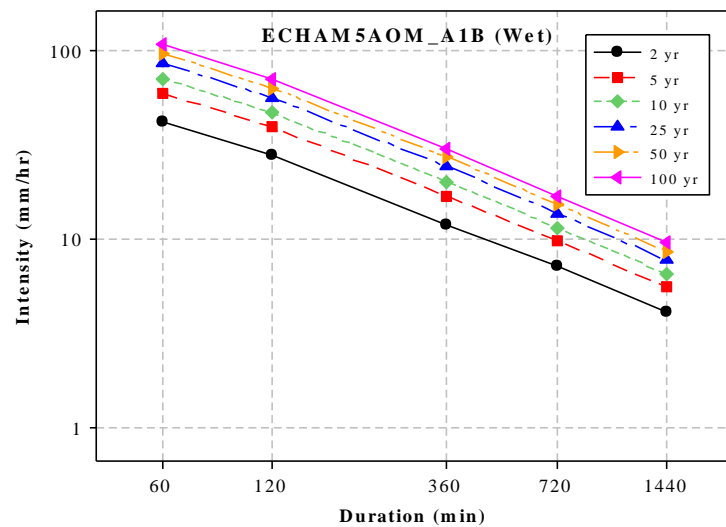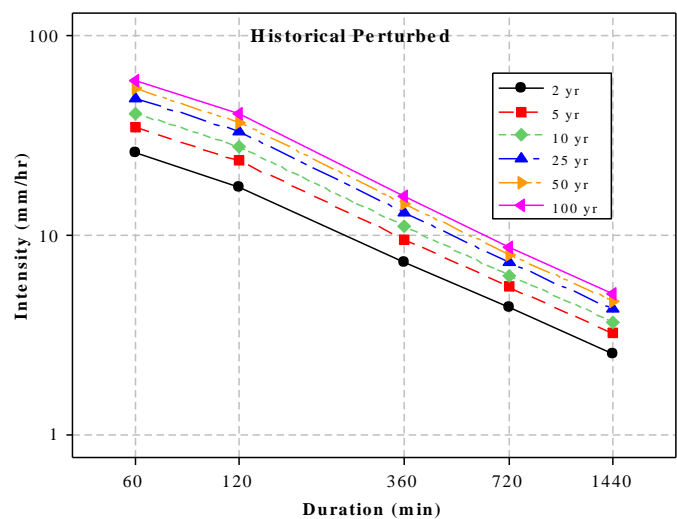
Appendix K: Steps of Research

This section provides the technical details necessary for reproducing the results developed in the study.

K-1: Assessment of Reanalysis-Hydro-climatic Data for Climate Change Studies

1) Data Description and Pre-processing

Data Type	Data Source	Data Format	Variables
Observed data	National Climate Data and Information Archive, Environment Canada (http://climate.weatheroffice.gc.ca/climateData/canada_e.html)	.txt	Precipitation, Maximum Temperature, Minimum Temperature
Global Reanalysis (NNGR) data	National Center for Environmental Protection/ National Center for Atmospheric Research (NCEP/NCAR) Reanalysis Project, Earth System Research Laboratory, National Oceanic and Atmospheric Administration, USA, (http://climate.weatheroffice.gc.ca/climateData/canada_e.html)	.netCDF	Precipitation Rate, Maximum Temperature, Minimum Temperature
Regional Reanalysis (NARR) data	National Center for Environmental Protection/ National Center for Atmospheric Research (NCEP/NCAR) Reanalysis Project, Earth System Research Laboratory, National Oceanic and Atmospheric Administration, USA, (http://climate.weatheroffice.gc.ca/climateData/canada_e.html) Processed data collected from Data Access Integration Portal of Global Environmental and Climate Change Center (GEC3), Environment Canada and the Drought Research Initiative (DRI) (http://loki.qc.ec.gc.ca/DAI/login-e.php)	.txt	Precipitation Rate, Maximum Temperature, Minimum Temperature

Preprocessing of NNGR:

- The NNGR data obtained in .netCDF extension which is a binary format and needs an extraction tool to convert the data into any readable format. In this study, the Grid Analysis and Display System (GrADS), [developed by Brian E. Doty of the Center for Ocean-Land-Atmosphere Studies, USA] is programming tool is used to convert the data into .txt. format.

- The variable 'precipitation rate' ($kg/m^2/sec$) is converted into precipitation (mm/day)

2) Interpolation of the Gridded data into Station Scale

Both NNGR and NARR are gridded data. So an inverse distance weighted method is used to convert them into the stations grid using the nearest grid points.

3) Hydrologic Modeling

The continuous hydrologic model used in this work is developed and modified by Cunderlik and Simonovic (2004) and Prodaovic and Simonovic (2006). The current program runs in Java program (Prodanovic and Simonovic, 2006) to add for more flexibility of the input variables. The necessary codes for developing the model can be downloaded from the FIDs website at

(http://www.eng.uwo.ca/research/iclr/fids/publications/products/ContinuousModelReport2.pdf, retrieved on 3/17/2011).

4) Performance Check of Reanalysis Data

The interpolated NNGR, NARR data and the observed station data and the hydrologic model results are analyzed using the methods mentioned in sections 4.2.1 and 4.2.3.

K-2: Estimating Uncertainties in the Modelled Estimates of Extreme Precipitation Events

1) Data Description

Data Type	Data Source	Data Format	Variables
Observed data	National Climate Data and Information Archive, Environment Canada (http://climate.weatheroffice.gc.ca/climateData/canada_e.html)	.txt	Precipitation, Maximum Temperature, Minimum Temperature
Regional Reanalysis (NARR) data	National Center for Environmental Protection/ National Center for Atmospheric Research (NCEP/NCAR) Reanalysis Project, Earth System Research Laboratory, National Oceanic and Atmospheric Administration, USA, (http://climate.weatheroffice.gc.ca/climateData/canada_e.html)	.txt	Mean Sea Level Pressure, Relative Humidity, Wind Speeds at Northward and Eastward directions
	Processed data collected from Data Access Integration Portal of Global Environmental and Climate Change Center (GEC3), Environment Canada and the Drought Research Initiative (DRI) (http://loki.qc.ec.gc.ca/DAI/login-e.php)		

2) Selection of appropriate predictor variables

For selecting appropriate set of predictor variables, several combinations of inputs are considered and run into weather generator to search for an optimal set of predictors. Monthly outputs from those different combinations are then evaluated using their mean, variance, maximum and minimum values. A compromise programming tool called "compro" is used to rank the combinations using the above four criteria and provide the best combination.

3) Future Climate Scenarios

- For generating future climate scenarios, 15 different climate models and scenarios, described in Table 4.2 are used. These are downloaded in .csv format from the CCCSN website (CCCSN, 2011).

- Like the reanalysis fata, AOGCMs also provide gridded data. So, an inverse distance weighted method is used to convert them into the stations grid using the nearest grid points.

- The interpolated station data are then used to calculate change change fields to generate synthetic climate data for input into the weather generator.

4) Weather Generator

The weather generator used in this study is originally developed by Sharif and Burn (2006) in C+ programming language. The model is further re-written in to a java program and modified to account for leap year (Prodanovic and Simonovic, 2008) and incorporate principal component analysis to calculate the mahalanobis distance using the principal components (Eum et al., 2009). These versions of weather generator were set to run using use three inputs and same number of outputs. In the present work, codes are modified to add additional inputs. The previous versions provided the same number of inputs and outputs. In the present version, only the output of interest is set to produce.

5) Bayesian Reliability Enssemble Average (BA-REA)

The Bayesian reliability ensemble average method is developed in r programming language by Tebaldi et al., (2004; 2005). The necessary codes to run the program can be downloaded from NCAR (2010).

6) Kernel Density Estimator

The kernel density estimator method used in this program is calculated using two step procedure.

First, specific bandwidths for each year time step are calculated by writing simple codes in r program.

The bandwidths are then input into the matlab program to develop a cumulative distribution function using the kernel estimator program called "@KDE", developed by Alex Ihler and Mile Mandel (2003). The program is a general matlab class for k-dimensional kernel density. It is written in a mix of matlab '.m' files and MEX/C++ code. Thus in order to use it, the user needs to compile the C++ code in Matlab. The program is available to download from (http://www.ics.uci.edu/~ihler/code/kde.html, Retrieved, 3/18/2011).

7) Probabilities of Extreme Precipitation Indices

The parametric distribution of the extreme precipitation indices are compared for a handful of 7 different distributions for each scenarios for summer and winter seasons. The performances of the distributions are assessed in terms of three goodness-of-fit tests. A sample table for comparing 5 day maximum precipitation for winter using CGCM3T63 A1B model is included next:

5 day Maximum Precipitation for Winter 2050s
CGCM3T63 A1B

#	Distribution	Kolmogorov Smirnov		Anderson Darling		Chi-Squared	
		Statistic	Rank	Statistic	Rank	Statistic	Rank
1	Frechet	0.07169	8	3.9815	8	12.372	6
2	Frechet (3P)	0.03747	3	0.39337	3	2.1107	2
3	Gamma	0.0498	7	1.0924	6	12.95	7
4	Gamma (3P)	0.0258	1	0.1845	1	2.007	1
5	Gen. Extreme Value	0.0331	2	0.35071	2	2.2295	3
6	Gen. Pareto	0.04807	6	57.529	13	N/A	
7	Gumbel Max	0.03984	4	0.5051	4	7.3627	5
8	Normal	0.10334	11	5.3168	9	35.053	10
9	Pareto	0.304	13	51.716	12	271.03	12
10	Rayleigh	0.12668	12	9.9044	11	64.458	11
11	Rayleigh (2P)	0.08171	9	2.2674	7	13.143	8
12	Weibull	0.09622	10	5.5201	10	30.922	9
13	Weibull (3P)	0.0401	5	0.51736	5	4.1031	4

8) Probabilities of Extreme Precipitation Indices

Probabilities of extreme precipitation indices are calculated in matlab using the codes written by author. This works by calculating a cumulative distribution function of using the 'ksdensity' function. The cumulative distribution functions for the specific ranges of indices are deducted to calculate probability of that specific class of index.

K-3: Developing Probabilistic Intensity-Duration-Frequency (IDF) Curves for Future

1) Data Description

Data Type	Data Source	Data Format	Variables
Observed data	National Climate Data and Information Archive, Environment Canada (http://climate.weatheroffice.gc.ca/climateData/canada_e.html)	.txt	Daily and Hourly Rainfall

2) Selection of Appropriate Number of Stations

For selecting appropriate number of stations regression analysis and cross-correlation analysis is performed using Minitab statistical software (Minitab, 2007).

3) Generation of Future Climate Scenario

- For generating future climate scenarios, 27 different climate models and scenarios, described in Table 4.10 are used. The choice of AOGCMs is entirely based on the availability of AOGCM data into an easily readable format. These are downloaded in .csv format from the CCCSN website (CCCSN, 2011).

- The gridded AOGCMs are interpolated to station grid using the IDW method.

- The interpolated station data are then used to calculate change fields to generate synthetic climate data for input into the weather generator.

4) Weather Generator

The weather generator used for this section is based on the same model described in H 2.4.

5) Hourly Disaggregation Scheme

The daily downscaled outputs are disaggregated into an hourly interval using the codes developed in Matlab by Mansour and Burn (2010).

6) Frequency Analysis

7) Kernel Density Estimator

The kernel density estimator described in H-2.5 is used to combine the IDF information of different durations. The weights are calculated based on equation 5.1.

The probabilities of different duration and return periods of storm are presented in terms of cumulative distribution functions with codes written in Matlab.

CURRICULUM VITAE

Name: Tarana A. Solaiman

Education

2007   **M. A. Sc.** in Civil Engineering

McMaster University, Hamilton, ON

2004   **B. Sc.** in Civil Engineering

Bangladesh University of Engineering and Technology, Dhaka, Bangladesh

Awards and Honours

2010-2011   Ontario Graduate Scholarships in Science and Technology

2007-2010   Western Graduate Research Scholarship (WGRS)

2005-2007   McMaster Entrance and Graduate Scholarship

1998-2004   Comilla Board Talentpool Scholarship for Continuing Undergraduate Studies, Bangladesh

2003-2004   Bangladesh University of Engineering and Technology Merit Scholarship

Journal Publications

1) **Solaiman, T. A**., King, L., and Simonovic, S. P. (2010). "Extreme precipitation vulnerability in the Upper Thames River basin: uncertainty in climate model projections", *Int. Journal of Climatology,* DOI: 10.1002/joc.2244.

2) **Solaiman, T. A.**, Simonovic, S. P., and Burn, D. H. "Quantifying uncertainties in the modelled estimates of extreme precipitation events". *Water Resources Research,* Under Review.

3) **Solaiman, T. A.**, and Simonovic, S. P. (2010). "NCEP-NCAR reanalyses data for hydrologic modelling on a basin scale". *Canadian Journal of Civil Engineering*, 37(4), 611-623.

4) **Solaiman, T.A.**, Coulibaly, P., and Kanaroglou, P. (2008). "Ground level ozone forecasting using data-driven methods, for Hamilton, Ontario, Canada". *Air Quality, Atmosphere and Health*, 1(4), 179-235.

Conference Proceedings/ Workshops

1) **Solaiman, T. A.** And Simonovic, S. P. (2011). "How uncertain are the future extreme precipitation events? An Upper Thames River basin context". Poster presented in the *public workshop organized by the Upper Thames River basin Conservation Authority*, London, Ontario, 29 March, 2011.

2) **Solaiman, T. A.** And Simonovic, S. P. (2011). "Moving towards probability based intensity-duration-frequency curves under climate change". Poster presented in *the public workshop organized by the Upper Thames River Basin Conservation Authority*, London, Ontario, 29 March, 2011.

3) **Solaiman, T.A.** and Simonovic, S. P. (2009). "NCEP-NCAR reanalyses hydroclimatic data for rainfall-runoff modeling on a watershed scale". In the proceedings of *the 33rd International. Association of Hydraulic Engineering & Research (IAHR) Congress*, Vancouver, Canada, 10-14 August, 2009.

4) **Solaiman, T.A.** (2009). "Partial least square (PLS) model for air quality modelling". Abstract published in the proceedings of *the 20th Annual Conference of the Intl. Environmetrics Soc.*, Bologna, Italy, 5-9 July, 2009.

5) **Solaiman, T.A.**, Coulibaly, P., Kanaroglou, P. (2007). "Spatio-temporal modeling of ozone and TSP pollution in Hamilton using Neural Network Models". Poster presented in the Graduate event day, Department of Geography and Earth Sciences, McMaster University, Hamilton, Ontario, 13 April, 2007.

6) Hoque, M., **Solaiman, T.A.**, Khondaker, B., Sarkar, S. (2005). "Road safety in Bangladesh: overview of problem, progress, priorities and options". In the proceedings of *the 13th International Conference on Road Safety on Four Continents*, Warsaw, Poland, 5-7 October, 2005.

7) Hoque, M. M., **Solaiman, T. A.**, And Alam, D. M., (2005), "Improving metropolitan road safety in Bangladesh". Abstract published in the proceedings of *the 3ʳᵈ Asian Regional Conference on Safe Communities*, Taipai, Taiwan, 19-22 October, 2005.